Cell Journal (Yakhteh)

Guide for Authors

Aims and Scope: The "Cell Journal (Yakhteh)" is a peer review and monthly English publication of Royan Institute of Iran. The aim of the journal is to disseminate information through publishing the most recent scientific research studies on exclusively Cellular, Molecular and other related topics. **Cell J**, has been certified by the Ministry of Culture and Islamic Guidance since 1999 and also accredited as a scientific and research journal by HBI (Health and Biomedical Information) Journal Accreditation Commission since 2000 which is an open access journal. **This journal holds the membership of the Committee on Publication Ethics (COPE).**

1. Types of articles

The articles in the field of Cellular and Molecular can be considered for publications in **Cell J.** These articles are as below:

A. Original articles

Original articles are scientific reports of the original research studies. The article consists of English Abstract (structured), Introduction, Materials and Methods, Results, Discussion, Conclusion, Acknowledgements, Author's Contributions, and References **(Up to 40).**

B. Review articles

Review articles are the articles written by well experienced authors and those who have excellence in the related fields. The corresponding author of the review article must be one of the authors of at least three published articles appearing in the references. The review article consists of English Abstract (unstructured), Introduction, Conclusion, Author's Contributions, and References **(Up to 70).**

C. Systematic Reviews

Systematic reviews are a type of literature review that collect and critically analyzes multiple research studies or papers. The Systematic reviews consist of English Abstract (unstructured), Introduction, Materials and Methods, Results, Discussion, Conclusion, Acknowledgements, Author's Contributions, and References **(Up to 70).**

D. Short communications

Short communications are articles containing new findings. Submissions should be brief reports of ongoing researches. The short communication consists of English Abstract (unstructured), the body of the manuscript (should not hold heading or subheading), Acknowledgements, Author's Contributions, and References **(Up to 30).**

E. Case reports

Case reports are short discussions of a case or case series with unique features not previously described which make an important teaching point or scientific observation. They may describe novel techniques or use equipment, or new information on diseases of importance. It consists of English Abstracts (Unstructured), Introduction, Case Report, Discussion, Acknowledgements, Author's Contributions, and References **(Up to 30).**

F. Editorial

Editorials are articles should be written in relevant and new data of journals' filed by either the editor in chief or the editorial board.

G. Imaging in biology

Images in biology should focus on a single case with an interesting illustration such as a photograph, histological specimen or investigation. Color images are welcomed. The text should be brief and informative.

H. Letter to the editors

Letter to the editors are in response to previously published **Cell J** articles, and may also include interesting cases that do not meet the requirement of being truly exceptional, as well as other brief technical or clinical notes of general interest.

I. Debate

Debates are articles which show a discussion of the positive and negative view of the author concerning all aspect of the issue relevant to scientific research.

2. Submission process

It is recommended to see the guidelines for reporting different kinds of manuscripts. This guide explains how to prepare the

manuscript for submission. Before submitting, we suggest authors to familiarize themselves with **Cell J** format and content by reading the journal via the website (www.celljournal.com). The corresponding author ensures that all authors are included in the author list and agree with its order, and they must be aware of the manuscript submission.

A. Author contributions statements

It is essential for authors to include a statement of responsibility in the manuscript that specifies the contribution of every one of them. This participation must include conception and design of the manuscript, data acquisition or data analysis and interpretation, drafting of the manuscript and/or revising it for critically important intellectual content, revision and final approval of the manuscript and statistical analysis, obtaining funding, administrative, technical, or material support, or supervision. Authors who do not meet the above criteria should be acknowledged in the **Acknowledgments section.**

B. Cover letter and copyright

Each manuscript should be accompanied by a cover letter, signed by all authors specifying the following statement: "The manuscript has been seen and approved by all authors and is not under active consideration for publication. It has neither been accepted for publication nor published in another journal fully or partially (except in abstract form). **Also, no manuscript would be accepted in case it has been pre-printed or submitted to other websites.** I hereby assign the copyright of the enclosed manuscript to **Cell J.**" Corresponding author must confirm the proof of the manuscript before online publishing. Also, it is needed to suggest three peer reviewers in the field of their manuscript.

C. Manuscript preparation

Authors whose first language is not English encouraged to consult a native English speaker in order to confirm his manuscripts to American or British (not a mixture) English usage and grammar. It is necessary to mention that we will check the plagiarism of your manuscript by iThenticate Software. The manuscript should be prepared in accordance with the "International Committee of Medical Journal Editors (ICMJE)". Please send your manuscript in two formats word and PDF (including: title, name of all the authors with their degree, abstract, full text, references, tables and figures) and also send tables and figures separately in the site. The abstract and text pages should have consecutive line numbers in the left margin beginning with the title page and continuing through the last page of the written text. Each abbreviation must be defined in the abstract and text when they are mentioned for the first time. Avoid using abbreviation in the title. Please use the international and standard abbreviations and symbols

It should be added that an essential step toward the integration and linking of scientific information reported in published literature is using standardized nomenclature in all fields of science and medicine. Species names must be italicized (*e.g., Homo sapiens*) and also the full genus and species written out in full, both in the title of the manuscript and at the first mention of an organism in a paper.

It is necessary to mention that genes, mutations, genotypes, and alleles must be indicated in italics. Please use the recommended name by consulting the appropriate genetic nomenclature database, e.g., HUGO for human genes. In another words; if it is a human gene, you must write all the letters in capital and italic (*e.g., OCT4, c-MYC*). If not, only write the first letter in capital and italic (*e.g., Oct4, c-Myc*). **In addition, protein designations are the same as the gene symbol but are not italicized.**

Of note, Cell J will only consider publishing genetic association study papers that are novel and statistically robust. Authors are advised to adhere to the recommendations outlined in the STREGA statement (http://www.strega-statement.org). The following criteria must be met for all submissions:

1. Hardy-Weinberg Equilibrium (HWE) calculations must be carried out and reported along with the P-values if applicable [see Namipashaki et al. 2015 (Cell J, Vol 17, N 2, Pages: 187-192) for a discussion].

2. Linkage disequilibrium (LD) structure between SNPs (if multiple SNPs are reported) must be presented.

3. Appropriate multiple testing correction (if multiple independent SNPs are reported) must be included.

Submissions that fail to meet the above criteria will be rejected before being sent out for review.

Each of the following manuscript components should begin in the following sequence:

Authors' names and order of them must be carefully considered (full name(s), highest awarded academic degree(s), email(s), and institutional affiliation(s) of all the authors in English. Also, you must send mobile number and full postal address of the corresponding author).

Changes to Authorship such as addition, deletion or rearrangement of author names must be made only before the manuscript has been accepted in the case of approving by the journal editor. In this case, the corresponding author must explain the reason of changing and confirm them (which has been signed by all authors of the manuscript). If the manuscript has already been published in an online issue, an erratum is needed.

Title is providing the full title of the research (do not use abbreviations in title).

Running title is providing a maximum of 7 words (no more than 50 characters).

Abstract must include Objective, Materials and Methods, Results, and Conclusion (no more than 300 words).

Keywords, three to five, must be supplied by the authors at the foot of the abstract chosen from the Medical Subject Heading (MeSH). Therefore; they must be specific and relevant to the paper.

The following components should be identified after the abstract:

Introduction: The Introduction should provide a brief background to the subject of the paper, explain the importance of the study, and state a precise study question or purpose.

Materials and Methods: It includes the exact methods or observations of experiments. If an apparatus is used, its manufacturer's name and address should be stipulated in parenthesis. If the method is established, give reference but if the method is new, give enough information so that another author can perform it. If a drug is used, its generic name, dose, and route of administration must be given. Standard units of measurements and chemical symbols of elements do not need to be defined.

Statistical analysis: Type of study and statistical methods should be mentioned and specified by any general computer program used.

Ethical considerations*:* Please state that informed consent was obtained from all human adult participants and from the parents or legal guardians of minors and include the name of the appropriate institutional review board that approved the project. It is necessary to indicate in the text that the maintenance and care of experimental animals complies with National Institutes of Health guidelines for the humane use of laboratory animals, or those of your Institute or agency.

Clinical trial registration: All of the Clinical Trials performing in Iran must be registered in Iranian Registry of Clinical Trials (www.irct.ir). The clinical trials performed abroad, could be considered for publication if they register in a registration site approved by WHO or www.clinicaltrials.gov. If you are reporting phase II or phase III randomized controlled trials, you must refer to the CONSORT Statement for recommendations to facilitate the complete and transparent reporting of trial findings. Reports that do not conform to the CONSORT guidelines may need to be revised before peer-reviewing.

Results: They must be presented in the form of text, tables, and figures. Take care that the text does not repeat data that are presented in tables and/or figures. Only emphasize and summarize the essential features of the main results. Tables and figures must be numbered consecutively as appeared in the text and should be organized in separate pages at the end of the manuscript while their location should be mentioned in the main text.

Tables and figures: If the result of your manuscript is too short, it is better to use the text instead of tables & figures. Tables should have a short descriptive heading above them and also any footnotes. Figure's caption should contain a brief title for the whole figure and continue with a short explanation of each part and also the symbols used (no more than 100 words). All figures must be prepared based on cell journal's guideline in color (no more than 6 Figures and Tables) and also in TIF format with 300 DPI resolution.

Of Note: Please put the tables & figures of the result in the results section not any other section of the manuscript.

Supplementary materials would be published on the online version of the journal. This material is important to the understanding and interpretation of the report and should not repeat material within the print article. The amount of supplementary material should be limited. Supplementary material should be original and not previously published and will undergo editorial and peer review with the main manuscript. Also, they must be cited in the manuscript text in parentheses, in a similar way as when citing a figure or a table. Provide a caption for each supplementary material submitted.

Discussion: It should emphasize the present findings and the variations or similarities with other researches done by other researchers. The detailed results should not be repeated in the discussion again. It must emphasize the new and important aspects of the study.

Conclusion: It emphasizes the new and important aspects of the study. All conclusions are justified by the results of the study.

Acknowledgements: This part includes a statement thanking those who contributed substantially with work relevant to the study but does not have authorship criteria. It includes those who provided technical help, writing assistance and name of departments that provided only general support. You must mention financial support in the study. Otherwise; write this sentence "There is no financial support in this study".

Conflict of interest: Any conflict of interest (financial or otherwise) and sources of financial support must be listed in the Acknowledgements. It includes providers of supplies and services from a commercial organization. Any commercial affiliation must be disclosed, regardless of providing the funding or not.

Of Note: If you have already any patent related to the subject of your manuscript, or you are going to apply for such a patent, it must be mentioned in this part.

References: The references must be written based on the Vancouver style. Thus the references are cited numerically in the text and listed in the bibliography by the order of their appearance. The titles of journals must be abbreviated according to the style used in the list of Journals Indexed in PubMed. Write surname and initials of all authors when there are six or less. In the case of seven or more authors, the names of the first six authors followed by "et al." must be listed. You can download Endnote file for Journal references style: endnote file

The reference of information must be based on the following order:

Article:

Surname(s) and first letter of name &middle name(s) of author(s) .Manuscript title. Journal title (abbr).publication date (year); Volume & Issue: Page number.

Example: Manicardi GC, Bianchi PG, Pantano S, Azzoni P, Bizzaro D, Bianchi U, et al. Presence of endogenous nicks in DNA of ejaculated human spermatozoa and its relationship to chromomycin A3 accessibility. Biol Reprod. 1995; 52(4): 864-867.

Book:

Surname(s) and first letter of name & middle name(s) of author(s).Book title. Edition. Publication place: publisher name; publication date (year); Page number.

Example: Edelman CL, Mandle CL. Health promotion throughout the lifespan. 2nd ed. ST Louis: Mosby; 1998; 145-163.

Chapter of book:

Surname(s) and first letter of name & middle name(s) of author(s).Chapter title. In: Surname(s) and first letter of name & middle name(s) of editor(s), editors. Book title. Edition. Publication place: publisher name; publication date (year); Page number.

Example: Phillips SJ, Whisnant JP. Hypertension and stroke. In: Laragh JH, Brenner BM, editors. Hypertension: pathophysiology, diagnosis, and management. 2nd ed. New York: Raven Press; 1995; 465-478.

Abstract book:

Example: Amini rad O.The antioxidant effect of pomegranate juice on sperm parameters and fertility potential in mice. Cell J. 2008;10 Suppl 1:38.

Thesis:

Name of author. Thesis title. Degree. City name. University. Publication date (year).

Example: Eftekhari Yazdi P. Comparison of fragment removal and co-culture with Vero cell monolayers on development of human fragmented embryos. Presented for the Ph.D., Tehran. Tarbiyat Modarres University. 2004.

Internet references

Article:

Example: Jahanshahi A, Mirnajafi-Zadeh J, Javan M, Mohammad-Zadeh M, Rohani M. Effect of low-frequency stimulation on adenosineA1 and A2A receptors gene expression in dentate gyrus of perforant path kindled rats. Cell J. 2008; 10 (2): 87-92. Available from: http://www.celljournal.org. (20 Oct 2008).

Book:

Example: Anderson SC, Poulsen KB. Anderson's electronic atlas of hematology.[CD-ROM]. Philadelphia: Lippincott Williams & Wilkins; 2002.

D. Proofs are sent by email as PDF files and should be checked and returned within 72 hours of receipt. It is the authors' responsibility to check that all the text and data as contained in the page proofs are correct and suitable for publication. **We are requested to pay particular attention to author's names and affiliations as it is essential that these details be accurate when the article is published.**

E. Pay for publication: Publishing an article in **Cell J** requires Article Processing Charges (APC) that will be billed to the submitting author following the acceptance of an article for publication. For more information please see www.celljournal.org.

F. Ethics of scientific publication: Manuscripts that have been published elsewhere with the same intellectual material will refer to duplicate publication. If authors have used their own previously published work or work that is currently under review, as the basis for a submitted manuscript, they are required to cite the previous work and indicate how their submitted manuscript offers novel contributions beyond those of the previous work. Research and publication misconduct is considered a serious breach of ethics.

The Journal systematically employs iThenticate, plagiarism detection and prevention software designed to ensure the originality of written work before publication. Plagiarism of text from a previously published manuscript by the same or another author is a serious publication offence. Some parts of text may be used, only where the source of the quoted material is clearly acknowledged.

3. General information

A. You can send your manuscript via online submission system which is available on our website. If the manuscript is not prepared according to the format of **Cell J**, it will be returned to authors.

B. The order of article appearance in the Journal is not demonstrating the scientific characters of the authors.

C. Cell J has authority to accept or reject the manuscript.

D. The received manuscript will be evaluated by associate editor. **Cell J** uses a single-blind peer review system and if the manuscript suits the journal criteria, we select the reviewers. If three reviewers pass their judgments on the manuscript, it will be presented to the editorial board of **Cell J.** If the editorial board has a positive judgment about the manuscript, reviewers' comments will be presented to the corresponding author (the identification of the reviewers will not be revealed). The executive member of journal will contact the corresponding author directly within 3-4 weeks by email. If authors do not receive any reply from journal office after the specified time, they can contact journal office. Finally, executive manager will respond promptly to authors' request.

The Final Checklist

The authors must ensure that before submitting the manuscript for publication, they have to consider the following parts:

1. The first page of manuscript should contain title, name of the author/coauthors, their academic qualifications, designation & institutions they are affiliated with, mailing address for future correspondence, email address, phone, and fax number.

2. Text of manuscript and References prepared as stated in the "guide for authors" section.

3. Tables should be on a separate page. Figures must be sent in color and also in JPEG (Jpg) format.

4. Cover Letter should be uploaded with the signature of all authors.

5. An ethical committee letter should be inserted at the end of the cover letter.

The Editor-in-Chief: Ahmad Hosseini, Ph.D.

Cell Journal *(Yakhteh)*

P.O. Box: 16635-148, Iran

Tel/Fax: + 98-21-22510895

Emails: Celljournal@royaninstitute.org

info@celljournal.org

IN THE NAME OF GOD

Dr. Saeed Kazemi Ashtiani

Gone But not Forgotten

In the memory of the late Director of Royan Institute, Founder of Stem Cells Research in Iran and Chairman of ***Cell Journal*** *(Yakhteh)*. May he rest in peace.

PUBLISHED & SPONSORED BY:
Publication of Royan Institute (ACECR)

Indexed in:
1. Thomson Reuters (ISI)
2. PubMed
3. PubMed Central (PMC)
4. National Library Medicine (NLM)
5. Biosis Preview
6. Index Medicus for the Eastern Mediterranean Region (IMEMR)
7. Regional Information Center for Sciences and Technology (RICeST)
8. Index Copernicus International
9. Cambridge Scientific Abstract (CSA)
10. EMBASE
11. Scopus
12. Cinahl Database
13. Google Scholar
14. Chemical Abstract Service (CAS)
15. Proquest
16. Directory of Open Access Journals (DOAJ)
17. Open Academic Journals Index (OAJI)
18. Directory of Research Journals Indexing (DRJI)
19. Scientific Information Database (SID)
20. Iranmedex
21. Islamic World Science Citation Center (ISC)
22. Magiran
23. Science Library Index
24. Biological Abstracts
25. Essential Science Indicators
26. EuroPub

Editorial Office Address (Dr. Ahmad Hosseini):
Royan Institute, P.O.Box: 16635-148,
Tehran, Iran
Tel & Fax: (+9821)22510895
Website: www.celljournal.org
Emails: info@celljournal.org
celljournal@royaninstitute.org

Printing Company:
Naghshe e Johar Co.
No. 103, Fajr alley, Tehranpars Street,
Tehran, Iran.

Cell Journal$_{(Yakhteh)}$, Vol 24, No 10, October 2022, Serial Number: 105, Pages: 555-636

CONTENTS

Review Article

• **Angiogenesis and Its Targeting in Glioblastoma with Focus on Clinical Approaches**
Fatemeh Daneshimehr, Zahra Barabadi, Shahrokh Abdolahi, Masoud Soleimani, Javad Verdi, Somayeh Ebrahimi-Barough, Jafar Ai **555**

Original Articles

• **Differential Expression Pattern of *linc-ROR* Spliced Variants in Pluripotent and Non-Pluripotent Cell Lines**
Fatemeh Mirzadeh Azad, Elham Taheri Bajgan, Parisa Naeli, Alexander Rudov, Mahrokh Bagheri Moghadam, Mozhgan Sadat Akhtar, Akram Gholipour, Seyed Javad Mowla, Mahshid Malakootian **569**

• **Moderate Endurance Training and MitoQ Improve Cardiovascular Function, Oxidative Stress, and Inflammation in Hypertensive Individuals: The Role of miR-21 and miR-222: A Randomized, Double-Blind, Clinical Trial**
Yaser Masoumi-Ardakani, Hamid Najafipour, Hamid Reza Nasri, Soheil Aminizadeh, Shirin Jafari, Zohreh Safi **577**

• **Itaconic Acid as A Differential Transcription Regulator of Apoptosis and Autophagy Pathways Genes: A Rat Adipose Mesenchymal Stem Cells Model**
Mohammad Reza Tabandeh, Fatemeh Soroush, Dian Dayer **586**

• **Production of *CFTR* Mutant Gene Model by Homologous Recombination System**
Hanieh Rezaee, Mohammad Salehi, Mojgan Bandepour, Sima Kalantari, Sara Hosseini, Khosrow Agin, Bahram Kezemi **596**

• **Alpha-Lipoic Acid Ameliorates Sperm DNA Damage and Chromatin Integrity in Men with High DNA Damage: A Triple Blind Randomized Clinical Trial**
Masoud Habibi, Behzad Abbasi, Zohreh Fakhari Zavareh, Vahid Esmaeili, Abdolhossein Shahverdi, Mohammad Ali Sadighi Gilani, Marziyeh Tavalaee, Mohammad Hossein Nasr-Esfahani **603**

• **Effect of Mechanical Micro-Vibrations on The Efficiency of Leopard Inter-Species Somatic Cell Nuclear Transfer**
Maryam Shahverdi, Vahid Akbarinejad, Azam Dalman, Mostafa Hajinasrollah, Mehdi Vodjgani, Nima Tanhaei Vash Mohammad Hossein Nasr-Esfahani, Poopak Eftekhari-Yazdi **612**

• **Granulosa Cell Conditioned Medium Enhances The Rate of Mouse Oocyte *In Vitro* Maturation and Embryo Formation**
Zeinab Bahrami, Narges Hatamian, Mahmood Talkhabi, Elnaz Zand, David G. Mottershead, Rouhollah Fathi **620**

• **Effect of Single Embryo Blastomere Biopsy from Human Frozen Embryos on Assisted Reproductive Outcomes**
Shahrzad Aghajani, Ali Salehzadeh, Fatemeh Ghasemian, Marzieh Mehrafza, Ahmad Hosseini **628**

• **Front page of Cell Journal$_{(Yakhteh)}$: Figure 5 A, Page: 616**

Review Article

Angiogenesis and Its Targeting in Glioblastoma with Focus on Clinical Approaches

Fatemeh Daneshimehr, Ph.D.[1], Zahra Barabadi, Ph.D.[2], Shahrokh Abdolahi, M.Sc.[1], Masoud Soleimani, Ph.D.[3, 4], Javad Verdi, Ph.D.[1], Somayeh Ebrahimi-Barough, Ph.D.[1], Jafar Ai, Ph.D.[1]*

1. Department of Tissue Engineering and Applied Cell Sciences, School of Advanced Technologies in Medicine, Tehran University of Medical Sciences, Tehran, Iran
2. Department of Tissue Engineering and Biomaterials, School of Advanced Medical Sciences and Technologies, Hamadan University of Medical Sciences, Hamadan, Iran
3. Department of Hematology, School of Medical Sciences, Tarbiat Modares University, Tehran, Iran
4. Medical Nanotechnology and Tissue Engineering Research Center, Shahid Beheshti University of Medical Sciences, Tehran, Iran

Corresponding Address: P.O.Box: 14177-55469, Department of Tissue Engineering and Applied Cell Sciences, School of Advanced Technologies in Medicine, Tehran University of Medical Sciences, Tehran, Iran
Email: jafar_ai@tums.ac.ir

Received: 31/July/2021, Accepted: 27/October/2021

Abstract

Angiogenesis is a characteristic of glioblastoma (GBM), the most fatal and therapeutic-resistant brain tumor. Highly expressed angiogenic cytokines and proliferated microvascular system made anti-angiogenesis treatments a thoroughly plausible approach for GBM treatment. Many trials have proved to be not only as a safe but also as an effective approach in GBM retardation in a certain time window as seen in radiographic response rates; however, they have failed to implement significant improvements in clinical manifestation whether alone or in combination with radio/chemotherapy. Bevasizumab, an anti-vascular endothelial growth factor-A (VEGF-A) antibody, is the only agent that exerts meaningful clinical influence by improving progression-free survival (PFS) and partially alleviate clinical symptoms, nevertheless, it could not prolong the overall survival (OS) in patients with GBM. The data generated from phase II trials clearly revealed a correlation between elevated reperfusion, subsequent to vascular normalization induction, and improved clinical outcomes which explicitly indicates anti-angiogenesis treatments are beneficial. In order to prolong these initial benefits observed in a certain period of time after anti-angiogenesis targeting, some aspects of the therapy should be tackled: recognition of other bypass angiogenesis pathways activated following anti-angiogenesis therapy, identification of probable pathways that induce insensitivity to shortage of blood supply, and classifying the patients by mapping their GBM-related gene profile as biomarkers to predict their responsiveness to therapy. Herein, the molecular basis of brain vasculature development in normal and tumoral conditions is briefly discussed and it is explained how "vascular normalization" concept opened a window to a better comprehension of some adverse effects observed in anti-angiogenesis therapy in clinical condition. Then, the most targeted angiogenesis pathways focused on ligand/receptor interactions in GBM clinical trials are reviewed. Lastly, different targeting strategies applied in anti-angiogenesis treatment are discussed.

Keywords: Angiogenesis Pathway, Cell Adhesion Molecules, Clinical Trial, Glioblastoma, Tyrosine-Kinase Receptors

Cell Journal(Yakhteh), Vol 24, No 10, October 2022, Pages: 555-568

Citation: **Daneshimehr F, Barabadi Z, Abdolahi Sh, Soleimani M, Verdi J, Ebrahimi-Barough S, Ai J. Angiogenesis and its targeting in glioblastoma with focus on clinical approaches. Cell J. 2022; 24(10): 555-568. doi: 10.22074/cellj.2022.8154.**

Introduction

Compensatory angiogenesis has been long introduced as the fuel for the tumor progression engine as well as an appealing target to curb tumor propagation. Glioblastoma multiforme (GBM) is a highly vascularized tumor that has been vastly investigated in anti-angiogenesis therapy (1), partly because of its resistance to current standard therapies including surgical resection, radiation, and chemotherapy. Moreover, patients with GBM show a survival period of less than 15 months. Also, patients with recurrent GBM have minimal treatment options and the survival time is less than 6 months. Therefore, GBM remains as one of the deadliest malignancies. Recent studies have demonstrated promising results from new anti-angiogenesis approaches that raise hope treating several solid tumors including GBM. Among these treatments, several FDA (U.S. Food and Drug Administration)-approved anti-vascular endothelial growth factor (VEGF) agents have been demonstrated satisfactory results such as bevacizumab (Avastin) for GBM, advanced colorectal cancer, non-small cell lung cancer, and breast cancer, Sorafenib (Nexavar) for patients with advanced renal cell and hepatocellular carcinoma, and sunitinib (Sutent) for advanced renal cell carcinoma and progressive gastrointestinal stromal tumor (2). Also, it has been shown that a combination of Sorafenib and administration of mesenchymal stem cell (MSC) improve the anti-angiogenesis effect of the drug in hepatocellular carcinoma (HCC) (3). Such promising results support the need for additional investigations.

This review summarizes angiogenesis in tumor tissue with a focus on angiogenic pathways in GBM, their targeting, the approaches' pros and cons, and related clinical trials.

Development of brain vasculature

Brain is a metabolically active organ in the body and its metabolism and physiochemical activity are absolutely oxygen dependent. The constant rate of oxygen

consumption in brain tissue is 3.5 ml of O_2/100 g of brain tissue/minutes accounting for 20% of total oxygen consumption in the body's rest state in a conscious young man. This oxygen is delivered and distributed precisely and unevenly throughout the brain based on different regions' activity and metabolism. A highly developed architecture of the brain vasculature is responsible for such a delicate oxygenation and blood supply with different perfusion rates in different areas (4).

Many studies have suggested the formation of embryonic brain vasculature from a primary surrounding peri-neural vascular plexus (PNVP) at certain stages of development in which brain is invaded in specific stereotypical patterns (5). The cellular basis for development of neurovascular plexus seems to be the interactions between endothelial and neural cells that are also involved in developing the blood-brain barrier (BBB). Somatic angioblasts have been proven to be the source of ECs contributing to the ingression of vessel sprouts in the avian neural tube. Signals from the developing nervous system direct sprouting vessels into the distinct areas of the brain. Contribution of neurovascular unit composed of ECs, pericytes, neurons, and astrocytes results in the development of the BBB and regulation of cerebral blood flow (6).

Molecular basis of vascular development in the nervous system

Although numerous molecules have been identified as angiogenic factors so far, the number of these factors is still expanding. Fibroblast growth factor1 (FGF1) is one of the first pre-angiogenic factors reported to be involved in vasculogenesis in developing the brain. Besides, VEGF as another pre-angiogenic factor with known effect on PNVP formation and subsequent vessel sprouts ingression into the developing neural tube, induces migration and patterning of angioblasts migrating from somitic mesoderm (7). Also, the role of integrin signaling pathways in the maturation of neurovascular structure through enhanced interaction of ECs and pericytes as well as induction of BBB development has been reported in many studies.

The other signaling pathways contributing to neurovascular development are semaphorins/plexin receptors, slits/Robo receptors, neuropilins (co-receptors of both VEGF and plexin receptors), netrins receptor UNC/DCC, and canonical Wnt signaling pathways (8).

Angiogenesis in brain tumors

Judah Folkman suggested that solid tumors meet tumor cells' need to excess nutrient and oxygen supply as well as their pervasiveness by provoking angiogenesis. Numerous studies have been conducted since then in an attempt to unveil the underlying mechanisms in malignancies and their differences form physiologic angiogenesis for more precisely modulate angiogenesis applying anti-angiogenesis therapy (9).

There are some differences between angiogenesis in cancer and normal tissues in terms of vascular structure, interactions between vascular ECs and pericytes, rate of blood flow, vascular permeability, and the maturation level (10). Similar to other cancer tissues, pathological vessels in GBM are tangled, unorganized, highly permeable and leaky, significantly larger in diameter, and thick in the basement membrane. Besides, the loose interaction between ECs and pericytes, and low pericyte coverage led to the development of a leaky, hemorrhagic vascular network as well as an impaired BBB leaving tumor tissue hypoxic and necrotic. Other common features of the vasculature architecture in cancer tissues are their irregularity, heterogeneity in shape and tissue distribution, uneven vessels diameter, excessive branching with some dead-end vessels, tortuosity, as well as chaotic structure of vascular network at all levels of arterioles, venules and capillaries (11).

Furthermore, the tight balance between pro and anti-angiogenesisfactors is one of the main regulators of physiologic vasculogenesis, whereas in GBM the balance heavily tips in favor of the expression of pro-angiogenic genes activated in response to tissue hypoxia, hypoxia-inducible factor1 (HIF-1) and acidosis. Highly active angiogenesis leads to glomeruloid tuft formation comprising perivascular and endothelial cells multilayered (12).

Some important molecules which are active in tumor vasculogenesis are VEGF, stromal-derived factor 1 (SDF1), platelet-derived growth factor (PDGF), granulocyte macrophage-colony stimulating factor (GM-CSF), insulin-like growth factor1 (IGF1), plasminogen activation factor 1 (PAI1), nitric oxide (NO), cyclooxygenase2 (COX2) and thrombospondin 2 (TSP2) (13).

It has been shown that VEGF increases vascular permeability through an increase in vascular wall pore size and number as well as a decrease in pericyte coverage. Besides, SDF1, as a very important modulator of brain tumor vasculogenesis, mediates its effect via the recruitment of intra-tumoral marrow-derived precursors into tumor endothelium. Vasculature maturation status is also different in tumor tissues; while most of the normal vessels are mature, stable and quiescent in normal tissue. They constantly proliferate and expand from the pre-existing vessels in tumor (14).

Vascular normalization theory

Since Folkman's proposition in anti-angiogenesis therapy to entirely block vessel growth in tumor settings in 1970s, it has been shown that applying excessive anti-angiogenesis factors may result in aggravating hypoxia recurrence fueling tumor progression. To conquer the unfavorable outcomes, "vascular normalization" concept was suggested by Jain in 2014 aiming to normalize tumor vasculature by restoring the balance between pro- and anti-angiogenesis agents to improve blood supply and drug access in the tumor region rather than totally destroying abnormal vessels. The concept was successfully examined using bevacizumab in mouse models of neuroblastoma in which the treatment led to

normal vasculature function and structure (11).

Angiogenesis pathways and anti-angiogenesis strategies

Many factors are known to affect ECs to promoting or eliminating angiogenesis. ECs receive these signals from the microenvironment either through their growth factor tyrosine kinase receptors (RTKs) such as VEGFR and epidermal growth factor receptor (EGFR), or via other growth factor receptors including TGF-β/TβRII and Wnt /Frizzled (Fzd) family receptor in addition to receptors involved in cell adhesion like integrins. Many studies have been conducted to target these signaling pathways for their potential effects in anti-angiogenesis therapy in GBM.

Growth factor tyrosine kinase receptors (RTKs)

The angiogenic effect of several growth factors including VEGFs, EGFs, FGFs, platelet-derived growth factors (PDGFs), angiopoietins (Ang-1 and Ang-2), hepatocyte growth factor (HGF) and ephrins is mediated through tyrosine kinase receptors. Ligand binding to the receptors leads to receptor homo- or hetero-dimerization and downstream signal activation. Some clinically targeted RTK are briefly discussed in the following section.

VEGF/VEGFR pathway

VEGFs are secreted by different cell types, including tumor cells, fibroblasts, and inflammatory cells, mostly in response to increasing tissue hypoxia in cancer. VEGF family including VEGFAs (VEGFA-165, -121, -145, -189 and -(xxx) b), VEGFB, VEGFC, VEGFD and placenta growth factor (PGF) bind to their receptors such as VEGFR1 (FLT-1), VEGFR2 (FLK1 or KDR) and VEGFR3 (FLT4) in addition to co-receptors proteoglycans and neurophilins in both physiologic and pathologic conditions. Depending on which VEGF/VEGFR is activated the outcome is different: VEGFAs (VEGF-165, -145, -189)/VEGFR-1,-2 activation is predominantly in favor of angiogenesis while VEGF-12, –(xxx)b/VEGFR1, -2 activation is anti-angiogenic, VEGFB/VEGFR1 activation is involved in fatty acid uptake in EC , VEGFC, VEGFD/VEGFR3, -2 induce lymphangiogenesis and PIGF/VEGFR1 recruits inflammatory cells. Besides, it has been demonstrated that VEGFAs/VEGFR2 activation develops immune privileged area in tumor site by suppression of T-cell function and dendritic cells (DCs) activation, as well as recruitment of regulatory T-cells (Tregs) and myeloid-derived suppressor cells (MDSCs) (15). Hence, targeting this pathway especially the interaction between VEGF-A and VEGFR-2, the main intra-tumoral angiogenesis pathway, has been vastly studied in cancer. For instance, Atorvastatin and deforolimus have been successfully used to reduce VEGF concentration in both glioma spheroids (16) and endometrial stromal cells (17), respectively. Some of the agents with proven efficiency in anti-angiogenesis therapy in cancer preclinical and clinical trials are now being marketed and prescribed to patients with cancer. To date, four inhibitors have been approved by the FDA: sunitinib and pazopanib for metastatic renal-cell carcinoma and gastrointestinal stromal tumors, vandetanib for medullary thyroid cancer and sorafenib for unresectable hepatocellular carcinoma and metastatic renal cell carcinoma (RCC). Besides, bevacizumab (Avastin) (Table 1), an anti-VEGF aptamer, is being used as an off-label drug for wet age-related macular degeneration that has FDA full approval for the treatment of adult patients with GBM (Fig.1) (2).

Despite examining a wide range of agents to target VEGF/VEGFR in clinical trials, almost all trials have failed to improve overall survival (OS) except Bevasizumab. Although the radiographic responses, progression-free survival (PFS) and brain edema improve in many cases for a period of time, GBM relapse following anti-VEGF/anti-VEGFR treatments has been reported. Hence several problems should be considered to enhance the benefits observed from a cumulative number of studies on VEGF/VEGFR targeting: alternative pathways activated after anti-VEGF/anti-VEGFR treatments should be explored, some biomarkers should be defined to better classify and recognize those patients most benefit from the treatments and an optimum dosing and timing should be defined.

High affinity and low affinity ligands /EGFR

EGFR, also designated as HER1 (human EGFR) or ErbB1 (named after its homology to a viral oncogene called erythroblastic leukemia viral oncogene), is one of the four members of the ErbB family; HER2/neu (ErbB-2), HER3 (ErbB-3), and HER4 (ErbB-4). The receptor activation triggers manifold responses depending on the type of ligands binding to the receptor. More than 40 ligands have been recognized that can be classified into high-affinity ligands, such as EGF, transforming growth factor alpha (TGF-α), and heparin-binding EGF-like growth factor (HB-EGF); and low-affinity ligands, such as amphiregulin (AREG), epiregulin (EREG), and epigen (EPGN). There is evidence showing the alteration of gene expression in the receptor in different types of cancers like GBM in which EGFR amplification induces GBM proliferation, invasion and drug resistance. Also, EGFR alterations are applied as a prognostic marker for GBM. There have been around 20 clinical trials to target EGFR using agents such as Cetuximab, Afatinib, Erlotinib, Gefitinib, Lapatinib, Nimotuzumab, to name a few. Most of the drugs have produced poor results in terms of clinical outcomes, because of EGFR heterogeneity, drug low specificity and low BBB penetration (Table 1). Besides, it has been interestingly proposed that clinical successes achieved applying tyrosine kinase inhibitors (TKIs) against EGFRSs are associated with particular mutations in EGFR rather than the type of tumor as the same non-respondent mutations in GBM do not respond to treatments in lung adenocarcinoma (LUAD) as well. More importantly, it has been demonstrated that the drugs with the same target have clinically varied outcomes. Therefore, this pathway response to treatment is highly specific and any improvements in the field depend on the recognition and classification of mutations in EGFRs as well as precisely identification of target sites for drugs (18).

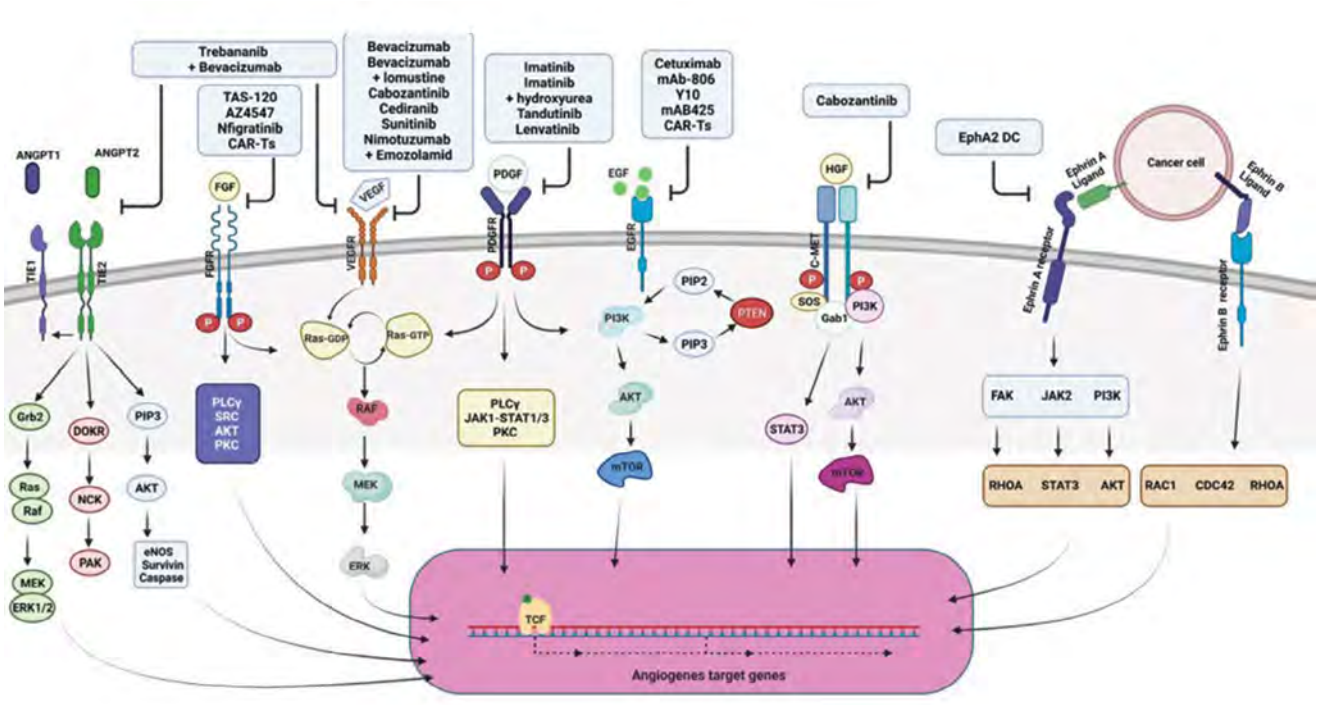

Fig.1: Tyrosine kinase receptor-dependent angiogenesis pathways and their targeting in clinical trials on glioblastoma. Different types of inhibitors (shown in upper blue boxes) targeting RTK-dependent angiogenesis pathways (RTKs are shown on the cell membrane) have been investigated in clinical trials on GBM to modulate angiogenesis. RTK; Tyrosine kinase receptor, ANGPT; Angiopoietin, FGF; Fibroblast growth factor, VEGF; Vascular endothelial growth factor, PDGF; Platelet-derived growth factor, EGF; Epidermal growth factor, HGF; Hepatocyte growth factor, and TCF; Transcription factor.

Table 1: Anti-angiogenesis clinical trials in GBM-targeting receptor tyrosine kinases (RTKs)

Target class	Treatments	Target	Clinical trial result	No. /phase	Trial reference No.
VEGF/VEGFR	Bevacizumab (Avastin)	VEGF-A	rGBM ORR: %:28.2, PFS (months): - PFS6 (%):42.6, OS (months): 8.6	II/ 167	NCT00345163
	Bevacizumab (Avastin), Lomustine	VEGF-A	rGBM Ongoing	III/ 592	NCT01290939
EGF/EGFR	Nimotuzumab (OSAG101) + Temozolamid, + standard treatment	L2 domain of EGFR	Cerebral GBM ORR %: 72.2, PFS (months): 11.9 PFS6(%): -, OS (months): 24.5	II/ 39	NCT03388372
	CAR-T cell	EGFRvIII	MG Recruiting	/I	NCT01454596
	CAR-T cell	EGFRvIII	GBM Recruiting	/I	NCT02209376
	CAR-T cell	IL13Rα2	rMG Completed	6/I	NCT01082926

Table 1: Continued

Target class	Treatments	Target	Clinical trial result	No. /phase	Trial reference No.
FGF/FGFR	AZ4547	FGFR1-3 IGF1 R KDR	rGBM Suspended	I/II 14	NCT02824133
	Infigratinib (BGJ398)	FGFR1-3	rGBM ORR %: 7.7, PFS (months): 1.7 PFS6(%): -, OS (months): 6.7	II/ 26	NCT01975701
	TAS-120	FGFR1-4	Advanced solid tumor like GBM Recruiting patients	386/ I/II	NCT02052778
PDGF/PDGFR	Lenvatinib (E7080)	VEGFR FGFR PDGFR	rGBM ORR %: -, PFS (months): 1.911.9 PFS6(%):8.3, OS (months): 28	II / 32	-
	Imatinib mesylate (Gleevec/ST1571)	PDGFRα PDGFRβ Bcr-Abl c-FMS	rGBM PFS6%: 33	I/II/ 50	-
HGF/c-MET	Cabozantinib	c-Kit MET VEGFR2	nGBM ORR (%): 17. 6, PFS (months): 3.7 PFS6(%): 22.3 OS (months): -	II/ 152	NCT00704288
Ephrins/Eph	α-type-1 polarized DC vaccine loaded with IL-13, receptor-α2, YKL-40, and gp100	EphA2, IL-13 receptor-α2 YKL-40 gp100	MG Proved safety, immunogenicity, and preliminary clinical activity of poly-ICLC-boosted αDC1-based vaccines.	I/II / 41	NCT00766753
Tandutinib		PDGFRβ FMS-like TK3 c-Kit	GBM Terminated due to unmet prespecified goal of SFP	I/II /19,30	

VEGF; Vascular endothelial growth factor, PDGFR; Platelet-derived growth factor, FLT-3 TKI; Fms-like tyrosine kinase 3 tyrosine kinase inhibitor, EGF; Epidermal growth factor, EGFR; Epidermal growth factor receptor, FGFR; Fibroblast growth factor receptor, HER2; Human epidermal growth factor receptor, IGFR1R; Insulin-like growth factor type 1 receptor, KDR; Kinase insert domain receptor, PDGFR; Platelet-derived growth factor, ANG; Angiopoietin, Tie; Tyrosine kinase with immunoglobulin-like and EGF-like domains 1, HGF; Hepatocyte growth factor, c-MET; Tyrosine-protein kinase Met, Eph; Erythropoietin-producing human hepatocellular receptors, DC; Dendritic cell, YKL-40; Chitinase-3-like protein 1, gp100; Glycoprotein 100, EphA2; EPH receptor A2, Bcr-Abl; Breakpoint cluster region – Abelson murine leukemia virus, c-FMS; Feline McDonough sarcoma, FMS-like TK3; FMS-like tyrosine kinase 3, Met; Mesenchymal-epithelial transition factor, GBM; MG; Malignant glioma, Glioblastoma, rGBM; Recurrent GBM, ORR; Overall response rate, PFS; Progression free survival, PFS6; Progression-free survival at 6 months, OS; Overall survival, and mOS; Median survival rate.

FGF/FGFR pathway

FGFs family are secreted mostly from fibroblasts and deposited close to the ECs' basement membrane. There are 23 members in the family, FGF1 through FGF23, which all bind to FGFR1, -4 except FGF11 through FGF-14 that play role in intracellular processes other than FGFs related functions. Accumulating data propose that the interaction of these factors with their corresponding transmembrane tyrosine kinase receptors affect tumor angiogenesis both in early (basal lamin degradation, migration and proliferation) and in late phase (morphogenesis and vessel maturation). For instance, FGF-2/FGFR-2 increases the expression of matrix metalloproteinase 9 (MMP9) and enhances vascular smooth muscle cell (VSMC) migration.

Furthermore, there is a growing number of reports showing the relationship between upregulation of FGFs or FGFRs and the occurrence of different cancers. For example, FGF7 and FGF10 are present in stroma in prostate, FGFR-3 is overexpressed in t (4;14) multiple myeloma, FGF-1, FGF-2 and FGF-5 are overexpressed in pancreatic ductal adenocarcinoma (PDAC), FGF-1 induces chemoresistance and highly expressed FGFR-1 is a hall mark for tumor progression (19, 20). There are some small molecule inhibitors that target FGFR1–3 like PD173074, AZ4547, BGJ398 and JNJ-493 which are not specific for either FGFR subtypes or isoforms. Amongst them, AZ4547, dovitinib, PD173074 and ponatinib effectively reduced pediatric glioma cell growth *in vitro* in comparison to the chemotherapeutic agent Temozolomide. AZ4547and BGJ398 (Table 1) were investigated in a clinical phase I/II and a phase II trial, respectively in patients with recurrent isocitrate dehydrogenase 1 (IDH) wild-type gliomas. The trials are suspended due to some side effects in the patients. Furthermore, the results of a clinical trial on BGJ398 (Table 1) in malignant glioma patients have not yet been published (21). Besides, a phase I/II trial of TAS-120 (Table 1), an irreversible FGFR inhibitor, is registering those suffering from advanced solid tumors, including brain tumors such as GBM (Fig.1) (22).

Among all FGFs/FGFRRs, FGF2/FGFR axis seems the most important axis for target therapy in GBM for the determinative role of FGF2 in glioma vascularization, GSC self-renewal and tumor growth. Although targeting tyrosine kinase domain of FGFRs by available inhibitors can block a prominent step in signal transduction, their lack of specificity provokes off-target effects and/or other complications. Therefore, it is critical to design more specific FGFRs inhibitors for highly sensitive and more precise target therapy.

PDGF/PDGFR pathway

Platelet-derived growth factors (PDGFs) are secreted by a variety of cells like tumor cells, ECs, macrophages, and transformed fibroblasts. The growth factors consist of PDGF-A, -D peptides which are in interaction with their receptors, PDGFR-a and PDGFR-b, evoke signalings comparable with those in VEGF/VEGFR signaling especially in recruiting pericytes to neo-vessels and secretion of a broad range of proangiogenic cytokines (23). Therefore, PDGF/PDGFR pathway has been a promising target in cancer therapy and the results of numerous investigations were so encouraging that several agents could get approval as anti-PDGF/PDGFR drugs in several solid tumors, such as Sorafenib (Nexavar) for metastatic RCC and unresectable HCC, Sunitinib (Sutent) for gastrointestinal stromal tumor (GIST) and unresectable pancreatic neuroendocrine tumors, Pazopanib (Votrient) for metastatic RCC and advanced soft tissue sarcoma, and Axitinib (Inlyta) for metastatic RCC (24).

Although improvements in other solid tumors were impressive, anti-angiogenesis therapy has still remained ineffective in GBM. Preclinical trials have demonstrated that imatinib (Table 1), a PDGF receptor kinase inhibitor augments the radiotoxicity; however, the effect was minor in Phase II clinical trials in GBM patients (25). Moreover, in Phase II and Phase III of a clinical trial in which a combination of imatinib and hydroxyurea (Table 1) was investigated, no beneficial effect for recurrent GBM (rGBM) treatment was observed (Fig.1) (26).

There is solid evidence that high expression of PDGF and PDGFR can be detected in most GBMs. Also, induction of PDGF and PDGFR overexpression, mostly PDGFB, induces GBM in laboratory animals. These data suggest that there is definitely a positive correlation between GBM and PDGF/PDGFR mutation and the lack of exact PDGF/PDGFR mutations profile is the key factor in clinical trials failure. Also, PDGFR profiling could hopefully improve clinical indices through early detection of the responsive subgroups of patients.

ANG/TIE pathway

ANGs are a family of growth factors (ANG-1, -4) secreted by endothelial and parenchymal cells that can bind to tyrosine kinase receptors (TIE-1 and TIE-2) on ECs. The abnormal activity of ANG-1, -2/TIE2 signaling mediates EC sprouting, pericytes recruitment, vascular remodeling and tumor plasticity. Although targeting each of these two ligands or both has improved clinical pre-targeted outcome, concomitant hindrance of both VEGF (using bevacizumab) and ANG2 (using Trebananib) (Table 1) results in both vasculature normalization and the survival benefit in comparison to inhibition of either pathway alone in GBM (Fig.1) (2).

A growing number of studies are revealing that ANG2 inhibition not only improve vascular normalization but also induces anti-tumor immunity which suggests ANG2 targeting as a favorable approach in combination therapy of treatment- resistant tumors.

HGF/c-MET pathway

The cellular mesenchymal-epithelial transition protein (c-MET), a transmembrane tyrosine kinase family, is activated by binding to the pleiotropic HGF and triggers proliferation, survival and motility of both normal and tumor-associated cells and ECs. It has been evidenced that

MET expression is elevated in tumor cells, blood vessels, and peri-necrotic areas of glioma sample (27). Moreover, HGF secretion from vasculature and neurons accelerates glioma invasion and proliferation in MET-positive cells (28). Due to the crucial role of HGF/c-MET pathway in GBM development and possibly in anti-VEGF therapy resistance induction, its inhibition has been considerably studied in numerous preclinical and clinical studies (29). Some of the monoclonal antibodies used for this purpose in clinical trials are as follow: Rilotumumab (AMG102), a neutralizing antibody against HGF (30) Onartuzumab, a humanized monovalent monoclonal anti-MET antibody (31), Crizotinib, an available ATP competitive selective inhibitor for MET inhibition (32) and Volitinib, a highly selective small molecule and ATP competitive MET kinase inhibitor (33). None of these mAbs showed positive clinical outcomes for their toxicity as Rilotumumab and for GBM stem cells heterogenicity as Crizotinib. Besides, many of the clinical studies were terminated without any published data such as those on Volitinib and small molecule inhibitor, SGX523. Amongst these mAbs, only cabozantinib (Table 1) treatment, a MET and VEGFR2 inhibitor, showed only modest clinical benefits in patients with GBM (Fig.1) (34).

Notwithstanding the fact that a wide range of agents from small-molecule inhibitors to mAbs have been long investigated on the pathway, there has been no phase III trial so far. A fact that reinforces an urgent need for a comprehensive review of the past trials to build up a solid conclusion on HGF/c-MET mutations and their responsiveness to therapy to more effectively select the patients who most benefit from the targeted therapies.

Ephrins/Eph pathway

Erythropoietin-producing human hepatocellular receptors (Ephs) are grouped into two subgroups EphAs (EphA1-8 and EphA10 in human) and EphBs (EphB1-4 and EphB6 in human). The receptor interacts with Eph receptor-interacting proteins (Ephrins)and subsequently exerts its effects on angiogenesis and stem cell differentiation. Recent studies in GBM have proven that these proteins play a role in both tumorigenesis and tumor progression in adult brain tumors, which proposes them as valuable therapeutic targets (35). Encouraging results from targeting Eph in pre-clinical GBM models have led to several vaccine trials targeting Ephrins. Amongst them EphA2 vaccine (Table 1) constructed by loading four of the glioma-associated antigen epitopes (EphA2, interleukin (IL)-13 receptor-α2, YKL-40, and gp100) on α-type 1 polarized dendritic cells has been proven to be safe in men with GBM (Fig.1) (36).

Since Ephs exert both tumorigenesis and anti-tumor effect depending on the tumor stage and the type of the receptor, it is crucial to specify the drugs for specific tumor stage and tumor subgroup. Besides, it has been shown that the expression pattern of Ephrins/Eph is different among patients which strongly suggests personalized therapy for a particular subgroup of patients with specific gene expression pattern.

RTK-independent angiogenesis signaling

Those signalings not classified as RTKs are discussed under this category here such as serin/tyrosine kinase TGF-β/TβRII and cell adhesion molecules such as integrins.

TGF-β/TβRII

TGF superfamily, secreted from immune cells, stromal cells and tumor cells, comprises more than 30 growth factors including TGF-βs (TGF-β1, -β2, and -β3), growth and differentiation factors (GDFs), activin, bone morphogenetic proteins (BMPs), nodal, and anti-mullerian hormone (AMH). Among these factors, TGF-βs are correlated with angiogenesis and modulate cell proliferation, differentiation, and tissue homeostasis following binding to their receptors, TGF-βRII and its disturbed function has been reported in fibrosis and tumorigenesis. It has been shown that TGF-βs, especially TGF-β1and -β2, have a crucial role in angiogenesis mediating up-regulation and induction of different angiogenic factors including VEGF, FGF and PAI-1 in GBM (37). Hence, TGF- β has been targeted in numerous studies in preclinical and clinical studies in a varied range of diseases and cancers such as sclerosis, pancreatic cancer (PAC), HCC, RCC and GBM.

Although both preclinical and clinical trials strongly propose TGF- β signaling, particularly TGF-β/TβRII, targeting as an effective treatment for metastatic tumors, serious adverse effects have been repetitively reported after long-term hindrance of the signaling in several animal studies. For example, hemorrhage and inflammation in ulcers of heart valves have been observed following TβRI blockade. Also, some cases of chronic inflammation resulting in precancerous conditions have been detected after TGF-β signaling hindrance. Therefore, targeting of the pathway should be applied with caution considering the pleiotropic function of the pathway both in normal and pathological condition.

There are currently several clinical trials on glioma to inhibit TGF-β signaling via different approaches:

Antisense oligonucleotide (AON): in a Phase IIb and III clinical trials the efficiency of an AON called AP12009 (Table 2) to block TGF-β2 mRNA translation has been studied (38).

Soluble receptors or their ectodomain constructs to sequester the ligand: in a Phase I trial i LY2157299 (Table 2), a Kinase inhibitor targeted for TGFβR1 (ALK-5), is going to be examined on volunteers (39).

Antibodies: in a Phase I/II trial GC1008 (Table 2), an antibody against TGF-β, has been tested to suppress TGF-β receptor kinase activity (Fig.2) (40).

There is solid evidence that the pathway can be a promising target in spite of documented adverse side effects and many pharmaceutical companies that are still interested in producing drugs to target TGF-β/TβRII. To reduce the intricacy of the results and guarantee the safety of the drugs, designing agents that can specifically target either particular subgroups of the receptors or the molecules in downstream of TGF-β signaling is critical (41).

Table 2: Anti-angiogenesis clinical trials in GBM – targeting RTK-independent angiogenesis pathways

Target class	Treatments	Target	Clinical trial result	No. /phase	Trial reference No.
TGFβ/TGF- βR	Galunisertib (LY2157299)	TGFβR1	MG Recruiting	65/ I, I/II	NCT01682187
	Fresolimumab (GC1008)	TGF-β	Glioma No significant clinical benefits	12/ II	-
	Trabedersen (AP12009)		Refractory anaplastic astrocytoma or secondary glioblastoma Terminated for recruitment issues The survival rate with 10 μM OS:(months):35.7 for AP12009; OS:(months): (23.1) for AP12009 + chemotherapy	27/ III	NCT00761280
IFN/IFNR	Cationic liposome-mediated IFN-β gene transfer	IFN-β	High grade glioma 50% reduction in disease severity and fewer CD34− immunoreactive vessels	5/ I	-
	Conventional radiation therapy followed by recombinant human IFN-β	IFN-β	GBM survival benefit in patients who remained stable after radiation therapy	109/ II	-
	Nimustine (ACNU) +Vincristine, +Carboplatin, + IFN-β + Radiotherapy	IFN-β	rGlioma Improved survival in patients with GBM	97/ II	11A0232177
IFN/IFNR	Peginterferon α-2b (PEG-Intron)	IFN α-2b	rGBM Confirmed safety and mild efficacy	7/ II	NCT00047879
	TMZ, +IFN α-2b and/or TMZ, +Long-acting IFN α-2b(PEG)		rGBM Confirmed safety and mild efficacy PFS6: 31% for patients on IFN PFS6: 38% for patients on PEG	34 on IFN and 29 on PEG/ II	-

Table 2: Continued

Target class	Treatments	Target	Clinical trial result	No. /phase	Trial reference No.
	TMZ and/or TMZ + IFN-α		High grade glioma Recruiting	-/ III	NCT01765088
Notch/NotchR	R4733 (RO4929097)		rGBM Terminated, no results available	/I, II	NCT01189240 NCT01131234 NCT01269411 NCT01122901
TNF/TNFR	VB-111 +Bevacizumab	VB-111	rGBM ORR %: -, PFS (months): - PFS6(%): -, mOS:(months): 6.8	256/III	NCT02511405

TGF-β; Transforming growth factor beta, VB-111; Adenoviral vector expressing PPE & Fas-TNFR1 chimera, TNFR; Tumor necrosis factor receptor, IFNR; Interferon receptor, IFNR; Interferon receptor, Integrin L; Integrin ligand, TMZ; Temozolomide, MG; Malignant Glioma, rGlioma; Recurrent Glioma, PFS; Progression free survival, ORR; Overall response rate, PFS; Progression free survival, PFS6; Progression-free survival at 6 months, OS; Overall survival, and PEG; Polyethylene glycol.

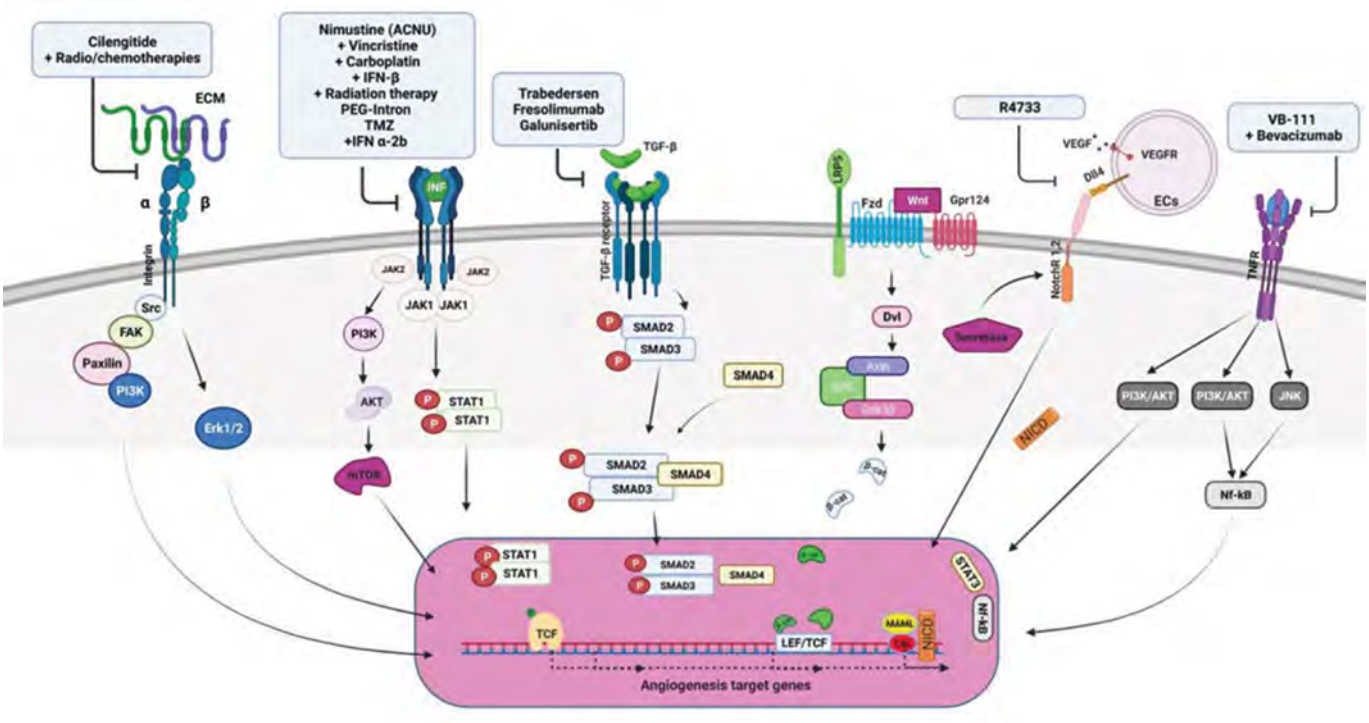

Fig.2: RTK-independent angiogenesis pathways alongside their clinical targeting in glioblastoma. Different clinical inhibitors (upper blue boxes) targeting signalings involved in GBM angiogenesis through RTK-independent angiogenesis pathways (growth factor receptors: TGF-β/TβR2, TNFα/TNFR1 and TNFR2, Interferons/IFNsR, Wnt/Fzd receptor) and cell adhesion molecules **(**Notch and Integrins) are shown here. ECM; Extracellular matrix, INF; Interferon, TGF; Transforming growth factor, LRP5; Low-density lipoprotein receptor-related protein 5, FZD; Frizzled, Gpr124; G-protein coupled receptor 124, Dll4; Delta-like 4, TNF; Tumor necrosis factor, ECs; Endothelial cells, MAML; Mastermind-like proteins, TCF; Transcription factor, NICD; Notch intracellular domain, and Dvl; Dishevelled limits.

TNFα/TNFR1 and TNFR2

Tumor necrosis factor alpha (TNFα, TNF, cachectin), an inflammatory cytokine, belongs to TNF superfamily and is mostly secreted by immune system cells. It is indicated that the cytokine possesses a pro-angiogenic effect which may be either directly by induction of ECs differentiation or indirectly through triggering the secretion of other angiogenic factors. Also, it is shown that expression of TNFR2 is elevated in six cancer types including GBM.

Although TNF blockers have been successfully administered for autoimmune diseases and are among the best seller biologics, they have failed to meet the pre-targeted clinical expectations as anti-tumor drugs for their severe side effects. Different experiments have suggested α as a potential target in glioma, however, it couldn't be clinically translated due to its high systemic toxicity at therapeutic doses (Fig.2) (42). To achieve more satisfactory results and reduce off-target effects localized therapies such as isolated organ perfusion in soft tissue sarcoma and melanoma has been developed. Yet, the problem remains unsolved for many cancers, particularly for highly metastatic ones (43).

Interferon-α/β/interferon-α/β receptor (IFNAR) and interferon-gamma/interferon-gamma receptor (IFNGR)

Interferons (IFN), initially discovered as antiviral responsiveness mediators, are currently recognized as multifunctional proteins involved in inflammation, proliferation, and differentiation and fall into 3 categories; IFN type I (IFN-α, IFN-β, IFN-ε, IFN-κ and IFN-ω), IFN type II (IFN-γ in humans) and IFN type III. They trigger a cascade of responses following binding to their glycoprotein receptors. It has been demonstrated that IFN-α and -β possess anti-angiogenesisproperties mediated by angiogenic factors inhibition (44). 50% reduction in disease severity and less $CD34^{-}$immunoreactive vessels have been shown in 2 patients in a clinical trial phase II in which *IFN-β* gene therapy (Table 2) was applied for 5 patients with high-grade glioma (45). Also, in a Phase II clinical trial, recombinant human *IFN-β* (Table 2) was administered after radiation therapy and the results showed little survival benefit and high tolerance in GBM patients (46). Furthermore, a Phase II clinical trial proved to be safe that showed mild survival benefit of applying a combination of nimustine (ACNU), vincristine, carboplatin, and IFN-β (Table 2) in addition to radiotherapy in GBM patients (Fig.2) (47).

The efficacy of peginterferon α-2b (Table 2), an anti-angiogenesisfactor, alone and in combination with thalidomide, an anti-angiogenesisdrug, in patients with glioma is being assessed in a phase II clinical trial (48). In another phase II trial, patients with GBM were treated with standard therapy using TMZ (Table 2), in combination with either short-acting IFNα-2b (non-pegylated) or long-acting IFNα-2b (pegylated). Safety and mild efficacy were observed in both regimens (49). In a phase III trial on cytokine therapy in patients with newly diagnosed GBM, TMZ was utilized with or without IFN-α (Table 2) (50) and results published. Some other trials are under investigation and attempt to find the best combination therapies (Fig.2) (51).

Despite encouraging results in preclinical trials on gliomas, clinical outcomes are puzzling: the results from IFN-*γ* targeting were dissatisfying, IFN-*β* targeting produced perplexing results and IFN-*β* targeting is still under investigation both alone and in combination with other approaches (52).

Wnt/Frizzled (Fzd) family receptor

Wnt signaling as a complex signaling pathway is implicated in proliferation, differentiation and migration of cells particularly stem cells in embryonic and adult tissues. There are three signaling pathways of Wnt signaling: canonical Wnt pathway, noncanonical planar cell polarity pathway, and noncanonical Wnt/calcium pathway which regulate gene transcription, cell cytoskeleton and cell inner calcium, respectively. There are convincing reports on the positive correlation between altered expressions of different members of Wnt, GBM genesis and progression which are proposed as a factor to discriminate between normal and malignant cells in the human brain. Abnormalities in canonical Wnt signaling are associated with GBM stem cells (GSCs) formation, chemo- and radiotherapy resistance, and poor prognosis while non-canonical Wnt dysfunction is more related to the invasiveness of GBM. Therefore, a variety of agents targeting Wnt have been examined such as non-steroidal anti-inflammatory drugs (NSAIDs) and Resveratrol which may be opening windows to clinical trials (Fig.2) (53).

Notch signaling pathway

Notch signaling is activated when cell interaction is mediated by membrane bound Notch receptors (Notch-1, -4) and related membrane-bound ligands (Jagged-1, Jagged-2; Delta-like 1, 3, and 4). All the receptors and ligands are expressed on the cell surface of ECs membrane except Notch-3 and Dll-3 and mediate tip-to-tip contact between blood vessel sprouts and endothelial cells (54). It has been demonstrated that Notch activity is correlated with hypoxia and some cancer-related molecular pathways like ERK/MAPK and PI3K/AKT/mTOR which amplify malignancy in GBM and its targeting reduces malignancy characteristics. For instance, high Notch-1 expressing GBM surgical samples affect stem cell and angiogenesis pathways. Notch inhibition using treatment with DAPT (a chemical compound and γ-secretase inhibitor) showed reduction in Nestin and elaboration in Ki-67 (a proliferation marker). In another study, it has been shown that a combination of radiation therapy and Notch inhibition hinders self-renewal and propagation in tumor explants. There have been several clinical trials using RO4929097 (a g-secretase inhibitor) (Table 2) to

unravel the correlation between Notch pathway and GBM patients' survival. All the trials were discounted due to the drug suppliers' decision not manufacturing the drug anymore (Fig.2) (55).

The importance of Notch signaling not only in the induction of tumor but also in the development of therapy resistance highlights exploring the best combination therapy to hinder tumor progression as well as tumor recurrence after applying standard cytotoxic therapies.

Integrins

Integrins (ITG) are transmembrane proteins comprised of two non-covalently associated α (18) and β (with 8) subunits that form 24 heterodimers responsible for cross-talk between a cell and another cell or ECM. As Intrgrin's expression pattern is different in normal and GBM tissues, they may serve both as prognosis biomarkers (some of them like αvβ5 are assumed to be expressed specifically on GBM cells) and as radio/chemotherapy specificity (αvβ3 and α3β1 high expression were associated with poor prognosis in patients with GBM). Also, it has been evidenced that αvβ3, αvβ5 and αvβ8 are related to angiogenesis in GBM and their targeting is vastly studied in anti-angiogenesis therapy: αvβ3/αvβ5 were targeted by Cilengitide (Table 2) in phase I/II clinical trials in GBM, in combination with radio/chemotherapies, both in recurrent and in newly diagnosed GBM. The results showed clinical benefit on progression free survival (PFS) and good tolerance in overall survival (OS) (Fig.2).

Integrins are definitely promising molecules in GBM therapy either as targets or as diagnostic tools. Future investigation should discover a correlation between different subtypes of GBM and expression pattern of integrins for both better prediction of radio/chemo-resistant patients and more personalized targeting of the tumors (56).

All in all, the initial achievements from these pre-clinical and clinical trials encourage more discoveries in laboratories to pave the way from bench to bedside where a combination of approaches could more effectively curb tumor growth. Proper dosing and targeting can meaningfully affect the outcomes achieved by selecting a perfectly designed vehicle for the desired drug to guarantee both the drug and the recipient's safety. In the following section the most prominent targeting strategies in GBM therapy is discussed.

Targeting strategies

Monoclonal antibodies (mAbs)

Monoclonal antibodies can specifically target a mutated ligand or its receptors. Bevacizumab (Table 2), an anti-VEGF-A, is the first FDA-approved anti-angiogenesis monoclonal antibody as the first-line treatment for recurrent GBM patients (2). While, the outcome was favorable in both phase I and II; the side effects were overwhelming in phase III. Yet there are hopes for Bevacizumab to be used as an adjuvant in addition to traditional therapy. Although some anti-EGFR antibodies such as Cetuximab, mAb-806 and Y10 (Table 2) have shown promising preclinical results, that the clinical findings did not meet the expectations (Fig.1).

There have been numerous clinical trials examining monoclonal antibodies on different tumors like GBM, yet the most important concern is their side effects which stem from on/off-target toxicities, leading to an autoimmune reaction in both normal and tumor tissues. Hence, clinicians should take the assessment of risk-benefit ratio between anti-tumor efficacy and related side effects into account when determining optimal therapies (Fig.2) (57).

MicroRNAs (miRNAs)

A network of different miRNAs is involved in GBM angiogenesis; while some are angiogenesis promotors like miR-296, miR-21, and miR-210-3p, others are angiogenesis inhibitors like miR-15b and miR-299. Some miRNAs that promote glioma invasion are vastly studied: miR-10b, miR-21, miR-221/222 which are upregulated and miR-124, miR-34a, miR-181, miR-451, miR-146, miR-218, miR-326 which are downregulated in GBM.

miR-10b inactivation using antagomiR in a mouse GBM model resulted in a dramatic decrease in tumor growth. Several miRNA-targeted therapeutics have reached clinical trials including a mimic of the tumor suppressor miRNAs: miR-34 in phase I clinical trials for cancer and anti-miR122 in phase II trials for hepatitis. Also, there are currently two miRNA-based Phase I trials on cancer, there are no trials on GBM as of yet (58).

Aptamers

Aptamers, high affinity single-stranded DNA/RNA molecules, have been proved to be safe and effective as both diagnostic and therapeutic tools. They efficiently discriminate not only between normal and tumor tissues but also between different tumor types.

There is an anti-VEGF aptamer called pegaptanib approved by FDA for the treatment of wet age-related macular degeneration. Other aptamers have been investigated in clinical trials for a range of diseases including coronary artery disease, renal cell carcinoma, type 2 diabetes mellitus and albuminuria, chronic lymphocytic leukemia, hemophilia, and anemia from chronic inflammation. Although there is no clinical trial on GBM, a magnetic nanocrystal-conjugated VEGF receptor 2-specific aptamer was successfully evaluated using MRI in GBM-bearing mice for GBM diagnosis (59).

Gene therapy

Gene delivery using either viral or non-viral carriers in combination with current standard-of-care treatments delivers suicide genes, immunomodulatory genes, tumor-

suppressor genes and oncolytic viruses to the target region. A number of gene therapy-based anti-angiogenesis clinical trials are now active on GBM: in a clinical trial HSV-1 expressing IL-12 (M032) (NCT02062827) is being investigated and in another trial VB-111 (Table 2) and bevacizumab are being used simultaneously. Although limited therapeutic benefits have been reported to date, a number of clinical trials verified gene therapy using various methods as a safe method (60).

Small molecules

There has been a growing interest in using anti-angiogenesis small molecules targeting various components of angiogenic pathways to overcome the BBB obstacles. For instance, AZD2171 (Cediranib) (Table 1), a VEGFR inhibitor, increased therapy response rate by 30% in patients with recurrent GBM in a non-randomized phase II trial (61). In a phase II study, tivozanib and pazopanib exerted a slight anti-tumour activity with no prolonged PFS in patients with recurrent GBM (62). Imatinib (Glivec-Novartis), one of the most widely used anti-PDGF receptors and its downstream pathway, has been well tolerated with almost no beneficial effect on high-grade glioma in adults (63). Tandutinib a multikinase inhibitor has been investigated in phase II studies in combination with bevacizumab. Although the approach was effective, it was more toxic than bevacizumab monotherapy (64). Also, Sunitinib (Table 2) proved to be feasible and safe with promising antitumor activity in phase I/II in patients with GBM has entered the phase II/III (65). The majority of clinical trials on small molecules for GBM therapy have fallen lack of clinical benefits in brain (i.e., gefitinib and erlotinib) because tumor cells develop new mutations after exposure to drugs and become drug resistant. Additionally, low efficacy of small molecules for heterogeneity of GBM cell population leads to target therapy inefficiency. Nevertheless, there still are hopes for development of combination therapy using these molecules (66).

Angiostatin and endostatin

Angiogenesis is orchestrated by a fine-tuned balance between angiogenesis promotors and inhibitors in adult normal tissues. Angiostatin and endostatin are endogenous angiogenesis inhibitors whose overexpression is of particular interest in many diseases. Viral gene transfer of these two proteins is currently being investigated in phase I and II clinical trials on advanced head/neck carcinoma and macular degeneration. Even though it proved to be beneficial in GBM animal models, no clinical trials have been done yet (67).

Cell therapy using chimeric antigen receptor T-cells (CAR-T cells)

One particularly encouraging area in cancer therapy is chimeric antigen receptors (CARs) in which T-cells are genetically engineered to produce the desired T-cell receptor to target a specific protein. Since the approach has been successful in treating some of the hematological malignancies, they are currently under investigation for a range of solid tumors including GBM. Among several CAR-Ts against six GBM-associated antigens, four are currently being tested in clinical trials to target EGFRvIII, IL13Rα2, HER2, and EphA2 (Table 1). Although the outcomes were not as satisfactory as the results obtained from treatment of acute lymphoblastic leukemia (ALL) and chronic lymphoblastic leukemia (CLL) therapy, the strategy is being improved to overcome the intrinsic obstacles of GBM immune therapy such as GBM ability to evade immune surveillance, to suppress the local immune response and to induce T-cell apoptosis as well as GBM's antigens heterogeneity (68).

Resistance to anti-angiogenesis treatment

Although mono anti-angiogenesis therapy raised enthusiasm at first, no or unsustainable beneficial effects set the scene for combination therapy to increase therapy effectiveness. It is proposed that adaptive and intrinsic resistance mediate the unresponsiveness in anti-angiogenesis therapy. Adaptive resistance include: activation of alternative angiogenesis pathways to restore angiogenesis in response to shortage of blood supply and oxygen, shifts in tumor cell metabolism, invasion of tumor cells, activation of autophagy, trans-differentiation of GBM cells to ECs and increase in glioblastoma stem cell (GSC) self-renewal. In intrinsic resistance, patients or tumors are naturally insensitive to that particular anti-angiogenesis therapy as tumor cells in pancreatic ductal adenocarcinoma grow in a hypoxic environment with no or little vascularity (69). Despite the mechanisms mentioned above as the inducers of the resistance, further investigation is still required to more effectively curb angiogenesis.

Conclusion

Longitudinal studies on anti-angiogenesis therapy have led to successful management of some abnormal conditions such as inflammatory and autoimmune diseases. However; the effect of the strategy seems incongruous when it comes to GBM therapy; while some of the patients show normalized vasculature in a particular time frame following anti-angiogenesis therapy, others present no beneficial and/or severe adverse effects. This partly reflects the fact that highly progressive tumor like GBM may survive in the absence of blood circulation. Besides, conceptually, anti-angiogenesis treatment could totally block angiogenesis that the invasive single tumor cells still can spread through the brain.

Despite the failure of anti-angiogenesis therapy to improve clinical courses in patients with GBM in the majority of clinical trials, the concept is strengthening with the continuing discovery of angiogenic factors. These findings can be applied in either multi-target therapy or combination therapy to more rigorously hinder tumor progression as multi-targeted RTKI and decoy receptors that are recently of particular interest in anti-angiogenesis therapy. Furthermore, in the absence of a profile of biomarkers associated with GBM, any improvement

in this field of therapy is impossible. Therefore, a very essential step to move forward in angiogenesis targeting is to define GBM-related biomarkers to fulfil these requirements: to predict the therapy-responsive subpopulation of patients, determine the proper molecular target in individual patient and provide a tracking way for following up with the efficiency of therapy. These biomarkers can be the expression pattern of GBM-related genes and/or circulating biomarkers. Last but not the least, issues regarding possible toxicity of the treatments, drug dosing and timing, and the drug delivery approaches should be addressed.

Acknowledgments

We are grateful to Dr. Mohammad Vasei for all his help and support and Mr. Behrad Rastgar for writing and editing assistance. This study was supported by a grant from Tehran University of Medical Sciences (project number: 9121607002). The authors declare no conflict of interest.

Authors' Contributions

F.D.; Participated in explicit literature search and classification as well as summarizing papers and writing the manuscript. Sh.A.; Contributed to writing the manuscript and preparation of the figures. Z.B.; Contributed in manuscript writing. S.E.-B., J.V., M.S.; Contributed in manuscript revision. J.A.; Supervised the study. All authors read and approved the final manuscript.

References

1. Carmeliet P, Jain RK. Principles and mechanisms of vessel normalization for cancer and other angiogenic diseases. Nat Rev Drug Discov. 2011; 10(6): 417-427.
2. Fukumura D, Kloepper J, Amoozgar Z, Duda DG, Jain RK. Enhancing cancer immunotherapy using antiangiogenics: opportunities and challenges. Nat Rev Clin Oncol. 2018; 15(5): 325-340.
3. Hajighasemlou S, Nikbakht M, Pakzad S, Muhammadnejad S, Gharibzadeh S, Mirmoghtadaei M, et al. Sorafenib and mesenchymal stem cell therapy: a promising approach for treatment of HCC. Evid Based Complement Alternat Med. 2020: 9602728.
4. Rink C, Khanna S. Significance of brain tissue oxygenation and the arachidonic acid cascade in stroke. Antioxid Redox Signal. 2011; 14(10): 1889-1903.
5. Feeney Jr JF, Watterson RL. The development of the vascular pattern within the walls of the central nervous system of the chick embryo. J Morphol. 1946; 78(2): 231-303.
6. Lok J, Gupta P, Guo S, Kim WJ, Whalen MJ, van Leyen K, et al. Cell-cell signaling in the neurovascular unit. Neurochem Res. 2007; 32(12): 2032-2045.
7. Hogan KA, Ambler CA, Chapman DL, Bautch VL. The neural tube patterns vessels developmentally using the VEGF signaling pathway. Development. 2004; 131(7): 1503-1513.
8. Bautch VL, James JM. Neurovascular development: the beginning of a beautiful friendship. Cell Adh Migr. 2009; 3(2): 199-204.
9. Bairey D, Blickstein D, Shaklai M. Tumor angiogenesis--prognostic and therapeutic implications. Harefuah. 1997; 132(2): 117-120.
10. Bergers G, Benjamin LE. Tumorigenesis and the angiogenic switch. Nat Rev Cancer. 2003; 3(6): 401-410.
11. Wu JB, Tang YL, Liang XH. Targeting VEGF pathway to normalize the vasculature: an emerging insight in cancer therapy. Onco Targets Ther. 2018; 11: 6901-6909.
12. Kleihues P, Louis DN, Scheithauer BW, Rorke LB, Reifenberger G, Burger PC, et al. The WHO classification of tumors of the nervous system. J Neuropathol Exp Neurol. 2002; 61(3): 215-225.
13. Jain RK, di Tomaso E, Duda DG, Loeffler JS, Sorensen AG, Batchelor TT. Angiogenesis in brain tumours. Nat Rev Neurosci. 2007; 8(8): 610-622.
14. Winkler F, Kozin SV, Tong RT, Chae SS, Booth MF, Garkavtsev I, et al. Kinetics of vascular normalization by VEGFR2 blockade governs brain tumor response to radiation: role of oxygenation, angiopoietin-1, and matrix metalloproteinases. Cancer Cell. 2004; 6(6): 553-563.
15. Yang J, Yan J, Liu B. Targeting VEGF/VEGFR to modulate antitumor immunity. Front Immunol. 2018; 9: 978.
16. Bayat N, Izadpanah R, Ebrahimi-Barough S, Norouzi Javidan A, Ai A, Mokhtari Ardakan MM, et al. The anti-angiogenic effect of atorvastatin in glioblastoma spheroids tumor cultured in fibrin gel: in 3D in vitro model. Asian Pac J Cancer Prev. 2018; 19(9): 2553-2560.
17. Ai J, Ebrahimi S, Ai A, Karimi R, Bahrami N. Effect of deforolimus and VEGF on angiogenesis in endometrial stromal cells following three-dimensional culture. Stem Cell Discov. 2013; 3(1): 7-12.
18. Oprita A, Baloi SC, Staicu GA, Alexandru O, Tache DE, Danoiu S, et al. Updated insights on EGFR signaling pathways in glioma. Int J Mol Sci. 2021; 22(2).
19. Korc M, Friesel RE. The role of fibroblast growth factors in tumor growth. Curr Cancer Drug Targets. 2009; 9(5): 639-651.
20. Khalid EB, Ayman EE, Rahman H, Abdelkarim G, Najda A. Natural products against cancer angiogenesis. Tumour Biol. 2016; 37(11): 14513-14536.
21. Dieci MV, Arnedos M, Andre F, Soria JC. Fibroblast growth factor receptor inhibitors as a cancer treatment: from a biologic rationale to medical perspectives. Cancer Discov. 2013; 3(3): 264-279.
22. Jimenez-Pascual A, Siebzehnrubl FA. Fibroblast growth factor receptor functions in glioblastoma. Cells. 2019; 8(7): 715.
23. Zhao Y, Adjei AA. Targeting angiogenesis in cancer therapy: moving beyond vascular endothelial growth factor. Oncologist. 2015; 20(6): 660-673.
24. Manzat Saplacan RM, Balacescu L, Gherman C, Chira RI, Craiu A, Mircea PA, et al. The role of PDGFs and PDGFRs in colorectal cancer. Mediators Inflamm. 2017; 2017: 4708076.
25. Holdhoff M, Kreuzer KA, Appelt C, Scholz R, Na IK, Hildebrandt B, et al. Imatinib mesylate radiosensitizes human glioblastoma cells through inhibition of platelet-derived growth factor receptor. Blood Cells Mol Dis. 2005; 34: 181-185.
26. Dresemann G, Weller M, Rosenthal MA, Wedding U, Wagner W, Engel E, et al. Imatinib in combination with hydroxyurea versus hydroxyurea alone as oral therapy in patients with progressive pretreated glioblastoma resistant to standard dose temozolomide. J Neurooncol. 2010; 96: 393-402.
27. Al-Abd AM, Alamoudi AJ, Abdel-Naim AB, Neamatallah TA, Ashour OM. Anti-angiogenic agents for the treatment of solid tumors: Potential pathways, therapy and current strategies - a review. J Adv Res. 2017; 8(6): 591-605.
28. Kunkel P, Muller S, Schirmacher P, Stavrou D, Fillbrandt R, Westphal M, et al. Expression and localization of scatter factor/hepatocyte growth factor in human astrocytomas. Neuro Oncol. 2001; 3(2): 82-88.
29. Cheng F, Guo D. MET in glioma: signaling pathways and targeted therapies. J Exp Clin Cancer Res. 2019; 38(1): 270.
30. Affronti ML, Jackman JG, McSherry F, Herndon JE 2nd, Massey EC Jr, Lipp E, et al. Phase II study to evaluate the efficacy and safety of rilotumumab and bevacizumab in subjects with recurrent malignant glioma. Oncologist. 2018; 23(8): 889-e898.
31. Cloughesy T, Finocchiaro G, Belda-Iniesta C, Recht L, Brandes AA, Pineda E, et al. Randomized, double-blind, placebo-controlled, multicenter phase II study of onartuzumab plus bevacizumab versus placebo plus bevacizumab in patients with recurrent glioblastoma: efficacy, safety, and hepatocyte growth factor and O(6)-methylguanine-DNA methyltransferase biomarker analyses. J Clin Oncol. 2017; 35(3): 343-351.
32. Junca A, Villalva C, Tachon G, Rivet P, Cortes U, Guilloteau K, et al. Crizotinib targets in glioblastoma stem cells. Cancer Med. 2017; 6(11): 2625-2634.
33. Jia H, Dai G, Weng J, Zhang Z, Wang Q, Zhou F, et al. Discovery of (S)-1-(1-(Imidazo[1,2-a]pyridin-6-yl)ethyl)-6-(1-methyl-1H-pyrazol-4-yl)-1H-[1,2,3]triazolo[4,5-b]pyrazine (volitinib) as a highly potent and selective mesenchymal-epithelial transition factor (c-Met) inhibitor in clinical development for treatment of cancer. J Med Chem. 2014; 57(18): 7577-7589.
34. Cloughesy TF, Drappatz J, de Groot J, Prados MD, Reardon DA, Schiff D, et al. Phase II study of cabozantinib in patients with progressive glioblastoma: subset analysis of patients with prior antian-

giogenic therapy. Neuro Oncol. 2018; 20(2): 259-267.
35. Genander M, Frisen J. Ephrins and Eph receptors in stem cells and cancer. Curr Opin Cell Biol. 2010; 22(5): 611-616.
36. Okada H, Kalinski P, Ueda R, Hoji A, Kohanbash G, Donegan TE, et al. Induction of CD8+ T-cell responses against novel glioma-associated antigen peptides and clinical activity by vaccinations with {alpha}-type 1 polarized dendritic cells and polyinosinic-polycytidylic acid stabilized by lysine and carboxymethylcellulose in patients with recurrent malignant glioma. J Clin Oncol. 2011; 29(3): 330-336.
37. Han J, Alvarez-Breckenridge CA, Wang QE, Yu J. TGF-beta signaling and its targeting for glioma treatment. Am J Cancer Res. 2015; 5(3): 945-955.
38. Bogdahn U, Hau P, Stockhammer G, Venkataramana NK, Mahapatra AK, Suri A, et al. Targeted therapy for high-grade glioma with the TGF-beta2 inhibitor trabedersen: results of a randomized and controlled phase IIb study. Neuro Oncol. 2011; 13(1): 132-142.
39. Rodon J, Carducci MA, Sepulveda-Sanchez JM, Azaro A, Calvo E, Seoane J, et al. First-in-human dose study of the novel transforming growth factor-beta receptor I kinase inhibitor LY2157299 monohydrate in patients with advanced cancer and glioma. Clin Cancer Res. 2015; 21(3): 553-560.
40. den Hollander MW, Bensch F, Glaudemans AWJM, Enting RH, Bunskoek S, Munnink THO, et al. zr-GC1008 PET imaging and GC1008 treatment of recurrent glioma patients. J Clin Oncol. 2013; 31(15).
41. Kim BG, Malek E, Choi SH, Ignatz-Hoover JJ, Driscoll JJ. Novel therapies emerging in oncology to target the TGF-beta pathway. J Hematol Oncol. 2021; 14(1): 55.
42. Burton ER, Libutti SK. Targeting TNF-alpha for cancer therapy. J Biol. 2009; 8(9): 85.
43. Fischer R, Kontermann RE, Pfizenmaier K. Selective targeting of TNF receptors as a novel therapeutic approach. Front Cell Dev Biol. 2020; 8: 401.
44. Lakka SS, Rao JS. Antiangiogenic therapy in brain tumors. Expert Rev Neurother. 2008; 8(10): 1457-1473.
45. Wakabayashi T, Natsume A, Hashizume Y, Fujii M, Mizuno M, Yoshida J. A phase I clinical trial of interferon-beta gene therapy for high-grade glioma: novel findings from gene expression profiling and autopsy. J Gene Med. 2008; 10(4): 329-339.
46. Colman H, Berkey BA, Maor MH, Groves MD, Schultz CJ, Vermeulen S, et al. Phase II radiation therapy oncology group trial of conventional radiation therapy followed by treatment with recombinant interferon-beta for supratentorial glioblastoma: results of RTOG 9710. Int J Radiat Oncol Biol Phys. 2006; 66(3): 818-824.
47. Aoki T, Takahashi JA, Ueba T, Oya N, Hiraoka M, Matsui K, et al. Phase II study of nimustine, carboplatin, vincristine, and interferon-beta with radiotherapy for glioblastoma multiforme: experience of the Kyoto Neuro-Oncology Group. J Neurosurg. 2006; 105(3): 385-391.
48. National Institutes of Health Clinical Center (CC). Phase II trial of peginterferon alpha-2b and thalidomide in adults with recurrent gliomas. 2002. Available from: https://clinicaltrials.gov/ct2/show/record/NCT00047879 (31 Jul 2021).
49. Groves MD, Puduvalli VK, Gilbert MR, Levin VA, Conrad CA, Liu VH, et al. Two phase II trials of temozolomide with interferon-alpha2b (pegylated and non-pegylated) in patients with recurrent glioblastoma multiforme. Br J Cancer. 2009; 101(4): 615-620.
50. Chen Z. A phase III trial on adjuvant temozolomide with or without interferon-alpha in newly diagnosed high-grade gliomas. 2013. Available from: https://clinicaltrials.gov/ct2/show/record/NCT01765088 (31 Jul 2021).
51. Mooney J, Bernstock JD, Ilyas A, Ibrahim A, Yamashita D, Markert JM, et al. Current approaches and challenges in the molecular therapeutic targeting of glioblastoma. World Neurosurg. 2019; 129: 90-100.
52. Jackson C, Ruzevick J, Phallen J, Belcaid Z, Lim M. Challenges in immunotherapy presented by the glioblastoma multiforme microenvironment. Clin Dev Immunol. 2011; 2011: 732413.
53. Zuccarini M, Giuliani P, Ziberi S, Carluccio M, Iorio PD, Caciagli F, et al. The role of wnt signal in glioblastoma development and progression: a possible new pharmacological target for the therapy of this tumor. Genes (Basel). 2018; 9(2): 105.
54. Kofler NM, Shawber CJ, Kangsamaksin T, Reed HO, Galatioto J, Kitajewski J. Notch signaling in developmental and tumor angiogenesis. Genes Cancer. 2011; 2(12): 1106-1116.
55. Gersey Z, Osiason AD, Bloom L, Shah S, Thompson JW, Bregy A, et al. Therapeutic targeting of the Notch pathway in glioblastoma multiforme. World Neurosurg. 2019; 131: 252-263.
56. Malric L, Monferran S, Gilhodes J, Boyrie S, Dahan P, Skuli N, et al. Interest of integrins targeting in glioblastoma according to tumor heterogeneity and cancer stem cell paradigm: an update. Oncotarget. 2017; 8(49): 86947-86968.
57. Farber SH, Elsamadicy AA, Atik AF, Suryadevara CM, Chongsathidkiet P, Fecci PE, et al. The safety of available immunotherapy for the treatment of glioblastoma. Expert Opin Drug Saf. 2017; 16(3): 277-287.
58. Beyer S, Fleming J, Meng W, Singh R, Haque SJ, Chakravarti A. The role of miRNAs in angiogenesis, invasion and metabolism and their therapeutic implications in gliomas. Cancers (Basel). 2017; 9(7): 85.
59. Catuogno S, Esposito CL. Aptamer cell-based selection: overview and advances. Biomedicines. 2017; 5(3): 49.
60. Kane JR, Miska J, Young JS, Kanojia D, Kim JW, Lesniak MS. Sui generis: gene therapy and delivery systems for the treatment of glioblastoma. Neuro Oncol. 2015; 17 Suppl 2: ii24-ii36.
61. Batchelor TT, Duda DG, di Tomaso E, Ancukiewicz M, Plotkin SR, Gerstner E, et al. Phase II study of cediranib, an oral pan-vascular endothelial growth factor receptor tyrosine kinase inhibitor, in patients with recurrent glioblastoma. J Clin Oncol. 2010; 28(17): 2817-2823.
62. Kalpathy-Cramer J, Chandra V, Da X, Ou Y, Emblem KE, Muzikansky A, et al. Phase II study of tivozanib, an oral VEGFR inhibitor, in patients with recurrent glioblastoma. J Neurooncol. 2017; 131(3): 603-610.
63. Raymond E, Brandes AA, Dittrich C, Fumoleau P, Coudert B, Clement PM, et al. Phase II study of imatinib in patients with recurrent gliomas of various histologies: a European organisation for research and treatment of cancer brain tumor group study. J Clin Oncol. 2008; 26: 4659-4565.
64. Odia Y, Sul J, Shih JH, Kreisl TN, Butman JA, Iwamoto FM, et al. A phase II trial of tandutinib (MLN 518) in combination with bevacizumab for patients with recurrent glioblastoma. CNS Oncol. 2016; 5(2): 59-67.
65. Brahm CG, van Linde ME, Labots M, Kouwenhoven MC, Aliaga ES, Enting RH, et al. A phase II/III trial of high-dose, intermittent sunitinib in patients with recurrent glioblastoma: the STELLAR study. Ann Oncol. 2019; 30: v157-8.
66. de Vries NA, Buckle T, Zhao J, Beijnen JH, Schellens JH, van Tellingen O. Restricted brain penetration of the tyrosine kinase inhibitor erlotinib due to the drug transporters P-gp and BCRP. Invest New Drugs. 2012; 30: 443-449.
67. Clavreul A, Pourbaghi-Masouleh M, Roger E, Menei P. Nanocarriers and nonviral methods for delivering antiangiogenic factors for glioblastoma therapy: the story so far. Int J Nanomedicine. 2019; 14: 2497-2513.
68. Mao G, Sampath P, Sengupta S. Updates on chimeric antigen receptor-mediated glioblastoma immunotherapy. R I Med J (2013). 2017; 100(6): 39-42.
69. Sofuni A, Iijima H, Moriyasu F, Nakayama D, Shimizu M, Nakamura K, et al. Differential diagnosis of pancreatic tumors using ultrasound contrast imaging. J Gastroenterol. 2005; 40(5): 518-525.

Original Article

Differential Expression Pattern of *linc-ROR* Spliced Variants in Pluripotent and Non-Pluripotent Cell Lines

Fatemeh Mirzadeh Azad, Ph.D.[1, 2], Elham Taheri Bajgan, Ph.D.[1], Parisa Naeli, Ph.D.[1, 2], Alexander Rudov, Ph.D.[3], Mahrokh Bagheri Moghadam, M.Sc.[4], Mozhgan Sadat Akhtar, M.Sc.[1], Akram Gholipour, Ph.D.[5], Seyed Javad Mowla, Ph.D.[1], Mahshid Malakootian, Ph.D.[4]*

1. Molecular Genetics Department, Faculty of Biological Sciences, Tarbiat Modares University, Tehran, Iran
2. Patrick G. Johnston Centre for Cancer Research, Queen's University Belfast, Belfast, UK
3. Department of Biomolecular Sciences, University of Urbino, Via Saffi Urbino, Italy
4. Cardiogenetic Research Center, Rajaie Cardiovascular Medical and Research Center, Iran University of Medical Sciences, Tehran, Iran
5. Department of Biology, Science and Research Branch, Islamic Azad University, Tehran, Iran

**Corresponding Address: Cardiogenetic Research Center, Rajaie Cardiovascular Medical and Research Center, Iran University of Medical Sciences, Tehran, Iran*
Email: malakootian@rhc.ac.ir

Received: 22/August/2021, Accepted: 14/February/2022

Abstract

Objective: The human large intergenic non-coding RNA-regulator of reprogramming program (*linc-ROR*) is known as a stem cell specific linc-RNA. *linc-ROR* counteracts differentiation via sequestering microRNA-145 (miR-145) that targets OCT4 transcript. Despite the research on the expression and function, the exact structure of *Linc-ROR* transcripts is not clear. Considering the contribution of alternative splicing in transcripts structures and function, identifying different spliced variants of *linc-ROR* is necessary for further functional analyses. We aimed to find the alternatively spliced transcripts of *linc-ROR* and investigate their expression pattern in stem and cancer cell lines and during neural differentiation of NT2 cells as a model for understanding *linc-ROR* role in stem cell and differentiation.

Materials and Methods: In this experimental study, *linc-ROR* locus was scanned for identifying novel exons. Different primer sets were used to detect new spliced variants by reverse transcription polymerase chain reaction (RT-PCR) and direct sequencing. Quantitative PCR (qPCR) and RT-PCR were employed to profile expression of *linc-ROR* transcripts in different cell lines and during neural differentiation of stem cells.

Results: We could discover 13 novel spliced variants of *linc-ROR* harboring unique array of exons. Our work uncovered six novel exons, some of which were the product of exonized transposable elements. Monitoring expression profile of the *linc-ROR* spliced variants in a panel of pluripotent and non-pluripotent cells exhibited that all transcripts were primarily expressed in pluripotent cells. Moreover, the examined *linc-ROR* spliced variants showed a similar down-regulation during neural differentiation of NT2 cells.

Conclusion: Altogether, our data showed despite the difference in the structure and composition of exons, various spliced variants of *linc-ROR* showed similar expression pattern in stem cells and through differentiation.

Keywords: *linc-ROR*, Pluripotency, Spliced Variants, Stem Cell

Cell Journal(Yakhteh), Vol 24, No 10, October 2022, Pages: 569-576

Citation: Mirzadeh Azad F, Taheri Bajgan E, Naeli P, Rudov A, Bagheri Moghadam M, Sadat Akhtar M, Gholipour A, Mowla SJ, Malakootian M. Differential expression pattern of linc-ROR spliced variants in pluripotent and non-pluripotent cell lines. Cell J. 2022; 24(10): 569-576. doi: 10.22074/cellj.2022.8205.

Introduction

One of the main achievements of genomic era was the discovery of myriads of long non coding RNA transcripts (lncRNAs) that show state specific expression in different samples and biological processes. This finding suggested lncRNAs as new regulators of diseases and biological events (1, 2). lncRNAs could be detected in the nucleus and cytoplasm and they could exert their regulatory functions through a broad range of mechanisms entailing hybridization to RNA (3) or DNA sequences (4), interaction with transcription factors (5), epigenetic regulators (6). One functional manifestation that showcased the dependency of lncRNAs on interactions with different molecules, was discovery of lncRNAs that operate as competitive endogenous RNA (ceRNA) to compete with mRNAs for binding to regulatory miRNAs (7). However, there are still incomplete experimental evidences to validate the exact mechanisms of lncRNA-disease associations (8). Previous studies demonstrated that some long noncoding RNAs such as metastasis associated lung adenocarcinoma transcript 1 (*MALAT1*) and psoriasis susceptibility 1 candidate 3 (*PSORS1C3*) were able to exert their various regulatory roles at transcriptional and post-transcriptional levels through production of different transcript spliced variants (9-11).

Among lncRNAs, long intergenic non coding RNAs (linc-RNAs) are located between two protein coding genes and usually display high expression levels. lincRNAs exhibit specific expression patterns in different cell types and tissues. They are involved in cellular processes like stemness maintenance, cell cycle regulation and differentiation, however, their exact mechanism of function is still unresolved (12, 13).

The large intergenic non-coding RNA-regulator of reprogramming (*linc-ROR, lincRNA-ROR*), was firstly

introduced in 2010 by Loewer et al. (14) as a 2.6 kb long transcript. This linc-RNA modulates reprogramming of the human induced pluripotent stem cells by sequestering miR-145 (15). Deregulation of *linc-ROR* expression is associated with tumorigenesis in various malignancies such as esophageal (16), pancreatic (17), gastric (18), colon (19), ovarian (20) and breast cancers (21). However, complete transcript repertoire of this lncRNA has not been clarified yet.

In this study, we experimentally validated novel transcript variants for *linc-ROR* (Fig.1A, B). We also monitored expression pattern of some of these novel spliced variants in different cells and during the neural differentiation of NTera-2 cells to see if they behaved differently.

Materials and Methods

The study was approved by Research Ethics Committee of Rajaie Cardiovascular Medical and Research Center (IR.RHC.REC.1397.016).

Bioinformatic analysis

Using the UCSC genome browser, *linc-ROR* genomic locus was scanned for the conserved regions and existence of TE elements specifically long interspersed nuclear elements (LINE) and short interspersed nuclear elements (SINE) repeats.

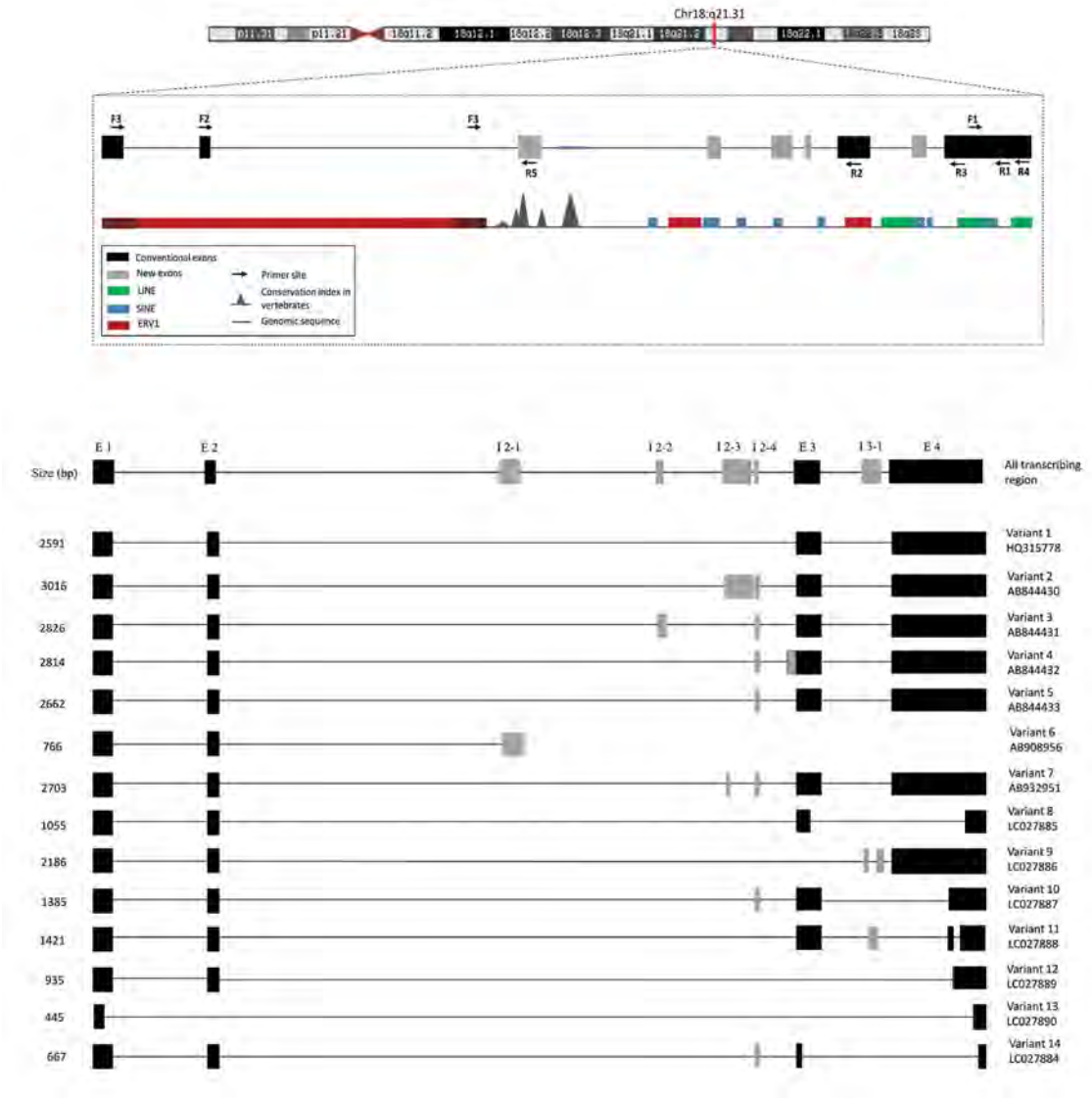

Fig.1: Genomic region of *linc-ROR* and its spliced transcript variants. **A.** The genomic location of *linc-ROR* in Chr.18:q21.31. The conserved regions in *linc-ROR* sequence along with LINE, SINE, ERV1, conventional and new exon sequences are represented here. Orientations of the primers were depicted in *linc-ROR* sequence. **B.** *linc-ROR* spliced transcript variants. Some isoforms contain new exons (gray) besides the conventional ones (black).

Cell culture

Dr. Peter Andrews, University of Sheffield was generously provided the human embryonic stem-like cell line NTERA2cl.D1 (NT2). The human embryonic stem cell lines, including hESC-RH5, hESC-RH6 (22), human induced pluripotent stem cell line 1 and human induced pluripotent stem cell lines 4 (hiPSC1 and hiPSC4 respectively) were obtained from Royan institute (Tehran, Iran) and cultured as described previously (23).

Human cell lines emanated from bladder carcinoma (5637), breast adenocarcinoma (MCF-7), hepatocellular carcinoma (HepG2), prostate cancer (PC3), prostatic adenocarcinoma (LNCAP), colorectal adenocarcinoma (HT-29), malignant glioma cell lines (U-87MG, A172), brain astrocytoma (1321N1), medulloblastoma (DAOY), cervix adenocarcinoma (Hela), hepatoblastoma (Huh-7), colon adenocarcinoma (SW480), esophageal squamous cell carcinoma (KYSE-30) and gastric carcinoma (AGS), were obtained from Pasture Institute of Iran (Tehran, Iran).

The human embryonic kidney 293 (HEK293T), human lung adenocarcinoma (A549), human USSC (unrestricted somatic stem cells) and fibroblast cells were purchased from the Stem Cell Technology Company (Tehran, Iran).

The cells were cultivated to reach 70% confluency before collection at 37°C with 5% humidified CO_2 in RPMI 1640 (for U-87MG, A172, 1321N1, DAOY) or high glucose Dulbecco's Modified Eagle Medium (DMEM, Invitrogen, USA) supplemented with 10% FBS (Invitrogen), 100 U/Ml penicillin, 100 mg/ml streptomycin and 25 ng/ml amphotericin B.

RNA isolation and cDNA synthesis

Total RNA was extracted from cell lines using TRIzol reagent (Invitrogen, USA), according to the manufacturer's instructions. RNase free DNaseI (TaKaRa, Japan) treatment was applied to remove any possible traces of DNA contamination. Reverse transcription of RNA was primed using an oligo (dT) primer and random hexamer by applying the PrimeScript TM Reagent kit (TaKaRa, Japan). Each sample had a no-reverse transcription (No-RT) control in parallel with the DNase-treated RNA to detect any potential non-specific amplification of genomic DNA.

Quantitative and qualitative reverse-transcriptional polymerase chain reaction

The GeneRunner (version 3.02, Hastings Software Inc., USA), PerlPrimer v1.1.16 and Oligo v 6.54 softwares were utilized to design the specific amplifying primers for qualitative and quantitative reverse-transcription PCR (RT-PCR) of both *linc-ROR* (GenBank accession numbers NR_048536 (HQ315778), AB844430, AB844431, AB844432, AB844433, AB908956 and AB932951) and β2 microglobulin (*β2M*, as an internal control; GenBank accession number: NM_004048.2), human glyceraldehyde 3-phosphate dehydrogenase (*GAPDH*, as an internal control; GenBank accession number: NM_002046). RT-PCR reactions were carried out using 2 µl of the synthesized cDNA, 0.5 mM of each primer and 10 µl of Taq DNA polymerase master mix RED (Ampliqon, Denmark).

PCR cycling parameters were comprised of initial cDNA denaturation of 5 minutes at 94ºC, followed by 45 seconds at 94ºC, 45 seconds at annealing temperature 60ºC and DNA extension for 1 minute at 72ºC for 35 and 26 cycles (for *linc-ROR* and *β2M* amplification, respectively). A final extension step was performed at 72ºC for 10 minutes. All PCR reactions incorporated no template controls or no RT reaction. Sequences of the designed oligos were listed in Table 1. PCR products were electrophoresed on 1% or 1.5% agarose gel electrophoresis, followed by staining with ethidium bromide and visualization through UV light exposure.

Quantitative RT-PCR (qRT-PCR) was carried out applying 2 µl of the synthesized cDNA, 10 µl of SYBR-Green ready mix (TaKaRa, Japan), 0.1 µl of Rox and 0.5 µM of each specific primer. *β2M* gene was utilized as an internal control, and expression of the other genes was normalized to its expression level using the $2^{-\Delta Ct}$ method.

ABI 7500 real-time PCR system (Applied Biosystems, USA) was employed to execute the PCR reactions using the following cycling conditions: initiation at 95°C for 15 minutes, amplification for 40 cycles with denaturation at 95°C for 15 seconds, annealing at 62.5°C for 30 seconds and extension at 72°C for 30 seconds. Melt curves were analyzed to validate the PCR products and amplified products were sequenced.

Cloning constructs and sanger sequencing

All *linc-ROR* PCR products were purified from agarose gel with ExpinTM combo kit (GeneAll, South Korea). Then, PTG19-T vector (Vivantis, Malaysia) was applied to clone the purified products using T4 DNA ligase (Fermentas, USA) and transformed to DH5α competent cells (TaKaRa, Japan).

Recombinant colonies with resistance to ampicillin (Sigma-Aldrich, USA) were selected as positive ones. Universal M13 primers were employed to select different variants of the *linc-ROR* gene via colony check PCR. Sanger sequencing (Microgen, South Korea) was utilized to validate identity and validity of the PCR products.

Induction of neural differentiation of NT2 cells

Peter Andrews protocol, which was described before (24), was applied to induced neural differentiation of NT2 cells. Concisely, NT2 cells were treated with 10-5 M all-trans-retinoic acid (RA, Sigma-Aldrich, USA) for up to 21 days. Then, the cells were passaged and re-cultured without retinoic acid for additional two weeks. NT2 cells were also treated with 1% DMSO (RA solvent) as a control group. The cells were then collected at different time points (3rd, 7th, 14th, 21st, 25th and 32nd days) for further analyses.

Table 1: Sequence of the utilized primers in the study

Gene	Name	Sequences (5´-3´)	Products (bp)
linc-ROR variant 6	F1	GCCATGTT CTCACACAAAG	1149
	R3	CTCATGGCTAATTGCACTGG	
linc-ROR	F3	ACCAATTTCAAATCCAGACCC	320
	R1	TCTTACTTAGCGACAATGCCATC	
linc-ROR	F3	ACCAATTTCAAATCCAGACCC	787
	R2	TTTGAGGTGGCTGGTGAGAG	
linc-ROR	F4	ACAAGGAGGAAAGGGCTGAC	124
	R4	TTCTGGAAGCTAAGTGCACATG	
OCT4A	F	CTTCTCGCCCCCTCCAGGT	496
	R	AAATAGAACCCCCAGGGTGAGC	
OCT4B1	F	AGACTATTCCTTGGGGCCACAC	272
	R	CTTAGAGGGGAGATGCGGTCA	
OCT4B	F	AGACTATTCCTTGGGGCCACAC	244
	R	GGCTGAATACCTTCCCAAATAGA	
Nanog	F	AGGAGCGACGAAGAGTACTAC	253
	R	ACTCTGCTTTCACCAAATTG	
SOX2	F	CATGGCTCTGGTGCTCTG	160
	R	GCTGGGAATTTCTGGTCG	
GAPDH	F	GTGAACCATGAGAAGTATGACAAC	123
	R	CATGAGTCCTTCCACGATACC	
B2M	F	GGGTTTCATCCATCCGACATTG	167
	R	TGGTTCACACGGCAGGCATAC	
miR-145	F	TAIAGCTAGACTCCGGGCGATG	202
	R	GCTCATTGTAGAAGGTGTGGTG	
OCT4A	F	TGCCCATCCAGTCAATCTCA	444
	R	TCCAGAGACGGCAGCCAAG	
linc-ROR	F	CAGTCGGGAAAGGAGGAACA	124
	R	GTACACGTGAATCGAAGGTCTT	
linc-ROR variant 4	FB22	TATCGTCAGAGTGTCAGGGT	251
	R2NEW	TACTTAGCGACAATGCCATC	
linc-ROR variant 3	FC3	AGATCACACCACTGCACTC	145
	RC3	AAGGGATTGAAGTTGAGTCT	
linc-ROR	F11	TGGTGATGTGACTCGGATAGG	448
	R22	TCTTACTTAGCGACAATGCCATC	
linc-ROR	FEA1	AAGCAGCTGTGACCTGGC	288
	R2	TCTTACTTAGCGACAATGCCATC	
linc-ROR (whole transcript)	Fex	GGTGAAATAAACAGCCATGTT	2580
	Rex	GAGGAACTGTCATACCGTTT	

Statistical analysis

All experiments were replicated at least three times. GraphPadPrism 8 software (GraphPad Software,USA) was employed to perform Student T test. All values were presented as means ± standard error of mean (means ± SEM) and $P<0.05$ were considered statistically significant.

Results

linc-ROR spliced variants has different patterns of expression in various cell lines

To profile expression of *linc-ROR* in different stem and cancer cell lines, we firstly designed a primer set on the lncRNA terminal exon (F4R4 primers, Fig.1A) with the idea to detect all possible spliced variants (Fig.1B). Our initial investigation on the expression of *linc-ROR* transcripts by qRT-PCR revealed that NT2 cells had the highest expression levels for *linc*-ROR (Fig.2A). Among the cancer cells, Huh-7, HEK293T and DAOY showed a relatively higher expression level for *linc-ROR*. Expression of *linc-ROR* was undetectable in fibroblast cells representing somatic normal cells.

Our bioinformatics analysis on the *linc-ROR* locus revealed that this lncRNA was overlapped with different transposable elements (TEs, Fig.1A). Based on the previous researches, TEs could contribute to create new alternatively spliced variants since they provide splice site acceptors and donors and they can be exonized into the transcript (25). To find out whether *linc-ROR* transcripts contained any TE driven exons, we specifically designed different sets of oligos mapping on different TEs to capture those potential transposon containing exons (Fig.1A, B).

Primers, designed on the junction of *linc-ROR* first and second exons (F3) and reverse primers on exon 3 (R1), were used to capture transcripts with possible TEs as exon. These primers were used in RT-PCR on NT2 cells since they showed the highest expression level of *linc-ROR*. In this experiment, we could detect several amplicons with different sizes that differ from what we expected to see from the RefSeq sequence (320 bp, Fig.2B).

To uncover the identity and structure of these bands, they were isolated from the gel, cloned, sequenced and aligned against the human genome (hg19) and transcript sequences. The results demonstrated existence of five novel *linc-ROR* spliced variants retaining different parts of the intron 2 sequence, as novel exons, some overlapped with TE elements. To examine whether we could also detect transcripts with extra exons in different cancer cells, we carried out RT-PCR analysis with the same set of primers in a panel of different cells. The result revealed a diverse pattern of expression for different variants in those cell lines (Fig.2C). The HT-29 and 5637 cells displayed almost the same expression pattern as NT2 cells.

Furthermore, our bioinformatic analysis displayed that there are three highly conserved regions approximately in the middle of the second intron of *linc-ROR* and we hypothesized that maybe these parts also could take part in creating new variants as well. Our RT-PCR outcomes using F1R3 primers in NT2 cells exhibited a novel spliced variant of *linc-ROR* (Fig.2D) with the AB908956 accession number (variant 6) that contained exon 1, 2 and a part of the conserved sequence in the second intron (Fig.1A, B).

To find whether we could detect the transcripts containing novel exons in full length, we designed two sets of primers, located on the beginning (Fex) of exon 1 and the end of exon 4 (Rex), followed by performing RT-PCR on human pluripotent cells (hiPSC1, hiPSC4, hESC-RH5 and hESC-RH6). The expected band for the transcript containing all exons was about 2.6 kb. Our results exhibited that there were additional bands with alternative sizes (Fig.2E). To confirm identity of the bands and presence of novel exons, all bands were extracted from the gel, cloned, sequenced and aligned to the human genome and transcript sequences (UCSC genome browser, hg19). Aside from validating the spliced variants that we first detected in NT2 cells, we identified eight novel variants for *linc-ROR*. Blat analysis exhibited two of the newly identified variants, retained some parts of LINE and SINE sequences which are located in intron 2 of the *linc-ROR* gene (Fig.1A, B).

linc-ROR variants are downregulated following differentiation

To scrutinize the correlation between the expression of *Linc-ROR* spliced variants and the undifferentiated state of human embryonic stem and embryonic carcinoma cells, NT2 human cells were treated with all-trans-retinoic acid (24). qRT-PCR results (using primers which could detect all transcripts) demonstrated that expression of *linc-ROR* was downregulated in the course of neural differentiation. Surprisingly, decline in *linc-ROR* expression was detected before downregulation of master regulators of pluripotency *OCT4A*, *SOX2*, *NANOG* and *miR-302b*. Adversely, expression of *miR-145* was upregulated gradually during differentiation (Fig.3A).

To see if the observed downregulation for *linc-ROR* was a trend affecting different variants, we used semi-qRT-PCR. Our results revealed that all detected *linc-ROR* spliced variants were downregulated the same way in the course of neural differentiation (Fig.3B, C), a pattern that was not seen in tumor samples, where some isoforms showed upregulation and some exhibited downregulation [unpublished data, (16)].

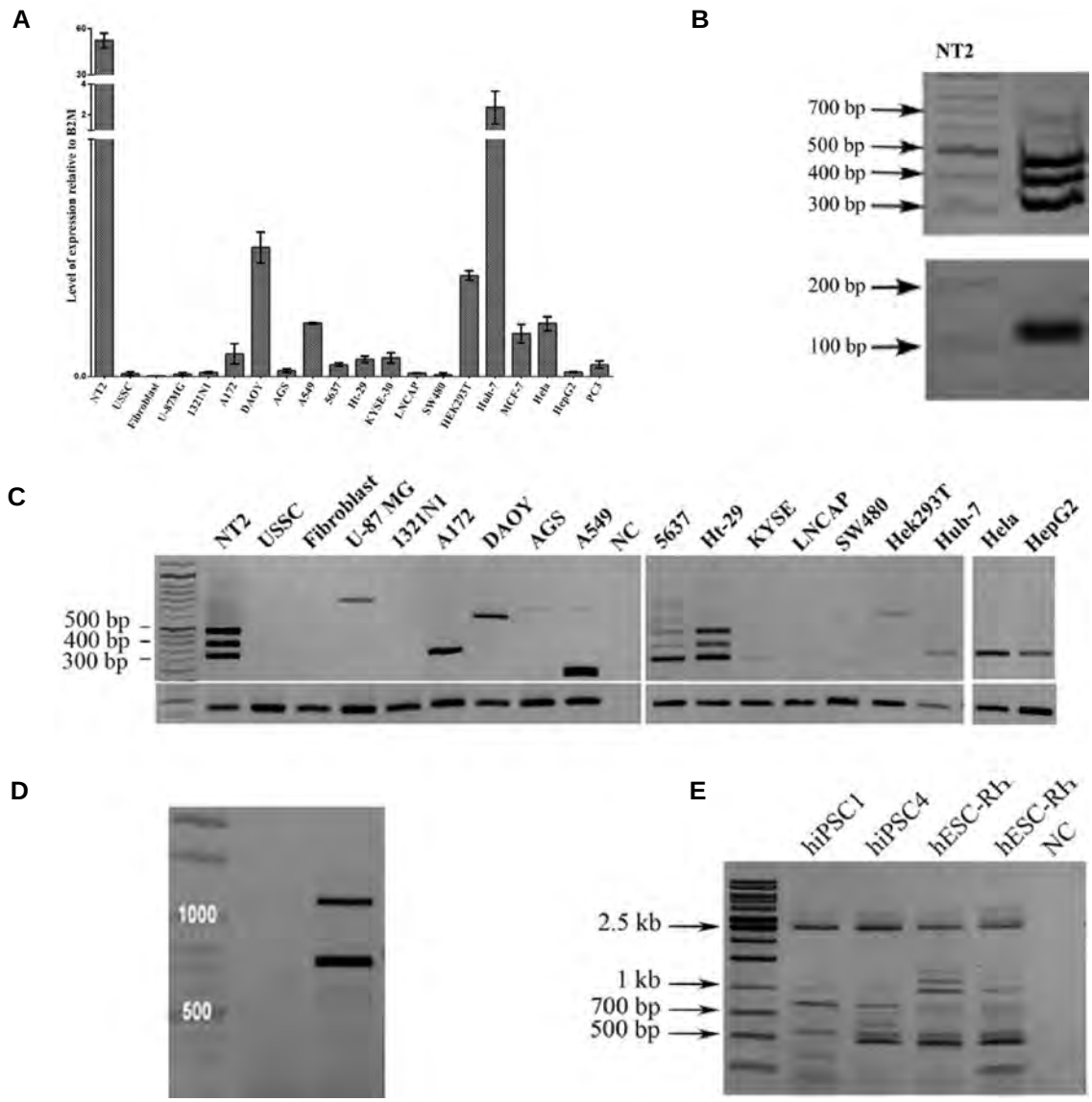

Fig.2: *linc-ROR* expression pattern in different cell lines. **A.** Expression profile of *linc-ROR* in a variety of pluripotent and non-pluripotent cell lines (F4R4; normalized to *B2M*). Expression of *linc-ROR* reaches the highest level in NT2 cell line. **B.** Reverse transcription polymerase chain reaction (RT-PCR) detection of *linc-ROR* isoforms in NT2 cell line (F3R1). **C.** Semi-quantitative RT-PCR results of *linc-ROR* detection in different pluripotent and non-pluripotent cell lines (F3R1). **D.** RT-PCR products in NT2 cell line using primers for variant 6 (F1R3), and **E.** RT-PCR products of *linc-ROR* spliced variants in human pluripotent cells using Fex and Rex oligos.

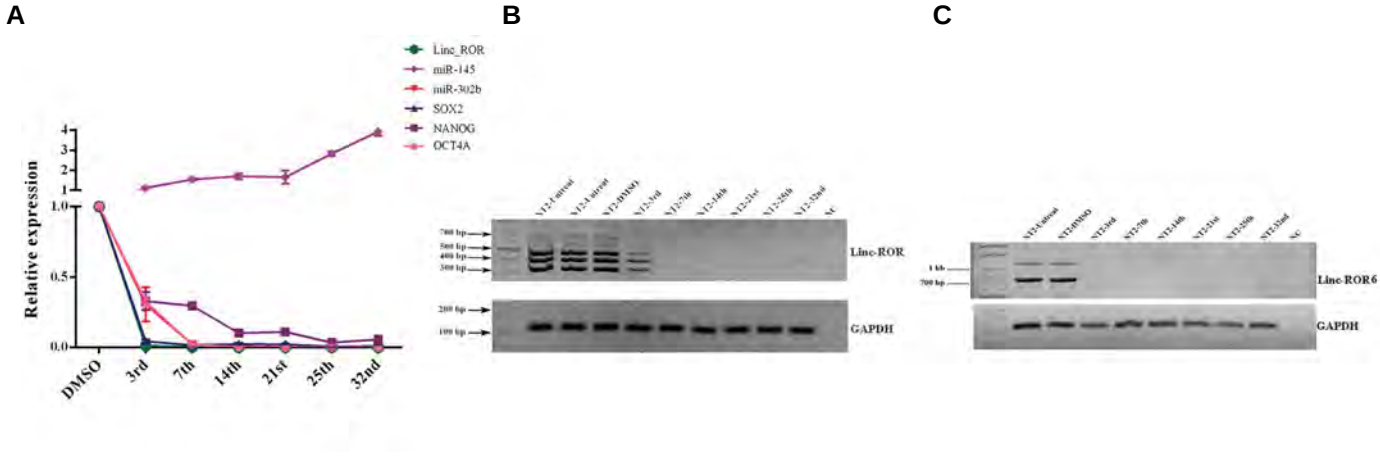

Fig.3: Expression of *linc-ROR* and its spliced variants during NT2 cells differentiation. **A.** Expression levels of *linc-ROR* (normalized to *B2M*), *miR-145, miR-302b, SOX2, NANOG* and *OCT4A* during differentiation. **B, C.** Expression pattern of *linc-ROR* spliced variants and *linc-ROR* variant 6 during differentiation of NT2 by means of semi-quantitative reverse transcription polymerase chain reaction (RT-PCR). DMSO; Dimethyl sulfoxide.

Discussion

linc-ROR plays a pivotal role in regulating self-renewal and reprogramming of pluripotent stem cells (12, 15). *linc-ROR*, some of the major regulators of pluripotency and self-renewal such as *OCT-4* share common expression signatures in some tumors and cancer cell lines (26) which advocate the hypotheses of the involvement of cancer stem cells and potential association of these factors in tumorigenesis. By scanning the genomic location of *Linc-ROR* which harbored transposon elements, we predicted there must be some transcript spliced variants of *Linc-ROR*. Our study has introduced and confirmed existence of the 14 different spliced variants of *lincROR* expressing in different stem and non-stem cells and in the course of differentiation. Our group previously reported differential expression of the three spliced variants of *linc-ROR* in human esophageal squamous cell carcinoma (16). In this study, we introduced 13 novel spliced variants for *linc-ROR*. Our investigations showed these variants were highly expressed in stem-like cells and differentially detectable in different cancer cell lines. For instance, *linc-ROR* expression level was not similar in different glioblastoma cell lines that we examined in this research. This could be due to differences in cancer stem cell pool, represented grade and stage and intra population heterogeneity of these cell lines.

The evolutionary role of alternative splicing in fine-tuning gene function and transcriptome dynamics in eukaryotes has been established previously (27) and it is known for many protein coding (28) and noncoding genes (10) with different transcript spliced variants. For instance, *OCT4*, a master regulator of pluripotency, has various isoforms with different expression and distinct functional roles (10, 26, 29). Our team also previously reported this phenomenon for long noncoding RNA *PSORS1C3*, which has 24 spliced variants with different expression pattern and function in pluripotent and non-pluripotent cells (10, 11, 30). Another example is *MALAT1*, one of the well-studied lncRNAs with various spliced variants that differ greatly in their expression patterns and functions in different cells and tissues (9, 31). There is an increasing number of publications on the function of *linc-ROR* and its expression. However, differential expression of its spliced variants in different cell types and tissues needs to be elucidated.

Here we detected new variants of *linc-ROR* transcripts in pluripotent stem cells and cancer cells, showing their expression alteration during neural differentiation. Our data indicated that many of *linc-ROR* spliced variants behaved similarly and their abrupt downregulation upon differentiation fit with their suggested role as guardians of stemness circuits.

Furthermore, the genomic location of *linc-ROR* contained transposon elements (TE), which are considered as selfish genomic parasites (32). Several studies argued that TE were involved in different transcriptional regulatory networks (32-34), as well as harboring splicing signals, leading to being spliced as new exons (25, 35). Our result exhibited that these elements could contribute to *linc-ROR* transcripts as new exons. TE derived sequences are considered as functional domains of lncRNAs which enable them to interact with and regulate RNA species and proteins (36). It is possible that *linc-ROR* exonized TEs are also involved in different functional abilities of their harboring transcripts. To validate this, further investigations are required.

Here, we showed that *linc-ROR* had higher expression level in NT2 cells, as a pluripotent human embryonal carcinoma cell line. This data is in line with the published association of *linc-ROR* with stemness state (14). Our data also pinpointed the significant decrease in *linc-ROR* and its transcript spliced variants expression throughout neural differentiation in both quantitative and semi-quantitative approaches which is in line with previous findings on the contribution of *linc-ROR* in self renewal and pluripotency through regulating core stemness factors (15, 37-39).

Mis-regulation of mRNA splicing can affect signaling pathways and contribute to diseases like cancer (40). The alternative splicing of lncRNAs might also impact various cellular processes, however, understanding the exact molecular effect of alternatively spliced exons needs to be further investigated.

Conclusion

The detailed picture of *linc-ROR* regulatory network is still missing. We identified 13 novel splice variants for *linc-ROR* that were expressed in pluripotent and some cancer cells. Our results, together with those from previous studies, depicted new insights into investigations of the molecular repertoire of lncRNAs, suggested a new angle for the scrutinizing lncRNA genes and showed the missing pieces that are needed for lncRNAs expression and function investigations.

Acknowledgements

We would like to thank Professor Hossain Baharvand (Royan Institute, Iran) for providing us the pluripotent cells. This work was supported in part by a research grant to Dr. Malakootian from council for development of stem cell sciences and technologies (Tehran, Iran, Grant number: 186) and the Research Deputyship of Rajaie Cardiovascular Medical and Research Center (Tehran, Iran, Grant number: 9711). We also thank Iranian national science foundation (Grant number: 92031599) for supporting the work. There is no conflict of interest in this study.

Authors' Contributions

M.M., S.J.M; Contributed to experimental design and supervision, finalized the draft. F.M.A., E.T.B., P.N., A.R., M.S.A., M.B.M., A.Gh.; Participated in experimental

work and statistical analysis. M.M, F.M.A., E.T.B., P.N., A.R., M.S.A., M.B.M., A.Gh.; Contributed to writing and submitting the manuscript. All authors participated in the finalization of the manuscript and approved the final draft.

References

1. Fort V, Khelifi G, Hussein SM. Long non-coding RNAs and transposable elements: a functional relationship. Biochim Biophys Acta Mol Cell Res. 2021; 1868(1): 118837.
2. Statello L, Guo CJ, Chen LL, Huarte M. Gene regulation by long non-coding RNAs and its biological functions. Nat Rev Mol Cell Biol. 2021; 22(2): 96-118.
3. Szcześniak MW, Makałowska I. lncRNA-RNA interactions across the human transcriptome. PLoS One. 2016; 11(3): e0150353.
4. Yang Y, Chen Q, Piao HY, Wang B, Zhu GQ, Chen EB, et al. HNRNPAB-regulated lncRNA-ELF209 inhibits the malignancy of hepatocellular carcinoma. Int J Cancer. 2020; 146(1): 169-180.
5. Xue Z, Hennelly S, Doyle B, Gulati AA, Novikova IV, Sanbonmatsu KY, et al. A G-rich motif in the lncRNA braveheart interacts with a zinc-finger transcription factor to specify the cardiovascular lineage. Mol Cell. 2016; 64(1): 37-50.
6. Wang C, Wang L, Ding Y, Lu X, Zhang G, Yang J, et al. LncRNA structural characteristics in epigenetic regulation. Int J Mol Sci. 2017; 18(12): 2659.
7. Militello G, Weirick T, John D, Döring C, Dimmeler S, Uchida S. Screening and validation of lncRNAs and circRNAs as miRNA sponges. Brief Bioinform. 2017; 18(5): 780-788.
8. Chen X, Yan CC, Zhang X, You ZH. Long non-coding RNAs and complex diseases: from experimental results to computational models. Brief Bioinform. 2017; 18(4): 558-576.
9. Meseure D, Vacher S, Lallemand F, Alsibai KD, Hatem R, Chemlali W, et al. Prognostic value of a newly identified MALAT1 alternatively spliced transcript in breast cancer. Br J Cancer. 2016; 114(12): 1395-1404.
10. Malakootian M, Azad FM, Naeli P, Pakzad M, Fouani Y, Bajgan ET, et al. Novel spliced variants of OCT4, OCT4C and OCT4C1, with distinct expression patterns and functions in pluripotent and tumor cell lines. Eur J Cell Biol. 2017; 96(4): 347-355.
11. Azad FM, Malakootian M, Mowla SJ. lncRNA PSORS1C3 is regulated by glucocorticoids and fine-tunes OCT4 expression in non-pluripotent cells. Sci Rep. 2019; 9 : 8370.
12. Fico A, Fiorenzano A, Pascale E, Patriarca EJ, Minchiotti G. Long non-coding RNA in stem cell pluripotency and lineage commitment: functions and evolutionary conservation. Cell Mol Life Sci. 2019; 76(8): 1459-1471.
13. Ransohoff JD, Wei Y, Khavari PA. The functions and unique features of long intergenic non-coding RNA. Nat Rev Mol Cell Biol. 2018; 19(3): 143-157.
14. Loewer S, Cabili MN, Guttman M, Loh Y-H, Thomas K, Park IH, et al. Large intergenic non-coding RNA-RoR modulates reprogramming of human induced pluripotent stem cells. Nat Genet. 2010; 42(12): 1113-1117.
15. Wang Y, Xu Z, Jiang J, Xu C, Kang J, Xiao L, et al. Endogenous miRNA sponge lincRNA-RoR regulates Oct4, Nanog, and Sox2 in human embryonic stem cell self-renewal. Dev Cell. 2013; 25(1): 69-80.
16. Sahebi R, Malakootian M, Balalaee B, Shahryari A, Khoshnia M, Abbaszadegan MR, et al. Linc-ROR and its spliced variants 2 and 4 are significantly up-regulated in esophageal squamous cell carcinoma. Iran J Basic Med Sci. 2016; 19(10): 1131-1135.
17. Chen W, Wang H, Liu Y, Xu W, Ling C, Li Y, et al. Linc-RoR promotes proliferation, migration, and invasion via the Hippo/YAP pathway in pancreatic cancer cells. J Cell Biochem. 2020; 121(1): 632-641.
18. Yu X, Ding H, Shi Y, Yang L, Zhou J, Yan Z, et al. Downregulated expression of linc-ROR in gastric cancer and its potential diagnostic and prognosis value. Dis Markers. 2020; 2020: 7347298.
19. Li X, Chen W, Jia J, You Z, Hu C, Zhuang Y, et al. The long non-coding RNA-RoR promotes the tumorigenesis of human colorectal cancer by targeting miR-6833-3p Through SMC4. Onco Targets Ther. 2020; 13: 2573-2581.
20. Lou Y, Jiang H, Cui Z, Wang L, Wang X, Tian T. Linc-ROR induces epithelial-to-mesenchymal transition in ovarian cancer by increasing Wnt/β-catenin signaling. Oncotarget. 2017; 8(41): 69983-69994.
21. Peng Wx, Huang Jg, Yang L, Gong Ah, Mo YY. Linc-RoR promotes MAPK/ERK signaling and confers estrogen-independent growth of breast cancer. Mol Cancer. 2017; 16: 1-11.
22. Baharvand H, Ashtiani SK, Taee A, Massumi M, Valojerdi MR, Yazdi PE, et al. Generation of new human embryonic stem cell lines with diploid and triploid karyotypes. Dev Growth Differ. 2006; 48(2): 117-128.
23. Totonchi M, Taei A, Seifinejad A, Tabebordbar M, Rassouli H, Farrokhi A, et al. Feeder-and serum-free establishment and expansion of human induced pluripotent stem cells. Int J Dev Biol. 2009; 54(5): 877-886.
24. Malakootian M, Azad FM, Fouani Y, Bajgan ET, Saberi H, Mowla SJ. Anti-differentiation non-coding RNA, ANCR, is differentially expressed in different types of brain tumors. J Neurooncol. 2018; 138(2): 261-270.
25. Chen LL, Yang L. ALUternative regulation for gene expression. Trends Cell Biol. 2017; 27(7): 480-490.
26. Atlasi Y, Mowla SJ, Ziaee SA, Gokhale PJ, Andrews PW. OCT4 spliced variants are differentially expressed in human pluripotent and nonpluripotent cells. Stem Cells. 2008; 26(12): 3068-3074.
27. Bush SJ, Chen L, Tovar-Corona JM, Urrutia AO. Alternative splicing and the evolution of phenotypic novelty. Philos Trans R Soc Lond B Biol Sci. 2017; 372(1713): 20150474.
28. Rodriguez JM, Pozo F, di Domenico T, Vazquez J, Tress ML. An analysis of tissue-specific alternative splicing at the protein level. PLoS Comput Biol. 2020; 16(10): e1008287.
29. Poursani EM, Mehravar M, Soltani BM, Mowla SJ. OCT4B2, a novel alternative spliced variant of OCT4, is significantly upregulated under heat-stress condition and downregulated in differentiated cells. Tumour Biol. 2017; 39(10): 1010428317724280.
30. Mirzadeh Azad F, Malakootian M, Mowla SJ. The regulatory effect of lncRNA PSORS1C3 on different variants of OCT4 in non-pluripotent cells. J Cell Mol Med. 2019; 11(1): 8-13.
31. Arun G, Aggarwal D, Spector DL. MALAT1 long non-coding RNA: functional implications. Noncoding RNA. 2020; 6(2): 22.
32. Johnson R, Guigó R. The RIDL hypothesis: transposable elements as functional domains of long noncoding RNAs. RNA. 2014; 20(7): 959-976.
33. Babaian A, Mager DL. Endogenous retroviral promoter exaptation in human cancer. Mob DNA. 2016; 7: 24.
34. Bejerano G, Lowe CB, Ahituv N, King B, Siepel A, Salama SR, et al. A distal enhancer and an ultraconserved exon are derived from a novel retroposon. Nature. 2006; 441(7089): 87-90.
35. Zeng L, Pederson SM, Cao D, Qu Z, Hu Z, Adelson DL, et al. Genome-wide analysis of the association of transposable elements with gene regulation suggests that alu elements have the largest overall regulatory impact. J Comput Biol. 2018; 25(6): 551-562.
36. Kelley D, Rinn J. Transposable elements reveal a stem cell-specific class of long noncoding RNAs. Genome Biol. 2012; 13(11): R107.
37. Feng L, Shi L, Lu Yf, Wang B, Tang T, Fu Wm, et al. Linc-ROR promotes osteogenic differentiation of mesenchymal stem cells by functioning as a competing endogenous RNA for miR-138 and miR-145. Mol Ther Nucleic Acids. 2018; 11: 345-353.
38. Hou P, Zhao Y, Li Z, Yao R, Ma M, Gao Y, et al. LincRNA-ROR induces epithelial-to-mesenchymal transition and contributes to breast cancer tumorigenesis and metastasis. Cell Death Dis. 2014; 5(6): e1287-e1287.
39. Taheri Bajgan E, Gholipour A, Faghihi M, Mowla SJ, Malakootian M. Linc-ROR has a Potential ceRNA Activity for OCT4A by Sequestering miR-335-5p in the HEK293T Cell Line. Biochem Genet. 2022; 60(3): 1007-1024.
40. Chen J, Weiss W. Alternative splicing in cancer: implications for biology and therapy. Oncogene. 2015; 34: 1-14.

Original Article

Moderate Endurance Training and MitoQ Improve Cardiovascular Function, Oxidative Stress, and Inflammation in Hypertensive Individuals: The Role of miR-21 and miR-222: A Randomized, Double-Blind, Clinical Trial

Yaser Masoumi-Ardakani, M.Sc.[1, 2], Hamid Najafipour, Ph.D.[3]*, Hamid Reza Nasri, M.D.[3], Soheil Aminizadeh, Ph.D.[1], Shirin Jafari, M.D.[3], Zohreh Safi, B.Sc.[4]

1. Physiology Research Center, Institute of Neuropharmacology, Department of Physiology and Pharmacology, Kerman University of Medical Sciences, Kerman, Iran
2. Student Research Committee, Kerman University of Medical Sciences, Kerman, Iran
3. Cardiovascular Research Center, Institute of Basic and Clinical Physiology Sciences, Kerman University of Medical Sciences, Kerman, Iran
4. Endocrinology and Metabolism Research Center, Institute of Basic and Clinical Physiology Sciences, Kerman University of Medical Sciences, Kerman, Iran

Corresponding Address: P.O.Box: 7619813159, Cardiovascular Research Center, Institute of Basic and Clinical Physiology Sciences, Kerman University of Medical Sciences, Kerman, Iran
Email: najafipourh@kmu.ac.ir

Received: 25/May/2021, Accepted: 21/February/2022

Abstract

Objective: Hypertension (HTN) is among the leading causes of myocardial infarction, stroke, and kidney disease. The MitoQ supplement is a mitochondrial-targeted antioxidant that attenuates the generation of reactive oxygen species (ROS). miRNAs play an essential role in the pathophysiology of HTN. Regular aerobic exercise is recommended to decrease the risk of cardiovascular disease. We aimed to evaluate the effects of MitoQ supplementation and moderate endurance training (ET), alone and in combination, on cardiac function, blood pressure, the circulatory levels of miRNA-21 and miRNA-222, and oxidative status in individuals with HTN.

Materials and Methods: In a double-blind, randomized clinical trial (except for ET group), 52 male hypertensive subjects (40-55 years old) were randomly divided into four groups (n=13): Placebo, MitoQ (20 mg/day, oral), ET (Cycle ergometer, moderate intensity, 40-60% VO_2 peak, three sessions/week for six weeks), and MitoQ+ET. Cardiac echocardiography indices, serum oxidative and inflammation status, and miRNAs 21 and 222 were assessed before and after interventions.

Results: Left ventricular mass [effect size (ES): -6.3, 95% confidence interval (CI): -11.2 to -1.4] and end-systolic/diastolic diameters significantly improved in the intervention groups (ES: -0.05, 95% CI: -0.11 to 0.00 and -0.09, 95% CI: -0.16 to -0.02). Total serum antioxidant capacity (TAC) increased (ES: 36.0, 95% CI: 26.1 to 45.8), and malondialdehyde (MDA) (ES: -0.43, 95% CI: -0.53 to -0.32), IL-6 (ES: -1.6, 95% CI: -1.98 to -1.25), miR-21 (ES: -0.48, 95% CI: -0.61 to -0.35), and miR-222 (ES: -0.31, 95% CI: -0.44 to -0.18) significantly decreased in response to ET, MitoQ, and their combination.

Conclusion: MitoQ and ET, individually and more pronouncedly in combination, can improve cardiovascular health in people with high blood pressure (BP) by reducing inflammation and increasing antioxidant defense, in association with reduction in circulatory miR-21 and miR-222 levels (registration number: IRCT20190228042870N1).

Keywords: Endurance Training, Hypertension, miR-21, miR-222, MitoQ

Cell Journal(Yakhteh), Vol 24, No 10, October 2022, Pages: 577-585

Citation: **Masoumi-Ardakani Y, Najafipour H, Nasri HR, Aminizadeh S, Jafari Sh, Safi Z. Moderate endurance training and mitoq improve cardiovascular function, oxidative stress, and inflammation in hypertensive individuals: the role of miR-21 and miR-222: a randomized, double-blind, clinical trial. Cell J. 2022; 24(10): 577-585. doi: 10.22074/cellj.2022.8089.**

Introduction

Hypertension (HTN) is a risk factor for other notable cardiovascular diseases (CVDs) such as myocardial infarction and stroke (1). HTN causes 9.4 million deaths annually worldwide and is estimated to affect about 1.56 billion people by 2025 (2). Primarily because of the unhealthy and sedentary lifestyle in the new generation, the prevalence and incidence of HTN are still increasing in many countries despite the numerous antihypertensive drugs available. Therefore, having physical activity is being increasingly advised as a non-pharmaceutical treatment strategy to prevent and treat HTN. Regular aerobic exercise reduces blood pressure (BP) and attenuates the risk of CVDs (3).

Oxidative stress and inflammation have also been introduced as mediators for the initiation and progression of HTN (4). Exercise training has been shown to modify the production of cytokines involved in inflammatory processes, such as interlukin-1beta (IL-1β), IL-6 and tumor necrosis factor-alpha (TNF-α) (5), and long-term endurance training (ET) has been demonstrated to reduce IL-6 and hs-CRP levels (6). Gaeini et al. (7) showed that the oxidant factor malondialdehyde (MDA) decreases even after one session of ET. Other investigators have also reported that strength training decreases MDA and increases total antioxidant capacity (TAC) and glutathione

peroxidase (GPx) activity in older men and women (8, 9).

Mitochondria are the sites of energy production in cells but are also involved in the production of free radicals (10), and their dysfunction plays an essential role in the pathophysiology of hypertensive injuries. In this regard, MitoQ, a mitochondrial-targeted antioxidant, has been reported to reduce free radicals, improve heart function, and attenuate BP (11-13).

MicroRNAs (miRNAs) are short single-stranded endogenous RNAs that target mRNAs and are involved in the development of HTN (4, 14). MiR-21 is expressed in the cardiovascular system and is associated with CVD and different types of HTN (15). MiR-222 suppresses mitochondrial and endothelial cell function by reducing PGC-1α (16). This micro-RNA plays an essential role in cardiac physiology and pathophysiology and has been introduced as a cardiac function biomarker (17).

Due to the role of oxidative stress in HTN, the role of mitochondria in ROS production, the protective effect of MitoQ on mitochondrial free radical production, and the role of exercise training on reducing oxidative stress and amelioration of HTN, this study was aimed to evaluate the effects of MitoQ supplementation and ET, alone and in combination, on cardiac function and oxidative and inflammatory status in hypertensive individuals. In this regard, the effect of the described interventions was assessed on the circulating levels of miR-21 and miR-222 as probable mediators in the interaction between ET and MitoQ supplementation in hypertensive patients.

Materials and Methods

Materials

In this double-blind randomized clinical trial study, the materials used and their sources were MitoQ (MitoQ Ltd., New Zealand), TAC, MDA, IL-6 kit (Thermo Fisher Scientific, USA), RNA isolation kit (Norgen Biotek, Cat. No. 17200, Canada), cDNA synthesis kit (Norgen Biotek, Cat. No. 54410, Canada), cel-miR-39 (Norgen Biotek, Cat. No. 59000, Canada), SYBR green (Ampliqon, Cat. No. A325402, Denmark), universal primer (reverse) (Norgen Biotek, Cat. No. 59000, Canada), and forward primers (Metabion, Germany). MitoQ capsules contained MitoQuinol (as MitoQuinol Mesylate) 20 mg as active ingredient, and microcrystalline cellulose (MCC), tapioca, and silicon dioxide (SiO_2) as excipients. The role of these excipients compounds in capsule formulation are: SiO_2 as an anti-caking agent, adsorbent, or glidant to allow powder to flow freely; MCC as a segregation inhibitor to improve drug content uniformity; and tapioca starch, as diluent due to its good flow ability. These compounds are generally inactive ingredients especially when used in low amounts, and we did not find any evidence for them to have side effects on the cardiovascular system.

Subjects

We used G*Power:3.1.9.4 version software to calculate the study sample size. Based on the nature of the study; repeated measure ANOVA, within-between interactions (see below: statical analysis), number of groups=4, given the asumptions of α=0.05, 1-β=0.8, effect size (ES)=0.24, the total sample size was computed to be 52. In this double-blind, randomized clinical trial, middle-aged patients (40-55 years old) with moderately high BP (between SBP/DBP 140/90 to 150/100 mmHg) were entered into the study. Blinding was complete for the laboratory to measure inflammatory and oxidant factors; and for the cardiologist assessing cardiac hypertrophy and functional variables. It was not possible to make the protocol blinded in all aspects for those that exercise (ET group). Participants were selected mostly from participant in KERCADRS (Kerman Coronary Artery Disease Risk Factor Study with sample size of 10,000, aged 15- 80 years old) (45 subjects) and some from patients referred to the cardiovascular clinic of Shafa Hospital in Kerman, Iran (7 subjects) from May 2019 to March 2020. All protocols, goals, and potential benefits and risks of the study were explained to the participants, and they signed an informed consent form. All procedures followed the standards set by the latest revision of the Declaration of Helsinki and were reviewed and approved by the Ethics Committee of Kerman University of Medical Sciences (IR.KMU.REC.1397.595) and by the national RCT registry (IRCT20190228042870N1). Figure 1 shows the study flowchart.

HTN was defined according to the criteria from the European Heart Association as systolic BP (SBP) ≥ 140 mm Hg or diastolic BP (DBP) ≥ 90 mm Hg. Participants with kidney, liver, and lung diseases, diabetes, cancer, known CVDs other than HTN (e.g., valvular heart disease, coronary disease and heart failure), antihypertensive and diuretic medications, SBP>150 mmHg and/or DBP>100 mmHg, high body mass index (BMI≥30 kg/m^2), and orthopedic disabilities were excluded from the study. The participants' demographic information (age, sex, history of HTN, level of physical activity, alcohol consumption, and medications) was collected by face-to-face interviews using a validated questionnaire. In the KERCADR study the baseline level of physical activity is determined using the global physical activity questionnaire (GPAQ), which includes all kind of activities, working, playing, training, housekeeping, and recreational activities (18).

Fifty-two subjects were randomly divided on the basis of throwing dice into four groups of Placebo, MitoQ (20 mg/day, oral) (13), ET, and MitoQ+ET, with 13 individuals in each group (Fig.1). Moderate-intensity ET [40 to 60 % VO_2 peak, heart rate (HR) 120-140 b/minutes, duration 45 minutes, three sessions/week], was performed for six weeks. The blood samples were taken at baseline and at the end of the study (day 43). The clotted blood sample was centrifuged (3000 g for 10 minutes), and the serum was stored at -80˚C for determining miRNAs 21 and 222, TAC, MDA, and IL-6.

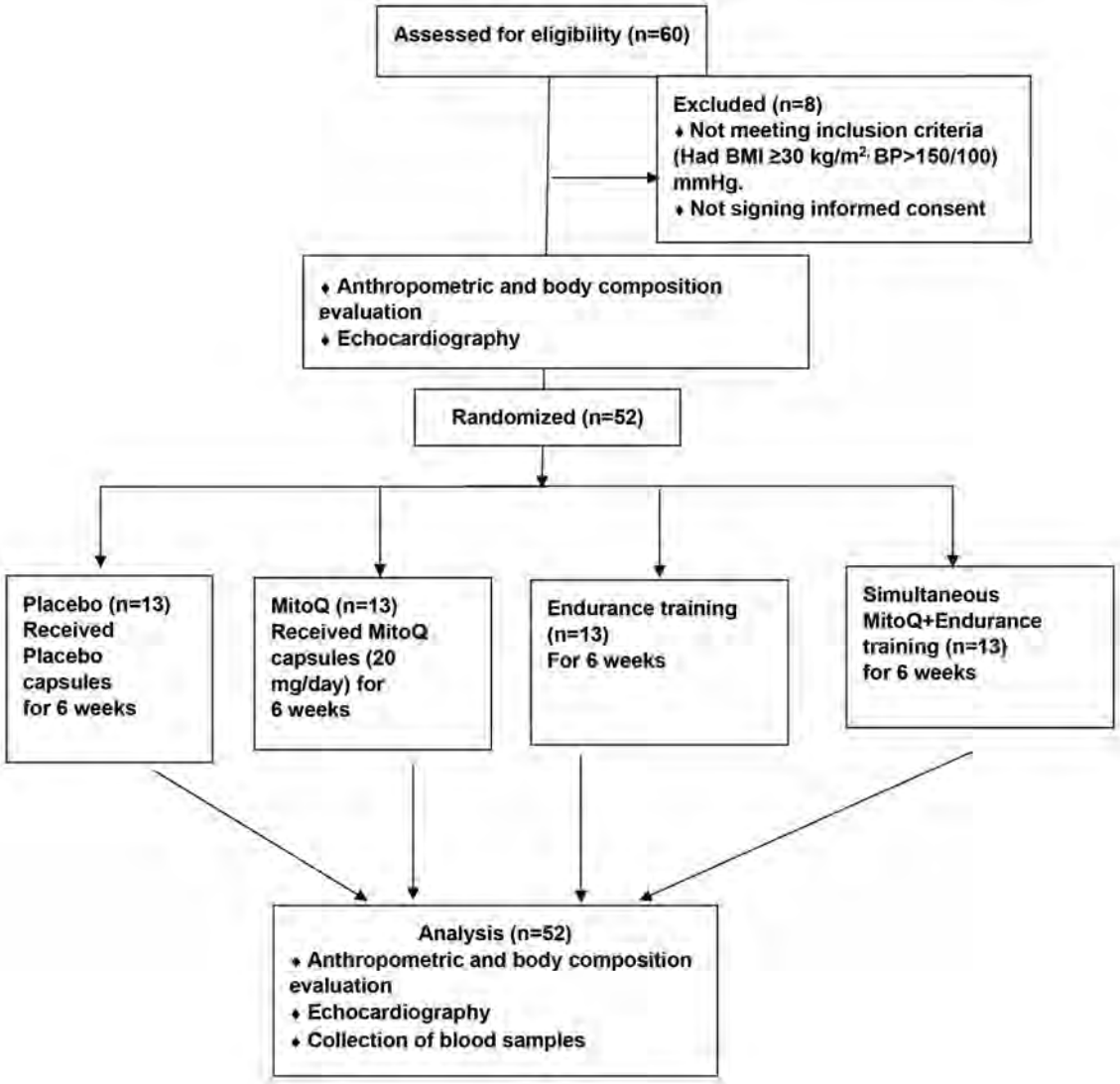

Fig.1: Study flow diagram. BMI; Body mass index.

Blood pressure measurement

BP (SBP and DBP) was measured with an automated device (Omron, M6 Comfort, Japan) to avoid the possibility of investigator bias in measurement. Measurement was performed twice after at least 10 minutes at rest (30 minutes apart) in a sitting position, and the values were averaged. The participants were asked to avoid consuming coffee, tea, soft drinks, supplements, and alcohol at least two hours before BP recording.

Body composition measurements

Bodyweight was measured by a medical beam balance (Allegro Medical, USA), and BMI was calculated [weight (in Kg)/height (in meter)^2] and classified as normal (BMI<25), overweight (BMI between 25 and 29.9) and obese (BMI≥30). For assessing body fat, we used a caliper (Saehan skinfold caliper, South Korea) to measure skinfold thickness (at seven points). The Jackson and Pollock formula was used for calculating the percentage of body fat as follows (19):

Body fat (%)=495/((1.112-(0.00043499 s)+(0.00000055 s s)-(0.00028826 a))-450

s: Sum of skinfolds at seven points, a: Age in years.

Modified Astrand-Ryhming Cycle Ergometer Test (Measurement of VO_2 Peak)

This test is a kind of ergometer test that is used for measuring VO_2 max, as a factor for determining aerobic capacity and physical fitness. The subjects were asked to avoid drinking alcohol or caffeine-containing products, smoking, and doing strenuous activity for at least 12 hours before the test. In groups with ET, a cardiopulmonary exercise test (CPET) was performed for estimating the peak power and VO_2 peak by the ergometer. The Astrand test consisted of having subjects pedal for six minutes against a constant load. This was conducted on a cycle ergometer (Monark, Ergomedic 839 E, Sweden) coupled with a gas analyzer (Cortex, Metalyzer 3B, Germany) while participants cycled in an upright position. The test consisted of a steady-state resting period, 2 minutes of warm-up without load, followed by a constant protocol in

which participants pedaled at a rate of 50 ± 5 rpm for six minutes while maintaining the heart rate (HR) between 120 and 140 bpm (20) (the HR range was required to predict VO_2 peak from the nomogram, Fig.2). Oxygen saturation (SpO_2) (pulse oximeter, Beurer, Germany), HR, oxygen uptake (VO_2), and respiratory exchange ratio (RER) were determined. Mean HR and output wattage was used to calculate the maximum oxygen consumption, and finally, the age coefficient was added to the values (21). Successful tests were defined as the completion of the 6-min test at a workload to induce HRs within the range of 120-140 bpm.

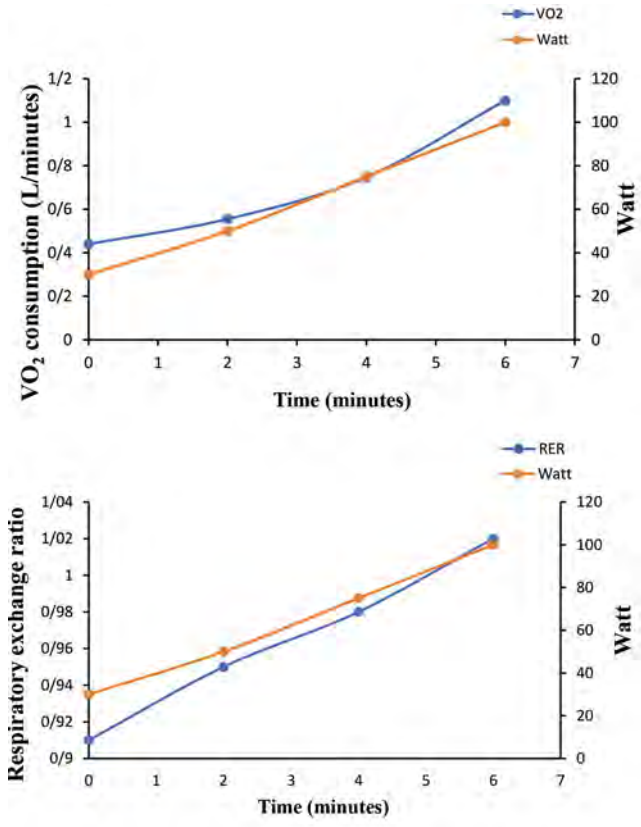

Fig.2: Oxygen uptake kinetics and changes in respiratory exchange ratio (RER) of participants in training groups in the Astrand test.

Endurance training protocol

Moderate intensity ET was performed on a cycle ergometer for six weeks, three sessions a week, in the Faculty of Sport Sciences of Shahid Bahonar University of Kerman under the guidance of an expert tutor. Based on the output wattage and the amount of oxygen consumption in the Astrand test, the first training session was performed for 15 minutes with 40% to 60% of the maximum output wattage. In subsequent sessions, an average of 2 minutes was added to the training time until the duration reached ~45 minutes. The ET duration and intensity were maintained constant at these levels in the last two weeks. Before and during training (at exercise peak), SBP, DBP, SpO_2 and HR were measured (22).

Cardiac function assessment by echocardiography

Cardiac function and hypertrophy parameters were assessed by a cardiologist. Parameters including left ventricle ejection fraction (EF), left ventricular end-systolic diameter (LVESD), left ventricular end-diastolic diameter (LVEDD), relative wall thickness (RWT), left ventricular mass (LV mass), LV mass index (LV mass per body surface area in m^2), and LV filling as measured by the early-to-late trans-mitral valve flow velocity ratio (E/A ratio) were obtained by a two-dimensional mode ultrasound machine (Philips, EPIQ, USA). Guided M-mode frames were scanned with simultaneous ECG for determination of HR. These parameters were assessed at baseline and the day after the end of the study.

Determination of total antioxidant capacity

A 5 mm fasting venous blood sample was taken from the participants at baseline and at the end of the study (day 43). The samples were centrifuged (3000 g for 10 minutes) after 20 minutes clotting time at room temperature. The ferric reducing ability of plasma (FRAP) method suggested by Benzie and Strain (1996) was used to quantify the serum TAC (23). At low pH, antioxidants present in the sample are able to reduce ferric (Fe III) tripyridyltriazine complex to an intense blue-colored ferrous (Fe II) form. This complex has a maximum absorbance at 593 nm and the blue color intensity is proportional to the antioxidant capacity of the sample. In brief, 5 µL of serum sample and 70 µL of FRAP reagent were incubated at 37˚C for 5 minutes. Then the absorbance at 593 nm was measured. For providing standard curve, known concentrations of ferrous iron were incubated with FRAP reagent and their optimal density (OD) was recorded at 593 nm to provide a concentration-response curve. Then the sample ODs were fitted on the curve to find out each serum TAC value.

Determination of serum malondialdehyde

MDA is an organic compound considered an index of cell membrane lipid peroxidation. The thiobarbituric acid (TBA) assay method was used (24). In a mixture of trichloroacetic acid (TCA) and TBA-hydrochloric acid, MDA reacts with TBA and develops a pink color with maximum absorbance at 535 nm. We used 20 ul of serum sample with the mixture mentioned above to determine MDA concentrations.

Determination of serum interlukin-6

Serum IL-6 concentration was measured by a specific human IL-6 ELISA kit (EH2IL6, Thermo Fisher Scientific,

USA). In this method, 50 µl of serum is loaded into the wells containing IL-6 antibody. Then a washing step was performed to wash the other analytes. In the next step, a substrate was added, resulting in a blue color development proportional to the amount of IL-6 in the serum. Finally, the reaction was stopped by adding the stop solution, and the amount of yellow color was assessed at a wavelength of 450 nm by an ELISA reader (DRG instrument, Cat. No. ELM-2000, Germany).

miR-21 and miR-222 measurement by RT-qPCR

miRs were measured by reverse transcription quantitative polymerase chain reaction (RT-qPCR) method. The total serum RNA was extracted using a total RNA extraction kit. Briefly, 150 µl of serum was incubated with RL buffer and then loaded into the column that specifically captured the RNA. Finally, these captured RNAs were washed from the column by RNAse-free water. The extracted RNA concentration and purity were determined by NanoDrop ND-2100 (Thermo Fisher Scientific, USA). To reduce sampling errors and normalize samples 3.5 µl Canorhabditis elegans miR-39 (cel-miR-39) was added to each sample as external control. Then, cDNA was synthesized from 5 µl extracted RNA using the microScript microRNA cDNA synthesis kit. To perform real-time PCR, we used synthesized cDNA, specific primers (for miR-21 and miR-222), and high ROX RealQ Plus Master Mix Green, and the mixture was amplified in the StepOnePlus instrument (Applied Biosystems, USA). The relative expressions of miR-21 and miR-222 were normalized to cel-miR-39 as external control. The expression was calculated as fold change according to the formula, Fold change=$2^{-\Delta\Delta CT}$, where $\Delta\Delta CT=[(CT\ gene\text{-}CT\ cel\text{-}miR\text{-}39)_{treatment}\text{-}(CT\ gene\text{-}CT\ cel\text{-}miR\text{-}39)]_{CTL}$ (25). The forward primer sequences of miRs were:

miR-21: 5′-TAGCTTATCAGACTGATGTTGA-3′

miR-222; 5′-AGCTACATCTGGCTACTGGGT-3′

cel-miR-39: 5′-UCACCGGGUGUAAAUCAGCUUG-3′

We used a universal primer that the company supplied as a reverse primer in the reactions.

Statistical analysis

Data analysis was performed by SPSS software (SPSS version 26, SPSS Inc., Chicago, IL, USA). The data distribution was determined by the Kolmogorov-Smirnov test, and if it was normal, two-way repeated measure ANOVA was used to assess the differences among the study groups, followed by Bonferroni post hoc test for pairwise comparisons. Nonparametric equivalent tests were used when the distribution of the data was not normal. Comparison of variables in each group between the baseline and its own follow up value (e.g., for HR, BMI, VO_2 peak values) was performed by the paired t test. The Chi-Square test was used for descriptive statistics (history of HTN, smoking, and the level of physical activity). $P\leq0.05$ was considered as the significance level.

Results

Anthropometric, demographic and clinical characteristics

The study groups were similar in demographic and general characteristics at baseline, and no significant differences were observed among them in these aspects (Table 1). The baseline parameters including: age (P=0.16), history of HTN (P=0.39), BMI (P=0.18), the basal level of physical activity (P=0.15), SBP (P=0.29), and DBP (P=0.09) were not significantly different among the groups. Body weight and BMI in the groups that performed ET significantly decreased ($P<0.05$) compared to the baseline values. Resting heart rates (HR) were 76 ± 1.8, 76 ± 1.9, 72 ± 1.8 and 74 ± 2.0 beats/minutes in placebo, MitoQ, ET and MitoQ+ET groups, respectively ($P>0.05$). Peak HR and baseline VO_2 in the ET group were 127 ± 2.5 beats/minutes and 3.1 ± 0.13 L/minutes, respectively; in MitoQ+ET group these values were 132 ± 2.5 beats/minutes and 3.0 ± 0.13 L/minutes, respectively. Both of these variables were in the range anticipated by executing moderate ET protocol.

Effects of MitoQ and ET on SBP and DBP

Exercise and MitoQ alone and in combination significantly decreased SBP compared to the baseline ($P<0.001$, Table 1), DBP decreased only in the combined (MitoQ+ET) group compared to the baseline ($P<0.01$).

Ventilatory parameters and body fat in hypertensive patients

Body fat percentage showed a significant decrease in the ET and the ET+MitoQ groups ($P<0.05$) compared to their baseline (Table 1). Also resting SpO_2s were 95 ± 0.1%, 93 ± 0.2%, 95 ± 0.2% and 95 ± 0.2% in the placebo, MitoQ, ET and MitoQ+ET groups, respectively ($P>0.05$). Peak SpO_2 in ET was 94 ± 0.2% and in MitoQ+ET was 93 ± 0.2%, which were both in the normal range.

Effects of MitoQ and ET on cardiac function

Table 2 shows that LV mass (normal range: 96-200 g) and LVESD (normal range: 2.5-4.0 cm) significantly decreased in the combined group compared to their pre-intervention values ($P<0.01$). However, EF (normal range: 52-72%), LV mass index (normal range: 50-102 g/m^2), LVEDD (normal range: 4.2-5.8 cm), RWT (normal range: 0.24-0.42 cm), and E/A ratio (normal value: 1.35 ± 0.5) were not changed significantly by the interventions (Table 2).

Table 1: Anthropometric, demographic and clinical characteristics of the study groups

Groups	Placebo (n=13)		MitoQ (n=13)		ET (n=13)		MitoQ+ET (n=13)	
Variable	**Baseline**	**Follow-up**	**Baseline**	**Follow-up**	**Baseline**	**Follow-up**	**Baseline**	**Follow-up**
Age (Y)	49 ± 0.7	NA	49 ± 0.7	NA	48 ± 0.9	NA	47 ± 1.1	NA
Weight (kg)	76 ± 1.5	76 ± 1.6	79 ± 2.0	79 ± 2.2	81 ± 2.4	80 ± 2.0*	83 ± 1.7	81 ± 1.7*
BMI (kg/m^2)	26 ± 0.5	26 ± 0.3	27 ± 0.5	26 ±0.6	26 ± 0.4	25 ±0.2*	27 ± 0.4	26 ± 0.3*
SBP (mmHg)	140.5 ± 1.3	139.5 ± 1.3	142.4 ± 1.4	136.8 ± 1.7***	139.6 ± 0.7	126.5 ± 1.1***	142.7 ± 1.4	128.1 ± 1.3***###
DBP (mmHg)	92 ± 1.9	90.7 ± 2	93.3 ± 1.4	89.2 ± 1.1	89.6 ± 0.9	85.6 ± 0.6	94.5 ± 1.8	89.2 ± 1.2**
Body fat (%)	23.3 ± 0.7	23.4 ± 0.8	23.9 ± 0.8	23.2 ± 0.6	25.1 ± 0.7	23.7 ± 0.7*	26.4 ± 0.8	24.9 ± 0.7*

Values are expressed as mean ± SEM. ∗; Significant vs. baseline (*; P<0.05, **; P<0.01, ***; P<0.001), #; significant vs. MitoQ follow-up (###; P<0.001), BMI; Body mass index, SBP; Systolic blood pressure, DBP; Diastolic blood pressure, and NA; Not applicable data.

Table 2: General echocardiographic and cardiac function indices at the baseline (pre-intervention) and follow-up (6 weeks) in hypertensive patients (n=52)

	Placebo (n=13)		MitoQ (n=13)		ET (n=13)		MitoQ+ET (n=13)	
Variable	**Pre-intervention**	**Follow-up**	**Pre-intervention**	**Follow-up**	**Pre-intervention**	**Follow-up**	**Pre-intervention**	**Follow-up**
EF (%)	59.6 ± 0.4	59.6 ± 0.4	60 ± 0.02	60 ± 0.02	59.2 ± 0.5	60 ± 0.01	58.8 ± 0.6	60 ± 0.03
LV mass (g)	156 ± 3.8	154 ± 3.1	175 ± 6.5	168 ± 5.5	172 ± 4.5	169 ± 6.6	188 ± 10.1	174 ± 9.3**
LV mass index (g/m^2)	87.3 ± 2.2	86.8 ± 2.8	86.8 ± 3.2	89.7 ± 2.6	84.2 ± 2.8	83.3 ± 3.4	94.3 ± 4.8	88.3 ± 5.7
LVESD (cm)	2.8 ± 0.10	2.8 ± 0.11	3.0 ± 0.08	3.0 ± 0.08	3.0 ± 0.07	2.9 ± 0.05	3.1 ± 0.08	2.9 ± 0.09*
LVEDD (cm)	4.8 ± 0.10	4.8 ± 0.11	4.9 ± 0.06	4.9 ± 0.06	4.8 ± 0.04	4.6 ± 0.07	5.0 ± 0.10	4.9 ± 0.14
RWT (cm)	0.33 ± 0.01	0.31 ± 0.01	0.32 ± 0.01	0.33 ± 0.01	0.39 ± 0.02	0.33 ± 0.01	0.36 ± 0.01	0.34 ± 0.01
E/A ratio	0.7 ± 0.07	0.7 ± 0.06	0.8 ± 0.05	0.8 ± 0.06	0.9 ± 0.05	0.9 ± 0.08	0.8 ± 0.06	0.8 ± 0.05

Data are presented as mean ± SEM. ∗; Significantly vs. baseline (pre-intervention) (∗; P<0.05, **; P<0.01), EF; Ejection fraction, LV mass; Left ventricular mass, LV mass index; Left ventricular mass index, LVESD; Left ventricular end-systolic diameter, LVEDD; Left ventricular end-diastolic diameter, RWT; Relative wall thickness, and E/A ratio; Early-to-late trans-mitral valve flow velocity ratio.

Effects of MitoQ and ET on serum TAC, MDA, and IL-6

After six weeks of ET and MitoQ intake, the serum TAC level significantly increased, and MDA and IL-6 significantly decreased in all intervention groups compared to their baseline values (P<0.001, Fig.3). The effect of combined therapy on TAC and MDA was more than the effect of ET or MitoQ alone.

Effects of MitoQ and ET on miR-21 and miR-222 expression

MitoQ, ET, and MitoQ+ET interventions caused a significant reduction in serum miR-21. ET and MitoQ+ET reduced serum miR-222 significantly as well (Fig.4).

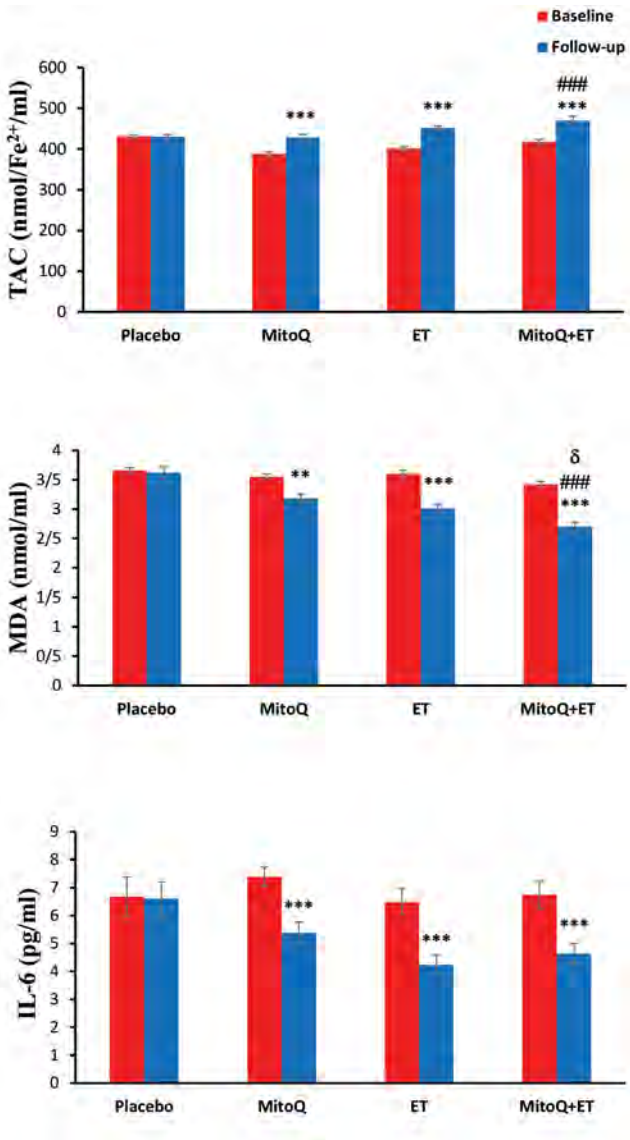

Fig.3: Serum TAC, MDA and IL-6 levels at baseline and follow-up in patients with HTN. Values are mean ± SEM. n=13 in each group. ***; P<0.001, significant difference vs. baseline, ###; P<0.001 significant difference vs. MitoQ follow-up, δ; Significant difference vs. ET follow-up, TAC; Total anti-oxidant capacity, MDA; Malondialdehyde, IL-6; Interlukine-6, HTN; Hypertension, and ET; Endurance training.

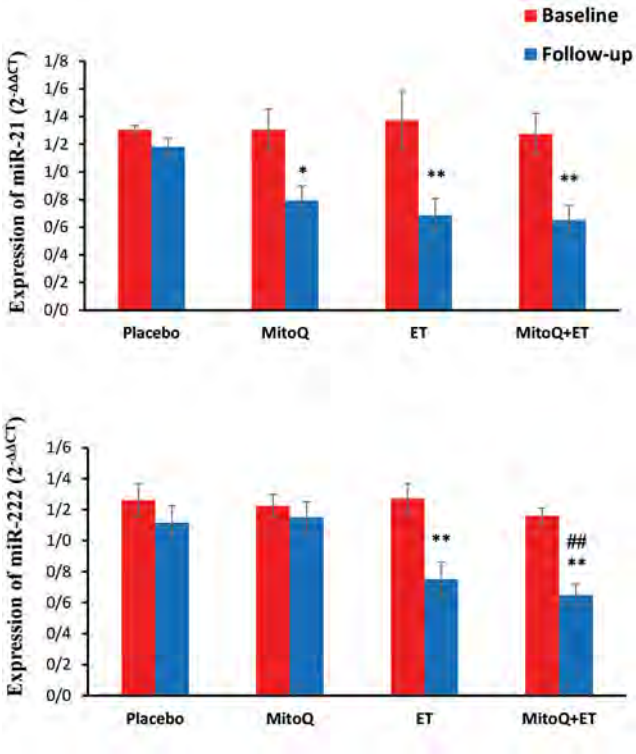

Fig.4: Relative expression (mean ± SEM) of circulating miR-21 and miR-222 in patients with hypertension, and the effect of treatment with MitoQ, ET, and MitoQ+ET combination. n=13 in each group. *; Significant difference vs. baseline (*; P<0.05, **; P<0.01), ##; P<0.01; Significant difference vs. MitoQ follow-up, and ET; Endurance training.

Discussion

The main results of the present study were that the combination of MitoQ and ET significantly decreased SBP and improved cardiac function indices, including LV mass and LVESD in hypertensive patients. Also, MitoQ, ET, and their combination reduced IL-6 levels and increased antioxidant defense capacity. Serum miR-21 levels decreased in all intervention groups, while ET and MitoQ+ET interventions reduced miR-222.

MiR-21 is related to vascular remodeling, ROS production, level of C-reactive protein (CRP), and arterial stiffness (15, 26, 27). MiR-21 was also related to left ventricular (LV) mass index in patients with HTN. Our results showed that MitoQ, ET, and their combination significantly lowered circulating miR-21 levels, which was associated with reducing LV mass and LVESD. This confirms the improving effect of ET, MitoQ, and their combined therapy on cardiac hypertrophy and on improving cardiac systolic function.

It has been well documented that oxidative stress, some miRNAs, and inflammation are involved in HTN development (4). Here, MitoQ and ET alone and in combination could reduce the expression of the two HTN-associated miRNAs, miR-21 and miR-222, caused a reduction in the inflammatory (IL-6) and oxidative (MDA) factors, and increased the antioxidant capacity (TAC) in our hypertensive participants. MitoQ and ET also reduced

SBP more efficiently when they were combined compared to their individual effects. The results are in line with our hypothesis that MitoQ, as a mitochondria-targeted antioxidant, may cause improvement in body redox state in association with reduction of miR-21 and miR-222. The more efficient effect of combination therapy in reducing HTN may be related to a more efficient reduction in MDA and a greater decrease in miR-222 expression.

On the other hand, it has been reported that exercise attenuates pro-inflammatory cytokines (IL-1, IL-6, and TNF-α) levels and increases anti-inflammatory cytokines (IL-10) (28). In this study, MitoQ and moderate ET, alone and in combination, reduced IL-6 and increased TAC serum levels in hypertensive individuals associated with lowering of miR-21 and miR-222 levels (especially miR-21). However, there are some studies whose findings are inconsistent with our results. For instance, in one study, two weeks of continuous ET (3 days/week) did not change CRP, IL-6, and IL-10 levels (29). In another study, after 16 weeks of ET, there was no change in IL-6 levels (30). Also, combined aerobic and resistance training (12 weeks) had no effects on IL-6 level (31). The discrepancies may be related to the differences in the intensity of training, which has been reported to be a determining factor affecting IL-6 release into the circulation (32). Also, the different periods and types of training may be factors that can affect the IL-6 production or release. In a study in young healthy men with MitoQ supplementation for 3 weeks during ET, it was observed that MitoQ did not affect skeletal muscle or whole-body aerobic adaptations to exercise training (33). These results verify that the responses to MitoQ may be dependent on healthy/diseased conditions, and/or the duration of supplementation. Meanwhile this study suggests that although MitoQ may not modulate the ET adaptations, it still potentiates the beneficial effects of exercise on HTN, being found in the present study.

Previous studies have proved that miR-21 exacerbates HTN by increasing IL-6 and TNF-α levels (15, 26). However, some studies have shown that miR-21 was not altered by exercise training (34). These discrepancies over miR-21 levels following exercise may be due to the different types of exercise or the sample used to measure miR-21 levels (blood or tissues). Similarly, there has been inconsistent data regarding miR-222 actions, including both its beneficial and detrimental effects. In one study on aortic endothelial cells, miR-222 caused mitochondrial dysfunction and ROS generation (16), and its inhibition reduced inflammation-induced ROS generation (35). Conversely, circulating miR-222 has been shown to be an athero-protective agent by affecting eNOS activity, thereby dilating blood vessels and lowering BP (36). It also protects cardiac tissue against ischemic injury (17). However, there is no data about the effect of MitoQ on miR-222 in human. This study showed that oral MitoQ supplementation did not change circulating miR-222 levels in hypertensive patients in spite of reducing their BP. At the same time, ET and the combination of MitoQ and ET significantly reduced miR-222 and BP levels. It seems that, unlike ET, the mechanism by which MitoQ reduces BP is independent of changes in miR-222 levels. That is why the BP lowering effect of MitoQ is added to the BP lowering effect of ET without more reduction in the level of miR-222 when they are combined.

Regarding the effect of exercise on miR-222, a study showed that circulating miR-222 increased after acute exhaustive cycling exercise (37). In the present study, in which the participants performed moderate ET, a reduction in the circulating miR-222 was observed. It seems that the expression of this miRNA and its beneficial/detrimental effects depend on the type, intensity, and duration of exercise (38).

We acknowledge the limitations of our study. Due to ethical considerations, we could not include patients with more severe HTN in the study as otherwise we had to discontinue their medications and put them at a high risk when performing ET. MitoQ may be found more effective in lowering BP in patients with more severe HTN, especially when combined with ET. Also, in a study with a higher sample size the effect of MitoQ may be more pronounced and the results may strengthen. Moreover, higher doses of MitoQ and more extended periods of treatment may show better outcomes. These modalities need further investigation.

Conclusion

Overall, the data from this study showed that concurrent moderate ET and MitoQ significantly reduced BP, MDA, and IL-6 serum levels in HTN subjects. It also increased TAC and either improved the antioxidant status or reduced free radicals. Other outcomes were reduction in serum miR-21 and miR-222 levels in hypertensive subjects, which was associated with improvement in cardiac LV mass index and systolic function. More studies with higher doses of MitoQ and more extended periods of treatment, alone and in combination with ET, are needed to further clarify the effects of these interventions on BP of patients with different levels of HTN.

Acknowledgements

The data presented in this paper are part of the thesis of Mr. Yaser Masoumi-Ardakani, Ph.D. candidate in Human Physiology. We are grateful to the Vice-Chancellor for Research and Technology of Kerman University of Medical Sciences, Kerman, Iran, for funding the research project (Grant No. IR.KMU.REC.97000973). We want to thank MitoQ Company for providing the MitoQ supplement. The authors declare no conflict of interest.

Authors' Contributions

H.N., Y.M.-A.; Contributed to the conception and design of the study. H.N.; Supervised the project. Y.M.-A., S.A., Z.S.; Wrote the first draft of the manuscript. H.R.N., Sh.J.; Performed the clinical examinations and helped in the interpretation of the echocardiography results. Y.M.-A., S.J., S.A., Z.S.; Performed data collection. All authors

contributed in reviewing and finalizing the manuscript.

References

1. Dorans KS, Mills KT, Liu Y, He J. Trends in prevalence and control of hypertension according to the 2017 american college of cardiology/american heart association (ACC/AHA) guideline. J Am Heart Assoc. 2018; 7(11): e008888.
2. Rajati F, Hamzeh B, Pasdar Y, Safari R, Moradinazar M, Shakiba E, et al. Prevalence, awareness, treatment, and control of hypertension and their determinants: results from the first cohort of noncommunicable diseases in a Kurdish settlement. Sci Rep. 2019; 9(1): 12409.
3. Tsai JC, Yang HY, Wang WH, Hsieh MH, Chen PT, Kao CC, et al. The beneficial effect of regular endurance exercise training on blood pressure and quality of life in patients with hypertension. Clin Exp Hypertens. 2004; 26(3): 255-265.
4. Bátkai S, Thum T. MicroRNAs in hypertension: mechanisms and therapeutic targets. Curr Hypertens Rep. 2012; 14(1): 79-87.
5. Drenth J, Van Uum S, Van Deuren M, Pesman GJ, Van der Ven-Jongekrijg J, Van der Meer J. Endurance run increases circulating IL-6 and IL-1ra but downregulates ex vivo TNF-alpha and IL-1 beta production. J Appl Physiol. 1995; 79(5): 1497-1503.
6. Sponder M, Campean IA, Emich M, Fritzer-Szekeres M, Litschauer B, Bergler-Klein J, et al. Long-term endurance training increases serum cathepsin S and decreases IL-6 and hsCRP levels. J Sports Sci. 2017; 35(21): 2129-2134.
7. Gaeini A, Sheykh Aleslami Vatani D, Alameh AA, Ravasi AA, Kordi MR, Mogharnasi M, et al. Effect of endurance training and a detraining period on lipid peroxidation and antioxidant system in wistar rats. Journal of Movement Science and Sports. 2008; 6(11): 51-63.
8. Dantas FFO, Brasileiro-Santos MdS, Batista RMF, do Nascimento LS, Castellano LRC, Ritti-Dias RM, et al. Effect of strength training on oxidative stress and the correlation of the same with forearm vasodilatation and blood pressure of hypertensive elderly women: a randomized clinical trial. PLoS One. 2016; 11(8): e0161178.
9. Fatouros IG, Jamurtas AZ, Villiotou V, Pouliopoulou S, Fotinakis P, Taxildaris K, et al. Oxidative stress responses in older men during endurance training and detraining. Med Sci Sports Exerc. 2004; 36(12): 2065-2072.
10. Eirin A, Lerman A, Lerman LO. Enhancing mitochondrial health to treat hypertension. Curr Hypertens Rep. 2018; 20(10): 1-8.
11. Graham D, Huynh NN, Hamilton CA, Beattie E, Smith RA, Cochemé HM, et al. Mitochondria-targeted antioxidant MitoQ10 improves endothelial function and attenuates cardiac hypertrophy. Hypertension. 2009; 54(2): 322-328.
12. Junior RFR, Dabkowski ER, Shekar KC, Hecker PA, Murphy MP. MitoQ improves mitochondrial dysfunction in heart failure induced by pressure overload. Free Radic Biol Med. 2018; 117: 18-29.
13. Rossman MJ, Santos-Parker JR, Steward CAC, Bispham NZ, Cuevas LM, Rosenberg HL, et al. Chronic supplementation with a mitochondrial antioxidant (MitoQ) improves vascular function in healthy older adults. Hypertension. 2018; 71(6): 1056-1063.
14. Santulli G. microRNA: medical evidence. From molecular biology to clinical practice. 1st ed. New York: Springer; 2015; 215-235.
15. Li X, Wei Y, Wang Z. microRNA-21 and hypertension. Hypertens Res. 2018; 41(9): 649-661.
16. Xue Y, Wei Z, Ding H, Wang Q, Zhou Z, Zheng S, et al. MicroRNA-19b/221/222 induces endothelial cell dysfunction via suppression of PGC-1α in the progression of atherosclerosis. Atherosclerosis. 2015; 241(2): 671-681.
17. Ding S, Huang H, Xu Y, Zhu H, Zhong C. MiR-222 in cardiovascular diseases: physiology and pathology. Biomed Res Int. 2017; 2017: 4962426.
18. Najafipour H, Kahnooji M, Baneshi MR, Yeganeh M, Ahmadi Gohari M, Shadkam Farokhi M, et al. The prevalence and 5-Year incidence rate of low physical activity in an urban population of 10,000 in southeastern Iran: relationship with other cardiovascular risk factors. J Phys Act Health. 2020; 17(4): 435-442.
19. Da Fonseca PHS, Marins JCB, Da Silva AT. Validation of anthropometric equations for the estimation of body density in professional soccer players. Rev Bras Med Esporte. 2007; 13(3): 135e-138e.
20. Pescatello LS. ACSM's guidelines for exercise testing and prescription. 9th ed. Philadelphia: Wolters Kluwer/Lippincott Williams & Wilkins Health; 2014; 1-456.
21. Liguori G. ACSM's guidelines for exercise testing and prescription. 11th ed. Wolters Kluwer; 2020; 541.
22. Pescatello LS, MacDonald HV, Lamberti L, Johnson BT. Exercise for Hypertension: a prescription update integrating existing recommendations with emerging research. Curr Hypertens Rep. 2015; 17(11): 87.
23. Benzie IF, Strain JJ. The ferric reducing ability of plasma (FRAP) as a measure of "antioxidant power": the FRAP assay. Anal Biochem. 1996; 239(1): 70-76.
24. Janero DR. Malondialdehyde and thiobarbituric acid-reactivity as diagnostic indices of lipid peroxidation and peroxidative tissue injury. Free Radic Biol Med. 1990; 9(6): 515-540.
25. Hijmans JG, Diehl KJ, Bammert TD, Kavlich PJ, Lincenberg GM, Greiner JJ, et al. Association between hypertension and circulating vascular-related microRNAs. J Hum Hypertens. 2018; 32(6): 440-447.
26. Fernandes T, Magalhães FC, Roque FR, Phillips MI, Oliveira EM. Exercise training prevents the microvascular rarefaction in hypertension balancing angiogenic and apoptotic factors: role of microRNAs-16,-21, and-126. Hypertension. 2012; 59(2): 513-520.
27. Wei C, Li L, Kim I, Sun P, Gupta S. NF-κB mediated miR-21 regulation in cardiomyocytes apoptosis under oxidative stress. Free Radic Res. 2014; 48(3): 282-291.
28. Tao L, Bei Y, Zhang H, Xiao J, Li X. Exercise for the heart: signaling pathways. Oncotarget. 2015; 6(25): 20773.
29. McLachlan J, Beattie E, Murphy MP, Koh-Tan CH, Olson E, Beattie W, et al. Combined therapeutic benefit of mitochondria-targeted antioxidant, MitoQ10, and angiotensin receptor blocker, losartan, on cardiovascular function. J Hypertens. 2014; 32(3): 555-564.
30. Libardi CA, De Souza GV, Cavaglieri CR, Madruga VA, Chacon-Mikahil MPT. Effect of resistance, endurance, and concurrent training on TNF-α, IL-6, and CRP. Med Sci Sports Exerc. 2012; 44(1): 50-56.
31. Stewart LK, Flynn MG, Campbell WW, Craig BA, Robinson JP, Timmerman KL, et al. The influence of exercise training on inflammatory cytokines and C-reactive protein. Med Sci Sports Exerc. 2007; 39(10): 1714-1719.
32. Tunc-Ata M, Turgut G, Mergen-Dalyanoglu M, Turgut S. Examination of levels pentraxin-3, interleukin-6, and C-reactive protein in rat model acute and chronic exercise. J Exerc Rehabil. 2017; 13(3): 279-283.
33. Shill DD, Southern WM, Willingham TB, Lansford KA, McCully KK, Jenkins NT. Mitochondria-specific antioxidant supplementation does not influence endurance exercise training-induced adaptations in circulating angiogenic cells, skeletal muscle oxidative capacity or maximal oxygen uptake. J Physiol. 2016; 594(23): 7005-7014.
34. Mooren FC, Viereck J, Krüger K, Thum T. Circulating microRNAs as potential biomarkers of aerobic exercise capacity. Am J Physiol Heart Circ Physiol. 2014; 306(4): H557-H563.
35. Song J, Ouyang Y, Che J, Li X, Zhao Y, Yang K, et al. Potential value of miR-221/222 as diagnostic, prognostic, and therapeutic biomarkers for diseases. Front Immunol. 2017; 8: 56.
36. Suárez Y, Fernández-Hernando C, Pober JS, Sessa WC. Dicer dependent microRNAs regulate gene expression and functions in human endothelial cells. Circ Res. 2007; 100(8): 1164-1173.
37. Ultimo S, Zauli G, Martelli AM, Vitale M, McCubrey JA, Capitani S, et al. Cardiovascular disease-related miRNAs expression: potential role as biomarkers and effects of training exercise. Oncotarget. 2018; 9(24): 17238.
38. Zhou Q, Shi C, Lv Y, Zhao C, Jiao Z, Wang T. Circulating microRNAs in response to exercise training in healthy adults. Front Genet. 2020; 11: 256.

Original Article

Itaconic Acid as A Differential Transcription Regulator of Apoptosis and Autophagy Pathways Genes: A Rat Adipose Mesenchymal Stem Cells Model

Mohammad Reza Tabandeh, Ph.D.[1]*, Fatemeh Soroush, D.V.M.[1], Dian Dayer, Ph.D.[2]

1. Department of Basic Sciences, Division of Biochemistry and Molecular Biology, Faculty of Veterinary Medicine, Shahid Chamran University of Ahvaz, Ahvaz, Iran
2. Cellular and Molecular Research Center, Medical Basic Sciences Institute, Ahvaz Jundishapur University of Medical Sciences, Ahvaz, Iran

**Corresponding Address: P.O.Box: 61355-145, Department of Basic Sciences, Division of Biochemistry and Molecular Biology, Faculty of Veterinary Medicine, Shahid Chamran University of Ahvaz, Ahvaz, Iran*
Email: m.tabandeh@scu.ac.ir

Received: 20/October/2021, Accepted: 23/February/2022

Abstract

Objective: Itaconate, a novel regulatory immunometabolite, is synthesized by inflammatory macrophage. It acts as an anti-inflammatory mediator and regulates several metabolic and signaling pathways particularly Nrf2 pathway. The immunometabolites can affect the stemness potency, differentiation ability and viability of stem cells, but little is known about the critical function of Itaconate on the stem cell fate. The objective of the present study was to determine the regulatory effects of Itaconic acid on the cell viability and transcription of apoptosis and autophagy pathways genes in the rat adipose derived mesenchymal stem cells (ADMSCs).

Materials and Methods: In this experimental study, the ADMSCs were incubated with 125 µM and 250 µM dimethyl itaconate (DMI) for 24 hours or 48 hours. The expression of apoptosis pathway genes (*Bax, Bcl2, Caspase 3, Fas, Fadd* and *Caspase 8*) and autophagy pathway genes (*Atg12, Atg5, Beclin, Lc3b* and *P62*) were determined using real time polymerase chain reaction (PCR) assay. Using the ELISA method, cellular level of phospho-NRF2 protein was measured.

Results: The results indicated that DMI increased the expression of NRF2 protein, altered the expression of some apoptosis genes (*Fadd, Bax* and *Bcl2*), and changed the expression of some autophagy related genes (*Lc3b, Becline* and *P62*) in ADMSCs. DMI had no obvious effect on the transcription of caspases enzymes.

Conclusion: Because autophagy activation and apoptosis suppression can protect stem cells against environmental stress, it seems Itaconate can affect the functions and viability of ADMSCs via converse regulation of these pathways.

Keywords: Adipose Derived Mesenchymal Stem Cells, Apoptosis, Autophagy, Itaconate

Cell Journal(Yakhteh), Vol 24, No 10, October 2022, Pages: 586-595

Citation: **Tabandeh MR, Soroush F, Dayer D. Itaconic acid as a differential transcription regulator of apoptosis and autophagy pathways genes: a rat adipose mesenchymal stem cells model. Cell J. 2022; 24(10): 586-595. doi: 10.22074/cellj.2022.8320.**

Introduction

Treatment application of mesenchymal stem cells (MSCs) for various diseases has been remarkably increased. The adipose derived MSCs (ADMSCs) are a type of adult stem cells with unique ability of proliferation, differentiation and immuno-modulation. ADMSCs have been regarded as excellent sources for cell therapy, tissue regeneration and autologous transplantation (1). ADMSCs are one of the best sources of MSCs due to simple isolation and abundant in number (2).

Recent studies have revealed a complex interaction between the inflammatory cells and MSCs. Interaction between MSCs and the inflammatory environment plays an important role in the regulating immune responses against transplanted cells. Although, the interaction between MSCs and immune cells have been confirmed in previous studies, there is little insight into the specific effect of the inflammatory immunometabolites on the MSCs fate. However, this molecular interaction is one main future area of research (3). MSCs have a dual effect on the inflammation process; depending on the environmental conditions they can intensify or alleviate the inflammation process (4, 5). MSCs regulate the function of innate and adaptive immune systems by affecting the inflammatory microenvironment. The immune factors secreted by inflammatory cells have various impacts on the MSCs phenotype such as stemness potency, differentiation ability, viability and efficiency of transplantation (3, 6). Several studies have demonstrated that long-term culture of MSCs can alter the proliferation potency and vital activity of MSCs by affecting the autophagy and apoptosis pathways (7). Autophagy and apoptosis are two evolutionarily conserved processes that play a crucial role in the stem cell fate determination. Apoptosis or programmed cell death is induced by death receptor-dependent (extrinsic) or mitochondrial (intrinsic) pathways. The extrinsic pathway is activated by TNF family ligands, while the intrinsic pathway is activated by different factors such as UV irradiation, chemotherapy, growth factor withdrawal

or cytokine deprivation (8). Autophagy contributes to the routine turnover of cytoplasmic components, and as part of tissue homeostasis. Different protein complexes control the formation and activation of the autophagosome. *Atg15*, *Atg5* and *Lc3b-II* genes are responsible for the formation of mature autophagosome. The P62 is an important autophagy protein that delivers ubiquitinated proteins to the proteasome for degradation and facilitates nuclear and cytosolic protein quality control (9). Autophagy can regulate different cellular processes in the stem cells, including self-renewal, differentiation, senescence, and apoptosis. Expression of several cellular proteins, including transcription factors, adhesion molecules and secreted proteins which are essential for self -renewal and stem cell differentiation are controlled by autophagy pathway (8, 9). It has been reported that autophagy helps cells survive during prolonged starvation and other microenvironment stresses. Recent studies have indicated that autophagy can act either as an inducer or as a suppressor of differentiation and apoptosis process in the MSCs (10, 11). Several effects of inflammatory factors on the MSCs are mediated through the regulation of apoptosis and autophagy pathways. Dang et al. (12) demonstrated that sepsis-induced inflammation stimulates autophagy and apoptosis in MSC. Generally, up-regulation of autophagy-related genes following oxidative stress and nutritional deprivation help MSCs to increase their survival. Following autophagy activation, defective mitochondria are removed by the autophagosomes and the production of free radicals that stimulate the inflammatory cytokine production are suppressed (9).

Previous studies have shown that immune cells produced several inflammatory mediators that affect stem cell functions and fate (3). Macrophages, a critical cell of the immune system can affect the cellular homeostasis in response to different microenvironmental cues. Recently, the complex cross-talk between MSCs functions and macrophages has been reported. MSCs affect macrophage polarization by secreting various factors such as IL-6, prostaglandin E2 (PGE2) and exosome (13). Recent studies have also shown that macrophages can also affect MSCs viability, proliferation and differentiation by secretion of various immune factors, indicating a critical interaction between MSCs and macrophages under the physiological condition (14).

Since anti-inflammatory effect, Itaconate, an immunometabolite, has attracted much attention. Itaconate is synthesized in response to LPS and certain infections by macrophages. The immune-responsive gene 1 (*Irg-1*) is expressed in mammalian macrophages under inflammatory conditions and encodes the mitochondrial enzyme cis-aconitic acid decarboxylase (CAD). CAD in turn catalyzes the cis-aconitic acid decarboxylation to produce itaconate during the tricarboxylic acid (TCA) cycle (15, 16). The process of itaconate production is also activated in myeloid cells under inflammatory conditions (17, 18). Recent published studies indicated that itaconate and its cell permeable derivatives, dimethyl itaconate (DMI) and 4-octyl itaconate (OI) markedly suppress the production of pro-inflammatory mediators in the lipopolysaccharide-treated macrophages and inflammatory associated diseases (19). Several molecular mechanisms have been reported for anti-inflammatory actions of itaconate in macrophage, including (node like receptor family pyrin domain containing 3 (NLRP3) inflammasome suppression, mitochondrial reactive oxygen species (ROS) production inhibition, NFκβ inflammatory pathway inactivation and nuclear factor erythroid 2-related factor 2 (NRF2) activation (20, 21). Previous studies have shown the anti-inflammatory actions of itaconate in the immune cells, to our knowledge, no study has yet been conducted to detect the effect of itaconate or its derivatives on the MSCs functions and fate. Therefore, the present study was designed to identify the effect of DMI on the vital activity and expression of apoptosis and autophagy related genes in the rat ADMSCs.

Materials and Methods

All animal work was carried out with approval from the Ethics Committee for research in animals and humans of Shahid Chamran University of Ahvaz (ee/97.24.03.93442/scu.ac.ir). Working with animals was also carried out on the basis of the guideline for the care and use of laboratory animals (NIH publication no. 86-23).

Animals

In this experimental study, six Sprague Dawley rats (8 weeks old, ~180 g) were obtained from the center of laboratory animals of the faculty of veterinary medicine of Shahid Chamran University of Ahvaz, Khozestan, Iran. They were kept under our animal facilities (22 ± 1℃), with a 12-hours light: 12-hours dark cycle beginning at 7:00 a.m. During experiments, the animals had free access to water and rat pellet diet (Pars, Tehran, Iran). Animals were euthanized with a combination of ketamine hydrochloride (Alfasan, Nederland) and xylazine (Alfasan, Nederland) (100 mg/kg of Ketamine and 10 mg/kg of Xylazine).

Isolation and culture of ADMSCs

Adipose tissue was surgically attained from the inguinal and epididymal fat pads and sliced into small pieces. The adipose tissues were digested with DMEM-HG medium (BI-1001, Bioidea, Iran) containing 0.1% collagenase type 1 (C0130, Sigma-Aldrich, USA) and 1% penicillin/streptomycin (BI-1230, Bioidea, Iran) for 40 minutes at 37°C in a shaking bath. Collagenase was neutralized by adding DMEM-HG containing 10% fetal bovine serum (FBS, BI-1201, Bioidea, Iran) and centrifuged at 1200 × rpm for 7 minutes to obtain a pellet. The supernatant was removed and precipitated cells were re-suspended in the DMEM-

HG medium containing 15% FBS and1% penicillin/streptomycin (BI-1230, Bioidea, Iran) and seeded in 25 cm^2 culture flask and incubated at 37˚ C with 5% CO_2. The residual non-adherent red blood cells were removed by washing with the DMEM-HG medium. The medium was changed every 3 days and after the cells reached the third passage, the cells were passaged using 0.25% trypsin-EDTA (BI-1602, Bioidea, Iran). The cells in the third passage were used for the next steps of the experiment.

Identification of ADMSCs phenotype

To confirm the phenotype of ADMSCs, the expression of CD31, CD44, CD45 and CD90 surface markers was determined using the flow cytometry method as described previously. To determine the lineage differentiation potency of ADMSCs, the cells were cultured in osteogenic and adipogenic differentiation medium for 14 days as described previously. Then the cells were fixed with 4% Paraformaldehyde (158127, Sigma-Aldrich, USA) for 10 minutes and stained with 40 m*M* Alizarin Red (58005, Merck, USA) or 0.5% Oil Red O (23125, Merck, USA) to identify the calcium deposition and fat droplet formation (22).

Treatment of ADMSCs with itaconate

The third passage of ADMSCs was seeded at a density of 1.5×10^5 cells/ml in the DMEM-LG medium containing 125 µM and 250 µM of DMI for 24 hours or 48 hours The culture media were supplemented with 5 % FBS and 1% pen/strep antibiotics. Compounds were prepared as 125 µM and 250 µM stock solutions in cell media and diluted directly into the culture media. DMI was prepared directly in the DMEM-HG cell media in order to avoid solvent effects. Control cells were cultured in the absence of DMI for the indicated times. At the end of experimental periods, the cells were detached using 0.25% Trypsin-EDTA (BI-1602, Bioidea, Iran) and used for subsequent experiments. We performed all experiments using 125 uM and 250 uM of DMI a dose shown to reduce LPS-induced inflammation in previous studies (17, 23).

Effect of DMI on cell proliferation

A sulforhodamine B (SRB) assay was performed to examine cell proliferation. Briefly, ADMSCs were seeded in 96-well plates in DMEM-LG (BI-1002, Bioidea, Iran) growth medium at a density of 5000 cells/well, respectively and settled overnight at 37˚C with 5% CO_2. The cells were then treated with 125 uM and 250 uM of DMI. At days 1, 3, 5 and 7 after DMI treatment, cells were fixed with cold 10% (w/v) Trichloroacetic acid (TCA) (T6399, Merck, Germany). The plates were washed with water, stained with 0.4% SRB (w/v, dissolved in 1% acetic acid) (10056, Merck, USA) and washed with 1% acetic acid (10056, Merck, USA). The protein-bound dye was subsequently dissolved in 10 mmol/L Tris-HCl (252859, Sigma Aldrich, USA). Absorbance values at 540 nm were recorded using a colorimetric plate reader (SP2, BioTek, USA) (24).

RNA extraction and cDNA synthesis

The RNAs were extracted using the RNX isolation reagent (EX6101, SinaClon, Iran) according to manufacturer's protocol. The samples were treated with DNase I enzyme (mo5401, SinaClon, Iran) to avoid DNA contamination. The quality and concentration of the extracted RNAs were assessed using a NanoDrop (2000c, Thermo Scientific, USA). High pure RNA, *OD* 260/280 ratios ≥1.8, was used for cDNA synthesis. The cDNA was synthesized using YTA cDNA synthesis kit (YT4500, Yekta Tajhiz, Iran) and random hexamer primer (YT4550, Yekta Tajhiz, Iran) by using 0.5 µg of RNA as recommended by the manufacturer.

Real time polymerase chain reaction assay

Real-time polymerase chain reaction (PCR) was performed using the StepOnePlus™ Real-Time PCR System (StepOnePlus™, Applied Biosystems, USA) by the qPCR™ Green Master Kit for SYBR Green I® (YT2551, Yektatajhiz, Iran). The primers were designed using the Primer3 software version 4.1.1 (Table 1). Relative expression levels of the target genes were compared to rat *Gapdh* as a housekeeping gene. The thermal program was consisted of 95˚C for 5 minutes, followed by 40 cycles of 94˚C for 15 seconds, 60˚C for 15 seconds and 72˚C for 30 seconds. All experiments were performed in triplicate. Two separate reactions without cDNA or with RNA were performed in parallel as controls. The results were analyzed by comparative $2^{-\Delta\Delta Ct}$ method using Lightcycler 96® software.

Determination of nuclear NRF2 protein

The nuclear NRF2 protein concentration was measured using Nuclear/Cytosol Fractionation Kit (K266, Biovision, USA) as recommended by the manufacturer. Protein concentration of the nuclear fraction was estimated using the Bradford method. NRF2 concentration was determined using rat specific NWLSS™ NRF2 ELISA kit (NWK-NRF2H, Northwest Life Science Specialties, Canada) and the concentration was expressed as ng/10^6 cells. All experiments were performed in duplicates.

Statistical analysis

Statistical analysis was conducted using GraphPad Prism8 software (GraphPad Software, Inc., San Diego, CA). All data were presented as mean ± standard deviation (SD). The normality of data or equality of error variances was determined using Shapiro–Wilk or Levene's tests. Two-way analysis of variance (ANOVA) was used to determine the interactions of sampling times and DMI concentration on each factor. Mean values were compared between different treated groups at different time points using one-way ANOVA and Tukey multiple-comparison post hoc tests. A statistically significant difference between different experimental groups at each sampling time was represented as follows: *P<0.05, **P<0.01, ***P<0.001, and ****P<0.0001.

Table 1: Characteristics of primers that used in the present study

Gene name	Primer sequences (5´-3´)	Size (bp)	GenBank accesion No
Gapdh	F: AGTTCAACGGCACAGTCAAG R: TACTCAGCACCAGCATCACC	119	XM_017593963.1
Caspase 3	F: CTATCCATGGAAGCAAGTCGATG R: TTGCGAGCTGACATTCCAGT	136	NM_012922.2
Bcl2	F: ATCGCTCTGTGGATGACTGAGTAC R: AGAGACAGCCAGGAGAAATCAAAC	135	NM_016993.2
Bax	F: ATCGCTCTGTGGATGACTGAGTAC R: AGAGACAGCCAGGAGAAATCAAAC	144	NM_017059.2
FADD	F: AGGGATCTGTGAGCAAGAGT R: GGCACTTGGTGCTACATCAT	143	AJ441127.1
FASL	F: AGCACACCCTCTGAAACCAA R: ATACGAAGTACAACCCAGCCTC	172	NM_012908.1
Caspase 8	F: AGGTTTCTGCCTACAGGGTT R: GCTCGAGTTGTCTTGCAGTT	125	XM_039084164.1
P62	F: CAGCTGCTGTCCGTAGAAATTG R: ACCCGCTCTTTCAGCTTCAT	113	NM_130405.2
Beclin1	F: TCAGGAACTCACAGCTCCATT R: ACCATCCTGGCGAGTTTCAA	112	NM_053739.2
Atg5	F: GAGAAGCAGAGCCATACTATTTGC R: TTTCAGGGGTGTGCCTTCAT	146	NM_001014250.1
Atg12	F: TGTCCAAGCACTCATCGACTT R: CCATCACTGCCAAAACACTCAT	141	NM_001038495.1
LC3	F: GACAGCACTGGCTGTTACAT R: AGCAGAGGCTTGCTTTAGTTG	109	XM_017601351.1

Results

Characterization of isolated ADMSC

To determine the phenotype of isolated ADMSCs, we determine their morphology, surface markers expression and differentiation potency. Flow cytometry analysis revealed ADMCs were positive for expression of cluster of differentiation (CD) CD90 and CD105, but negative for CD31 and CD45 (Fig.1A). In passage 3, ADMCs exhibited a spindle-shaped morphology (Fig.1B1). To investigate the differentiation capacity of isolated ADMSCs, cells were cultured in the osteogenic and adipogenic differentiating media and lineage potential was tested by staining for the typical lineage markers. Osteogenesis was determined by a bone-type marker, Alizian red staining (Fig.1B2) and adipogenesis was stained with oil Red O, cytoplasmic lipid droplets (Fig.1B3). These results confirmed that isolated ADMSCs successfully differentiate into the multiple cell types including osteoblasts and adipocytes.

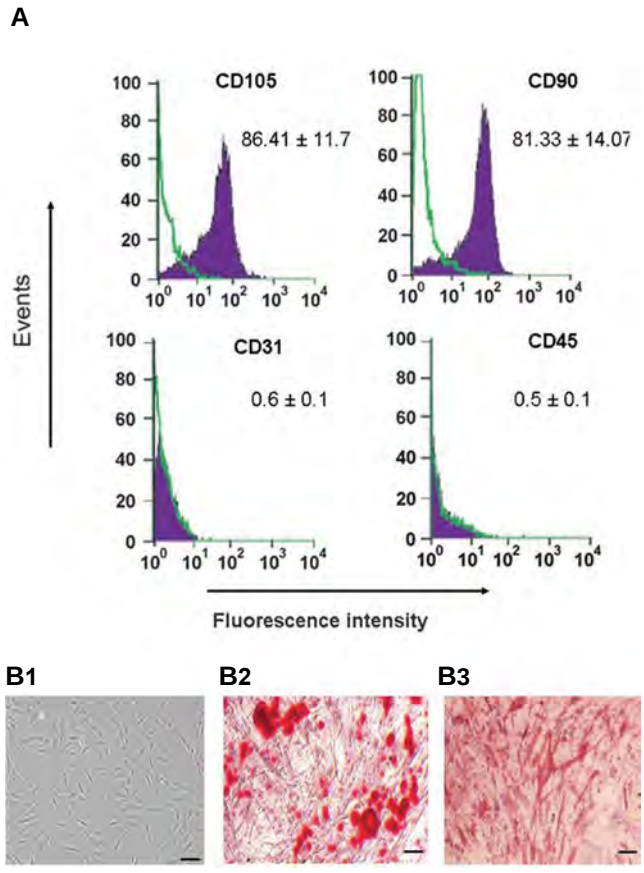

Fig.1: Characterization of adipose derived mesenchymal stem cells (ADMSCs) isolated from epididymal and inguinal adipose fat pads of rats. **A.** Flow cytometer analysis revealed the positive expression of CD105 and CD90 and negative expression of CD31 and CD45 in the ADMSCs. **B1.** Morphology of cultured ADMSCs. ADMSCs exhibited spindle-shaped morphology. **B2.** Osteogenic differentiation was confirmed by Alizian red staining. **B3.** Adipogenesis was detected by accumulated lipid vacuoles within the cytoplasm that stained with oil red O (scale bar: 50 µm, magnification: 100×). Numbers on graphs represents the percentage of cells that express each cell surface marker.

Effect of DMI on cell proliferation and nuclear Nrf2 concentration

We observed that ADMSCs exposure to a dose of 125 uM DMI resulted in higher cell density at days 3, 5 and 7 after treatment in comparison with the untreated cells ($P<0.05$). ADMSCs that treated with 250 µM DMI showed higher cell density at day 3, 5 and 7 after exposure in comparison with the untreated cells and cells treated with another dose of DMI ($P<0.01$, $P<0.001$, Fig.2A). These findings indicated that DMI could increase the cell proliferation in a dose dependent manner in MSCs.

Because it has been previously found that DMI exerts its effects in other cells through the NRF2 pathway, we determined the nuclear levels of NRF2 in DMI treated ADMSCs to determine the activation of the NRF2 pathway by DMI in ADMSCs. Our results showed that DMI in a dose and time dependent manner could increase the nuclear level of NRF2 protein in ADMSCs in comparison with untreated cells. DMI at a dose of 250 µM for 48 hours. had the maximal stimulatory effect on the translocation of NRF2 protein to nucleus compared to other dose and incubation time ($P<0.0001$, $P<0.001$, Fig.2B).

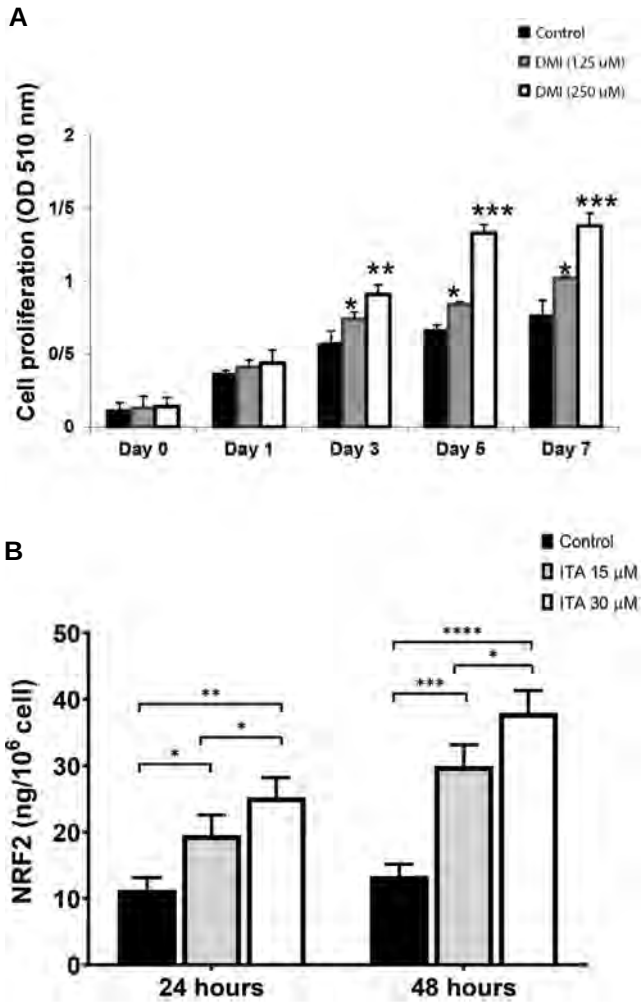

Fig.2: Evaluation of cell proliferation and cellular NRF2 protein levels in the dimethyl itaconate (DMI) treated adipose derived mesenchymal stem cells (ADMSCs). **A.** Cell proliferation assay using Sulforhodamine B method. ADMSCs proliferation was assessed up to 7 days, in the presence of 125 µM and 250 µM of DMI. **B.** The nuclear concentration of NRF2 protein in the ATDMCs following different treatment. For each concentration, the mean ± SD for at least three independent experiments is represented. *, **, ***, **** represent the significant difference between DMI treated groups and the control group at $P<0.05$, $P<0.01$, $P<0.001$ and $P<0.0001$, respectively.

Effect of DMI on transcription of external apoptosis pathway genes

Treatment of ADMSCs with both concentrations of DMI significantly reduced the *Fadd* expression after 24 hours and 48 hours exposure in comparison with the untreated group ($P<0.01$, $P<0.001$). Down regulation of the *Fadd* transcription level after exposure to 250 µM DMI at 48 hours was more than 24 hours time period ($P<0.01$, Fig.3A). Treatment of ADMSCs with both concentrations of DMI at 24 hours and 48 hours had no significant effect on the genes expression, *Fasl* and *Caspase 8* (Fig.3B, C).

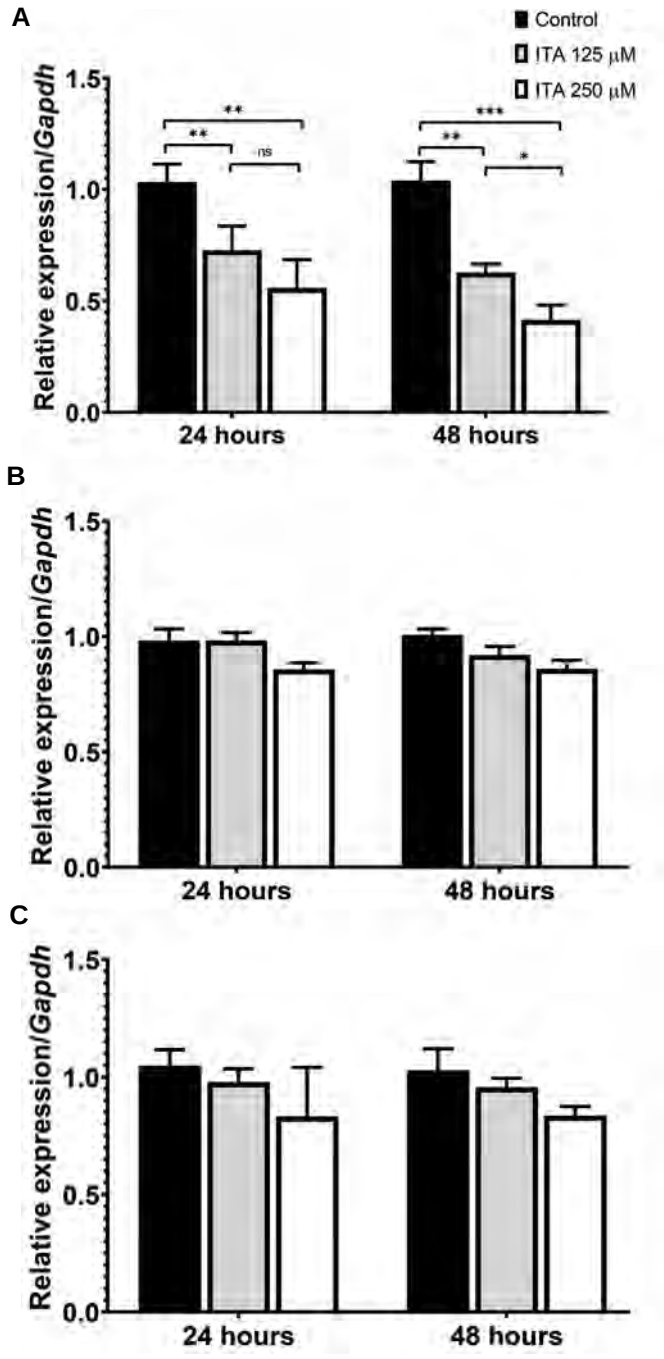

Fig.3: The mRNA levels of *Fadd*, *Fasl* and *Caspase 8* in adipose derived mesenchymal stem cells (ADMSCs) following different treatment. **A.** *Fadd*, **B.** *Fasl*, and **C.** *Caspase 8. Gapdh* was used as a housekeeping gene. *, **, *** represent the significant difference between dimethyl itaconate (DMI) treated groups and the control group at P<0.05, P<0.01, and P<0.001, respectively. ns; Non significant.

Effect of DMI on transcription of internal apoptosis pathway genes

Our results revealed that exposure of ADMSCs with the 125 μM DMI for 24 hours or 48 hours had no significant effect on the transcription level of the *Bax* gene (Fig.4A). DMI at a dose of 250 uM caused a downregulation of the *Bax* gene in the ADMSCs at both incubation times in comparison with the untreated cells (P<0.01, P<0.001) and down regulation of *Bax* transcription level in 48 hours was more than 24 hours time period (P<0.01, Fig.4A). ADMSCs cells that treated with the 250 μM DMI for 24 hours or 48 hours showed a significant increase in the mRNA level of the antiapoptotic *Bcl2* gene in comparison with the untreated cells (P<0.001, P<0.0001, Fig.4B). Treatment of ADMSCs cells with the 125 μM DMI for 24 hours had no significant effect on the transcription level of the *Bcl2* gene (P<0.01, Fig.4B). The highest upregulation of the *Bcl2* transcription level was observed in the ADMSCs after exposure to the 250 μM DMI for a 48 hours time period (P<0.0001, Fig.4B). Our results showed that treatment of ADMSCs with both doses of DMI in the different time periods had no significant effect on the *Caspase 3* expression level (Fig.4C).

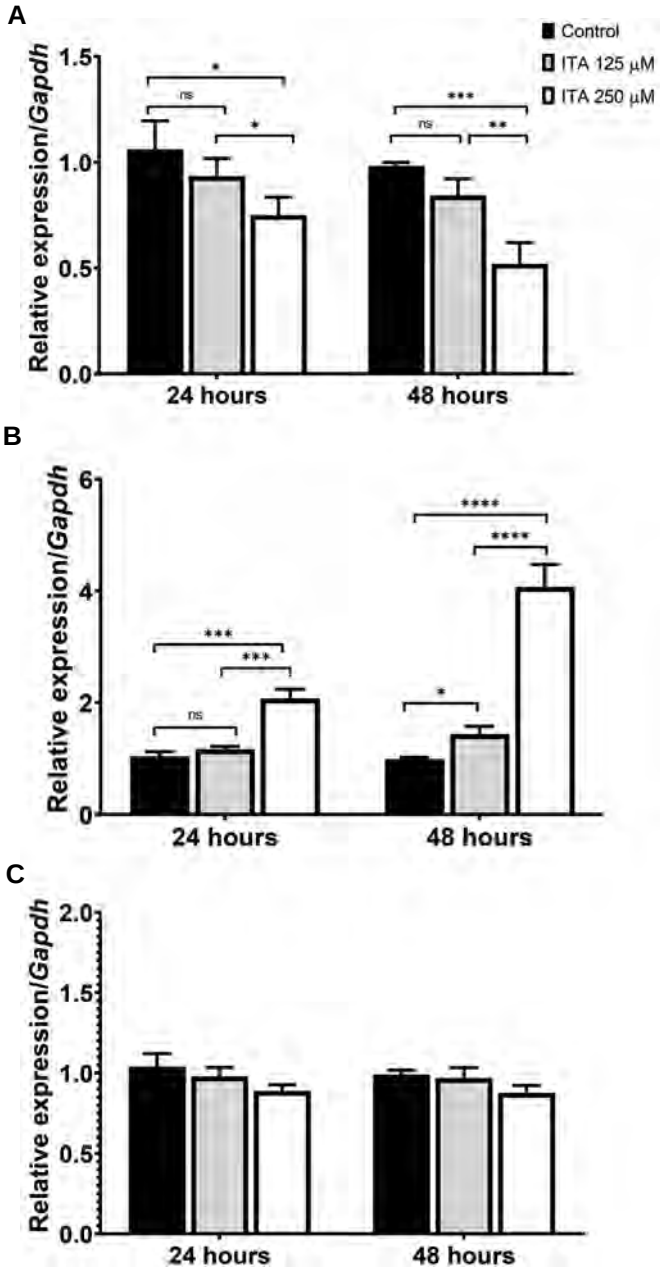

Fig.4: The mRNA levels of *Bax*, *Bcl2* and *Caspase 3* in the adipose derived mesenchymal stem cells (ADMSCs) following different treatment. **A.** *Bax,* ***B.*** *Bcl2*, and **C.** *Caspase 3*. *Gapdh* was used as a housekeeping gene. *, **, ***, **** represent the significant difference between dimethyl itaconate (DMI) treated groups and the control group at both time periods at P<0.05, P<0.01, P<0.001, and P<0.0001, respectively.

Effect of DMI on transcription of autophagy associated genes

qRT-PCR analysis revealed that DMI at both doses for 24 hours and 48 hours time period could stimulate the transcription of the *Lc3b* gene in ADMSCs in comparison with the untreated cells (P<0.01, P<0.001, Fig.5A). DMI at a dose of 250 µM at 48 hours incubation time had the maximum stimulatory effect on the expression level of *Lc3b* in comparison with other doses and incubation time (P<0.0001, Fig.5A). Following treatment with DMI at a dose of 125 µM and 250 µM for 24 hours or 48 hours the expression level of *Beclin* gene was increased in comparison with the untreated cells (P<0.0001). High and low concentrations of DMI at both incubation time had a similar stimulatory effect on the expression level of the *Beciln* gene in ADMSCs *(*Fig.5B). Exposure of ADMSCs to 125 µM DMI for 24 hours had no obvious effect on the transcription level of the *P62* gene, while a 48 hours exposure of ADMSCs to this dose could significantly induce the transcription level of the *P62* gene in comparison with the untreated cells (P<0.01). DMI at a dose of 250 µM had a more stimulatory effect on the expression level of the *P62* gene in comparison with another dose of DMI at both exposure times (P<0.01, P<0.05, Fig.5C). DMI at both concentrations for 24 hours and 48 hours had no significant effect on the mRNA levels of *Atg5* and *Atg12* genes in the ADMSCs in comparison with the untreated cells (Fig.5D, E).

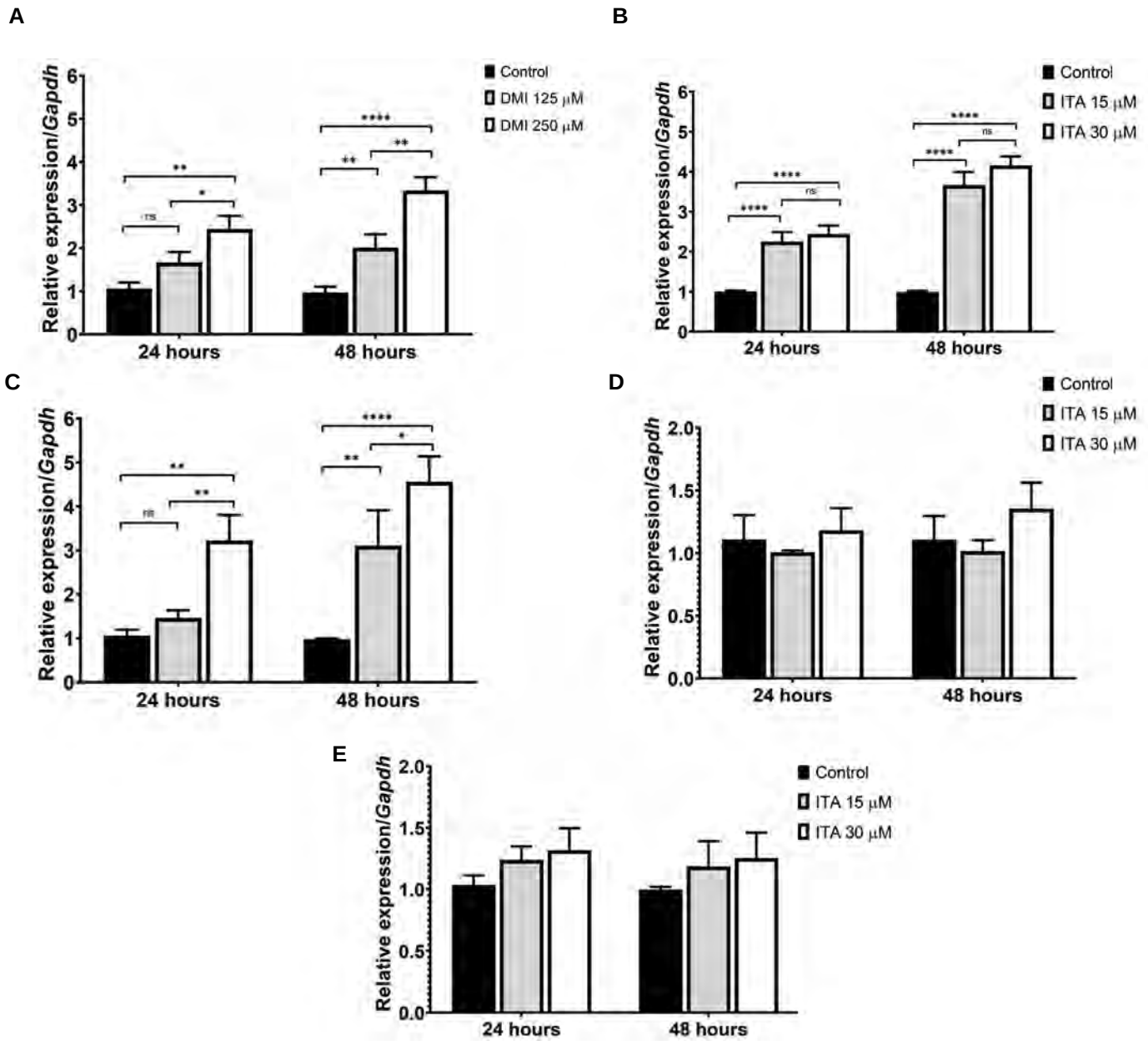

Fig.5: The mRNA levels of *L3b, Belin, P62, Atg5,* and *Atg12* in the adipose derived mesenchymal stem cells (ADMSCs) treated with different concentrations (125 µM and 250 µM) of dimethyl itaconate (DMI) at different exposure time (24 hours and 48 hours). **A.** *Lc3b*, **B.** *Beclin*, **C.** *P62*, **D.** *Atg5*, and **E.** *Atg12*. Gapdh was used as a housekeeping gene. *, **, ***, **** represent a significant difference between the DMI treated groups and the control group at both time periods at P<0.05, P<0.01, P<0.001, and P<0.0001, respectively.

Discussion

Itaconate is a novel anti-inflammatory mediator which is produced by mammalian immune cells (19). The role of itaconate as a novel immunometabolite on the stem cell fate in physiological condition is still not well understood. The present study investigated the effect of DMI, a membrane permeable non-ionic form of itaconate, on the vital activity and transcription level of apoptosis and autophagy associated genes in the rat ADMSCs. Here, we demonstrated a novel data that have not been previously reported. Our results showed that DMI increases the proliferation of ADMSCs in a dose dependent manner under in vitro condition. Our experiment was performed using 125 µM and 250 µM of DMI, doses that have been shown to reduce LPS-induced inflammation in the other mammalian cells (19, 25). These doses had no inhibitory effect on the ADMSCs viability. Our qRT-PCR analysis revealed that treatment of ADMSCs with different doses DMI for 24 hours and 48 hours downregulated the transcription of *Fadd* and *Bax* genes and upregulated the transcription of *Bcl2* gene. Both doses of DMI had no obvious effect on the expression of *Caspase 8*, *Fasl* and *Caspase 3* genes. Here, we also demonstrated for the first time that DMI enhances the transcription level of autophagosome formation genes, including *Lc3b*, *Beclin1* and *P62*, while, it had no regulatory effect on transcription of *Atg5* and *Atg12* genes.

In accordance with our results, Lampropoulou et al. (17), has shown that treatment of bone marrow derived dendritic cells (BMDCs) with the DMI can protect them from hypoxia, an inducer cell death. A recent report by Muri et al have demonstrated that 4 octyl itaconate (4-OI) at low concentration protects the BMDCs against inflammation, while it promotes inflammatory apoptosis at high concentration (480 µM) (26). Functional study by Liu et al. (11) showed that 4-OI attenuated H_2O_2-induced neuronal cell death and apoptosis. Moreover, 4-OI treatment can reduce ischemia-reperfusion damage in the hepatocytes, which indicated an anti death effect of itaconate in the nonimmune cells (27). Taken together, these findings highlighted the protective effect of itaconate against cell death and apoptosis in various cells and this protection is depended on the cell type, dose of itaconate and physiological or pathological conditions of exposed cells.

Our results showed that DMI could upregulate the expression of autophagy associated genes, including *P62*, *Beclin1* and *Lc3b* concomitant with upregulation of the *Bcl2* as an anti-apoptosis gene. Despite the considerable advances in the biology of stem cells, understanding of the dual role of various immunometablites on the stem cell autophagy and apoptosis and their connections in the different physiological and pathological conditions remains incomplete. Understanding the actions of novel immunometabolites on the both of these pathways in the stem cells is an important area of research. It has been reported that autophagy, protection against stress condition, was induced by prolonged starvation, inflammatory agents and extrinsic death signals (28). Previous works have shown that *P62* can act as a main regulator of cell fate by controlling the autophagosomal degradation of several cellular proteins related to apoptosis and survival pathways (29). It has been reported that caspase-8 is degraded via autophagy pathway by interaction with p62 protein (30). BECLIN1 is another critical regulator of autophagy that directly interacts with anti-apoptotic BCL2 protein. Autophagy is induced by release of BECLIN1 from BCL2 by pro-apoptotic BH3 proteins (31). In addition, Caspase-3 inhibits the autophagy process by cleavage of BECLIN1 and production of an inactive, truncated form of BECLIN1 (32). In bone marrow MSCs, rapamycin induces autophagy markedly via reduction P62 accumulation and apoptosis, that suggests a protective role against apoptosis in the BMSCs for autophagy (11). Taken together we concluded that DMI by upregulation of *P62* and *Beclin1* may affect the components of the apoptosis machinery and enhance the cell viability and proliferation in the physiological condition.

Previous research indicated that ATG5 is required for autophagy induced vacuole formation by conjugation to human ATG12 homologue in a non-ubiquitin dependent pathway (9). It has been reported that ATG5 contributes to autophagic cell death by interacting with the FADD via Lys residue located in middle and C-terminal regions of ATG5. These data suggest that the induction of cell death by the ATG5 requires FADD as a downstream mediator (33). Although, the transcription of *Atg5* and *Atg12* was not altered in our study, down-regulation of *Fadd* transcription after exposure of ADMSCs to the DMI might result to enhance proliferation of ADMSCs following exposure to the DMI via inhibition of ATG5-ATG12 formation and an external pathway of apoptosis.

Our results showed that increasing of the cell proliferation potency of ADMSCs and upregulation of autophagy genes and anti-apoptotic genes after exposure to the DMI was accompanied by an increase in nuclear concentration of NRF2 protein. The NRF2 is a multifunctional and indispensable transcription factor that contributes to the autophagy and apoptosis of cells under stress condition via regulating the expression of several cytoprotective genes. Under normal conditions, Kelch-like ECH-associated protein 1 (KEAP1) binds to NRF2 in the cytoplasm, and act as an inhibitor of NRF2 activation. Different cellular stresses result in dissociation of KEAP1 from NRF2, consequently, *Nrf2* translocates to the nucleus where it activates the transcription of a host of cell defense genes (34). In accordance with our results, recent findings demonstrated that itaconate or its derivatives increases the alkylation of cysteine residues on the KEAP1, which enhances the degradation of KEAP1 and leads to translocation of NRF2 to the nucleus and its further activation of NRF2 and downstream gene transcription in the BMDCs and neuronal cells (11, 19, 23). Increased survival and proliferation along with altered expression of apoptotic genes and autophagy genes in the DMI treated

ADMSCs might be due to increased activation of NRF2 protein. To confirm this opinion several previous reports demonstrated that NRF2 overexpression improves MSCs survival under oxidative stress and protects MSCs against hypoxia induced apoptosis (35). According to our results, it is likely that DMI is involved in the transcription of apoptosis associated genes in the ADMSCs through activation of NRF2 pathway.

The relationship between NRF2 activation and autophagy has been indicated in previous reports and it was suggested that DMI might increase intranuclear NRF2 protein and cellular protection by affecting the expression of autophagy genes. To support this opinion, a recent study by Jiang et al. (36) has shown that P62 contributes to the activation of NRF2 by direct binding to KEAP1 and its autophagic degradation. This event induces KEAP1 degradation via autophagy and leaves NRF2 free to accumulate and translocate in the nucleus and facilitates the activation of NRF2 target genes. It has also reported that the suppression of NRF2 leads to autophagy and the osteoblastic differentiation of ASCs (37). These findings indicate that overexpression of *P62* in DMI treated ADMSCs in our study might contribute cell proliferation enhancement by activation of NRF2 and creating a positive feedback loop. Further researches are needed to confirm these mechanisms.

There are some limitations in this study that can be addressed in future research. The present study focused on determination of abundance of mRNA transcripts of apoptosis and autophagy associated genes and cell proliferation rate in the DMI treated ADMSCs. Application of specialized apoptosis and autophagy detection methods such as Annexin-V/propidium iodide method, Terminal deoxynucleotidyl transferase dUTP nick end labeling (*TUNEL*) assay, caspases activity assay and specific staining methods such as Hoechst 33258 and Acridine orange/ethidium bromide staining are suggested in future studies to better understanding of itaconate actions on stem cell fate and functions.

Conclusion

It has been demonstrated that MSCs gradually lose their proliferation and differentiation potential after long-term *ex vivo* culture. Our findings demonstrated that DMI by upregulation of some autophagy and anti-apoptosis associated genes and by activation of NRF2 may serve as a new cellular protective mechanism against stressful environment induced by exposure of stem cells to *ex vivo* condition. It is undeniable that the action of itaconate; as a novel immunometabolite, on MSCs is complex, and the relationship between itaconate and stem cell fate still requires further in vitro experiments. Knowing how itaconate acts on the complicated apoptosis and autophagy pathways may open the new research area for the development of novel protocols for culture and differentiation of MSCs in the *in vitro* condition.

Acknowledgements

This work was funded by a Grant from Shahid Chamran University of Ahvaz Research Council (grant No: 98/3/02/16670). The authors declare that they have no conflicts of interest.

Authors' Contributions

All authors contributed to the study conception and design. F.S.; Performed the study and collected the data. M.R.T., D.D.; Designed the study, analyzed the results, drafted and revised the manuscript, critically for important intellectual content. All authors gave final approval of the version to be published.

References

1. Argentati C, Morena F, Bazzucchi M, Armentano I, Emiliani C, Martino S. Adipose stem cell translational applications: from bench-to-bedside. Int J Mol Sci. 2018; 19(11): 3475.
2. Han Y, Li X, Zhang Y, Han Y, Chang F, Ding J. Mesenchymal stem cells for regenerative medicine. Cells. 2019; 8(8): 886.
3. Kizil C, Kyritsis N, Brand M. Effects of inflammation on stem cells: together they strive? EMBO Rep. 2015; 16(4): 416-426.
4. Weiss AR, Dahlke MH. Immunomodulation by mesenchymal stem cells (MSCs): mechanisms of action of living, apoptotic, and dead MSCs. Front Immun. 2019; 10: 1191.
5. Wang M, Yuan Q, Xie L. Mesenchymal stem cell-based immunomodulation: properties and clinical application. Stem Cells Int. 2018; 2018.
6. Planat-Benard V, Varin A, Casteilla L. MSCs and inflammatory cells crosstalk in regenerative medicine: concerted actions for optimized resolution driven by energy metabolism. Front Immunol. 2021; 12: 626755.
7. McKee C, Chaudhry GR. Advances and challenges in stem cell culture. Colloids Surf B Biointerfaces. 2017; 159: 62-77.
8. Cruciani S, Santaniello S, Montella A, Ventura C, Maioli M. Orchestrating stem cell fate: novel tools for regenerative medicine. World J Stem Cells. 2019; 11(8): 464.
9. Chen X, He Y, Lu F. Autophagy in stem cell biology: a perspective on stem cell self-renewal and differentiation. Stem Cells Int. 2018; 21; 2018.
10. Fairlie WD, Tran S, Lee EF. Crosstalk between apoptosis and autophagy signaling pathways. Int Rev Cell Mol Biol. 2020; 352: 115-158.
11. Liu WJ, Ye L, Huang WF, Guo LJ, Xu ZG, Wu HL, et al. p62 links the autophagy pathway and the ubiqutin–proteasome system upon ubiquitinated protein degradation. Cell Mol Biol Lett. 2016; 21(1): 1-4.
12. Dang S, Yu ZM, Zhang CY, Zheng J, Li KL, Wu Y, et al. Autophagy promotes apoptosis of mesenchymal stem cells under inflammatory microenvironment. Stem Cell Res Ther. 2015; 6(1): 1-9.
13. Wang J, Xia J, Huang R, Hu Y, Fan J, Shu Q, et al. Mesenchymal stem cell-derived extracellular vesicles alter disease outcomes via endorsement of macrophage polarization. Stem Cell Res Therap. 2020: 11(1): 1-2.
14. Zhao H, Shang Q, Pan Z, Bai Y, Li Z, Zhang H, et al. Exosomes from adipose-derived stem cells attenuate adipose inflammation and obesity through polarizing M2 macrophages and beiging in white adipose tissue. Diabetes. 2018; 67(2): 235-247.
15. Michelucci A, Cordes T, Ghelfi J, Pailot A, Reiling N, Goldmann O, et al. Immune- responsive gene 1 protein links metabolism to immunity by catalyzing itaconic acid production. Proc Nat Acad Sci USA. 2013; 110: 7820-7825.
16. Strelko CL, Lu W, Dufort FJ, Seyfried TN, Chiles TC, Rabinowitz JD, et al. Itaconic acid is a mammalian metabolite induced during macrophage activation. J Am Chem Soc. 2011; 133(41): 16386-16389.
17. Lampropoulou V, Sergushichev A, Bambouskova M, Nair S, Vincent EE, Loginicheva E, et al. Itaconate links inhibition of succinate dehydrogenase with macrophage metabolic remodeling and regulation of inflammation. Cell Metab. 2016; 24(1): 158-166.
18. O'Neill LA, Artyomov MN. Itaconate: the poster child of metabolic reprogramming in macrophage function. Nat Rev Immun. 2019; 19(5): 273-281.
19. Mills EL, Ryan DG, Prag HA, Dikovskaya D, Menon D, Zaslona Z, et al. Itaconate is an anti-inflammatory metabolite that activates

Nrf2 via alkylation of KEAP1. Nature. 2018; 556(7699): 113-117.
20. Németh B, Doczi J, Csete D, Kacso G, Ravasz D, Adams D, et al. Abolition of mitochondrial substratelevel phosphorylation by itaconic acid produced by LPS- induced Irg1 expression in cells of murine macrophage lineage. FASEB J. 2016; 30(1): 286-300.
21. Hooftman A, Angiari S, Hester S, Corcoran SE, Runtsch MC, Ling C, et al. The immunomodulatory metabolite itaconate modifies NLRP3 and inhibits inflammasome activation. Cell Metab. 2020; 32(3): 468-478.
22. Hashemi Tabar M, Tabandeh MR, Moghimipour E, Dayer D, Ghadiri AA, Allah Bakhshi E, et al. The combined effect of Pdx1 overexpression and Shh manipulation on the function of insulin-producing cells derived from adipose-tissue stem cells. FEBS Open Bio. 2018; 8(3): 372-382.
23. Bambouskova M, Gorvel L, Lampropoulou V, Sergushichev A, Loginicheva E, Johnson K, et al. Electrophilic properties of itaconate and derivatives regulate the IkappaBzeta-ATF3 inflammatory axis. Nature. 2018; 556(7702): 501-504.
24. Orellana EA, Kasinski AL. Sulforhodamine B (SRB) assay in cell culture to investigate cell proliferation. Bio Protoc. 2016; 6(21): e1984.
25. Sun KA, Li Y, Meliton AY, Woods PS, Kimmig LM, Cetin-Atalay R, et al. Endogenous itaconate is not required for particulate matter-induced NRF2 expression or inflammatory response. eLife. 2020; 9: e54877.
26. Muri J, Wolleb H, Broz P, Carreira EM, Kopf M. Electrophilic Nrf2 activators and itaconate inhibit inflammation at low dose and promote IL-1β production and inflammatory apoptosis at high dose. Redox Biol. 2020; 36: 101647.
27. Yi Z, Deng M, Scott MJ, Fu G, Loughran PA, Lei Z, et al. Immune-responsive gene 1/Itaconate activates nuclear factor erythroid 2–related factor 2 in hepatocytes to protect against liver ischemia–reperfusion injury. Hepatology. 2020; 72(4): 1394-1411.
28. Chang NC. Autophagy and stem cells: self-eating for self-renewal. Front Cell Dev Biol. 2020; 8: 138.
29. Liu WJ, Ye L, Huang WF, Guo LJ, Xu ZG, Wu HL, et al. p62 links the autophagy pathway and the ubiqutin–proteasome system upon ubiquitinated protein degradation. Cell Mol Biol Lett. 2016; 21(1): 1-4.
30. Yan XY, Zhong XR, Yu SH, Zhang LC, Liu YN, Zhang Y, et al. p62 aggregates mediated Caspase 8 activation is responsible for progression of ovarian cancer. J Cell Mol Med. 2019; 23(6): 4030-4042.
31. Chen Y, Zhang W, Guo X, Ren J, Gao A. The crosstalk between autophagy and apoptosis was mediated by phosphorylation of Bcl-2 and beclin1 in benzene-induced hematotoxicity. Cell Death Dis. 2019; 10(10): 1-5.
32. Zhu Y, Zhao L, Liu L, Gao P, Tian W, Wang X, et al. Beclin 1 cleavage by caspase-3 inactivates autophagy and promotes apoptosis. Protein Cell. 2010; 1(5): 468-477.
33. Mnich K, Koryga I, Pakos-Zebrucka K, Thomas M, Logue SE, Eriksson LA, et al. The stressosome, a caspase-8-activating signalling complex assembled in response to cell stress in an ATG5-mediated manner. J Cell Mol Med. 2021; 25(18): 8809-8820.
34. Katsuragi Y, Ichimura Y, Komatsu M. Regulation of the Keap1-Nrf2 pathway by p62/SQSTM1. Curr Opin Toxicol. 2016; 1: 54-61.
35. Dai X, Yan X, Wintergerst KA, Cai L, Keller BB, Tan Y. Nrf2: redox and metabolic regulator of stem cell state and function. Tren Mol Med. 2020; 26(2): 185-200.
36. Jiang T, Harder B, De La Vega MR, Wong PK, Chapman E, Zhang DD. p62 links autophagy and Nrf2 signaling. Free Radic Biol Med. 2015; 88: 199-204.
37. Tao J, Wang H, Zhai Y, Park H, Wang J, Ji F, et al. Downregulation of Nrf2 promotes autophagy-dependent osteoblastic differentiation of adipose-derived mesenchymal stem cells. Exp Cell Res. 2016; 349(2): 221-229.

Original Article

Production of *CFTR* Mutant Gene Model by Homologous Recombination System

Hanieh Rezaee, Ph.D.[1], Mohammad Salehi, Ph.D.[1, 2*], Mojgan Bandepour, Ph.D.[2], Sima Kalantari, Ph.D.[1, 3], Sara Hosseini, Ph.D.[4], Khosrow Agin, M.D.[5], Bahram Kezemi, Ph.D.[1, 2*]

1. Department of Medical Biotechnology, School of Advanced Technologies in Medicine, Shahid Beheshti University of Medical Sciences, Tehran, Iran
2. Cellular and Molecular Biology Research Center, Shahid Beheshti University of Medical Sciences, Tehran, Iran
3. Regenerative Medicine Group (REMED), Universal Scientific Education and Research Network (USERN), Tehran, Iran
4. Mom Fertility and Infertility Research and Innovation Center, Tehran, Iran
5. Toxicological Research Center, Loghman-Hakim Hospital, Department of Clinical Toxicology, School of Medicine, Shahid Beheshti University of Medical Sciences, Tehran, Iran

Corresponding Address: P.O.Box: 193954717, Department of Medical Biotechnology, School of Advanced Technologies in Medicine, Shahid Beheshti University of Medical Sciences, Tehran, Iran
Emails: m.salehi@sbmu.ac.ir, kazemi@sbmu.ac.ir

Received: 04/January/2022, Accepted: 27/April/2022

Abstract

Objective: The most common mutation in cystic fibrosis (CF), (ΔF508-CFTR), results in impaired protein maturation, folding and transportation to the surface of the cell. As a consequence of impaired protein maturation and/or transport from the extracellular matrix to the cell, different systems are influenced, including gastrointestinal system and glandular system, reproductive system and respiratory systems. CF models are essential tools to provide further knowledge of CF pathophysiology. With this aim, we designed a transgenic CF model based on the homologous recombination (HR) system.

Materials and Methods: In this experimental study, a specifically designed construct containing the *CFTR* gene with F508del was cloned into a PTZ57R cloning vector and then the construct was transformed into the male pronucleus by microinjection after *in vitro* fertilization (IVF). Then the rates of blastocyst formation and embryonic development at 72 hours after IVF, were evaluated using the inverted microscope and the insertion of the construct was approved by polymerase chain reaction (PCR) method.

Results: The *CFTR* gene was successfully cloned into the PTZ57R cloning vector and overall, from 22 injected cells, 5 blastocysts were observed after pronuclear injection of the *CFTR* gene construct. PCR verification of the blastocyst with *CFTR*-specific primers represented complete recombination of *CFTR* into the mouse genome.

Conclusion: For the first time we designed a unique genome construction that can be detected using a simple PCR method. The pronuclear injection was performed for the transformation of the genome construct into the male pronuclei using microinjection and the development of zygote to the blastocyst stage has been observed following transgenesis.

Keywords: Animal Model, Cystic Fibrosis, Homologous Recombination, Polymerase Chain Reaction

Cell Journal(Yakhteh), Vol 24, No 10, October 2022, Pages: 596-602

Citation: **Rezaee H, Salehi M, Bandepour M, Kalantari S, Hosseini S, Agin Kh, Kezemi B. Production of CFTR mutant gene model by homologous recombination system. Cell J. 2022; 24(10): 596-602. doi: 10.22074/cellj.2022.8408.**

Introduction

The cystic fibrosis transmembrane conductance regulator (*CFTR)* gene contains about 189.36 kilo base pairs and produces a 1,480 amino acids protein. Over 2,000 distinct variants of *CFTR* have been identified as a cause of CF (1). These different mutations are classified based on the mechanism of *CFTR* dysfunction, including impaired protein synthesis, protein instability, channel regulation and electrolyte imbalance (2). The F508del variation is the most prevalent variation and is observed in 70% of patients. The deletion of three nucleotides results in a phenylalanine acid amine deletion. This change in the 508th position of the protein structure causes impaired protein folding, maturation, and/or electrolyte transportation between cells and extracellular matrix (3).

Apart from the earlier description, late 1930's century, CF is a major challenge. There isn't any significant treatment for patients suffering from CF disease, and most of treatment strategies are focused on aleiviation of symptoms and increase the life expance of patients up to 40 years (4). Therefore, designing an animal model that accurately mimics the disease pattern and counterpoises various micro-environments can efficiently produce good insights into CF disease (5). The recent revolution in producing animal models brought up some genome editing techniques such as transcription activator-like effector nucleases (TALENs); zinc-finger nuclease (ZFNs); and clustered regularly interspaced short palindromic repeats Cas9 (CRISPR-Cas9); as well as homologous recombination (HR) system for CF research (6).

HR system accounts as a simple system that the desired gene can be integrated into the specific site through either embryonic stem cells or somatic cell nuclear transfer, as well as pronucleus transfer (PNT) (7). In order to increase the porportion of integration rate, the genomic content is flanked into

homology arms. These homology arms consist of long genomic regions with a thousand base pairs that are a complement of the desired region of the genome. It is called site specific recombination that generates a line of a transgenic animal harboring the desired gene inserted into the genome. Using homologous-directed repair (HDR), a double-strand DNA breaks down and a donor DNA with a 200 to 800 bp homology arm is inserted into the site of genomic DNA breakage. To increase the efficiency of homologous recombination, the use of longer homology arms and the Crispr/cas9 system for genome modification is recommended (8).

In the present study, to produce a transgenic model, we designed an artificial genetic construct of the *CFTR* gene containing F508del by performing some necessary modifications. Then desired construct had synthesized and cloned into the bacterial vector. There are different CF animal models, including pig (9), ferret (10, 11), rabbit (12), and rat (13). But, according to a systematic review study performed in 2020, the majority of studies in the generation of transgenic CF models were performed on different mouse models using either pronuclear injection or other recombination systems (14). In order to test our novel construct, the bacterial vector harboring the *CFTR* construct was injected into the male pronucleus of mature mouse zygotebased on an HR system. The embryo development up to a mature blastocyst formation was monitored, and the presence of an injected gene was detected using a simple polymerase chain rection (PCR) method.

Material and Methods

This experimental study was approved by the Research and Ethics Committee of the Shahid Beheshti University of Medical Sciences (IR.SBMU.RETECH.REC.1395.753). All animal treatments were carried out in accordance with US NIH guidelines for the care and use of laboratory animals (15).

Animals

Approximately 210 oocytes were obtained from five healthy female B6D2F1 mice (C57BL/6×DBA2). These 4-8 weeks old mice (weighing 11.9 ± 0.9 g) were purchased from the Royan Institute, Tehran, Iran. Hybrid mice such as B6D2F1 have a high fertility rate, as well as a high quality and the number of releasing oocytes which were suitable for reproductive research. Spermatozoa were obtained from five healthy male B6D2F1 mice (C57BL/6×DBA2) at 8 weeks of age.

All animals were housed at a constant temperature and humidity (22-28°C, 55 ± 5%), under a 12-hour light/dark cycle, and their food and water were provided according to the libitum standard laboratory diet. The animals were adapted to laboratory conditions for 10 days before the experiment. In order to have a minimum animal suffering and applying for our transgenesis method evaluation, the study was conducted on a small group of mice.

Construct designing

The human *CFTR* gene sequence was obtained from the UniProt database (www.uniprot.org) and compared with the mouse *CFTR* gene sequence using the Clustal Omega tool (plugged in UniProt) to identify the rate of similarity between human *CFTR* and mouse *CFTR* gene sequences. Then, the entire *CFTR* gene sequence was screened and the intron regions across the length of the gene were omitted and all exon sequences were merged respectively. Some necessary modifications had been performed, including the insertion of a promotor site along with modification in the initial and terminal sequences of the promotor to have a restriction site for *SacI* and *NdeI* restriction enzymes (RE), respectively. After insertion into the mouse genome the mouse promotor would render the transcription procedure. Also, to digest the construct genome from the vector, a modification was performed at the end of the genome sequence to have a restriction site for the *BglII* RE. To have a frameshift mutation in the *CFTR* sequence, a stuffer sequence containing 200 nucleotides was inserted at the position of 508th nucleotide, the most common CF mutations. Following, the codon optimization was performed to make a *BamHI* restriction site to remove the stuffer for further evaluation and gene therapy approaches. Finally, codon optimization was performed in an amino acid codon to have a unique sequence. This alternation aimed to determine the inserted sequence in the mouse genome using a simple PCR method. The designed *CFTR* gene sequence, then was incorporated within the PCC1 cloning vector (GenCArt Bioneer, Korea). The schematic model of the designed construct is illustrated in Figure 1.

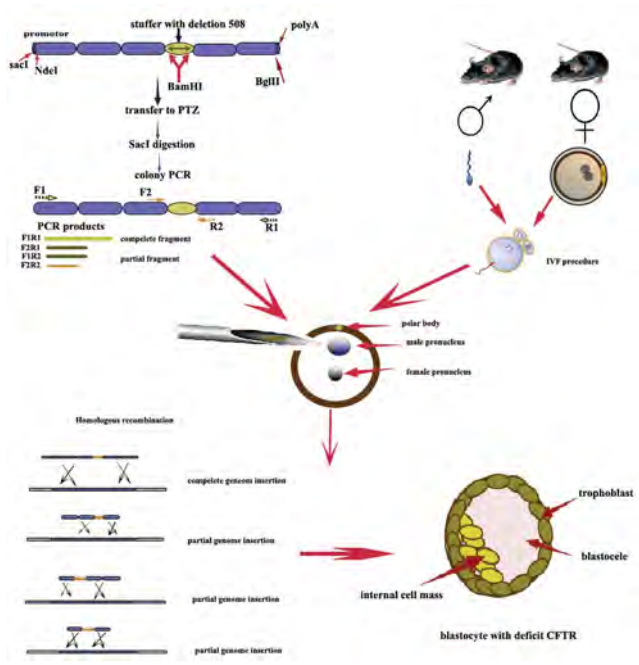

Fig.1: Graphical abstract of the study.

Cloning of the *CFTR* gene in the PTZ57R cloning vector

For cloning the *CFTR* construct into the PTZ57R vector, the *CFTR* gene construct was amplified using specific primer sets designed for the initial and end sites of the *CFTR* construct. We used NCBI BLAST and Oligo7 software (Molecular Biology Insights, Inc., Cascade Co.) to design and validate primer sets. The sequence of the primers is presented in the Table 1. The amplification was performed using the PCR Qiagen kit (201445., Qiagen, Hilden, Germany) under the following program: initial denaturation at 94°C (5 minutes), followed by 29 cycles with denaturation at 94°C (45 seconds), annealing at 57°C (45 seconds), extension at 72°C (120 seconds), with the final extension step at 72°C (10 minutes). The PCR products were electrophoresed and the results were observed on the 1% agarose gel (A9539, Sigma-Aldrich, Germany). The 1 µl of PCR product was ligated with a 10 µl PTZ57R vector using T4 DNA ligase (L6030-W-L, Qiagen, Hilden, Germany), and after 3 hours incubation at 37°C, the ligation was confirmed by gel electrophoresis. Then, the $CaCl_2$ transformation method (16) was employed to transform the ligated *CFTR* and PTZ57R vector into the *E.coli* Top10 as a competent host. The colonies were cultured on a LB (Luria-Bertani) agar plate containing 100 µg/mL ampicillin. The assessment of the transformation was performed using colony PCR and RE digestion with the *SacI* RE (1078A, Takara, Dalian, China) because due to the ligation, the orientation of the gene was changed, and double digestion was performed with *SacI* RE.

Table 1: Sequence of primers used for cloning and polymerase chain reaction

Primer	Primer sequencing (5´-3´)
CFTR	F1: GAG CTC GGA TCC AGG AAC CCA GG
	R1: AGA TCT AAG CCT TGT ATC TTG CAC C
	F2: CCT AAC TGA GAC CTT ACA CCG TTT
	R2: AAA CGG TGT AAG GTC TCA GTT AGG

In vitro fertilization procedure

IVF procedurewas performed on8- week-old female mice by superovulation with 10 IU Pregnant male serum Gonadotropin (PMSG, C0434, Sigma-Aldrich, Germany), following injection of 10 IU human choronic gonadotropin (hCG, 9002-61-3, Sigma Aldric, Germany) after 50 hours. Cumulus-oocyte complexes (COCs) were separated from the ampulla of the oviduct 14 hours after a single dose injection hCG. For sperm collection, the 8 to10-week-old male mice were euthanized by cervical dislocation. Then spermatozoa were isolated from the cauda epididymis as well as the vasa deferentia. The sperm suspension was collected and cultured in the human tubal fluid (HTF) medium, containing 4 mg/mL bovine serum albumin (BSA, MR-070-D, Sigma Aldric, Germany) and incubated at 37°C with 5% CO_2 for 45 minutes. Then, COCs were inseminated with approximately 1×10^6 sperm/mL in 100 µl of HTF medium and then incubated for 6 hours. The pronuclear injection was applied on mature zygote with two pronuclei following about6 hours incubation at the incubator and rested on an ice plate for 30 minutes, they were placed in a potassium simplex optimized (KSOM) medium (MR-107-D, Sigma-Aldrich, Germany) that riches in essential amino acids supplemented with a 4% BSA. The rates of blastocyst formation and embryo development was evaluated at 24 and 96 hours after IVF, respectively (17).

Pronuclear plasmid microinjection

The concentration of the purified plasmids was measured using Nanodrop (ND2000, NanoDrop Technologies, USA). The amount of 4 µg/µl was needed for the injection of PCR product to the male pronucleus. Thus, 1 µl of purified PCR product was diluted with a sterile Tris/Editium (TE) buffer. The diluted PCR product was then inserted into an injection needle with a Pasteur pipette. Approximately 210 mature oocytes were obtained from female mice, resulting in the development of 170 MII stage zygotes with two pronuclei which were selected for pronuclear injection.

The magnitude of the microscope (Nikon TE2000, Narishige, USA) was adjusted at 60X and then the mature zygote with two distinct pronuclei was transferred in Flushing Holding medium (FHM) media and fixed with a holder needle; then injection was performed by pushing the diluted PCR product with a TE buffer (1:50) into the male pronucleus. All procedures were performed under the cold chain to keep the integrity of the cell membrane of the zygote. After injection, they were placed on an ice plate to heal the zygote's cell wall and then transferred into the KSOM buffer. The presence of mature blastocyst was observed after 24 and 96 days of the micro-injection. Approximately 210 mature oocytes were obtained from female mice, resulting in the development of 170 MII stage zygotes with two pronuclei which were selected for pronuclear injection. Mature 2PN zygotes were then transferred to the 5ml FHM media. Each FHM media consisted of about 5 to 10 zygotes. The concentration of PCR products was measured after purifying with drop dialysis using Nanodrop for calculation of the amount of DNA for injection.

The concentration of the PCR products applied for pronuclear injection was about 520 µl/ml. Around 4 ng/ml was needed to inject into the male pronucleus. Therefore, 1 µl of PCR products were diluted with a 99 µl sterile TE buffer. The diluted PCR product was transferred to the injection needle and whilst the orientation of the polar body was at top of the cell, the

construct was injected into male pronuclei. Then the injection dish was kept in the cold plate to repair the zygote's cell wall and finally transferred to the KSMO culture plate.

construction insertion confirmation

The PCR method was employed to confirm the presence of corresponding *CFTR* gene sequences in mature blastocytes and morulae. The PCR was performed using all primer sets including F1R1, F1R2, F2R2, and F2R1 primers for identification of either complete or partial insertion of the *CFTR* gene construct (The PCR program was mentioned in the cloning section). Primers, applied for amplification of *CFTR*, were specific for the designed construct that just attached to the genome while the *CFTR* gene construct was inserted. The F1R1 primers amplified both the initial and end of the *CFTR* gene construct, while F2R2 attached to the middle of the construct contained a 200 bp fragment inserted at the 508th position of the CFTR protein. F1R2 and F2R1 amplified the partial sequence of the genome within the inserted stuffer site. Therefore, even in the case of partial insertion of the *CFTR* gene, the function of the whole genome would knock down the entire genome.

Results

Gene construction

The sequence of the human *CFTR* gene was compared with the mouse *CFTR* gene. Using the Clustal Omega tool (plugged in UniProt), 78.5% identity between human *CFTR* and mouse *CFTR* based on reference gene was observed. To design the construct, the *CFTR* gene was screened and all the intron regions were excluded while exon regions connected to each other. The *CFTR* gene exons were listed in Table 2.

Table 2: The list of *CFTR* gene exons

Region	Start	End	Region length	Phase at end	Region	Start	End	Region length	Phase at end
UTR	117,120,016	117,120,148			Exon	117,234,984	117,235,112	129	0
Exon	117,120,149	117,120,201	53	2	Exon	117,242,880	117,242,917	38	2
Exon	117,144,307	117,144,417	111	2	Exon	117,243,586	117,243,836	251	1
Exon	117,149,088	117,149,196	109	0	Exon	117,246,728	117,246,807	80	0
Exon	117,170,953	117,171,168	216	0	Exon	117,250,573	117,250,723	151	1
Exon	117,174,330	117,174,419	90	0	Exon	117,251,635	117,251,862	228	1
Exon	117,175,302	117,175,465	164	2	Exon	117,254,667	117,254,767	101	0
Exon	117,176,602	117,176,727	126	2	Exon	117,267,576	117,267,824	249	0
Exon	117,180,154	117,180,400	247	0	Exon	117,282,492	117,282,647	156	0
Exon	117,182,070	117,182,162	93	0	Exon	117,292,896	117,292,985	90	0
Exon	117,188,695	117,188,877	183	0	Exon	117,304,742	117,304,914	173	2
Exon	117,199,518	117,199,709	192	0	Exon	117,305,513	117,305,618	106	0
Exon	117,227,793	117,227,887	95	2	Exon	117,306,962	117,307,162	201	0
Exon	117,230,407	117,230,493	87	2	UTR	117,307,163	117,308,718		
Exon	117,231,988	117,232,711	724	0	Chromosome: chr7, Genbank ID: NM_000492 , Length coding sequence : 4440 nucleotides				

Cloning and confirmation of DNA construct

The *CFTR* gene was successfully cloned into the PTZ57R cloning vector and the insertion of gene construct was confirmed on colonies observed after transformation using colony PCR method with the F1R1 primers. PCR results indicated the presence of 4,600 bp related fragment on the 1% gel agarose. Also, after ligation of the *CFTR* construct in to PTZ57R cloning vector, the vector was digested using the *SacI* RE confirmed the insertion of the *CFTR* gene into the PTZ57R cloning vector. The results of PTZ+ *CFTR* gene cloning into *E. coli* TOP10 cells are shown in Figure 2.

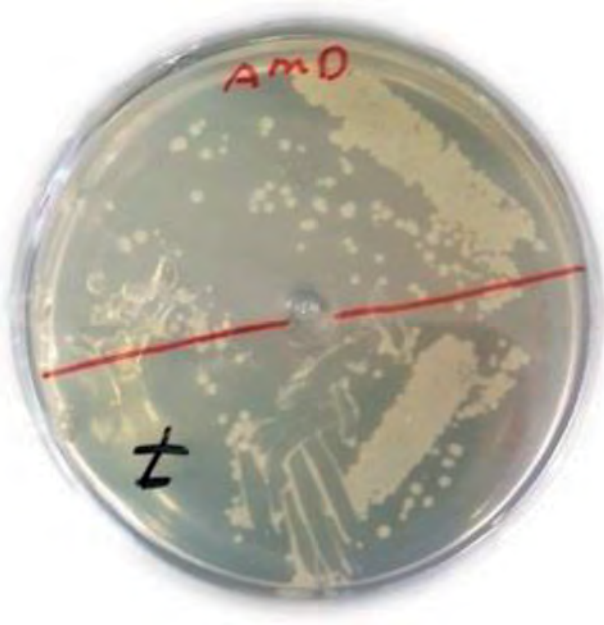

Fig.2: Cloning of PTZ+*CFTR* gene into *E. coli* TOP10 cells. AMD; Ampliciline supplimented dish.

Pronuclear injection

Following injection of *CFTR* gene construct Approximately 170 MII stage zygotes with two pronuclei were developed, and the developmental rate was about 80.9%.

The presence of mature blastocysts was examined at 24 and 96 hours after micro-injection in which about 22 blastocysts along with 10 morulae were developed after being injected. The overall rate of development of either morula and blastocytes cells in transgenic zygotes was 18.8%, while the rate of blastocyte development was 12.9%. The developed blastocysts and morulae are illustrated in Figure 3.

Confirmation of mutant *CFTR* gene insertion

All mature blastocysts along with morula stages of injected cells lysed with lysis buffer and the PCR technique was conducted using either F1R1, F2R1, F1R2, and F2R2 primers. PCR results were shown in Figure 4. In accordance with PCR results, 5 blastocysts out of 22 mature injected blastocytes and 2 morulae out of 10 injected morulae showed a positive PCR for the presence of *CFTR* either in a partial or complete insertion.

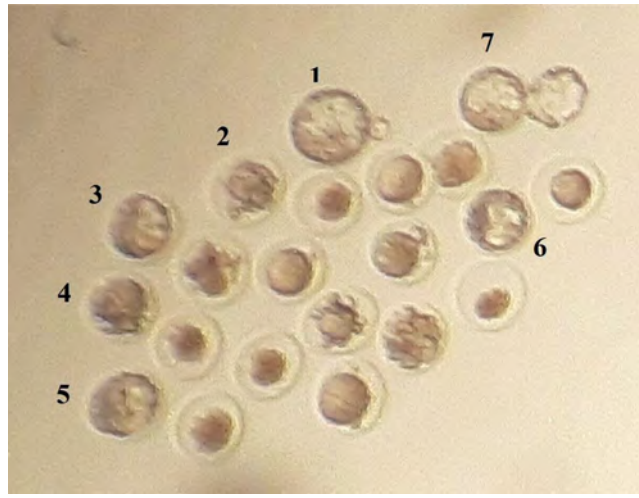

Fig.3: Pronuclear injection of *CFTR* in the mouse zygote. Embryo numbers 1, 3, 5, 6, 7; Blastocysts stage and Embryo numbers 2, 4; Morulae stage, and the rest didn't develop.

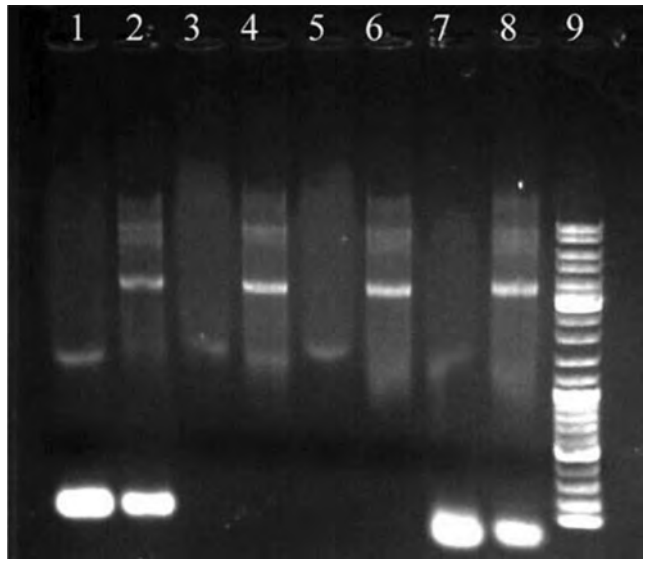

Fig.4: PCR products of the blastocyst with *CFTR* primers. Line numbers 2, 4, and 6 represent complete recombination of *CFTR* into the mouse genome, while sample number 1 represents a partial insertion of the construct as the F2R1 primers could amplify this region. The last band is the controlling band and the PCR result of the plasmid alone. 1 F2R1 (about 2600 bp); 2, 4, 6 F1R1 primer (4600 bp), number 8 plasmid as a positive control, and number 9, 5 kb DNA ladder.

Discussion

The first transgenic mouse model of CF was created in 1994 based on the HR system, that contained 78%

similarity in amino acid sequences with human *CFTR* protein (18). Other mouse models were developed using replacement and/or insertional strategies in which this procedure resulted in the knockout of the gene, whilst insertional procedure produces less than 10% of normal *CFTR* mRNA. Inducing mutation at the site of *CFTR* gene construct insertion by double-strand HR, 'hit and run', various mouse models of CF would be produced. It is worth noting that the mutated mice are less fertile than normal mice. Also, the CF mutant mice breeding is much laborious work and needs a hard attempt. Recently the G542X CF mouse model was generated using a CRISPR/Cas9 genome editing system that leading to 40.9% of mice expressing the G542X mutation (19). HR was a predominant way for the alteration of genetic information, hence, it contributed to the important process of genetic replication with a double-strand break, formation of the replication fork, and horizontal gene transfer through meiosis, leading to the genome integrity and diversity (20-22).

Our study was aimed to use an HR system by introducing the foreign DNA into the male pronucleus. This was through the pronuclear injection method to produce a *CFTR* mutant model. We use codon optimization to design a unique construct whilst inserted into the genome, that made it easily detectable. We used a simple PCR technique without genome sequencing after insertion.

There is a variety of strategies to insert the exogenous DNA into the host genome. The majority applicable method is microinjection that the DNA is injected into the male pronucleus which has been shown to have a 100% efficiency. Although, the birth rate of offspring is about 4-8% (23). The pronuclear injection technology has been used to study the molecular and cellular functions of many genes (24). In this technology, the foreign gene, artificially introduced into cells, contributed to rearrangements of nucleotides and render the mutations. Thus, different copies of the gene were arranged randomly in a case of cytoplasmic insertion of DNA or direct injection into the nuclei. The integration of foreign DNA fragments into a genome may occur either by heterologous or HR with different mechanisms and frequencies. The heterologous recombination accounts as a most frequent recombination leading to random integration (25). In this current study following injection of *CFTR* gene construct, the mutated *CFTR* was randomly integrated into the host genome and development of zygotes to blastocyte stage was observed three days after the pronuclear injection and found that 22 blastocysts along with 10 morulae were developed after injection indicating the development of zygotes after *CFTR* gene construct insertion. The overall rate of development in transgenic zygotes was 18.8%, whilst the rate of blastocyst development was 12.9%. Hence, the birth rate of offspring after microinjection of DNA into the male pronucleus was very low (~ 4-8%) (23) which we also observed a low rate of blastocyte in our current study.

HR accounts as a common way of foreign DNA insertion into the host genome (26). The exogenic DNA integrated during the DNA replication mechanism of the host cell following breakage in double-strand DNA; as the breakage in DNA is random, the incorporation of exogenous DNA into the host genome would be random and consequently disrupt or prevent the expression of the host gene (27). But, the efficiency of integration is very low, hence HR is mostly followed by a double-strand break using TALEN, ZFNs, and CRISPR-cas9 technique that the CRISPR technique has been reported to have off-target effects (5). To successfully insert the gene in the animal model of diseases, it was necessary to include expression elements located at 5' and 3' ends of the gene sequence (28). To obtain a unique genome construct, some modification should be performed later verification test. This alternation included placement of RE sites to remove the designed gene construct and inserts it into the other vector, as well as identification of an inserting gene into the interest site within the animal genome (29). Therefore, after the introduction of the gene construct, the verification could be performed using RE and PCR products.

In the current study, we designed a specific *CFTR* gene construct and used an HR system without using breakage enzymes. The integration occurred during normal genome replication where two-strand DNA separated through the replication fork, and randomly the targeted exogenous gene incorporated with a homologs site in the genome. So, for a first time we succeed in insertion of gene construct and determine the insertion using simple PCR method.

Conclusion

We successfully designed and produced a transgenic model of CF based on a HR system. This was via transferring the specific designed artificial human *CFTR* gene into a male mouse pronucleus without the requirement of TALEN, ZFNs, or CRISPR-cas9 techniques to increase the efficiency of integration; and, we could then verify *CFTR* construct integration into the genome using simple PCR. The study can only be further developed after the blastocyst formation and implantation of the blastocyst passes through the embryonic development stages and gives birth to the CF fetuses. Hence, the production of the CF mouse model by this specifically designed *CFTR* construct is recommended for further studies.

Acknowledgments

The authors are thankful of the Cellular and Molecular Biology Research Center, Shahid Beheshti University of Medical Sciences, Tehran Iran, for their cooperation. There is no financial support and conflict of interest in this study.

Authors' Contributions

B.K., M.S.; Contributed to conception and design. H.R.; Contributed to all experimental work, data gathering, statistical analysis, and data interpretation. B.K., M.S., S.H.; Experimental work. Kh.A.; Clinical consultation and overall supervision. H.R., S.K.; Drafted the manuscript

and bioinformatic analysis. M.B.; Manuscript revision and cloning and experimental work. B.K., S.H.; Contributed in IVF procedure. All authors read and approved the final manuscript.

References

1. Lopes-Pacheco M. CFTR modulators: the changing face of cystic fibrosis in the era of precision medicine. Front Pharmacol. 2020; 101662.
2. Wang Y, Wrennall JA, Cai Z, Li H, Sheppard DN. Understanding how cystic fibrosis mutations disrupt CFTR function: from single molecules to animal models. Int J Biochem Cell Biol. 2014; 52: 47-57.
3. McCarron A, Donnelley M, Parsons D. Airway disease phenotypes in animal models of cystic fibrosis. Respir Res. 2018; 19(1): 1-12.
4. Hodson ME, Simmonds NJ, Warwick WJ, Tullis E, Castellani C, Assael B, et al. An international/multicentre report on patients with cystic fibrosis (CF) over the age of 40 years. J Cyst Fibros. 2008; 7(6): 537-542.
5. Rosen BH, Chanson M, Gawenis LR, Liu J, Sofoluwe A, Zoso A, et al. Animal and model systems for studying cystic fibrosis. J Cyst Fibros. 2018; 17(2): S28-S34.
6. Yu L, Batara J, Lu B. Application of genome editing technology to microrna research in mammalians. Kormann MSD, editor. Modern tools for genetic engineering. London: IntechOpen; 2016.
7. Leavitt AD, Hamlett I. Homologous recombination in human embryonic stem cells: a tool for advancing cell therapy and understanding and treating human disease. Clin Transl Sci. 2011; 4(4): 298-305.
8. Yu H, Wang X, Zhu L, He Z, Liu G, Xu X, et al. Establishment of a rapid and scalable gene expression system in livestock by site-specific integration. Gene. 2013; 515(2): 367-371.
9. Rogers CS, Hao Y, Rokhlina T, Samuel M, Stoltz DA, Li Y, et al. Production of CFTR-null and CFTR-ΔF508 heterozygous pigs by adeno-associated virus–mediated gene targeting and somatic cell nuclear transfer. J Clin Invest. 2008; 118(4): 1571-1577.
10. Engelhardt JF, Yankaskas JR, Ernst SA, Yang Y, Marino CR, Boucher RC, et al. Submucosal glands are the predominant site of CFTR expression in the human bronchus. Nat Genet. 1992; 2(3): 240-248.
11. Sun X, Sui H, Fisher JT, Yan Z, Liu X, Cho HJ, et al. Disease phenotype of a ferret CFTR-knockout model of cystic fibrosis. J Clin Invest. 2010; 120(9): 3149-3160.
12. Xu J, Livraghi-Butrico A, Hou X, Rajagopalan C, Zhang J, Song J, et al. Phenotypes of CF rabbits generated by CRISPR/Cas9-mediated disruption of the CFTR gene. JCI Insight. 2021; 6(1): e139813.
13. Dreano E, Bacchetta M, Simonin J, Galmiche L, Usal C, Slimani L, et al. Characterization of two rat models of cystic fibrosis—KO and F508del CFTR—Generated by Crispr-Cas9. Animal Model Exp Med. 2019; 2(4): 297-311.
14. Leenaars CH, De Vries RB, Heming A, Visser D, Holthaus D, Reijmer J, et al. Animal models for cystic fibrosis: a systematic search and mapping review of the literature–Part 1: genetic models. Lab Anim. 2020; 54(4): 330-340.
15. National Research Council (US) Committee for the Update of the Guide for the Care and Use of Laboratory Animals. Guide for the Care and Use of Laboratory Animals. 8th ed. Washington (DC): National Academies Press (US); 2011.
16. Zeng F, Hao Z, Li P, Meng Y, Dong J, Lin Y. A restriction-free method for gene reconstitution using two single-primer PCRs in parallel to generate compatible cohesive ends. BMC Biotechnol. 2017; 17(1): 32.
17. Vahdat-Lasemi M, Hosseini S, Jajarmi V, Kazemi B, Salehi M. Intraovarian injection of miR-224 as a marker of polycystic ovarian syndrome declines oocyte competency and embryo development. J Cell Physiol. 2019; 234(8): 13858-13866.
18. Colledge WH, Abella BS, Southern KW, Ratcliff R, Jiang C, Cheng SH, et al. Generation and characterization of a delta F508 cystic fibrosis mouse model. Nat Genet. 1995; 10: 445-452.
19. Scholte BJ, Davidson DJ, Wilke M, De Jonge HR. Animal models of cystic fibrosis. J Cyst Fibros. 2004; 3 Suppl 2: 183-190.
20. Dunham MA, Neumann AA, Fasching CL, Reddel RR. Telomere maintenance by recombination in human cells. Nat Genet. 2000; 26(4): 447-450.
21. Jasin M, Rothstein R. Repair of strand breaks by homologous recombination. Cold Spring Harb Perspect Biol. 2013; 5(11): a012740.
22. Symington LS, Rothstein R, Lisby M. Mechanisms and regulation of mitotic recombination in Saccharomyces cerevisiae. Genetics. 2014; 198(3): 795-835.
23. Popova E, Krivokharchenko A, Ganten D, Bader M. Efficiency of transgenic rat production is independent of transgene-construct and overnight embryo culture. Theriogenology. 2004; 61(7-8): 1441-1453.
24. Sosa MAG, De Gasperi R, Elder GA. Animal transgenesis: an overview. Brain Struct Funct. 2010; 214(2-3): 91-109.
25. Meyer M, de Angelis MH, Wurst W, Kühn R. Gene targeting by homologous recombination in mouse zygotes mediated by zinc-finger nucleases. Proc Natl Acad Sci USA. 2010; 107(34): 15022-15026.
26. Yan BW, Zhao YF, Cao WG, Li N, Gou KM. Mechanism of random integration of foreign DNA in transgenic mice. Transgenic Res. 2013; 22(5): 983-992.
27. Bouabe H, Okkenhaug K. Gene targeting in mice: a review. Methods Mol Biol. 2013; 1064: 315-336.
28. Hall B, Limaye A, Kulkarni AB. Overview: generation of gene knockout mice. Curr Protoc Cell Biol. 2009; Chapter 19: Unit 19.12 19.12.1-17.
29. Yaghobi Moghaddam MA, Dehghan Esmatabadi MJ. A review of artificial genetic constructs and their applications as positive controls. J Human Gen Genom. 2019; 3(1): e99853.

Original Article

Alpha-Lipoic Acid Ameliorates Sperm DNA Damage and Chromatin Integrity in Men with High DNA Damage: A Triple Blind Randomized Clinical Trial

Masoud Habibi, Ph.D.[1#], Behzad Abbasi, M.D.[2, 3#], Zohreh Fakhari Zavareh, B.Sc.[1], Vahid Esmaeili, M.Sc.[1], Abdolhossein Shahverdi, Ph.D.[1], Mohammad Ali Sadighi Gilani, M.D.[4], Marziyeh Tavalaee, Ph.D.[2], Mohammad Hossein Nasr-Esfahani, Ph.D. [2, 3*]

1. Department of Embryology, Reproductive Biomedicine Research Center, Royan Institute for Reproductive Biomedicine, ACECR, Tehran, Iran
2. Department of Animal Biotechnology, Reproductive Biomedicine Research Center, Royan Institute for Biotechnology, ACECR, Isfahan, Iran
3. Isfahan Fertility and Infertility Center, Isfahan, Iran
4. Department of Andrology, Reproductive Biomedicine Research Center, Royan Institute for Reproductive Biomedicine, ACECR, Tehran, Iran

#These authors contributed equally to this work.

Corresponding Address: P.O.Box: 8165131378, Department of Animal Biotechnology, Reproductive Biomedicine Research Center, Royan Institute for Biotechnology, ACECR, Isfahan, Iran
Email: mh.nasr-esfahani@royaninstitute.org

Received: 19/September/2021, Accepted: 06/March/2022

Abstract

Objective: Evidence suggests the contributory role of oxidative stress (OS) to sperm DNA damage and eventually, male infertility. Antioxidant supplementation has exhibited favorable results regarding seminal OS, sperm DNA damage, and chromatin integrity. We aimed to evaluate the effect of alpha-lipoic acid (ALA) supplementation on semen analysis, sperm DNA damage, chromatin integrity, and seminal/intracellular OS in infertile men with high sperm DNA damage.

Materials and Methods: In this randomized triple-blind placebo-controlled clinical trial study, we opted for a triple-blind controlled clinical trial design. Considering the study's inclusion criteria for the level of sperm DNA fragmentation (higher than the threshold of 30 and 15%), 70% of participants were selected for this clinical research study. Subjects were divided into case and control groups receiving oral ALA (600 mg/day) and placebo for eighty days, respectively. Sperm parameters and functional tests were examined and compared before and after treatment. The final sample size was 34 and 29 for ALA and placebo receivers, respectively.

Results: No significant differences were observed about anthropometrics and baseline measures of semen analysis, DNA damage, OS, and chromatin integrity between the two groups. Conventional semen parameters were enhanced insignificantly in both groups (P>0.05). DNA damage decreased significantly in the ALA group, as per sperm chromatin structure assay (SCSA, P<0.001). Moreover, chromomycin A3 (CMA3) staining results indicated a decrease in nuclear protamine deficiency post-ALA therapy (P=0.004). Lipid peroxidation decreased significantly after treatment with ALA (P=0.003). Further, seminal antioxidant capacity/activity did not differ significantly in either of the groups (registration number: IRCT20190406043177N1).

Conclusion: An 80-day course of oral ALA supplementation (600 mg/day) alleviates sperm OS, DNA damage, and chromatin integrity in men with high sperm DNA damage.

Keywords: Alpha-Lipoic Acid, DNA Damage, Male Infertility, Sperm

Cell Journal(Yakhteh), Vol 24, No 10, October 2022, Pages: 603-611

Citation: **Habibi H, Abbasi B, Fakhari Zavareh Z, Esmaeili V, Shahverdi AH, Sadighi Gilani MA, Tavalaee M, Nasr-Esfahani MH. Alpha-lipoic acid ameliorates sperm DNA damage and chromatin integrity in men with high DNA damage: a triple blind randomized clinical trial. Cell J. 2022; 24(10): 603-611. doi: 10.22074/cellj.2022.8273.**

Introduction

Infertility is defined as the failure to conceive despite the performance of regular unprotected coitus for a minimum of a year affecting 15-24% of couples (1). Of all infertility cases, approximately 50% are due to male factors and male suboptimal sperm parameters (2). The quality of sperm plays an indisputable leading role in male fertility. However, the criteria by which a spermatozoon is considered 'qualified' to induce pregnancy still need to be determined. Sperm concentration, motility, and morphology have classically been known as sperm quality representatives, although it is now believed that as many as 26% of the male population with 'normal' semen parameters could face infertility (i.e., unexplained infertility) (3, 4). Further, despite advances in human knowledge upon reproduction, the exact etiology behind 30-40% of impaired semen analyses remains unknown, nomenclature as idiopathic male infertility. The emerging evidence has drawn attention to sperm DNA damage as a potential underlying etiology (5, 6). On the other hand, it has been indicated that oxidative stress (OS) majorly contributes to infertility of unknown origin (in 30-80% of infertile men) (7). Similarly, men with unexplained infertility tend to exhibit higher reactive oxygen species (ROS) levels in their seminal fluid compared to fertile normozoospermic individuals (8).

ROS represents a vast number of free and non-free radical chemical compounds produced by oxidative metabolism. ROS generated at the levels of sperm mitochondria and plasma membrane and acts as signaling molecules that mediate capacitation, acrosome reaction, hyperactivation, and sperm-zona pellucida fusion (9). OS portrays a state in which the homeostatic equilibrium between the oxidizing and reductant molecules shifts in favor of the former. The OS occurs as a result of ROS overproduction in the seminal plasma by either morphologically abnormal sperms and/or leukocytes, or due to the lack of antioxidants. The sperm plasma membrane rich in polyunsaturated fatty acids and the simultaneous lack of compensatory mechanisms expose the cell to oxidative damage. Finally, OS is supposedly the main contributor to sperm DNA damage (10, 11).

Evidence shows that there is many studies have exhibited a meaningful association between the increase in sperm DNA damage and prolonged conception period, decreased fertilization rate, impairments in embryo cleavage, higher rates of miscarriage and pregnancy loss, and birth defects in the offspring (12). OS-alleviating role of oral antioxidant supplementation has been also widely explored in the context of male infertility and many studies have detected favorable outcomes regarding motility, OS-induced damage, and DNA fragmentation in sperm (13).

Alpha-lipoic acid (ALA), thiotic acid, is a natural Krebs cycle co-enzyme, reputed for its potent antioxidant characteristics. ALA and its reduced form, dihydrolipoic acid (DHLA), act in both aqueous and lipid phases and exert intense antioxidant properties. In addition to *in vitro*-confirmed direct ROS scavenging characteristics, DHLA regenerates non-enzymatic endogenous antioxidants, namely vitamin C and E, and augments enzymatic antioxidants such as glutathione and superoxide dismutase. Both ALA and DHLA serve as metal chelating agents by forming stable compounds with elements Cu, Mn, Zn, Ars, Cd, and Hg (14). Interestingly, DHLA does not turn into a free radical in the process of neutralizing these agents (14-16).

Many studies have underlined the beneficial impacts of ALA supplementation on OS-derived conditions, namely diabetic neuropathy, glaucoma, cataracts, and alcoholic liver disease (14). Also, the effects of ALA on male fertility have been the subject of several animal models and a few controlled clinical trials. As evidenced, ALA administration ameliorates enzymatic/non-enzymatic antioxidant features, mitigates OS-mediated damages to the testicular structure, and maintains sex-hormone balance; all of which may lead to the improvement in semen parameters and the consequent fertility efficacy (16-18). However, human studies are confined to two exclusive clinical trials: Through a clinical trial on asthenoteratospermic men, Haghighian et al. (18) indicated that ALA supplementation could enhance semen quality in terms of conventional semen parameters. Further, a recent controlled randomized trial has shown that ALA administration after microsurgical varicocelectomy could significantly improve sperm motility and DNA fragmentation in the patients (19). Therefore, both studies have underlined the need for further trials on the subject.

To fill the mentioned gap, we aimed to conduct a randomized, triple-blind placebo-controlled clinical trial to evaluate the effect of oral ALA administration on sperm DNA integrity, chromatin integrity, and sperm parameters as well as seminal OS markers in infertile human subjects with high sperm DNA damage.

Materials and Methods

Study design

The present randomized triple-blind placebo-controlled clinical trial was held in Royan Institute (Tehran, Iran) between July 2018 and June 2020, we randomized infertile men with sperm DNA damage over the threshold to evaluate ALA medication efficacy versus placebo regarding conventional sperm parameters, seminal/intracellular OS, and DNA damage alleviation capabilities (Fig.1). All the sperm analysis and sperm functional tests were conducted in native semen samples. The study protocol was approved by Royan Institute Ethics Committee for Research Involving Human Subjects (IR.ACECR.ROYAN.REC.1397.108) and the Iranian Registry for Clinical Trials (IRCT20190406043177N1).

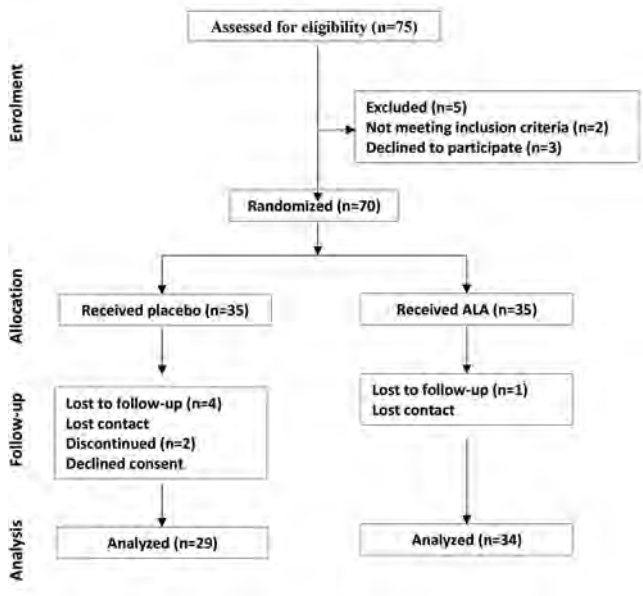

Fig.1: Study design according to CONSORT.

Patient recruitment

Men -referred to the Royan Institute clinic- with or without impaired semen analysis with high sperm DNA damage were eligible for our study. According to WHO guidelines, impaired semen analysis was defined as the presence of at least one of the following conditions: sperm

concentration < 15 million/ml, total motility < 40%, and normal morphology < 4%, otherwise semen analysis was considered to be normal (3). For all the couples, the extent of sperm DNA damage was defined with either sperm chromatin structure assay (SCSA) or terminal deoxynucleotidyl transferase dUTP nick end labeling (TUNEL) method, and individuals with values higher than the threshold of 30% and 15% were considered eligible, respectively (6, 20).

Medical conditions potentially affecting the fertility status were ruled out by available routine investigations for the participants and their female partners. We excluded the subjects with recent/ongoing history of varicocele, leukocytospermia, chemo-radiation, cytotoxic medication, and malignancies. Female partners were considered normal in the presence of normal menstrual cycles, vaginal ultrasounds, and hysterosalpingographies. Couples with female-related infertility, including polycystic ovary syndrome, endometriosis, and tubal factor, were excluded from the study.

Individuals were thoroughly educated on the aim and the rationale behind the study design and the interventional groups, randomization, sample collection, and delivery to the designated laboratory. Age, anthropometrics, and medical and medication/supplementation history were provided from each of the participants. After assuring the couples of not incurring any cost and their right to acquire the obtained results, a signed written consent form was obtained from each.

Interventions

Applying a computer-mediated random digits table and simple randomization method, we allocated the subjects to drug and control groups. Patients in the case group received a cumulative daily dose of 600 mg of ALA (Raha company, Isfahan, Iran), while controls were given the placebo (600 mg, made of starch) with identical appearance and taste, both daily for 80 consecutive days (18). There are no reports of adverse drug reactions for the oral intake of ALA in the literature and it is considered safe to consume (18, 19).

Two semen samples were obtained from every participant: one before the medication course initiation and the other promptly after its termination. Samples were given by masturbation following 2-7 days of sexual abstinence (3). Once delivered to the laboratory, samples were weighed, let to liquefy at room temperature, and subsequently evaluated in terms of viscosity and liquefaction by applying a wide-bore pipette.

Randomization

To randomly allocate the subjects to medication and control groups, we applied permuted blocks. According to our sample size, all the possible permutations of ten-unit blocks were obtained, and subsequently, a sequence of seven blocks was designated by applying a random number table. Randomization was carried out by persons unrelated to the study operations. ALA and placebo were packed identically and were indiscernible. The randomization sequence was not disclosed before the termination of statistical analysis, and patients, drug prescribers, data collectors, and statistical analysts were kept blinded to it.

Primary outcomes

Conventional semen analysis

Concentration

Samples were diluted by applying 1% formalin in sodium bicarbonate solution (1:10) and placed in the sperm counting chamber (Sperm meter, sperm processor, Garkheda, Aurangabad, India). Applying an optical microscope (LABOMED CxL; 20×), a trained laboratory technician counted the number of sperm (a minimum of 200 sperm per sample) and recorded the observations as million sperms/milliliter (3).

Motility

Semen (10 µl) was placed on a pre-warmed sperm counting chamber and was covered with a coverslip with a depth of 20 µm. The motility was assessed utilizing computer-assisted sperm analysis (CASA) and LABOMED CxL optical microscope in a minimum of five different microscopic fields (≥200 sperm evaluated per field). Four distinct sperm motions were determined: rapid progressive, slowly progressive, non-progressive, and immotile. Ultimately the percentage of total sperm motility and progressive sperm motility were reported (3).

Abnormal sperm morphology

According to Tygerberg's criteria, two smears were obtained and fixed by methanol-dissolved triarylmethane dye per sample. The smears were later stained by eosinophilic xanthene and basophilic thiazine solutions (Diff-Quick staining) (Fig.2A). The smears were evaluated regarding head, neck, and tail abnormalities under high microscopic magnification (×1000). At last, the percentage of sperm with abnormal morphology was expressed (3).

Viability

In short, 1 g of eosin Y (color index: 45380) and 10 g of nigrosine (color index: 50420) dyes were separately solved in 100 ml of distilled water. The semen sample was then mixed with eosin (one drop each), and after 30 seconds, three drops of the suspended nigrosine were added to the mixture. One minute later, a thin smear was obtained from the well-blended mixture and was left to dry up for five additional minutes. Subsequently, the slides were monitored using a bright-field optic microscope with ×100 magnification (LABOMED CxL). A minimum of 200 sperm was evaluated per replicate (3).

Sperm DNA integrity/damage evaluation

Terminal deoxynucleotidyl transferase dUTP nick end labeling (TUNEL)

A commercial detection kit was used for TUNEL (Apoptosis Detection System Fluorescein, Promega, Mannheim, Germany). Briefly, a semen aliquot containing 3×10^6 sperm was centrifuged (800 g, 5 minutes, room temperature). After removing the seminal plasma, phosphate-buffered saline (PBS, Sama Tashkhis, Iran) was added to the pellet. Next, each sample was equally divided into negative/positive control and the test tubes. The tube's pellet was then fixed in 4% paraformaldehyde (methanol-free) for 30 minutes (pH=7.4). Next, the samples were diluted with PBS and permeabilized with 0.2% Triton X-100 in PBS for 5 minutes followed by PBS -wash and were resuspension in 50 µl of the staining solution for one hour (37°C, dark room).

For negative control, the TdT enzyme from the kit was not added to the tube, and for the positive control, the samples were incubated with DNase I (40 IU/ml for 10 minutes) before the fixation. Finally, we analyzed the data by flow cytometry (FACScan BD FACS Calibur, Becton–Dickinson, San Jose, CA, USA). A minimum of 10,000 sperm was examined per assay (21).

Sperm chromatin structure assay

Two million sperms were separated from each sample, and container volume was raised to 1 ml using TNE buffer (Tris–HCl+sodium chloride+Ethylenediaminetetra acetic acid [EDTA]) buffer. Following the addition of 400 µl acid-detergent solution to 200 µl of the diluted semen sample, the mixture was stained with 1200 µl of acridine orange (Sigma, St. Louis, USA) staining solution (Fig.2B). Almost 10,000 sperm per sample were monitored/analyzed with a flow cytometer (FACSCalibur Becton Dickinson, San Jose, CA, USA), and the percentage of DNA fragmentation was calculated accordingly (22).

Aniline blue staining

Two smears were obtained and washed from each sample. Then, the slides were fixed and stained by glutaraldehyde (2.5%) and 5% aniline blue (AB, aqueous) in 4 % acetic acid, respectively. Afterward, the slides were dried out using consecutive ethanol baths (70%, 96%, and 100%) and embedded in xylol (5 minutes). Finally, the smears were coated with Entellan rapid mounting medium. Randomly, a minimum of 200 sperm was counted by an instructed individual applying an optical microscope (bluish sperm implied nuclear immaturity) (23).

Chromomycin A3

Briefly, from each sample, two smears of sperm were washed and later fixed with Carnoy's solution. Afterward, smears were stained with 200 µl of Chromomycin A3 (CMA3) staining solution (0.25 mg/ml). After washing with 1x-PBS (×3). By use of an epifluorescence microscope (Olympus, Japan) with suitable filters (460-470 nm, 100× magnified), a minimum of 200 sperm was evaluated: Sperm with insufficient protamine content ~ light yellow; sperm with adequate protamine content ~ dark yellow (Fig.2C) (24).

Reactive oxygen species generation

Mitochondrial membrane potential evaluation: JC1 staining assay (JC1-MMP)

Briefly, the samples were diluted with PBS to an approximate concentration of 3-5 million sperms/ml. JC-1 dye (preserved at -20°C) was thawed at 37°C and was added to the attenuated samples (1 µl to 1 ml) followed by incubation for 15 minutes at 37°C. Subsequently, the samples were centrifuged at 3000 RPM for five minutes. The resultant supernatant was removed, and the cell pellet was suspended again with 1 ml of PBS. For each sample, the level of JC-1 stainability was evaluated using a flow cytometer (FACSCalibur Becton Dickinson, San Jose, CA, USA). Red and green fluorescence implied normal and abnormal mitochondrial membrane potentials, respectively (Fig.2D). The results were eventually expressed as the percentage of green cells reflecting the sperm percentage possessing abnormal mitochondrial membrane potentials (25).

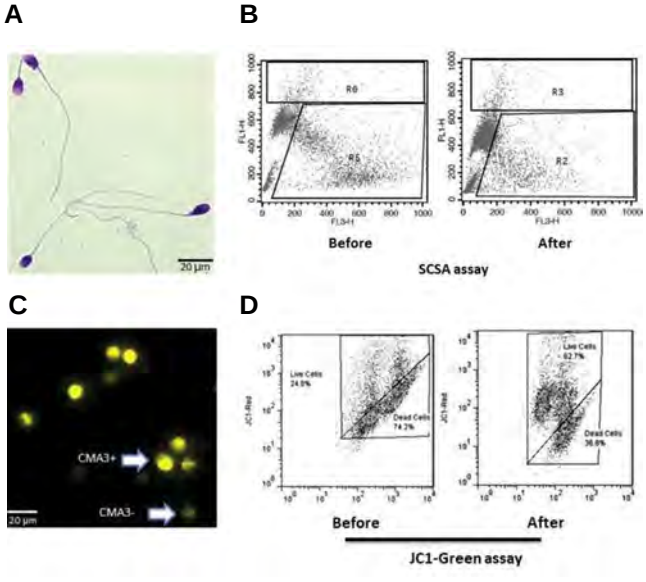

Fig.2: Assessment of sperm functional tests. **A.** Assessment of sperm morphology with Diff- Quick staining, **B.** Representative histograms of sperm chromatin structure assay (SCSA) test before and after ALA therapy in an infertile man, **C.** Chromomycin A3 (CMA3) staining for assessment of sperm protamine deficiency; CMA3 negative or the sperm with normal protamine content and CMA3 positive or protamine deficient sperm, and **D.** Representative histograms of sperm JC1 staining for assessment of mitochondrial membrane potential before and after alpha-lipoic acid (ALA) therapy in an infertile man (20 µm=100 magnification).

Lipid peroxidation

To assess the extent of seminal lipid peroxidation, we evaluated malondialdehyde (MDA) by utilizing a commercial colorimetric MDA assay kit (ZB-MDA-

96A, ZellBio GmbH, Ulm, Germany). Briefly, 100 µL of seminal samples were mixed with 100 µL and 200 µL of R4 reagent and Chromogenic solution, respectively. The mixture then was heated using a boiling water bath for one hour. Next, the tube was cooled in an ice bath and centrifuged for 10 minutes (10,000 rpm). 200 µL of the supernatant was pipetted into a microplate and read at 535 nm.

Total antioxidant capacity

We used a commercial kit (ZB-TAC-96A, ZellBio GmbH, Germany) to measure total antioxidant capacity (TAC) in the seminal plasma. As per manufacturer instructions, seminal plasma was initially centrifuged at 600 g for 10 minutes. Then, 10 µL of the sample was added to 190 µL working chromogen reagent on the microplates followed by covering and 2 minutes of incubation at room temperature. Lastly, the samples were read at the wavelength of 490 nm (26).

Superoxide dismutase activity

Superoxide dismutase (SOD) was also measured with the use of a ZellBio kit (ZB-SOD-96A, Zellbio GmbH, Ulm, Germany). Briefly, the sample was mixed with EDTA and centrifuged for 10 minutes (2000-3000 rpm). Then, the supernatant was added to the wells and blended with the reagents for homogenization. Afterward, applying an enzyme-linked immuno-absorbent assay (ELISA) microplate reader, the absorbance (412 nm) was then measured at 0 and 2 minutes.

Secondary outcome

We opted for pregnancy rate as the secondary outcome. To do so, patients were followed up to determine pregnancy occurrence for approximately six months after the medication's termination. The percentage of couples with clinically approved (confirmation by ultrasound) pregnancies in each interventional group was calculated and reported as the pregnancy rate. Recurrent pregnancy loss was defined and measured as the occurrence of two or more failed pregnancies (27).

Sample size and statistical analysis

Our estimate indicated that a total of 75 infertile men with damaged sperm DNA would correctly endorse a relative effect size of 22% in the composite outcome measure (μ_0=67; μ_1=0.87) with the power and one-tailed level of significance of 0.9 and 0.05, respectively (1-β=0.9; α=0.05) (18).

The analysis was performed utilizing IBM SPSS Statistics for Windows (version 26). As confirmed by the Kolmogorov-Smirnov test, the variables were normally distributed. Consequently, the independent-sample t-test was used to underlie the dispersion of the variables between ALA and placebo groups, while intra-group differences were evaluated applying the paired-sample t test. The data were expressed as mean ± standard deviation, and the P values calculated lower than 0.05 were considered significant. Flow cytometry data were analyzed using WIN MDI 2.9 software (The Scripps Institute, Flow Cytometry Core Facility, USA).

Results

In the current study, 35 individuals to each of the interventional groups were assigned by use of permuted blocks. One and six were lost in ALA and placebo groups due to refusal to continue therapy or not showing up for the endpoint sampling; consequently, the sample size was confined to the final 34 ALA and 29 ALA placebo receivers (Fig.1).

No statistically significant difference was observed between ALA and placebo receivers regarding mean anthropometric values namely age, height, weight, and body mass index. Likewise, the difference between baseline measures of conventional semen parameters, sperm DNA/chromatin indexes, and indicators of ROS generation showed no differences between two groups (P>0.05, Table 1). The abortion rate was higher in the ALA group in comparison with the placebo (97.06% vs. 70.37%, P=0.004). Moreover, a significantly higher prevalence of recurrent pregnancy loss was detected in the ALA group compared to the placebo receivers (85.29% vs. 55.56%, P=0.01).

The results of conventional semen analysis showed significant intra-group differences after the termination of treatment in neither of the interventional groups (Fig.3). We witnessed improvement in sperm chromatin represented by AB (remnant histones) and CMA3 staining (protamine deficiency) after ALA therapy (P=0.03 and P<0.005, respectively). In the ALA group, our analysis revealed a significant decrease in sperm DNA damage by the SCSA test (P<0.005) while the TUNEL results did not differ significantly (P=0.11). Conversely, the mean sperm DNA fragmentation increased significantly among placebo receivers (TUNEL, P=0.03, Fig.4). The extent of lipid peroxidation (i.e., MDA generation) and TAC decreased significantly after ALA medication (both P<0.005) while post-intervention levels of SOD did not differ significantly in either of the groups (P>0.05, Fig.5). Finally, no significant change in mean mitochondrial membrane potential was seen in the ALA (P=0.60) and placebo (P=0.24) groups.

Patients were further followed up for the occurrence of pregnancy: In the ALA group, eight patients achieved natural pregnancy, while the number for the control group was three (pregnancy rates 23.53% and 10.34%, respectively). Pearson's chi-square test revealed no statistically significant relationship between the type of treatment and the incidence of pregnancy (P=0.169).

Table 1: Comparison of the measures of conventional semen analysis and sperm DNA damage assays (SCSA and TUNEL) before and eighty days after initiation of the designated intervention for each experimental group: Alpha-lipoic acid (600 mg/day) versus placebo

Variable	Placebo		ALA		P value			
	a. Before	b. After	c. Before	d. After	a vs. b[1]	c vs. d[1]	a vs. c[2]	b vs. d[2]
Semen volume (ml)	3.43 ± 1.34	3.31 ± 1.22	4.24 ± 1.86	3.89 ± 1.72	0.379	0.132	0.069	0.161
Sperm concentration (10^6/ml)	63.54 ± 64.47	54.56 ± 35.24	50.09 ± 47.64	59.8 ± 43.49	0.335	0.181	0.353	0.614
Total motility (%)	47.16 ± 27.27	41.52 ± 22.56	45.64 ± 25.02	47.27 ± 26.43	0.144	0.653	0.819	0.364
Progressive motility (%)	34.73 ± 19.31	25.49 ± 15.88	28.64 ± 18.28	28.07 ± 22.55	0.997	0.849	0.239	0.631
Viability (%)	84.44 ± 13.54	80.63 ± 20.52	80.58 ± 18.1	83.87 ± 13.65	0.407	0.409	0.386	0.493
Normal morphology (%)	2.19 ± 2.27	1.67 ± 1.33	1.64 ± 1.52	1.48 ± 1.09	0.104	0.377	0.268	0.563
SCSA (%)	30.08 ± 14.24	32.41 ± 14.62	36.98 ± 15.67	25.38 ± 14.68	0.319	0.0005	0.085	0.072
TUNEL (%)	16.23 ± 9.2	20.54 ± 10.44	18.2 ± 12.64	13.7 ± 8.58	0.029	0.107	0.514	0.514

Data are presented as mean ± SD . [1]; Paired t test, [2]; Two-sample t test, SCSA; Sperm chromatin structure assay, and TUNEL; Terminal deoxynucleotidyl transferase dUTP nick end labeling.

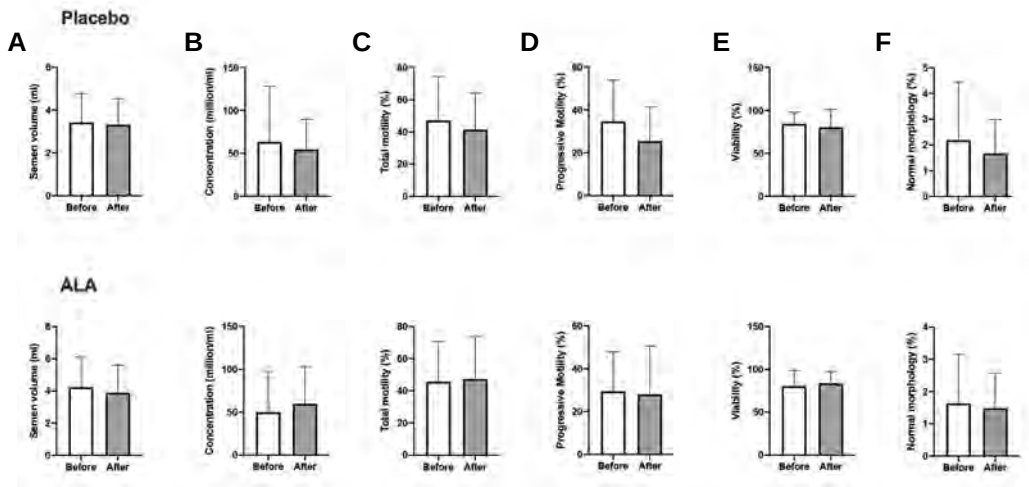

Fig.3: Comparison between the mean measures of seminal analysis parameters before and after intervention (paired t test). **A.** Semen volume, and sperm **B.** Concentration, **C.** Total motility, **D.** Progressive motility, **E.** Viability, and **F.** Normal morphology. ALA; Alpha lipoic acid.

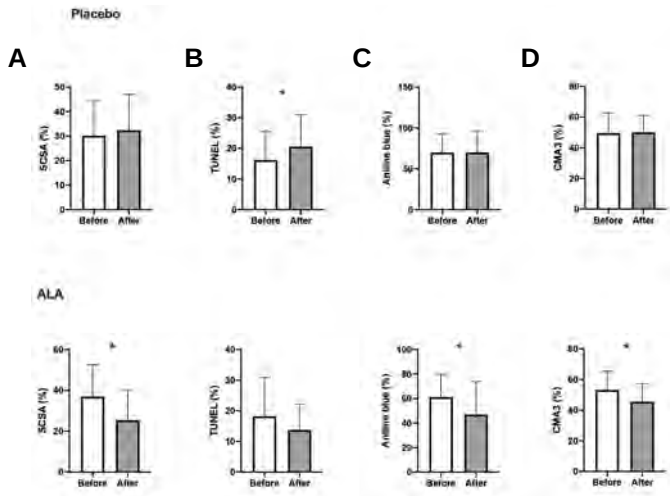

Fig.4: Intragroup comparison between the mean values of sperm DNA damage before and after intervention (paired t test). Examined by **A.** SCSA and **B.** TUNEL assays, and the level of sperm chromatin compaction/protamination as indicated by the results of **C.** Aniline blue and **D.** CMA3 staining techniques. *; Denotes P<0.05, ALA; Alpha lipoic-acid, SCSA; Sperm chromatin structure assay, TUNEL; Terminal deoxynucleotidyl transferase dUTP nick end labeling, and CMA3; Chromomycin A3.

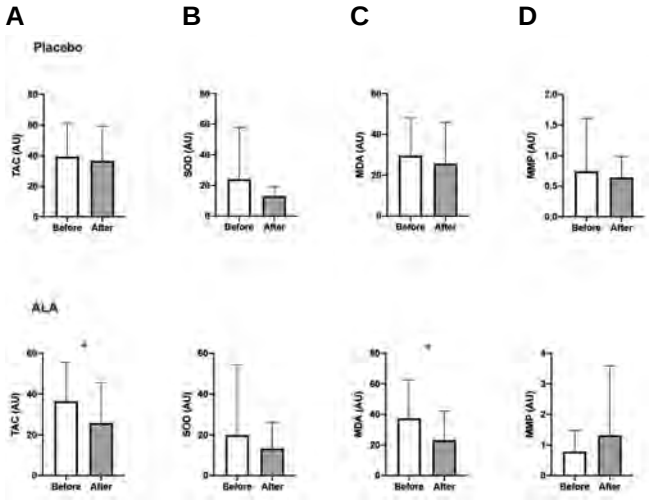

Fig.5: Comparison between levels of seminal oxidative determinants before and after intervention. **A.** Total antioxidant capacity, **B.** Superoxide dismutase, **C.** Malondialdehyde, and **D.** Mitochondrial membrane potential. *; Denotes P<0.05, ALA; Alpha lipoic-acid, TAC; Total antioxidant capacity, SOD; Superoxide dismutase, MDA; Malondialdehyde, MMP; Mitochondrial membrane potential, and AU; Arbitrary unit.

Discussion

As of today, the etiology behind a notable proportion of male infertility cases remains unknown. A recent study has unveiled that as much as 80% of infertile men exhibit some extent of OS in their seminal fluid, which is a potentially reversible condition (28). As mentioned, seminal enzymatic or non-enzymatic antioxidants provide the seminal fluid with oxidative homeostasis primarily through scavenging mechanisms, which ultimately leads to a reduction in ROS content to a satisfactory level. Lately, empirical antioxidant supplementation for infertility has drawn considerable attention. Despite enhancing sperm motility and attenuating seminal OS, however, most of the studied antioxidants confer minimal or no effect on the sperm DNA (29).

Opting triple-blind controlled clinical trial design, the present study is the first to evaluate the effects of ALA supplementation on sperm DNA in human subjects. Recruiting men with infertility of unknown origin, we aimed to focus on ROS overproduction as the principal contributor to sperm DNA damage and consequently to infertility. Generally, our results indicated that infertile men with over-threshold DNA damage could benefit from an 80-day course of ALA supplementation with the daily dosage of 600 mg: chromatin integrity and DNA damage status showed significant improvement post-medication, as assessed by SCSA, AB, and CMA3 assays. However, TUNEL results decreased insignificantly in the case group, while in contrast, placebo receivers gained a statistically significant increase in the TUNEL-assessed DNA damage. Also, both SCSA and TUNEL assays showed lower mean measures of sperm DNA damage in the ALA group compared to the placebo group after treatment.

The DNA integrity status outlines the degree of chromatin compaction, which in sperm is obtained by several mechanisms, most notably through exchanging histone nucleoproteins for protamines (30). Protamine provides more compacted sperm DNA compared to histones primarily through forming intra-/inter-DNA disulfide bonds. Compacted DNA is less vulnerable to damage, namely nicks and fragmentations (31, 32). Consistent with this, in the ALA group we observed a simultaneous decrease and increase in residual histone and sperm nuclear protamine content, respectively. In this regard, ALA has been shown to uphold intracellular cysteine concentration presumably through actively reducing cystine to cysteine or by increasing cellular cysteine uptake; all of which enhance one-carbon metabolism providing methyl groups mandatory for di-sulfide tight bonds needed for the optimum compaction of sperm DNA (33).

Moreover, in the ALA group, our analysis indicated a significant decrease in the mean sperm DNA damage according to the SCSA assay. Conversely, TUNEL results did not show a meaningful alleviation in sperm DNA fragmentation among ALA receivers while underlining a corresponding significant elevation in the placebo group. These findings are potentially attributable to the nature of damages that TUNEL and SCSA assays could detect. In short, the TUNEL assay measures the pre-existing double-strand DNA breaks (i.e., fragmentations) while SCSA evaluates the DNA's susceptibility to single-strand nicks (34). Meanwhile, the persistence of the pre-existing fertility-deteriorating condition through the course of the study (80 days) coupled with receiving a placebo could be explanatory for the observed increase of TUNEL-assessed sperm DNA damage in the control group.

No significant difference was observed in mean MMP after medication. High MMP has been linked to optimum mitochondrial function, high viability, and motility in sperm, while low MMP is a sign of early cell death and apoptosis and is associated with sperm DNA damage (35, 36). On the other hand, hydrogen peroxide and superoxide radicals are byproducts of normal mitochondrial activities (37). Therefore, these observations further verify that ALA may benefit independent of mitochondrial function.

Our analysis unveiled a significant decrease in the level of MDA post-ALA treatment. MDA is the ultimate product of lipid peroxidation (38). The disturbance in membrane structure induced by lipid peroxidation affects vital cellular functions namely signal transduction and maintenance of ion and metabolite gradient necessary for optimal sperm function. The peroxides are generally associated with decreased sperm function and viability, DNA damage, and the ultimate fertility decrease (39). ALA has been proposed to quip the sperm with an extracellular shield and prevent lipid peroxidation, which may account for the observed reduced MDA (18). Concurrently, no significant difference was detected between the baseline and final measures SOD activity in the case group. However, TAC content showed a significant decrease in the ALA receivers, hypothetically imputable to the

presence of a steady ROS scavenging process. Despite the findings mentioned above, no statistically significant changes were observed in favor of ALA supplementation efficacy regarding conventional semen parameters despite noticed alleviation in mean sperm DNA damage.

Finally, patients were monitored regarding the occurrence of pregnancy for a minimum of six months. As addressed in the result sections, we did not notice a significant association between the type of treatment (ALA or placebo) and the occurrence of natural. Considering the significant predominance in the case group regarding the abortion rate, the observed higher pregnancy rate might imply that ALA supplementation leads to enhanced pregnancy results in the infertile men with eminent DNA damage, possibly as a consequence of the lowered DNA damage enhancing the fertilizing capability of sperm, as well as a decrease in chromatin alterations incompatible with fetus viability which needs to be further investigated. Nevertheless, the statistical insignificance of improved pregnancy rate presumably stems from insufficiency in the sample size, proposing room for further clinical trials with larger sample sizes.

Conclusion

An 80-day course of ALA supplementation (600 mg/day) diminishes sperm DNA damage in men with high DNA damage. As indicated by our analysis, ALA medication ameliorates OS-derived lipid peroxidation leading to the consequent alleviation in DNA's damage susceptibility and endorsement of DNA integrity by means of maintaining the optimal nuclear protamine content. However, further investigation could unveil the clinical aspects of such an association.

Acknowledgments

The authors would like to express their gratitude to Raha company (Iran, Isfahan) for providing ALA and placebo packs. This research received no specific grant from any funding agency in the public, commercial, or not-for-profit sectors. The authors declare no conflict of interest.

Authors 'Contributions

M.H.N.-E., M.T.; Contributed to the conception, design, and coordination of the study, data analysis, revised the manuscript, and performed the final scientific manuscript revision. M.H., Z.F.Z., V.E.; Were in charge of patient recruitment and drug prescription, executed the laboratory analysis, and analyzed the data. B.A.; Analyzed the data, performed literature research, drafted the manuscript, revised the manuscript, and the final scientific manuscript revision. A.Sh., M.A.S.G.; Were in charge of patient recruitment and drug prescription. All authors read and approved the final manuscript.

References

1. Zegers-Hochschild F, Adamson GD, Dyer S, Racowsky C, de Mouzon J, Sokol R, et al. The International Glossary on Infertility and Fertility Care, 2017. Fertil Steril. 2017; 108(3): 393-406.
2. Agarwal A, Mulgund A, Hamada A, Chyatte MR. A unique view on male infertility around the globe. Reprod Biol Endocrinol. 2015; 13: 37.
3. World Health Organization. WHO laboratory manual for the examination and processing of human semen. 6th ed. Geneva: World Health Organization; 2021.
4. Moghissi K, Wallach E. Unexplained infertility. Fertil Steril. 1983; 39(1): 5-21.
5. Haddock L, Gordon S, Lewis SEM, Larsen P, Shehata A, Shehata H. Sperm DNA fragmentation is a novel biomarker for early pregnancy loss. Reprod Biomed Online. 2021; 42(1): 175-184.
6. Aitken RJ, Bakos HW. Should we be measuring DNA damage in human spermatozoa? New light on an old question. Hum Reprod. 2021; 36(5): 1175-1185.
7. Wagner H, Cheng JW, Ko EY. Role of reactive oxygen species in male infertility: an updated review of literature. Arab J Urol. 2017; 16(1): 35-43.
8. Pasqualotto FF, Sharma RK, Kobayashi H, Nelson DR, Thomas AJ, Agarwal A. Oxidative stress in normospermic men undergoing infertility evaluation. J Androl. 2001; 22(2): 316-322.
9. du Plessis SS, Agarwal A, Halabi J, Tvrda E. Contemporary evidence on the physiological role of reactive oxygen species in human sperm function. J Assist Reprod Genet. 2015; 32(4): 509-520.
10. Rashki Ghaleno L, Alizadeh A, Drevet JR, Shahverdi A, Valojerdi MR. Oxidation of sperm DNA and male infertility. Antioxidants (Basel). 2021; 10(1): 97.
11. Gualtieri R, Kalthur G, Barbato V, Longobardi S, di Rella F, Adiga SK, et al. Sperm oxidative stress during in vitro manipulation and its effects on sperm function and embryo development. Antioxidants. 2021; 10(7): 1025.
12. Lewis SEM, Simon L. Clinical implications of sperm DNA damage. Hum Fertil (Camb). 2010; 13(4): 201-207.
13. Duca Y, Calogero AE, Cannarella R, Condorelli RA, la Vignera S. Current and emerging medical therapeutic agents for idiopathic male infertility. Expert Opin Pharmacother. 2019; 20(1): 55-67.
14. Salehi B, Berkay Yılmaz Y, Antika G, Boyunegmez Tumer T, Fawzi Mahomoodally M, Lobine D, et al. Insights on the use of α-lipoic acid for therapeutic purposes. Biomolecules. 2019; 9(8): 356.
15. Shay KP, Moreau RF, Smith EJ, Smith AR, Hagen TM. Alpha-lipoic acid as a dietary supplement: Molecular mechanisms and therapeutic potential. Biochim Biophys Acta. 2009; 1790(10): 1149-1160.
16. Prathima P, Pavani R, Sukeerthi S, Sainath SB. α-Lipoic acid inhibits testicular and epididymal oxidative damage and improves fertility efficacy in arsenic-intoxicated rats. J Biochem Mol Toxicol. 2018; 32(2).
17. Truong T, Gardner DK. Antioxidants improve IVF outcome and subsequent embryo development in the mouse. Hum Reprod. 2017; 32(12): 2404-2413.
18. Haghighian HK, Haidari F, Mohammadi-Asl J, Dadfar M. Randomized, triple-blind, placebo-controlled clinical trial examining the effects of alpha-lipoic acid supplement on the spermatogram and seminal oxidative stress in infertile men. Fertil Steril. 2015; 104(2): 318-324.
19. Abbasi B, Molavi N, Tavalaee M, Abbasi H, Nasr-Esfahani MH. Alpha-lipoic acid improves sperm motility in infertile men after varicocelectomy: a triple-blind randomized controlled trial. Reprod Biomed Online. 2020; 41(6): 1084-1091.
20. Evenson D, Wixon R. Meta-analysis of sperm DNA fragmentation using the sperm chromatin structure assay. Reprod Biomed Online. 2006; 12(4): 466-472.
21. Henkel R, Hajimohammad M, Stalf T, Hoogendijk C, Mehnert C, Menkveld R, et al. Influence of deoxyribonucleic acid damage on fertilization and pregnancy. Fertil Steril. 2004; 81(4): 965-972.
22. Evenson DP. Sperm chromatin structure assay (SCSA ®). Methods Mol Biol. 2013; 927: 147-164.
23. Auger J, Mesbah M, Huber C, Dadoune JP. Aniline blue staining as a marker of sperm chromatin defects associated with different semen characteristics discriminates between proven fertile and suspected infertile men. Int J Androl. 1990; 13(6): 452-462.
24. Iranpour FG, Nasr-Esfahani MH, Valojerdi MR, Taki Al-Taraihi TM. Chromomycin A3 staining as a useful tool for evaluation of male fertility. J Assist Reprod Genet. 2000; 17(1): 60-66.
25. Sivandzade F, Bhalerao A, Cucullo L. Analysis of the mitochondrial membrane potential using the cationic JC-1 dye as a sensitive fluorescent probe. Bio Protoc. 2019; 9(1): e3128.
26. Agarwal A, Varghese AC, Sharma RK. Markers of oxidative stress and sperm chromatin integrity. Methods Mol Biol. 2009; 590: 377-402.

27. Bender Atik R, Christiansen OB, Elson J, Kolte AM, Lewis S, Middeldorp S, et al. ESHRE guideline: recurrent pregnancy loss. Hum Reprod Open. 2018; 2018(2): hoy004.
28. Agarwal A, Parekh N, Panner Selvam MK, Henkel R, Shah R, Homa ST, et al. Male oxidative stress infertility (MOSI): Proposed terminology and clinical practice guidelines for management of idiopathic male infertility. World J Mens Health. 2019; 37(3): 296-312.
29. Arafa M, Agarwal A, Majzoub A, Panner Selvam MK, Baskaran S, Henkel R, et al. Efficacy of antioxidant supplementation on conventional and advanced sperm function tests in patients with idiopathic male infertility. Antioxidants. 2020; 9(3): 219.
30. Hekmatdoost A, Lakpour N, Sadeghi MR. Sperm chromatin integrity: etiologies and mechanisms of abnormality, assays, clinical importance, preventing and repairing damage. Avicenna J Med Biotechnol. 2009; 1(3): 147-160.
31. Aoki VW, Moskovtsev SI, Willis J, Liu L, Mullen JBM, Carrell DT. DNA integrity is compromised in protamine-deficient human sperm. J Androl. 2005; 26(6): 741-748.
32. Manochantr S, Chiamchanya C, Sobhon P. Relationship between chromatin condensation, DNA integrity and quality of ejaculated spermatozoa from infertile men. Andrologia. 2012; 44(3): 187-199.
33. Cronan JE. Biotin and lipoic acid: synthesis, attachment, and regulation. EcoSal Plus. 2014; 6(1): 10.1128/ecosalplus.ESP-0001-2012.
34. Henkel R, Hoogendijk CF, Bouic PJD, Kruger TF. TUNEL assay and SCSA determine different aspects of sperm DNA damage. Andrologia. 2010; 42(5): 305-313.
35. Gallon F, Marchetti C, Jouy N, Marchetti P. The functionality of mitochondria differentiates human spermatozoa with high and low fertilizing capability. Fertil Steril. 2006; 86(5): 1526-1530.
36. Agnihotri SK, Agrawal AK, Hakim BA, Vishwakarma AL, Narender T, Sachan R, et al. Mitochondrial membrane potential (MMP) regulates sperm motility. In Vitro Cell Dev Biol Anim. 2016; 52(9): 953-960.
37. Mahfouz RZ, du Plessis SS, Aziz N, Sharma R, Sabanegh E, Agarwal A. Sperm viability, apoptosis, and intracellular reactive oxygen species levels in human spermatozoa before and after induction of oxidative stress. Fertil Steril. 2010; 93(3): 814-821.
38. Dutta S, Majzoub A, Agarwal A. Oxidative stress and sperm function: a systematic review on evaluation and management. Arab J Urol. 2019; 17(2): 87-97.
39. Agarwal A, Virk G, Ong C, du Plessis SS. Effect of oxidative stress on male reproduction. World J Mens Health. 2014; 32(1): 1-17.

Original Article

Effect of Mechanical Micro-Vibrations on The Efficiency of Leopard Inter-Species Somatic Cell Nuclear Transfer

Maryam Shahverdi, D.V.M.[1, 2], Vahid Akbarinejad, Ph.D.[2*], Azam Dalman, Ph.D.[1], Mostafa Hajinasrollah, Ph.D.[3], Mehdi Vojgani, Ph.D.[2], Nima Tanhaei Vash, B.Sc.[4], Mohammad Hossein Nasr-Esfahani, Ph.D.[4], Poopak Eftekhari-Yazdi, Ph.D.[1*]

1. Department of Embryology, Reproductive Biomedicine Research Centre, Royan Institute for Reproductive Biomedicine, ACECR, Tehran, Iran
2. Department of Theriogenology, Faculty of Veterinary Medicine, University of Tehran, Tehran, Iran
3. Animal Core Facility, Reproductive Biomedicine Research Center, Royan Institute for Biotechnology, ACECR, Tehran, Iran
4. Department of Animal Biotechnology, Reproductive Biomedicine Research Center, Royan Institute for Biotechnology, ACECR, Isfahan, Iran

**Corresponding Addresses: P.O.Box: 141556453, Department of Theriogenology, Faculty of Veterinary Medicine, University of Tehran, Tehran, Iran P.O.Box: 16635-148, Department of Embryology, Reproductive Biomedicine Research Center, Royan Institute for Reproductive Biomedicine, ACECR, Tehran, Iran*
Emails: v_akbarinejad@ut.ac.ir, eftekhari@royaninstitute.org

Received: Received: 29/January/2022, Accepted: 25/April/2022

Abstract

Objective: Scarcity of oocytes for assisted reproduction in endangered species can be bypassed by interspecies somatic cell nuclear transfer (iSCNT). In Felids, domestic cat (*Felis catus*) oocytes can serve as recipients for the nucleus of the endangered Persian leopard (*Panthera pardus saxicolor*). However, *in vitro* oocyte maturation is still suboptimal in cats, whereas it has been reported to benefit from micro-vibration in non-felid species. Therefore, the present study is aimed to determine whether micro-vibration, applied during *in vitro* maturation (IVM), improves the embryogenic potential of cat oocytes transplanted with fibroblast nuclei of the Persian leopard.

Materials and Methods: In the experimental study, cat cumulus-oocyte complexes (COCs) were randomly assigned to the treatment group (micro-vibration) or control group (static culture). Resultant metaphase II (MII) oocytes were enucleated and reconstructed with nucleus transplants from leopard fibroblasts, followed by artificial oocyte activation and embryo culture under the same condition (static) for 7 days.

Results: While cumulus cell expansion and oocyte maturation profited from micro-vibration ($P<0.05$), the quantity and quality of blastocysts were significantly lower in micro-vibration than in the control group ($P<0.05$). The total number of blastocyst cells tended to be lower in the micro-vibration than in the control group ($P=0.075$). Nevertheless, the proportion of ICM and TE cells did not differ between the micro-vibration and control groups ($P>0.05$).

Conclusion: The present study indicated that micro-vibration at a frequency of 44 Hz for 5 secs per hour enhanced nuclear maturation and cumulus cell expansion of cat oocytes. However, exposure to micro-vibration during IVM impaired the survival rate of reconstructed oocytes during the iSCNT process and their developmental competence toward the blastocyst stage.

Keywords: Domestic Cat, *In Vitro* Maturation, *Panthera Pardus Saxicolor*, Somatic Cell Nuclear Transfer, Vibration

Cell Journal(Yakhteh), Vol 24, No 10, October 2022, Pages: 612-619

Citation: Shahverdi M, Akbarinejad V, Dalman A, Hajinasrollah M, Vojgani M, Tanhaei Vash N, Nasr-Esfahani MH, Eftekhari-Yazdi P. Effect of mechanical micro-vibrations on the efficiency of leopard inter-species somatic cell nuclear transfer. Cell J. 2022; 24(10): 612-619. doi: 10.22074/cellj.2022.8425.

Introduction

According to the red list of the international union for conservation of nature, the population of the wild members of the Felidae family has dramatically dwindled over the past decades and all of them are presumed to be in jeopardy of extinction (1). This phenomenon has been attributed to various issues, including genetic, demographic, environmental, and human-associated factors restricting wild felids territory and rendering wildlife habitats uninhabitable (2, 3). In this regard, the Persian leopard (*Panthera pardus saxicolor*), which is one of the eight subspecies of leopard species (*Panthera pardus*), is mostly distributed in Iran and considered endangered; hence, protection of this subspecies is of utmost importance (4).

In the context of wildlife conservation, assisted reproductive technologies can be applied to protect endangered animals (5) and there are numerous successful reports in leopard cats (6), African lions (7), and black-footed cats (8). In this regard, interspecies somatic cell nuclear transfer (iSCNT), in which the nucleus of one species is transferred to the enucleated oocyte of another species, could serve as a promising technique, particularly in wild cats affected by oocyte scarcity (9). Indeed, iSCNT using domestic cat oocytes has been applied to rescue a number of endangered feline species such as the African wild cat (10), sand cat (11), tiger (12), and cheetah (13). In these cases, the domestic cat oocyte was utilized as the recipient for the nucleus since it is the only feline species which is not considered endangered (10, 13). Nevertheless, iSCNT technique in feline species suffers from limitations. Chief among them is the fact

that despite major progress over recent years, rates of *in vitro* maturation (IVM) of domestic cat oocytes are still unsatisfactory for large-scale applications in iSCNT (14).

To improve IVM rate in cats, most studies have relied on chemical modifications of culture media, for instance, incorporation of growth factors or antioxidants (15). However, the possibilities are not exhausted with chemistry, and physical parameters are an option as well. Dynamic *in vitro* culture (IVC) using micro-vibration has been proposed to resemble *in vivo* conditions more closely, supporting improved oocyte maturation and development of resultant embryos (16-20). In validation of this notion, evaluating the effect of micro-vibration during IVM and IVC of embryos in pig, Mizobe et al. (17) observed that application of micro-vibration during IVM enhanced development of embryos up to the blastocyst stage, irrespective of the micro-vibration treatment during IVC, and the beneficial effect of micro-vibration was more pronounced during IVM than IVC. Also, micro-vibration has shown positive effects on embryo development in mice, cattle, pigs, and humans in the frequency range of 20-44 Hz.

In this study, we hypothesized that micro-vibration during IVM would result in cat oocytes that are more supportive of iSCNT. We conducted the present study to test this hypothesis, using oocytes from the domestic cat as recipients and fibroblasts from the Persian leopard as nucleus donors.

Materials and Methods

All procedures were performed according to institutional guidelines on animal experimentation and care and approved by the Ethical Committee at Royan Institute (IR.ACECR.ROYAN.REC.1397.188). Unless otherwise mentioned, all materials used in this study were obtained from Sigma-Aldrich (St. Louis, MO, USA) and Gibco (Grand Island, NY, USA).

Oocyte collection and IVM

Ovaries were collected from queens following routine ovariohysterectomy in veterinary clinics and kept in phosphate-buffered saline (PBS, Sigma-Aldrich, USA) at 4°C during transportation to the laboratory. After transportation, ovaries were washed (3 times) using PBS supplemented with 100 IU/ml penicillin and 100 mg/ml streptomycin at room temperature. Each ovary was sliced by a scalpel blade to release cumulus-oocyte complexes (COCs) into a washing medium (WM) containing HEPES tissue culture medium 199 (HTCM 199) supplemented with 10% fetal bovine serum (FBS, Gibco, Ireland). COCs with good morphology and quality (uniform in morphology with intact and dark ooplasm and more than three layers of cumulus cells) were selected forIVM (13). Maturation medium consisted of tissue culture medium 199 (TCM 199) supplemented with 2.5 mM sodium pyruvate, 1 ng/ml estradiol, 1 mM L-glutamine, 3% bovine serum albumin (BSA, Sigma-Aldrich, USA), 100 IU/ml penicillin and 100 mg/ml streptomycin, 25 ng/ml EGF, 100 ng/ml IGF1. The selected COCs were cultured in IVM medium droplets (5 to 10 COCs in each 50 µL droplet), which were placed on tissue culture dishes and covered with mineral oil, at 38°C in 5% CO_2 for 24 hours. In the control (static) group, COCs received no more treatment, whereas, in the treatment (dynamic) group, COCs were subjected to mechanical micro-vibration at the frequency of 44 Hz for 5 seconds per hour using Viboviduct 1500 (SimSoTec GmbH, Cologne, Germany) (17, 18). Following IVM, cumulus expansion area was measured in 12 COCs using Fiji software (National Institutes of Health, Bethesda, MD, USA) as an image processing program, in which system units were changed to μm^2 by calibration. Afterward, cumulus cells were removed by treatment with hyaluronidase (300 IU/ml in HTCM199 containing 10% FBS) for 3 minutes, resulting in denuded oocytes. Oocyte maturation to metaphase II (MII) was scored by the presence of a polar body using a phase-contrast inverted microscope (Olympus CKX41, Tokyo, Japan), and the MII stage was confirmed by Hoechst staining (0.5 mg/ml) of 5 oocytes randomly selected from each group of denuded oocytes. Subsequently, the matured oocytes were deprived of the zona pellucida by incubation in pronase (2.5% in HTCM199 also containing 10% FBS) for 30 seconds on a warm plate and then allowed to recover for 15 minutes in 20% FBS.

Isolation and preparation of leopard fibroblast cell line

The skin biopsy from the Persian leopard was provided to the Royan Institution by Tehran Zoo in April 2018. This step was implemented based on the methodology described previously by Dalman et al. (21). In brief, a biopsy from the ear of a Persian leopard was punched. After washing three times with PBS containing antibiotics (penicillin G 250 U/ml and streptomycin 250 mg/ml), the dermis was dissected into small pieces. After washing, the explants were cultured in Dulbecco's Modified Eagle's Medium (DMEM) supplemented with 15% FBS, 1% penicillin and streptomycin, 2 mM L-glutamine, and 1 mM sodium pyruvate at 38°C in a 5% CO_2 incubator. After 10 days of culture when the cells reached confluency (80-90%), tissue explants were removed and cells were dissociated in trypsin (0.25% trypsin/EDTA) and centrifuged at 1200 rpm for 5 minutes and seeded. Early cell passages were cryopreserved in a medium containing 10% Dimethyl sulfoxide (DMSO, Sigma-Aldrich, USA) and stored in liquid nitrogen. For use in iSCNT experiments, cryopreserved fibroblasts were thawed, passaged 3 to 5 times in DMEM supplemented with 15% FBS at 38°C in a 5% CO_2 incubator, and

arrested in G0 by culturing them 48 hours in DMEM with 0.5% FBS (Fig.1).

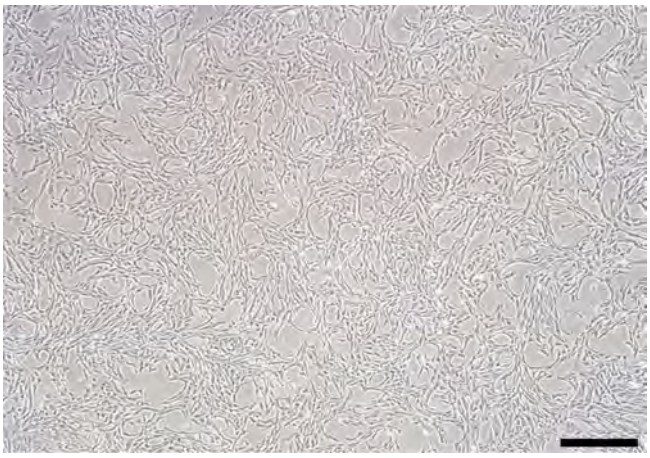

Fig.1: Cultured leopard fibroblast cells (scale bar: 200 µm).

Enucleation of oocytes

Enucleation was performed manually using a pulled Pasteur pipette as described previously by Hosseini et al. (22). In brief, zona-free oocytes were cultured in TCM199 supplemented with 0.41 µg /ml demecolcine, 10% FBS, 10 mg/ml BSA, and 3 mg/ml polyvinyl alcohol (PVA) for 1.5 to 2 hours to induce cytoplasmic protrusion. Thereafter, manual enucleation of the oocyte was implemented under a stereomicroscope by a pulled Pasteur pipette. Before nuclear transfer, enucleated oocytes were maintained for 30 minutes in TCM199 supplemented with 10% FBS, 10 mg/ml BSA, and 3 mg/ml PVA.

Interspecies somatic cell nuclear transfer

To place leopard cells in the vicinity of an enucleated oocyte, the population of fibroblast cells (about 500 cells) was transferred to 50 µl drops of HTCM199 supplemented with 10 mg/ml Phytohemagglutinin (PHA-P). Each enucleated oocyte was dropped on top of an intact and viable fibroblast and the two cells were pushed against each other with a Pasteur pipette. The resultant aggregates were placed in drops of HTCM199 supplemented with 1 mg/ml PVA before fusion. The electrodes of the fusion chamber, lying 0.5 mm apart, were overlaid with a fusion medium consisting of TCM199, 0.3 mM mannitol, and 0.05% BSA. The aggregates were aligned manually and the cell membranes were fused by applying two pulses of direct electric current (1.75 kV/cm for 80 seconds and 1-second delay, Cryologic, Australia). Resultant reconstructed oocytes were maintained in HTCM199 supplemented with 3 mg/ml PVA for 30 to 40 minutes to assess fusion success, before proceeding to activation.

Artificial oocyte activation and *in vitro* embryo culture

Reconstructed oocytes were incubated for 5 minutes in drops of activation medium composed of HTCM199, 1 mg/ml BSA, and 10 µg/ml calcium ionophore A23187. After brief washing in a drop of TCM199 supplemented with 10 mg/ml BSA and 1 mg/ml PVA, reconstructed oocytes were incubated 5 hours in 6-Dimethylamino purine (6-DMAP, 5 µg/ml). Given that zona-free oocytes were used for iSCNT; we chose a 'well of well' (WOW) culture system so as to prevent the embryos from sticking to each other while allowing for diffusion of embryo-derived growth factors between embryos (23). Six reconstructed oocytes were co-cultured in each WOW overlaid with 20 µl of synthetic oviductal fluid (SOF) medium with oil on top, at 39°C, under an atmosphere of 5% O_2, 5% CO_2, and maximum humidity. *In vitro* culture conditions were identical between control and micro-vibration groups.

Differential staining of embryos

Differential staining was used to identify inner cell mass (ICM) and trophectoderm (TE) cells by means of two DNA-specific fluorochromes, namely, propidium iodide (PI) and Hoechst 33342 (24). To this end, day-7 blastocysts were transferred to 2.5% Triton X100 in HTCM plus 5 mg/ml BSA for 15 seconds, and then, they were transferred into HTCM-BSA medium containing 30 µg/ml PI for 45 seconds and washed in HTCM-BSA medium. Afterward, blastocysts were transferred into 800 µl of Hoechst 33342 (10 µg/ml in Ethanol) for 15 minutes and were further mounted on glass slides and examined under a fluorescence microscope (Nikon Eclipse 50i, Tokyo, Japan). Counting of cell nuclei was performed on microphotographs taken with a digital camera. Following enumeration of cells in ICM and TE, the proportion of ICM and TE cells relative to total blastocyst cells (ICM+TE cells) were calculated for further analysis.

Statistical analysis

There were three biological replicates in each experimental group. Continuous data, including COC expansion (size) and the number of blastocyst cells, were initially tested for normality using the Kolmogorov-Smirnov test, and as they had normal distribution, they were analyzed by t test. Non-continuous data, including rates (of IVM, reconstructed oocytes formation, degeneration, cleavage, and blastocyst formation) as well as proportions (of ICM and TE cells) were analyzed using logistic regression (GENMOD procedure), which generated odds ratios (ORs), as the strength of the difference between groups, and 95% confidence intervals (95% CIs). All analyses were conducted in SAS version 9.4 (SAS, 2013). Data are presented as mean ± SEM. Differences at $P<0.05$ were considered statistically significant.

Results

The effect of micro-vibration on domestic cat oocyte IVM

Based on the projection area of the COCs (Fig.2A), micro-vibration during IVM supported greater expansion of the cumulus cells (9.48E+04 ± 1.37E+04 µm², n=12)

compared to the control group (4.74E+04 ± 0.18E+04 μm^2, n=12) (P=0.0007, Fig.2B). Based on the presence of a polar body (Fig.3A), a higher proportion of cat oocytes progressed to MII in the micro-vibration group (91.70 ± 1.77 %, n=383) compared to the control group (84.95 ± 2.85 %, n=383, OR=1.816, 95% CI=1.152-2.865, P=0.010, Fig.3B).

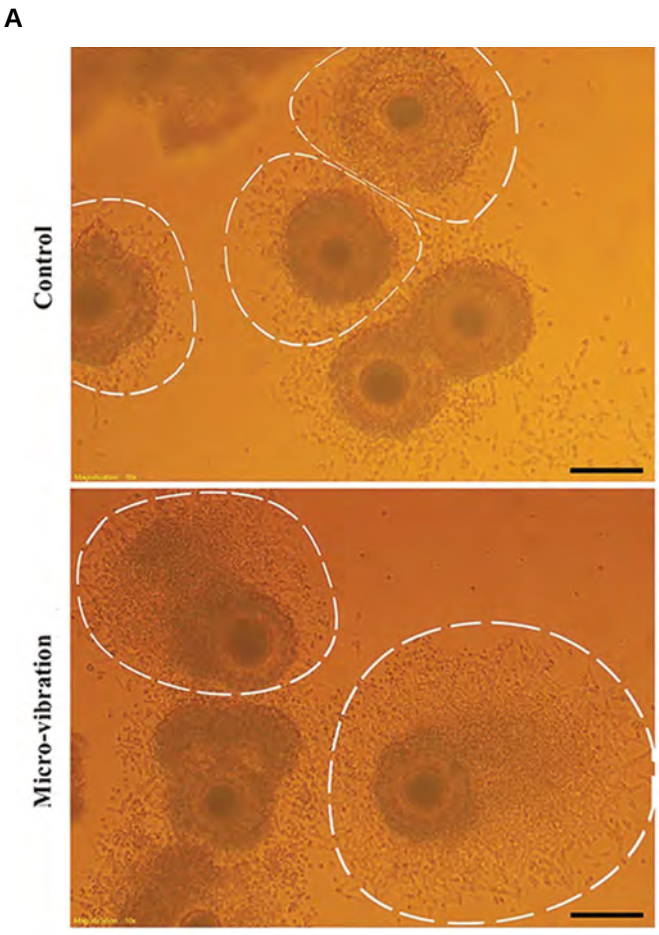

Fig.2: Expansion of cumulus cells. **A.** Expansion of cumulus cells was highlighted by the dashed circles in control and micro-vibration groups (scale bar: 100 µm). **B.** Comparison of cumulus cell expansion in control (n=12) and micro-vibration (n=12) groups. *; P<0.05.

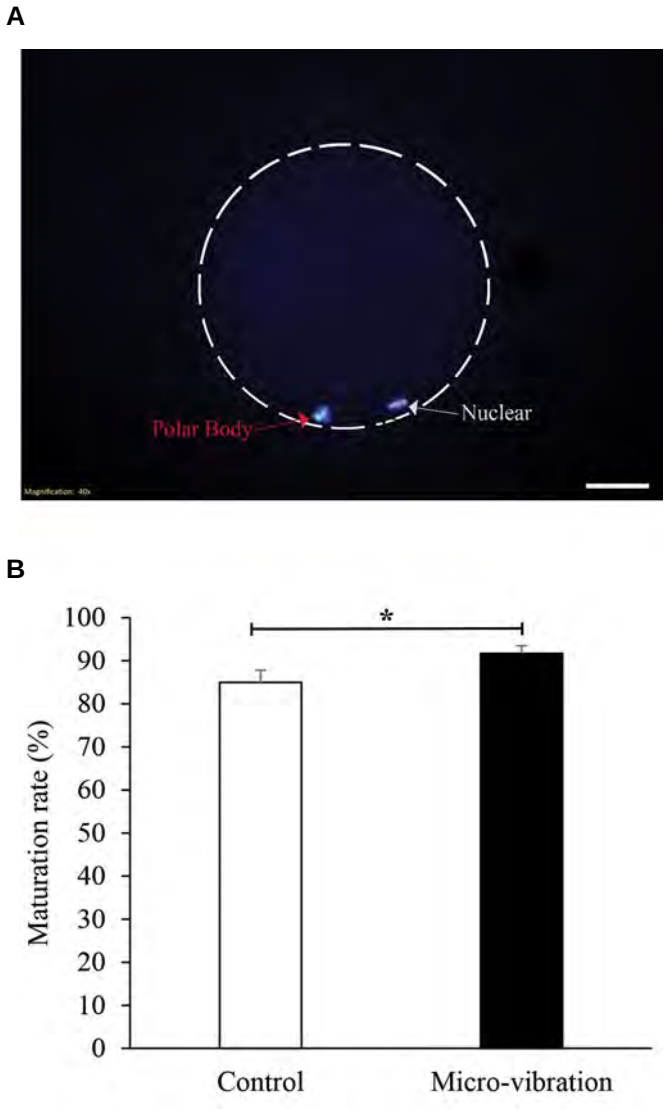

Fig.3: Oocytes maturation. **A.** Extrusion of the first polar body was substantiated by Hoechst staining in a subset of MII-stage oocytes (five oocytes per replicate) (scale bar: 20 µm). **B.** Maturation rate of domestic cat oocytes subjected to *in vitro* maturation (IVM) under control (n=383) and micro-vibration (n=383) conditions. *; P<0.05.

The effect of micro-vibration on iSCNT rate and embryo development

Rate of reconstructed oocyte formation was less in the micro-vibration group (n=350, 23.92 ± 5.82%) compared to the control group (n=327, 48.53 ± 4.90%, OR=0.334, 95% CI=0.240-0.465, P<0.0001, Fig.4). Following activation, similar proportions of reconstructed oocytes degenerated in the two groups (11.02 ± 0.26%, n=81, and 15.81 ± 5.72%, n=15, in the micro-vibration and control groups, respectively). Likewise, cleavage rates were similar in the two groups (83.19 ± 0.44%, n=72, and 90.63 ± 1.73%, n=130; in the micro-vibration and control groups, respectively) (P>0.10, Fig.4). However, the proportion of cleaved embryos that developed to the blastocyst stage after seven days of culture was lower in the micro-vibration (n=60, 6.61 ± 0.82%) than in the control group (18.70 ± 0.72%, n=118, OR=0.312, 95%

CI=0.102-0.951, P=0.041, Fig.4).

The effect of micro-vibration on iSCNT blastocysts quality

Based on the absolute cell counts after differential staining (3 blastocysts in each group) (Fig.5A), the number of ICM cells was lower in the micro-vibration (19.67 ± 1.20) than in the control (25.33 ± 0.88) group (P=0.019, Fig.5B), while the number of TE cells (70.00 ± 5.77, 86.33 ± 5.24) and total blastocyst cells (89.67 ± 6.94, 111.87 ± 6.01) were not significantly different in the micro-vibration and control groups, respectively (P>0.05, Fig.5B). According to the differential staining method, the ICM cell number did not differ between micro-vibration and control groups (22.00 ± 0.54% and 22.75 ± 0.66%, respectively), so did the TE cell number (78.00 ± 0.54% vs. 77.25 ± 0.66 %) (P>0.05, Fig.5B).

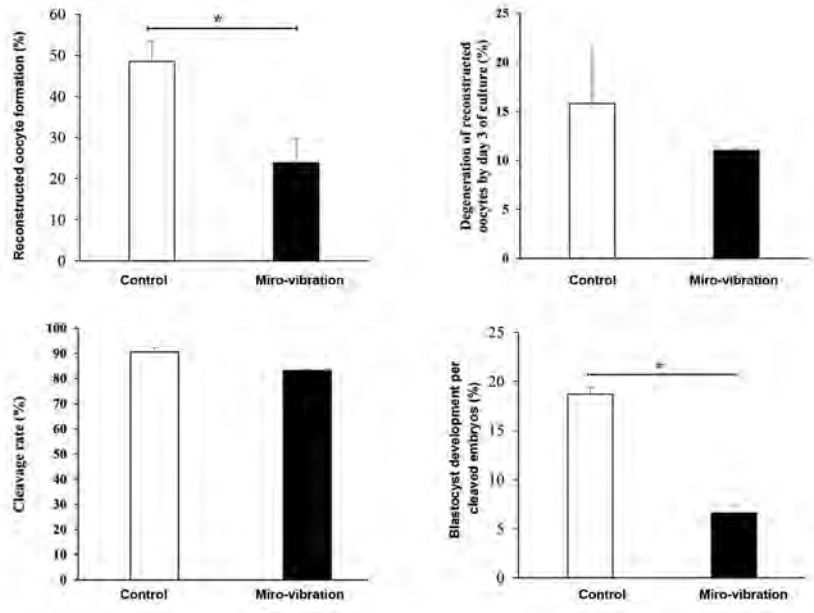

Fig.4: Rate of reconstructed oocyte formation, degeneration rate of reconstructed oocytes by day three of culture, cleavage rate of intact reconstructed oocytes, and rate of blastocyst formation relative to cleaved embryos in control and micro-vibration groups. *; P<0.05.

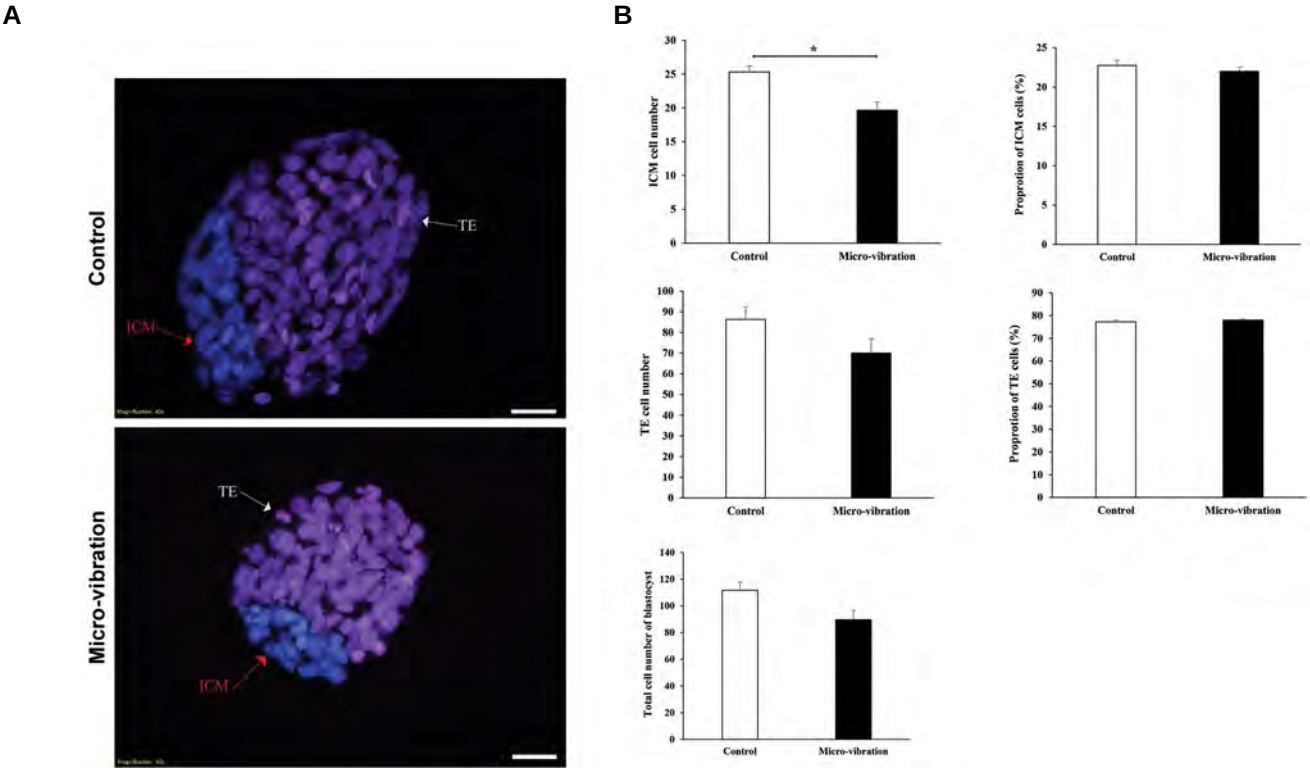

Fig.5: Interspecies somatic cell nuclear transfer (iSCNT) blastocysts. **A.** Differential staining of iSCNT-generated blastocysts in control and micro-vibration groups (scale bar: 20 µm). **B.** Number of embryonic cells and proportion of inner cell mass (ICM) and trophectoderm (TE) cells relative to the total number of blastocyst cells in the control (n=3) and micro-vibration (n=3) groups. *; P<0.05.

Discussion

An inadequate rate of IVM in the domestic cat impedes the success of iSCNT in wild felids (17, 18). The present study aimed to investigate the effect of micro-vibration, applied during IVM, on the maturation of domestic cat oocytes and their embryogenic potential after iSCNT from Persian leopard fibroblasts. The results showed that to apply micro-vibration with the frequency of 44 Hz for 5 seconds per hour, the maturation rate of oocytes was improved but the blastocysts formation rate was decreased.

Our results show that micro-vibration enhanced the expansion of COCs as well as the MII progression of oocytes in the domestic cat. This is consistent with reports in pigs (25, 28). In particular, Mizobe et al. (17) demonstrated a greater extent of cumulus cell expansion in porcine COCs exposed to mechanical micro-vibration during IVM, although these authors did not observe any significant influence of micro-vibration on the proportion of oocytes reaching the MII stage. Mechanical micro-vibration has also proven itself in somatic cell applications, augmenting the proliferation, differentiation, and secretion parameters (27-29). Since COCs are comprised of somatic cells encasing an oocyte, it seems logical that micro-vibration could enhance oocyte maturation through facilitation of expansion in cumulus cells, which govern the maturation and developmental competence of oocytes (30). As an expected result of the enhancement, the IVM oocytes could be better prepared for their biological tasks, including fertilization and embryonic development (31).

Contrary to our expectations, cat oocytes subjected to micro-vibration during IVM were more vulnerable to iSCNT procedure, as measured by rates of reconstructed oocyte formation, which were inferior in the micro-vibration group compared to the control group. This observation implies that despite improved cumulus cell expansion and oocyte maturation to MII, the oocytes were probably damaged in other ways, thereby detracting from their ability to survive the subsequent procedures. Since the settings of intensity, duration, and frequency of micro-vibration used in this study were adopted from studies in other species (e.g. pig (17), human (18), mice (19), and cows (20), it is conceivable that the settings did not suit feline oocytes, reducing their ability to support iSCNT in terms of embryo development (17,18). In this context, we speculate that the plasma membrane may be key to understanding what happened in our study. The plasma membrane is the outermost cellular component that receives the shear stress induced by micro-vibration, and plasma membrane also plays a critical role as a signal transduction interface between external and intracellular environment, subject to modulation by its structural and biochemical properties, particularly its lipid composition and organization (32-34). It is of note that lipid composition and organization determine plasma membrane integrity, prerequisite for cellular homeostasis, and tolerance to extracellular pressures and manipulations (32, 33, 35). Hence, the adverse effects of micro-vibration settings - adopted from other species - on cat oocyte survival during iSCNT could be attributed to the difference(s) between cat and other species in terms of oolemma' s physical and biochemical properties, including lipid composition (36).

After activation of the reconstructed oocytes, degeneration and cleavage rate did not differ between the two experimental groups, while the micro-vibration group produced fewer embryos with diminished proliferation. This negative effect of micro-vibration on embryonic development may have resulted from settings (e.g. duration and/or intensity of micro-vibration) which were inappropriate for the domestic cat oocyte. In this regard, while evaluating the effect of various durations of micro-vibration on IVM of porcine oocytes, Mizobe et al. (17) observed that prolonged exposure to mechanical micro-vibration reduced parthenogenetic development of oocytes up to the blastocyst stage. Moreover, aiming to ascertain the optimum frequency of micro-vibration for IVM and IVC of bovine oocytes and embryos, Takahashi et al. (20) found that an excessive micro-vibration intensity reduced development to the blastocyst stage as well as blastocyst cell proliferation. In the present study, the nuclear maturation rate was improved by micro-vibration, but cytoplasmic maturation remains to be assessed under static vs dynamic conditions. Therefore, the adverse effect of micro-vibration on oocyte developmental competence in the current study could have been mediated through the disruption of processes involved in oocyte cytoplasmic maturation. Indeed, normal development relies on coordinated nuclear and cytoplasmic maturation of oocytes (37, 38). Interference of micro-vibration with the oocytes' cytoplasmic maturation during IVM might have led to disruption of molecular mechanisms regulating proliferation of the future embryonic cells. Among these mechanisms, we envision, for example, the tissue growth factor β superfamily proteins (39) and the Hippo signaling pathway (40).

In this study, the most important limitation that we faced was the scarcity of cat ovaries and oocytes and it restricted the study from finding the optimal frequency for cat oocytes and iSCNT embryos.

Conclusion

Micro-vibration at the frequency of 44 Hz for 5 seconds per hour during IVM augmented cumulus cell expansion and meiotic maturation in domestic cat oocytes. However, the oocytes that matured under the influence of micro-vibration were less tolerant of iSCNT and produced lower numbers of reconstructed oocytes. In addition, these reconstructed oocytes were less capable of developing into blastocysts, which also contained fewer cells. Therefore, it appears that this field of research requires further studies to tailor the characteristics of micro-vibration during IVM of domestic cat oocytes for use in either intraspecies or interspecies purposes. In particular, it should be clarified if the low tolerance of micro-vibrated cat oocytes to iSCNT stemmed from the micro-vibration, or from the

specific settings used (intensity, duration, and frequency of micro-vibration). It would also be helpful to examine the expression of pluripotency and trophectoderm markers in the blastocysts like *OCT4, CDX2*.

Acknowledgments

We express gratitude to the staff of the cloning laboratory at Royan Biotechnology Institute and the Embryology Laboratory at Royan Institute. This study was supported by Royan institute (grant number 97000012); and the Faculty of Veterinary Medicine, University of Tehran (grant number 30854/6/3). The authors declare that there is no conflict of interest regarding the publication of this paper.

Authors' Contributions

M.Sh., A.D.; Participated in the investigation, methodology, writing, review, and editing. V.A., P.E.-Y.; Funding acquisition, project administration, supervision, formal analysis, review, and editing. M.H.; Prepared cat's ovaries following ovariohysterectomy. M.V., M.H.N-E.; Provided critical revision of the study. N.T.V.; Contributed to all experimental work and data. All authors read and approved the final manuscript.

References

1. Wildt D, Philips L, Simmons L, Chakraborty P, Brown J, Howard J, et al. A comparative analysis of ejaculate and hormonal characteristics of the captive male cheetah, tiger, leopard and puma. Biol Reprod. 1988; 38: 245-255.
2. Jacobson AP, Gerngross P, Lemeris JRJr, Schoonover RF, Anco C, Breitenmoser-Würsten C, et al. Leopard (Panthera pardus) status , distribution , and the research efforts across its range. PeerJ. 2016; 4: 1-28.
3. Thuwanut P, Tipkantha W, Siriaroonrat B, Comizzoli B, Chatdarong K. Beneficial effect of extracellular adenosine 5′ triphosphate treatment on the Indochinese leopard (Panthera pardus delacouri) sperm quality after cryopreservation. Reprod Domest Anim. 2017; 52(52): 269-274.
4. Naderi M, Farashi A, Erdi MA. Persian leopard 's (Panthera pardus saxicolor) unnatural mortality factors analysis in Iran. PLoS One. 2018; 13(4): 1-12.
5. Mikołajewska N, Müller K, Niżański W, Jewgenow K. Vitrification of domestic cat oocytes--effect on viability and integrity of subcellular structures. Reprod Domest Anim. 2012; 47 Suppl 6: 295-299.
6. Goodrowe KL, Miller AM, Wildt DE. In vitro fertilization of gonadotropin-stimulated leopard cat (Fezis bengdemis) follicdar oocytes. J exp Zool. 1989; 252(1): 89-95.
7. Goeritz F, Painer J, Jewgenow K, Hermes R, Rasmussen K, Dehnhard M, et al. Embryo retrieval after hormonal treatment to control ovarian function and non-surgical artificial insemination in African lions (Panthera leo). Reprod Domest Anim. 2012; 47 Suppl 6: 156-160.
8. Pope CE, Gómez MC, Galiguis J, Dresser Bl. Applying embryo cryopreservation technologies to the production of domestic and black-footed cats. Reprod Domest Anim. 2012; 47 Suppl 6: 125-129.
9. Cordova A, King WA, Mastromonaco GF. Choosing a culture medium for SCNT and iSCNT reconstructed embryos: from domestic to wildlife species. J Anim Sci Technol. 2017; 59: 24
10. Gómez MC, Pope CE, Giraldo A, Lyons LA, Harris RF, King AL, et al. Birth of african wildcat cloned kittens born from domestic cats. Cloning Stem Cells. 2004; 6(3): 247-258.
11. Gómez MC, Pope CE, Kutner RH, Ricks DM, Lyons LA, Ruhe M, et al. Nuclear transfer of sand cat cells into enucleated domestic cat oocytes is affected by cryopreservation of donor cells. Cloning Stem Cells. 2008; 10(4): 469-483.
12. Moro LN, Jarazo J, Buemo C, Hiriart MI, Sestelo A, Salamone DF. Tiger, Bengal and Domestic cat embryos produced by homospecific and interspecific zona-free nuclear transfer. Reprod Domest Anim. 2015; 50(5): 849-857.
13. Moro LN, Hiriart MI, Buemo C, Jarazo J, Sestelo A, Veraguas D, et al. Cheetah interspecific SCNT followed by embryo aggregation improves in vitro development but not pluripotent gene expression. Reproduction. 2015; 150(1): 1-10.
14. Amarnath D, Li X, Kato Y, Tsunoda Y. Gene expression in individual bovine somatic cell cloned embryos at the 8-cell and blastocyst stages of preimplantation development. J Reprod Dev. 2007; 53(6): 1247-1263.
15. Ochota M, Pasieka A, Nizański W. Superoxide dismutase and taurine supplementation improves in vitro blastocyst yield from poor-quality feline oocytes. Theriogenology. 2016; 85(5): 922-927.
16. Fauci LJ, Dillon R. Biofluidmechanics of reproduction. Annu Rev Fluid Mech. 2006; 38: 371-394.
17. Mizobe Y, Yoshida M, Miyoshi K. Enhancement of cytoplasmic maturation of in vitro matured pig oocytes by mechanical vibration. J Reprod Dev. 2010; 56(2): 285-290.
18. Isachenko V, Maettner R, Sterzik K, Strehler E, Kreinberg R, Hancke K, et al. In-vitro culture of human embryos with mechanical micro-vibration increases implantation rates. Reprod Bio Med Online. 2011; 22(6): 536-544.
19. Hur YS, Park JH, Ryu EK, Park SJ, Lee JH, Lee SH, et al. Effect of micro-vibration culture system on embryo development. J Assist Reprod Genet. 2013; 30(6): 835-841.
20. Takahashi M, Honda T, Hatoya S, Inaba T, Kawate N, Tamada H. Efficacy of mechanical micro-vibration in the development of bovine embryos during in vitro maturation and culture. J Vet Med Sci. 2018; 80(3): 532-535.
21. Dalman A, Eftekhari-Yazdi P, Valojerdi MR, Shahverdi A, Gourabi H, Janzamin E, et al. Synchronizing cell cycle of goat fibroblasts by serum starvation causes apoptosis. Reprod Domest Anim. 2010; 45(5): e46-e53.
22. Hosseini SM, Hajian M, Moulavi F, Asgari V, Forouzanfar M, Nasr-Esfahani MH. Cloned sheep blastocysts derived from oocytes enucleated manually using a pulled pasteur pipette. Cell Reprogram. 2013; 15(1): 15-23.
23. Vajta G, Peura TT, Holm P, Paldi A, Greve T, Trounson AO, et al. New method for culture of zona-included or zona-free embryos: the Well of the Well (WOW) system. Mol Reprod Dev. 2000; 55(3): 256-264.
24. Papaioannou VE, Ebert KM. The preimplantation pig embryo: cell number allocation to trophectoderm and inner cell mass of the blastocyst in vivo and in vitro. Development. 1988; 102(4): 793-803.
25. Comizzoli P, Wildt DE, Pukazhenthi BS. Overcoming poor in vitro nuclear maturation and developmental competence of domestic cat oocytes during the non-breeding season. Reproduction. 2003; 126(6): 809-816.
26. Fernandez-Gonzalez L, Hribal R, Stagegaard J, Zahmel J, Jewgenow K. Production of lion (Panthera leo) blastocysts after in vitro maturation of oocytes and intracytoplasmic sperm injection. Theriogenology. 2015; 83(6): 995-999.
27. Puig F, Rico F, Almendros I, Navajas D, Montserrat JM, Farre R. Vibration enhances interleukin-8 release in a cell model of snoringinduced airway inflammation. Sleep. 2005; 28(10): 1312-1316.
28. Kaupp JA, Waldman SD. Mechanical vibrations increase the proliferation of articular chondrocytes in high-density culture. Proc Inst Mech Eng H. 2008; 222(5): 695-703.
29. Ito Y, Kimura T, Nam K, Katoh A, Masuzawa T, Kishida A. Effects of vibration on differentiation of cultured PC12 cells. Biotechnol Bioeng. 2011; 108(3): 592-599.
30. Dhali A, Javvaji PK, Kolte AP, Francis JR, Roy SC, Sejian V. Temporal expression of cumulus cell marker genes during in vitro maturation and oocyte developmental competence. J Assist Reprod Genet. 2017; 34(11): 1493-1500.
31. De Matos DG, Miller K, Scott R, Tran CA, Kagan D, Nataraja SG, et al. Leukemia inhibitory factor induces cumulus expansion in immature human and mouse oocytes and improves mouse two-cell rate and delivery rates when it is present during mouse in vitro oocyte maturation. Fertil Steril. 2008; 90(6): 2367-2375.
32. White CR, Frangos JA. The shear stress of it all: the cell membrane

and mechanochemical transduction. Philos Trans R Soc Lond B Biol Sci. 2007; 362(1484): 1459-1467.
33. Le Roux AL, Quiroga X, Walani N, Arroyo M, Roca-Cusachs P. The plasma membrane as a mechanochemical transducer. Philos Trans R Soc Lond B Biol Sci. 2019; 374(1779): 1-15.
34. Tozzi C, Walani N, Arroyo M. Out-of-equilibrium mechanochemistry and self-organization of fluid membranes interacting with curved proteins. New J Phys. 2019; 21: 1-23.
35. McNeil PL, Steinhardt RA. Loss, restoration, and maintenance of plasma membrane integrity. J Cell Biol. 1997; 137(1): 1-4.
36. Apparicio M, Ferreira CR, Tata A, Santos VG, Alves AE, Mostachio GQ, et al. Chemical composition of lipids present in cat and dog oocyte by matrix-assisted desorption ionization mass spectrometry (MALDI- MS). Reprod Domest Anim. 2012; 47 Suppl 6: 113-117.
37. Watson AJ. Oocyte cytoplasmic maturation: a key mediator of oocyte and embryo developmental competence. J Anim Sci. 2007; 85(13 Suppl): E1-3.
38. Conti M, Franciosi F. Acquisition of oocyte competence to develop as an embryo: integrated nuclear and cytoplasmic events. Hum Reprod Update. 2018; 24(3): 245-266.
39. Anani S, Bhat S, Honma-Yamanaka N, Krawchuk D, Yamanaka, Y. Initiation of Hippo signaling is linked to polarity rather than to cell position in the pre-implantation mouse embryo. Development. 2014; 141(14): 2813-2824.
40. Liu C, Peng G, Jing N. TGF-β signaling pathway in early mouse development and embryonic stem cells. Acta Biochim Biophy Sin (Shanghai). 2018; 50(1): 68-73.

Original Article

Granulosa Cell Conditioned Medium Enhances The Rate of Mouse Oocyte *In Vitro* Maturation and Embryo Formation

Zeinab Bahrami, M.Sc.[1#], Narges Hatamian, M.Sc.[1#], Mahmood Talkhabi, Ph.D.[1*], Elnaz Zand, M.Sc.[2], David G. Mottershead, Ph.D.[3], Rouhollah Fathi, Ph.D.[2*]

1. Department of Animal Sciences and Marine Biology, Faculty of Life Sciences and Biotechnology, Shahid Beheshti University, Tehran, Iran
2. Department of Embryology, Reproductive Biomedicine Research Center, Royan Institute for Reproductive Biomedicine, ACECR, Tehran, Iran
3. School of Pharmacy and Bioengineering, Keele University, Staffordshire, UK

#These authors contributed equally to this work.

Corresponding Addresses: P.O.Box: 19395-4716, Department of Animal Sciences and Marine Biology, Faculty of Life Sciences and Biotechnology, Shahid Beheshti University, Tehran, Iran
P.O.Box: 16635-148, Department of Embryology, Reproductive Biomedicine Research Center, Royan Institute for Reproductive Biomedicine, ACECR, Tehran, Iran
Emails: m_talkhabi@sbu.ac.ir, rfathi79@royaninstitute.org

Received: 02/August/2021, Accepted: 12/April/2022

Abstract

Objective: *In vitro* maturation (IVM) and cryopreservation of oocytes are two important parts of assisted reproductive technology (ART), but their efficacy is low. This study aimed to improve the quality of *in vitro* vitrified-warmed maturated oocytes using granulosa cell conditioned medium (GCCM).

Materials and Methods: In the experimental study, fresh/non-vitrified and vitrified-warmed mouse germinal vesicle (GV) oocytes (as F and V) were *in vitro* maturated using basal medium (BM) and also BM supplemented with 50% GCCM as treated groups (GM), and categorized as FBM, FGM, VBM and VGM groups, respectively. The rate of successful IVM (MII oocyte formation), mitochondrial membrane potential and the viability of MII oocytes were determined using inverted microscopy, JC-1 and trypan blue staining. Then, the rate of *in vitro* fertilization (IVF) and subsequent two-cell embryo formation was calculated. Finally, the expression levels of *Oct4, Sox2, Cdk-2, Gdf9*, *Integrin beta1* and *Igf2* were analyzed using real-time polymerase chain reaction (PCR) in MII oocytes and two-cell embryos.

Results: These analyses showed that GCCM significantly increased the IVM rate, oocyte meiotic resumption and mitochondrial membrane potential (P<0.05). In addition, the rate of IVF and two-cell embryo formation was significantly higher in FGM and VGM compared to FBM and VBM (P<0.05). Interestingly, GCCM significantly affected the expression of the studied genes.

Conclusion: Our findings suggest that GCCM might be useful for improving the efficiency of IVM and the subsequent IVF outcomes.

Keywords: Conditioned Medium, *In Vitro* Fertilization, *In vitro* Maturation, Vitrification

Cell Journal(Yakhteh), Vol 24, No 10, October 2022, Pages: 620-627

Citation: **Bahrami Z, Hatamian N, Talkhabi M, Zand E, Mottershead DG, Fathi R. Granulosa cell conditioned medium enhances the rate of mouse oocyte in vitro maturation and embryo formation. Cell J. 2022; 24(10): 620-627. doi: 10.22074/cellj.2022.8155.**

Introduction

Assisted reproductive technology (ART) needs ovarian hyperstimulation to increase the number of oocytes. Oocyte cryopreservation is an important and promising adjunct to ART and helps to preserve women's fertility (1). Oocyte cryopreservation enhances the cumulative live-birth rate and promotes the formation of donor banks. It is also important for allowing patient synchronization and better management of medical risks, especially in women who want to freeze oocytes for medical reasons such as cancer, autoimmune diseases and medical conditions causing ovarian insufficiency (2). *In vitro* maturation (IVM) is another important part of ART, which involves the removal of oocytes from an ovary before they are fully developed, and allowing them to finish their maturation *in vitro* (3). IVM has benefits for patients with high antral follicle count (AFC) and/or polycystic ovarian syndrome (PCOS), and helps reduce the risk of ovarian hyperstimulation syndrome (OHSS) as well (4). Despite these benefits, the efficiency of *in vitro* fertilization (IVF) and the viability of embryos derived from *in vitro* maturated oocytes are lower than desired, highlighting the importance of further optimization of the IVM technique.

It is well known that both oocyte cytoplasm maturation (e.g. increasing mitochondrial potential) and nuclear maturation (e.g. progression of meiosis to metaphase II) are required for a successful fertilization and subsequent embryo development (5). The disappearance of the nuclear membrane can be considered as a distinctive sign for the resumption of meiosis morphologically, which is called germinal vesicle breakdown (GVBD) (6). During oocyte maturation *in vivo*, a series of mutual interactions play

roles between oocytes and their surrounding granulosa cells (7). Paracrine communication and gap junctions are the most active bidirectional interactions between oocytes and granulosa cells. Interestingly, granulosa cells-to-oocyte connections are mediated by paracrine signals, whereas the majority of oocyte-to-granulosa cells interaction take place via gap junctions (8, 9). For example, cAMP transferred from granulosa cells to oocytes induces CDK1 phosphorylation and MPF activation, thereby help oocyte to resumes meiosis (10). Moreover, granulosa cell conditioned medium (GCCM) contains various cytokines and growth factors such as epidermal growth factor (EGF), insulin-like growth factor (IGF) and transforming growth factor beta (TGFβ) (11, 12), which stimulate oocyte meiotic resumption via activating MPF subunits (i.e. *Cyclin b1* and *Cdk1*) (13). In addition, it was reported that bovine cumulus-oocyte complex conditioned medium significantly increases IVM of canine oocytes, particularly via nuclear maturation (14). Very recently it was showed that IL-6 concentration in single-blastocyst conditioned medium is linked to embryo quality, depending on the blastulation time (15). Moreover, conditioned media obtained from mesenchymal stem cells has been reported to induce preantral follicle growth, oocyte maturation and subsequent embryo development (16). All these studies suggest a vital role for granulosa cells and GCCM in oocyte maturation and the likelihood of IVF, embryo formation and implantation.

Based on such previous studies, we hypnotized that GCCM could improve the efficiency of IVM, IVF and subsequent embryo formation in mice. Therefore, the aim of this study was to investigate the effects of GCCM on IVM and embryo formation of fresh and vitrified-warmed mouse oocytes.

Materials and Methods

Animals and sample preparation

In the experimental study, Naval Medical Research Institute (NMRI) mice, originally derived from the Royan Institute, were housed in a conditioned environment (20-25°C), humidity (40-60%) and with 12 hours light:12 hours dark cycles. The GV-stage oocytes, preantral follicles and epididymal sperm were obtained from 6-8 week-old and 14 day-old female ovaries, and 10-12 week-old male mice, respectively. All animal experiments were accomplished under Ethics Committee of Royan Institute (IR.ACECR.ROYAN.REC.1398.102).

Granulosa cell culture and preparation of conditioned medium

Preantral follicles (100-120 μm) were isolated mechanically from 14 day-old female mice using 29 gauge insulin needles, placed into minimum essential medium alpha (α-MEM, Sigma, St Louis, MO, USA) supplemented with 10% fetal bovine serum (FBS, Gibco, Waltham, Massachusetts, USA) and 1% follicle-stimulating hormone (Merck, Darmstadt, Germany), and incubated at 37°C and 5% CO_2. After 3 days, non-adherent cells were removed through washing twice with phosphate-buffered saline (PBS) and the remaining adherent cells were cultured in the medium mentioned above until passage 3-4. When the cultured cells reached 70% confluency (approximately 28 days), GCCM was collected, filtered and stored at -20°C until subsequent using for IVM.

GV oocyte isolation and vitrification

Granulosa denuded GV-stage oocytes were obtained from the ovaries of 6-8-week-old NMRI female mice through mechanical dissection of the antral follicles.

To vitrify GV-stage oocytes, 3 droplets of 30 μl of equilibrium solution (ES) medium were placed separately in a dish, and then the collected GV oocytes were washed 3 times in those 3 ES droplets. The oocytes were kept in the third droplet for 5 minutes, and then were transferred to vitrification solution (VS) medium and washed 3 times again in VS medium. It should be noted that washing the oocytes in the second and third droplets and transferring them to cryotop were all done in one minute. Then the cryotops were transferred into the liquid nitrogen tank (-196°C). After 1 day, cryotops were taken out and oocytes were warmed through a specific warming process. To warm the oocytes, three media called W1, W2 and W3 were used. The oocytes were separated from the cryotop and nine washings were performed in three droplets of W1 for less than 1 minute. Then the oocytes were washed in W2 and W3, and for each they were left for 3 minutes in the last droplet. Then, oocytes were transferred to recovery medium containing α-MEM+FBS 10% and placed for 30 minutes in the incubator.

In vitro maturation

For IVM of vitrified-warmed GV-stage oocytes (V) and freshly isolated GV-stage oocytes (F), both types of oocytes were cultured in base medium (BM) and 50% filtered GCCM. In these experiments, α-MEM supplemented with human chorionic gonadotropin (HCG, 7.5 IU, Merck, Darmstadt, Germany), FSH (100 mIU) and FBS (10%) was considered as BM; and BM plus 50% GCCM was referred to as GM. Accordingly, IVM was accomplished in four groups: i. Fresh GV-stage oocytes cultured in the BM (FBM), ii. Fresh GV-stage oocytes cultured in GM (FGM), iii. Vitrified-warmed GV-stage oocytes cultured in the BM (VBM) and iv. Vitrified-warmed GV-stage oocytes cultured GM (VGM). The cultured oocytes in the four listed conditions were evaluated using inverted microscopy (Nikon-TS100) and first polar body extrusion was considered as the maturation criterion [also called metaphase II (MII) phase].

Trypan blue staining

In vitro matured oocytes (MII oocytes) were stained using 0.4% trypan blue (TB). Then, they were washed 3 times in PBS droplets and finally observed using inverted light microscopy. TB-negative MII oocytes and embryos were considered as viable. In contrast, cells with damaged membranes were stained and appeared with a distinctive blue color and were determined as dead cells.

Hoechst staining

Oocytes or two-cell embryos were placed in 70% paraformaldehyde. After 10-15 minutes, they were transferred into a Hoechst staining (Sigma, St Louis, MO, USA) droplet (20 µl). After 6 minutes, the oocytes or two-cell embryos were placed on slides, and observed using fluorescent microscopy (Olympus BX).

JC-1 staining: mitochondria membrane potential activity

To investigate the mitochondria membrane potential (ΔΨm) and localization of mitochondria, the *in vitro* matured oocytes was stained with JC-1 (Sigma, St Louis, MO, USA). JC-1 is a cationic dye that accumulates in energized mitochondria. Low and high concentrations of JC-1 yield green and red (to orange) fluorescence, respectively. Accordingly, A high ratio of red/green fluorescence points to an increase in ΔΨm, as well as mitochondria accumulation in the oocytes. To detect ΔΨm, the *in vitro* matured MII oocytes were stained with JC-1 as previously described (13). Briefly, the *in vitro* matured MII oocytes were stained with JC-1 for 18 hours. Then, they were treated with 0.25 µl/ml JC-1 for 30 minutes in an incubator. Next, they were washed with PBS and evaluated under a fluorescent microscope (Olympus IX71). Finally, Image J software (Java 1.8.0_172 (64-bit) was used to quantify the red/green ratio.

In vitro fertilization procedure

To study the effect of GCCM on the fertilization level and efficiency of embryo formation, the *in vitro* matured oocytes were subjected to IVF method. Briefly, the sperms were collected from the cauda epididymis of 6-8-weeks-old male NMRI mice, capacitated in T6+bovine serum albumin (BSA, 15 mg/ml) medium for 40-60 minutes in an incubator. Then, they were added to the *in vitro* matured oocytes in droplets containing T6 media supplemented with 10% BSA. After 4-6 hours, two pronuclei embryos (2PN) were isolated and washed carefully with IVF medium and transferred to the developmental droplets containing T6 medium supplemented with 10% BSA (4 mg/ml). The two-cell embryos were evaluated after 18 24-hours.

Gene expression following IVM and IVF

To analyze the expression levels of the genes involved in meiotic resumption (*Gdf9, Cdk1, Cyclin b1)* and embryo development (*Oct4, Sox2, Igf2, Cdk2, Integrin beta1)*, total RNA was extracted using PicoPure Kit (TaKaRa Bio Inc., Shiga, Japan) from the oocytes matured in the four previously mentioned conditions (FBM, FGM, VBM and VGM) and their subsequent two-cell embryos. The quality and concentration of RNA in each sample was determined using a NanoDrop 2000 spectrophotometer (Thermo Scientific). The possible genomic DNA contamination was removed by DNase I (Invitrogen) treatment for 15 minutes at room temperature. The total RNA was used for cDNA synthesis using a Takamed Kit (TaKaRa Bio Inc., Shiga, Japan), according to the manufacturer's instructions. Quantitative reverse transcription polymerase chain reaction (RT-qPCR) was performed using ABI Step One Plus Real-Time PCR detection system, in triplicate for each sample and each gene. The relative gene expression was calculated using $2^{-\Delta\Delta Ct}$ method. *Gapdh* was used as the internal control (housekeeping gene) to normalize the expression of genes (the primer sequences are provided in Table 1).

Table 1: The list of primers used for real-time polymerase chain reaction

Gene	Primer sequence (5´-3´)
Gdf9	F: TGAACAACTCTGCCTCTTCC
	R: ATGCTAAACACTCCGTCCTC
Cdk1	F: GACAAAGGAACAATCAAACTGG
	R: GCAAATATGGTCCCTATACTCC
Cyclin B	F: GTTGATAATCCCTCTCCAAGCC
	R: CTGCTCTTCCTCCAGTTGTC
Oct4	F: AGAACCTTCAGGAGATATGCAAA
	R: AGAACCATACTCGAACCACAT
Sox2	F: GCTGGGAGAAAGAAGAGGAG
	R: ATCTGGCGGAGAATAGTTGG
Integrin β1	F: GACACTCAGATACAACCA
	R: AGGTAGTAGAGATCAATAGGG
Igf2	F: AGTTCTGCTGCTGCTTATTG
	R: CTACCTGGCTAGTCATTGG
Cdk2	F: CCTGCTTATCAATGCAGAGGG
	R: TGCGGGTCACCATTTCAGC

Statistical analysis

All quantifications were performed using at least three independent replicates. In the present study, descriptive and inferential statistics were used to analyze the data. Descriptive statistics were used to prepare tables, draw charts and calculate statistical indices and one-way analysis of variance was used to analyze the data. Data were analyzed by GraphPad Prism 8 software (Dotmatics,

USA) and presented as proportions or mean ± standard deviation (SD). Differences with P<0.05 were considered significant.

Results

GCCM increases the rate of *in vitro* maturation

TB staining after IVM revealed that *in vitro* matured oocytes in all four groups (FBM, FGM, VBM and VGM) were viable (Fig.1A). The analysis of the first polar body release showed that its rate was significantly higher in VGM (75.8 %) compared to the groups FBM (53%) and VBM (43.5%, P<0.05, Fig.1B). In addition, the rate of the first polar body release was significantly higher in FGM (72.6%) compared to VBM (43.5%, P<0.05, Fig.1B). Moreover, determination of the number of oocytes, which degraded their nucleus and progressed to the MI and MII stages, showed that the meiotic resumption rate was significantly higher in FGM and VGM than in either one of FBM or VBM (P<0.05, Fig.1C).

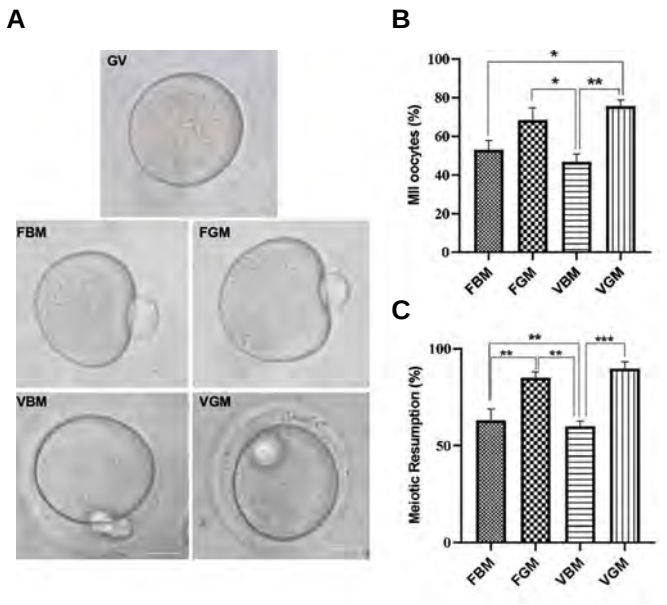

Fig.1: The effect of GCCM on IVM of mouse vitrified-warmed GV oocytes. **A.** Trypan blue staining of oocytes at GV-stage and after IVM (magnification: ×40), **B.** The rate of polar body release of *in vitro* maturated oocytes in the different experimental groups, and **C.** The rate of meiotic resumption of in vitro maturated oocytes in the experimental groups. Data are expressed as mean ± SD. *; P<0.05, **; P<0.01, ***; P<0.001, GCCM; Granulosa cell conditioned medium, IVM; *In vitro* maturation, GV; Germinal vesicle, FBM; *In vitro* matured of fresh/non-vitrified GV-stage oocytes in the basal medium, FGM; *In vitro* matured fresh/non-vitrified GV-stage oocytes in 50% GCCM, VBM; *In vitro* matured vitrified GV-stage oocytes in the basal medium, and VGM; *In vitro* matured vitrified GV-stage oocytes in 50% GCCM (scale bars: 80 µm).

GCCM increased the mitochondrial membrane potential (ΔΨm) activity

Fluorescence microscopy revealed that the JC-1 green signal, which indicates low ΔΨm, was observed in the cytoplasm of the *in vitro* matured oocytes in all experimental groups (FBM, FGM, VBM and VGM) (P<0.05, Fig.2A). Interestingly, the red signal of JC-1, which indicates high ΔΨm, was clearly observed in the cytoplasm of the matured oocytes in FGM and VGM, but it was not significant (P<0.05, Fig.2B). The quantification of red to green signals (Red/Green) showed insignificant differences among all experimental groups. However, the ratio of Red/Green was higher in VGM compared to FBM, FGM and VBM. Moreover, VBM showed the lowest ratio of Red/Green compared to the other groups (P<0.05, Fig.2B).

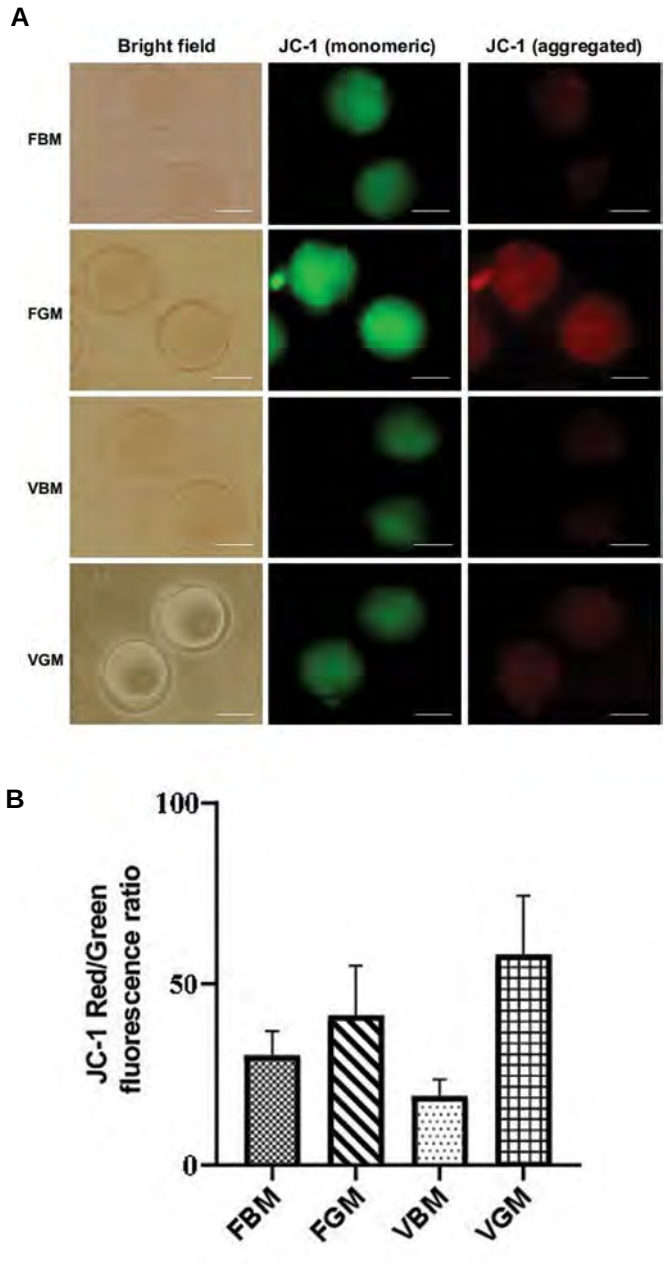

Fig.2: Effects of GCCM on mitochondrial membrane potential (ΔΨm) of *in vitro* maturated vitrified-warmed mouse GV oocytes. **A.** JC-1 staining to assay ΔΨm of *in vitro* maturated oocytes; Green indicates monomeric form of JC-1 generated at low ΔΨm and Red indicates JC-1-aggregated form generated at high ΔΨm) and **B.** The ratio of Red/Green fluorescenceof *in vitro* maturated oocytes in the experimental groups. Data are expressed as mean ± SD (P=0.9, P=0.1). GCCM; Granulosa cell conditioned medium, GV; Germinal vesicle, FBM; *In vitro* matured of fresh/non-vitrified GV-stage oocytes in the basal medium, FGM; *In vitro* matured fresh/non-vitrified GV-stage oocytes in 50% GCCM, VBM; *In vitro* matured vitrified GV-stage oocytes in the basal medium, and VGM; *In vitro* matured vitrified GV-stage oocytes in 50% GCCM (scale bars: 40 µm).

GCCM improves the rate of IVF and embryo formation

Light microscopy showed the MII oocytes, fertilized eggs and two-cell embryos derived from all experimental groups had normal morphology and structure (Fig.3A). The analysis of the second polar body release (as a sign of fertilization) showed that the rate was significantly higher in FGM (68.84 % ± 5.88) compared to FBM (52.23% ± 8.50) and in VGM (77.96% ± 9.29) compared to VBM (62.29% ± 6.70) ($P<0.05$, Fig.3B). Interestingly, the highest rate of IVF was observed in VGM. Analyzing the second polar body release over time revealed that IVF occurred significantly faster in VGM (4.5 hours) and FGM (5.2 hours) compared to VBM (6.6 hours) and FBM (6.4 hours) ($P<0.05$, Fig.3C).

Moreover, the evaluation of two-cell embryo formation revealed that FGM (71.79% ± 8.92) and VGM (76.08% ± 5.32) had higher rate of two-cell embryo formation than that in FBM (54.28% ± 11.66) and VBM (57.89% ± 6.55, $P<0.05$, Fig.3D). Similar to the results obtained from IVF analysis, the highest and lowest rates of two-cell embryo formation were observed in VGM and FBM, respectively (Fig.3B, D). The evaluation of the first cleavage over time demonstrated that FBM- and VBM-derived zygotes needed significantly longer time to complete their first cleavage (Fig.3E).

GCCM has a biphasic effect on gene expression during IVM and embryo formation

The relative expression of *Cyclin B1* (the regulatory subunit of MPF), *Cdk1 (*the catalytic subunit of MPF*)* and *Gdf9* (a growth factor involved in oocyte maturation) was analyzed in all experimental groups (FBM, FGM, VBM and VGM). It was found that *Cdk1* expression was significantly higher in VBM compared to FBM and VGM, but not to FGM ($P<0.05$, Fig.4A). In addition, relative expression of *Cyclin B1* and *Gdf9* was not statistically higher in VGM compared to the other groups (Fig.4A).

In addition, the expression levels of *Oct4* and *Sox2* (transcription factors controlling pluripotency), *Cdk2* (an important factor for cell division), *Itgb1* (integrin beta1; an adhesion molecule involved in implantation) and *Igf-2* (a key growth factor for fetal growth) were examined in two-cell embryos in all experimental groups. The highest expression levels of *Itgb1* and *Cdk2* were observed in VGM-derived embryos ($P<0.05$, Fig.4B). These two genes showed the lowest level of expression in FBM-derived embryos. The highest levels of *Oct4* and *Sox2* expression were detected in the VBM-derived embryos ($P<0.05$, Fig.4B); nonetheless, their expression patterns were different among other groups. It was also found that *Igf-2* expression was insignificantly higher in FBM-derived embryo (Fig.4B) compared to the other groups.

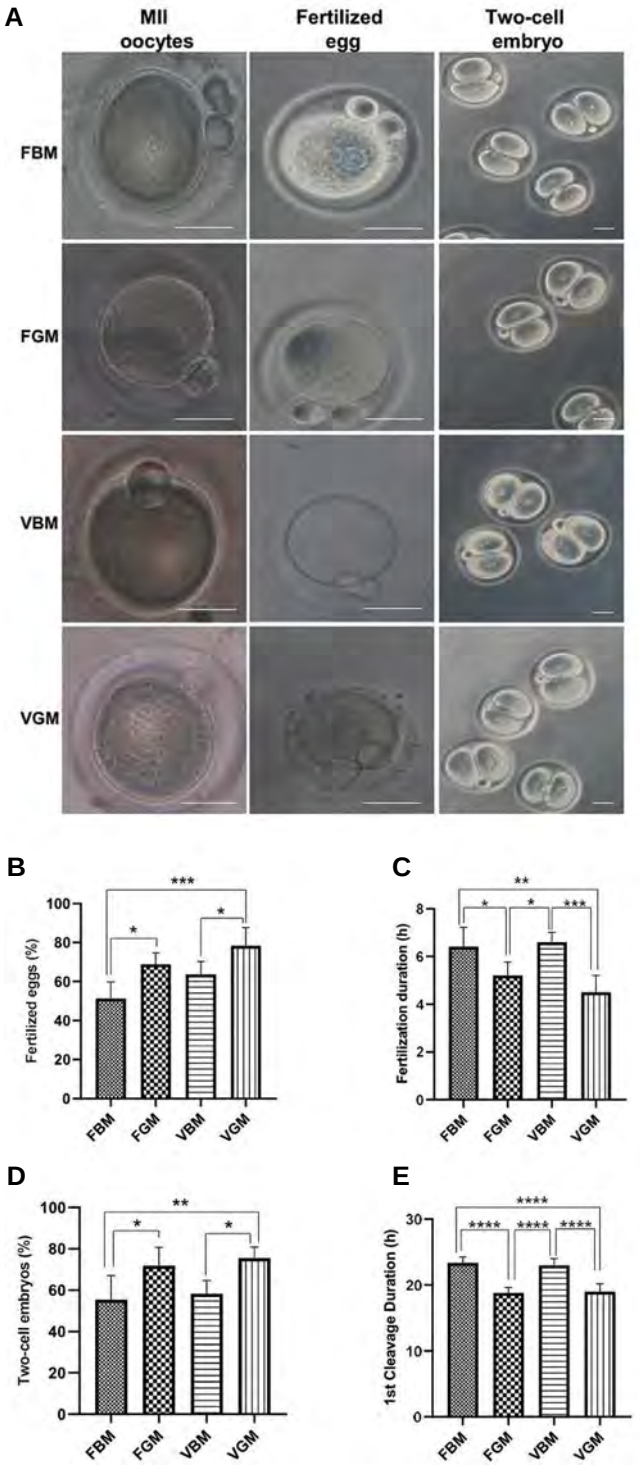

Fig.3: The effect of GCCM applied in IVM of mouse vitrified-warmed GV oocytes on subsequent IVF and two-cell embryo formation. **A.** The morphology of MII oocytes in the experimental groups before and after fertilization and at two-cell embryo stage (magnification 40X for MII oocytes and fertilized eggs, 10X for two-cell embryos). **B.** IVF rate in the experimental groups. **C.** The amount of time taken by the experimental groups to accomplish IVF. **D.** The rate of two-cell embryo formation in the experimental groups. **E.** The amount of time taken by the zygotes derived from the experimental groups to complete the first cleavage. Data are expressed as mean ± SD. *; P<0.05, **; P<0.01, ***; P<0.001, ****; P<0.0001), GCCM; Granulosa cell conditioned medium, IVM; *In vitro* maturation, GV; Germinal vesicle, IVF; *In vitro* fertilization, MII; Metaphase II, FBM; *In vitro* matured of fresh/non-vitrified GV-stage oocytes in the basal medium, FGM; *In vitro* matured fresh/non-vitrified GV-stage oocytes in 50% GCCM, VBM; *In vitro* matured vitrified GV-stage oocytes in the basal medium, and VGM; *In vitro* matured vitrified GV-stage oocytes in 50% GCCM (scale bars: 40 µm).

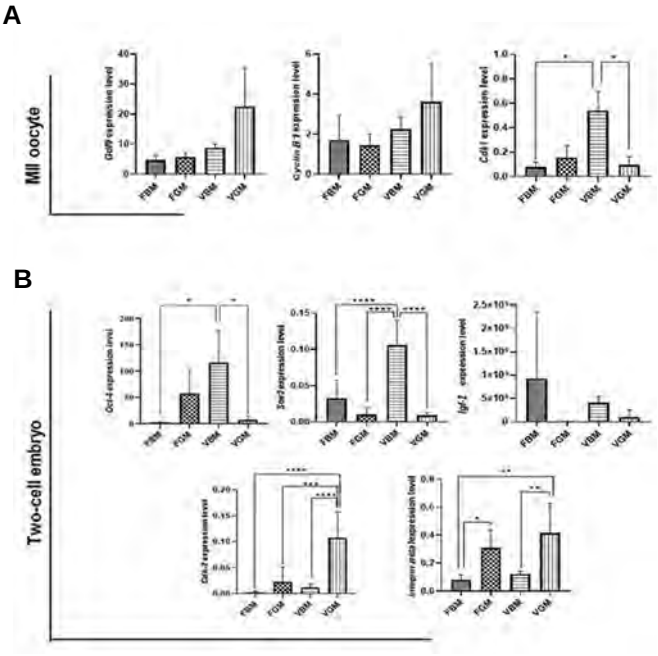

Fig.4: The effect of GCCM on gene expression of *in vitro* matured vitrified-warmed mouse GV oocytes. **A.** The relative gene expression analysis at MII oocytes and **B.** Derived two-cell embryos. Data are expressed as mean ± SD. *; P<0.05, **; P<0.01, ***; P<0.001, ****; P<0.0001, GCCM; Granulosa cell conditioned medium, GV; Germinal vesicle, MII; Metaphase II, FBM; *In vitro* matured of fresh/non-vitrified GV-stage oocytes in the basal medium, FGM; *In vitro* matured fresh/non-vitrified GV-stage oocytes in 50% GCCM, VBM; *In vitro* matured vitrified GV-stage oocytes in the basal medium, and VGM; *In vitro* matured vitrified GV-stage oocytes in 50% GCCM.

Discussion

Today, many different therapeutic strategies are available to treat or control different types of cancer. However, these strategies prolong the life expectancy in cancer patients, but they also reduce their fertility. In recent years, we and other researchers have focused on oncofertility and creating conditions outside the body to preserve and improve fertility in cancer patients. Vitrification is a promising technique for cryopreservation of oocytes and embryos collected from cancer patients. Unfortunately, vitrification increases the level of free radicals in oocytes, induces irreversible damage to the oocyte cell membrane and cytoplasm, decreases antioxidant capacity, mitochondrial membrane potential and ATP levels, and thus reduces fertilization rate and embryo development (17-19). Therefore, improvements in vitrification conditions or other cryopreservation techniques and enhancement of oocyte survival and maturation rate will ameliorate the current situation regarding the reduced fertilization rate and embryo development. In this study, we attempted to take a step towards making improvements in vitrified-warmed oocyte maturation using GCCM, which seems to have critical factors such as IL-6, IGF1, EGF and TGFβ, involved in oocyte maturation and the subsequent processes such as fertilization and embryo formation. In addition, granulosa cells secrete the factors that help the subsequent stages of fertilization like implantation and fertility maintenance. These secretions indicate different functions such as the effects of steroids and follicle stimulating hormone (FSH) on granulosa cells, and lead to estradiol production. Granulosa cells also secrete progesterone after the ovulation stage, which protects against possible pregnancy. The activity of the matrix metalloproteinase (MMP) protein, which is involved in uterine tissue regeneration, embryo development and cervix regeneration during pregnancy, is controlled by tissue inhibitors of metalloproteinases (TIMPs), which are only found *in vitro* by stimulating the granulosa cells with HCG. In addition to the known proteins that are found in the secretion of granulosa cells, proteins with unknown functions are also detected (20-22).

In the present study, the effects of GCCM on IVM of fresh/non-vitrified and vitrified GV-stage oocytes, mitochondrial membrane potential, IVF and two-cell embryo formation were evaluated.

Our results showed that GCCM enhanced the meiotic resumption and maturation in the fresh/non-vitrified GV oocytes (VGM) and vitrified-warmed GV oocytes (VGM). It has been reported that the expression levels of *Gdf9* (23) and *Cdk1* (24) decrease significantly after oocyte vitrification. We found that the relative expression levels of *Cyclinb1* and *Gdf9* were higher, but not significantly, in VGM compared to other groups, whereas *Cdk1* had a significantly higher expression level in VBM compared to other groups. Very recently, it was shown that GDF9 improves meiotic resumption in sheep oocytes (25). Importantly, vitrification-induced damage to the boundary between the nucleus and the cytoplasm results in the early activation of the *Cdk1* gene and the sudden entry of the oocyte into metaphase II (26). Interestingly, we found that *Cdk1* expression was significantly lower in VGM compared to VBM, suggesting that GCCM acts very precisely to promote oocytes to enter metaphase. Although, previous studies demonstrated that oocyte vitrification causes defects in oocyte chromosomal structure and arrangement (27, 28), it is possible that GCCM reduces the destructive effects of vitrification on chromosomal structure and arrangement. To provide a cryopreservation methodology with no destructive impact on embryo and gamete, is one of the most important challenges in the field of cryobiology. In our experiences, when dealing with cryopreservation of the reproductive samples, especially oocytes and embryos, we commonly observe this exciting result. It is accepted that when different treatments are integrated with cryopreservation in oocytes or embryos, the results are in favor of the cryopreserved samples against "fresh" or non-cryopreserved ones. There are several studies that represent a similar idea (29, 30). It is clear that there are many factors involved in this phenomenon, but only some of them have been understood by now. Rodriguez-Wallberg et al. (31), have compared the laboratory and clinical outcomes of embryo and gamete cryopreservation with non-cryopreserved samples. They concluded thatcryopreservation of embryos and gametes is a developing technology that makes frozen reproductive samples comparable to fresh ones.

Moreover, it has been reported that the conditioned media

obtained from embryonic stem cells (32), mesenchymal stem cells (16), and cumulus-oocyte-complexes (33) improve the rate of IVM in different species, suggesting that factors contained in such conditioned media regulate mechanisms involved in oocyte maturation.

We also found that the rate of IVF and embryo formation was significantly increased in FGM and VGM, compared to FBM and VBM, indicating that GCCM contains factors involved in the fertilization process and early embryo development. Our findings also suggest that GCCM eliminates the negative effects of vitrification on IVF and embryo formation and development. These results are supported by previous studies that demonstrated GCCM improves embryo formation and development through the blastocyst stage (12, 34). To better understand the effects of GCCM on fertilization and early embryo development, we analyzed the expression of *Oct4* and *Sox2* (transcription factors regulating pluripotency), *Cdk-2* (an important kinase regulating cell division), *Igf-2* (a key growth factor for fetal growth) and *Integrin beta1* (an important adhesion molecule for implantation) at the two-cell embryo stage. We found that GCCM reduces the expression of pluripotency regulating factors *Oct4* and *Sox2*. It will be interesting and important to investigate the next developmental stages in embryos derived from FGM and VGM. It has been shown that inhibition of maternal-*Oct4* expression has no effect on normal mouse embryo development (35). Moreover, a deliberate increase of *Sox2* gene expression in two-cell embryos impairs embryonic development during pre-implantation stages (36). *Integrin beta1* is another important factor that is necessary for embryo formation and development, and *Integrin beta1*-null embryos don't form inner cell mass (ICM) and die in the preimplantation phase (37). In the present study, there was a higher expression level of *Integrin beta1* in FGM and VGM, suggesting an inducing role for GCCM in *Integrin beta1* expression, which might support further development of embryos. Additional studies are needed to find cell and molecular mechanisms whereby GCCM exerted these effects on IVM, IVF, embryo formation and gene expression. However, it seems that secreted growth factors and cytokines such as IL-6, IGF1, EGF and TGFβ may be one of the more likely candidates, as it has been previously demonstrated that IVM medium supplemented with IGF-1 improves the rate of oocyte maturation, fertilization, and embryo formation (38), and IL-6 improves the quality of mouse embryos and the rate of hatching (39). In addition to above mentioned growth factors, GCCM might have different types of exosomes and miRNAs that could affect embryo quality and development, as it has been recently shown that human embryo culture media and blastocoel fluid have different soluble RNAs that might be used as biomarkers for embryo quality and viability (40).

Conclusion

Taken together, the results presented here indicate that supplementation of GCCM in IVM improve the meiotic resumption in both fresh and vitrified-warmed GV oocytes, and increase the oocyte maturation, fertilization and 2-cell embryo formation rates in GV oocytes derived from vitrification. Overall, it can be concluded that GCCM improves the vitrification outcomes in mouse GV oocytes.

Acknowledgements

This work was supported by Shahid Beheshti University and Royan Institute. The authors indicated no potential conflicts of interest.

Authors' Contribution

R.F., M.T.; Contributed to the design and implementation of the research. Z.B., N.H.; Carried out the experiment, collected, analyzed data, and wrote the manuscript. M.T.; Took the lead in writing the manuscript. E.Z.; Contributed to set up IVM and IVF tests. R.F., M.T., D.G.M.; Provided critical feedback and helped to finalize the manuscript structure. All authors read and approved the final manuscript.

References

1. Talaulikar VS, Conway GS, Pimblett A, Davies MC. Outcome of ovarian stimulation for oocyte cryopreservation in women with Turner syndrome. Fertil Steril. 2019; 111(3): 505-509.
2. Iussig B, Maggiulli R, Fabozzi G, Bertelle S, Vaiarelli A, Cimadomo D, et al. A brief history of oocyte cryopreservation: arguments and facts. Acta Obstet Gynecol Scand. 2019; 98(5): 550-558.
3. Khalili MA, Nottola SA, Shahedi A, Macchiarelli G. Contribution of human oocyte architecture to success of in vitro maturation technology. Iran J Reprod Med. 2013; 11(1): 1-10.
4. Delvigne A, Rozenberg S. Epidemiology and prevention of ovarian hyperstimulation syndrome (OHSS): a review. Hum Reprod Update. 2002; 8(6): 559-577.
5. Trounson A, Anderiesz C, Jones G. Maturation of human oocytes in vitro and their developmental competence. Reproduction. 2001; 121(1): 51-75.
6. Dekel N. Molecular control of meiosis. Trends Endocrinol Metab. 1995; 6(5): 165-169.
7. Liu W, Xin Q, Wang X, Wang S, Wang H, Zhang W, et al. Estrogen receptors in granulosa cells govern meiotic resumption of preovulatory oocytes in mammals. Cell Death Dis. 2017; 8(3): e2662-e2662.
8. Jahromi BN, Mosallanezhad Z, Matloob N, Davari M, Ghobadifar MA. The potential role of granulosa cells in the maturation rate of immature human oocytes and embryo development: a co-culture study. Clin Exp Reprod Med. 2015; 42(3): 111-117.
9. Wigglesworth K, Lee KB, O'Brien MJ, Peng J, Matzuk MM, Eppig JJ. Bidirectional communication between oocytes and ovarian follicular somatic cells is required for meiotic arrest of mammalian oocytes. Proc Natl Acad Sci USA. 2013; 110(39): E3723-E3729.
10. Webb RJ, Marshall F, Swann K, Carroll J. Follicle-stimulating hormone induces a gap junction-dependent dynamic change in [cAMP] and protein kinase a in mammalian oocytes. Dev Biol. 2002; 246(2): 441-454.
11. Dirnfeld M, Goldman S, Gonen Y, Koifman M, Calderon I, Abramovici H. A simplified coculture system with luteinized granulosa cells improves embryo quality and implantation rates: a controlled study. Fertil Steril. 1997; 67(1): 120-122.
12. Malekshah AK, Moghaddam AE, Daraka SM. Comparison of conditioned medium and direct co-culture of human granulosa cells on mouse embryo development. Indian J Exp Biol. 2006; 44(3): 189-192.
13. Zand E, Fathi R, Nasrabadi MH, Atrabi MJ, Spears N, Akbarinejad V. Maturational gene upregulation and mitochondrial activity enhancement in mouse in vitro matured oocytes and using granulosa cell conditioned medium. Zygote. 2018; 26(5): 366-371.
14. Abdel-Ghani MA, Abe Y, Asano T, Hamano S, Suzuki H. Effect of

bovine cumulus–oocyte complexes-conditioned medium on in-vitro maturation of canine oocytes. Reprod Med Biol. 2011; 10(1): 43-49.
15. Zhong H, Sun Q, Chen P, Xiong F, Li G, Wan C, et al. Detection of IL-6, IL-10, and TNF-α level in human single-blastocyst conditioned medium using ultrasensitive Single Molecule Array platform and its relationship with embryo quality and implantation: a pilot study. J Assist Reprod Genet. 2020; 37(7): 1695-1702.
16. Akbari H, Eftekhar Vaghefi SH, Shahedi A, Habibzadeh V, Mirshekari TR, Ganjizadegan A, et al. Mesenchymal stem cell-conditioned medium modulates apoptotic and stress-related gene expression, ameliorates maturation and allows for the development of immature human oocytes after artificial activation. Genes. 2017; 8(12): 371.
17. Succu S, Bebbere D, Bogliolo L, Ariu F, Fois S, Leoni GG, et al. Vitrification of in vitro matured ovine oocytes affects in vitro pre-implantation development and mRNA abundance. Mol Reprod Dev. 2008; 75(3): 538-546.
18. Massip A. Cryopreservation of bovine oocytes: current status and recent developments. Reprod Nutr Dev. 2003; 43(4): 325-330.
19. Lei T, Guo N, Tan MH, Li YF. Effect of mouse oocyte vitrification on mitochondrial membrane potential and distribution. J Huazhong Univ Sci Technol Med Sci. 2014; 34(1): 99-102.
20. Garzo VG, Dorrington JH. Aromatase activity in human granulosa cells during follicular development and the modulation by follicle-stimulating hormone and insulin. Am J Obstet Gynecol. 1984; 148(5): 657-662.
21. Nishi Y, Yanase T, Mu Y, Oba K, Ichino I, Saito M, et al. Establishment and characterization of a steroidogenic human granulosa-like tumor cell line, KGN, that expresses functional follicle-stimulating hormone receptor. Endocrinology. 2001; 142(1): 437-445.
22. De Leo V, Musacchio MC, Cappelli V, Massaro MG, Morgante G, Petraglia F. Genetic, hormonal and metabolic aspects of PCOS: an update. Reprod Biol Endocrinol. 2016; 14(1): 38.
23. Azari M, Kafi M, Ebrahimi B, Fatehi R, Jamalzadeh M. Oocyte maturation, embryo development and gene expression following two different methods of bovine cumulus-oocyte complexes vitrification. Vet Res Commun. 2017; 41(1): 49-56.
24. Niu HR, Zi XD, Xiao X, Xiong XR, Zhong JC, Li J, et al. Cloning of cDNAs for H1F0, TOP1, CLTA and CDK1 and the effects of cryopreservation on the expression of their mRNA transcripts in yak (Bos grunniens) oocytes. Cryobiology. 2014; 69(1): 55-60.
25. Monte AP, Santos JM, Menezes VG, Gouveia BB, Lins TL, Barberino RS, et al. Growth differentiation factor-9 improves development, mitochondrial activity and meiotic resumption of sheep oocytes after in vitro culture of secondary follicles. Reprod Domest Anim. 2019; 54(9): 1169-1176.
26. Kim SS, Olsen R, Kim DD, Albertini DF. The impact of vitrification on immature oocyte cell cycle and cytoskeletal integrity in a rat model. J Assist Reprod Genet. 2014; 31(6): 739-747.
27. Ebrahimi B, Valojerdi MR, Eftekhari-Yazdi P, Baharvand H. In vitro maturation, apoptotic gene expression and incidence of numerical chromosomal abnormalities following cryotop vitrification of sheep cumulus-oocyte complexes. J Assist Reprod Genet. 2010; 27(5): 239-246.
28. Succu S, Leoni GG, Berlinguer F, Madeddu M, Bebbere D, Mossa F, et al. Effect of vitrification solutions and cooling upon in vitro matured prepubertal ovine oocytes. Theriogenology. 2007; 68(1): 107-114.
29. Talreja D, Gupta C, Pai H, Palshetkar N. Oocyte vitrification: a comparative analysis between fresh and cryopreserved oocytes in an oocyte donation program. Fertil Reprod. 2020; 2(01): 9-13.
30. Elnahas A, Alcolak E, Marar EA, Elnahas T, Elnahas K, Palapelas V, et al. Vitrification of human oocytes and different development stages of embryos: an overview. Middle East Fertil Soc J. 2010; 15(1): 2-9.
31. Rodriguez-Wallberg KA, Waterstone M, Anastácio A. Ice age: cryopreservation in assisted reproduction - an update. Reprod Biol. 2019; 19(2): 119-126.
32. Miraki S, Mokarizadeh A, Banafshi O, Assadollahi V, Abdi M, Roshani D, et al. Embryonic stem cell conditioned medium supports in vitro maturation of mouse oocytes. Avicenna J Med Biotechnol. 2017; 9(3): 114-119.
33. Uhde K, van Tol HT, Stout TA, Roelen BA. Metabolomic profiles of bovine cumulus cells and cumulus-oocyte-complex-conditioned medium during maturation in vitro. Sci Rep. 2018; 8(1): 1-14.
34. Maeda J, Kotsuji F, Negami A, Kamitani N, Tominaga T. In vitro development of bovine embryos in conditioned media from bovine granulosa cells and vero cells cultured in exogenous protein- and amino acid-free chemically defined human tubal fluid medium. Biol Reprod. 1996; 54(4): 930-936.
35. Wu G, Schöler HR. Role of Oct4 in the early embryo development. Cell Regen. 2014; 3(1): 7.
36. Avilion AA, Nicolis SK, Pevny LH, Perez L, Vivian N, Lovell-Badge R. Multipotent cell lineages in early mouse development depend on SOX2 function. Genes Dev. 2003; 17(1): 126-140.
37. Stephens LE, Sutherland AE, Klimanskaya IV, Andrieux A, Meneses J, Pedersen RA, et al. Deletion of beta 1 integrins in mice results in inner cell mass failure and peri-implantation lethality. Genes Dev. 1995; 9(15): 1883-1895.
38. Toori MA, Mosavi E, Nikseresht M, Barmak MJ, Mahmoudi R. Influence of insulin-like growth factor-i on maturation and fertilization rate of immature oocyte and embryo development in NMRI mouse with TCM199 and α-MEM medium. JCDR. 2014; 8(12): AC05.
39. Kelley RL, Gardner DK. Addition of interleukin-6 to mouse embryo culture increases blastocyst cell number and influences the inner cell mass to trophectoderm ratio. Clin Exp Reprod Med. 2017; 44(3): 119-125.
40. Kirkegaard K, Yan Y, Sørensen BS, Hardarson T, Hanson C, Ingerslev HJ, et al. Comprehensive analysis of soluble RNAs in human embryo culture media and blastocoel fluid. J Assist Reprod Genet. 2020; 37(9): 2199-2209.

Original Article

Effect of Single Embryo Blastomere Biopsy from Human Frozen Embryos on Assisted Reproductive Outcomes

Shahrzad Aghajani, Ph.D.[1], Ali Salehzadeh, Ph.D.[1]*, Fatemeh Ghasemian, Ph.D.[2], Marzieh Mehrafza, M.D.[3], Ahmad Hosseini, Ph.D.[3]

1. Department of Biology, Rasht Branch, Islamic Azad University, Rasht, Iran
2. Department of Biology, Faculty of Science, University of Guilan, Rasht, Iran
3. Mehr Fertility Research Center, Guilan University of Medical Sciences, Rasht, Iran

Corresponding Address: P.O.Box: 41335-3516, Department of Biology, Rasht Branch, Islamic Azad University, Rasht, Iran
Email: salehzadeh@iaurasht.ac.ir

Received: 01/November/2021, Accepted: 22/February/2022

Abstract

Objective: Preimplantation genetic testing for aneuploidies (PGT-A) is used to determine chromosomal normality and achieve a successful live birth in infertile couples. There is a possible correlation between chromosomal aneuploidy, embryo development and pregnancy rate. This study evaluated the influence of single blastomere biopsy (SBB) on embryo development and pregnancy rates during frozen embryo transfer (FET) and fresh cycles.

Materials and Methods: This quasi-experimental study evaluated 115 intracytoplasmic sperm injection (ICSI) cycles, including 443 embryos (6-8 cells) with a grade A on day three, following PGT-A in the fresh or FET cycles from February 2018 to June 2020. In addition, the fresh cycles without PGT were included as a control group (n=166 embryos). SBB was done on day three and was grouped as FET-PGT (n=149) and the fresh-PGT (n=128).

Results: There is a more aneuploidy rate in the FET-PGT group compared to the fresh-PGT cycle (36.60% vs. 20.38%, P<0.001). There is a rate of higher development and blastocyst in the control group. While the embryos of PGT groups showed higher degrees of expansion (expansion 5) on day five. 8.6, 8.59, and 9.37% of expansion 3, 4, and 5 in the fresh-PGT embryos, 12.58, 2.78, and 14.84% of expansion 3, 4, and 5 in the FET-PGD embryos compared to 10.84and 33.73% of expansion 3 and 4 in the control group (without expansion 5; P<0.001). There was no significant relationship between 13, 18, and 21 chromosome aneuploidies with blastocyst development competence among the groups (P<0.1). Following embryo transfer (n=97), the spontaneous abortion rate was higher in the FET-PGT cycles compared to the fresh-PGT and control groups (50 vs. 22 and 11%, respectively; P<0.04).

Conclusion: The process of SBB following vitrification significantly decreased embryo development and pregnancy outcomes. Therefore, a morphological analysis could not be reliable in selecting chromosomally normal embryos.

Keywords: Aneuploidy, Biopsy, Blastocyst, Genetic Testing, Pregnancy Outcome

Cell Journal(Yakhteh), Vol 24, No 10, October 2022, Pages: 628-636

Citation: **Aghajani Sh, Salehzadeh A, Ghasemian F, Mehrafza M, Hosseini A. Effect of single embryo blastomere biopsy from human frozen embryos on assisted reproductive outcomes. Cell J. 2022; 24(10): 628-636. doi: 10.22074/cellj.2022.8328.**

Introduction

Selecting viable embryos for implantation to achieve successful live birth is a significant concern during intracytoplasmic sperm injection (ICSI) and *in vitro* fertilization (IVF) cycles. At present, morphological evaluation is the basic embryo selection approach. Preimplantation genetic testing for aneuploidies (PGT-A) determines embryos' chromosomal normality. Simultaneously, there is no permanent relationship between embryo morphology and chromosomal status. However, a considerable rate of human blastocysts with excellent morphological grades may have an abnormal chromosomal status (1).

Morphological characteristics include evaluating blastomere number, shape, size, and fragmentation rate, multinucleation of blastomeres, perivitelline space, and zona pellucida evaluation, a common approach for embryo quality assessment (2). However, the predictability of embryo morphology for implantation is controversial (3), while studies reported this association to be fragile (4).

Progression in cryopreservation permits almost 100% recovery of warmed embryos with minimum damage and chemical pregnancy rates similar to (or even higher) than fresh embryo transfer (5). In addition, a recent multicenter cohort study demonstrated that freeze-only transfer cycles had better implantation and pregnancy rates than fresh transfer cycles (6), stimulating a dispute on freeze-only IVF competence (7).

The rate of embryo development to the blastocyst stage has been studied in many studies. Many parameters related to semen quality, maternal age, and embryo gender on aneuploidy, as well as the developmental potential of biopsied and non-biopsied embryos in freeze and fresh embryo transfer cycles, were evaluated. The embryo's quality, determined by the morphological parameters, was not associated with the embryo's genetic status (8, 9).

In contrast, most studies evaluated blastocyst embryos with trophectoderm (TE) biopsy on day five. Therefore, physicians and patients can be informed about the

effect of single blastomere biopsy (SBB) on the embryo development potential to choose an alternative embryo transfer approach and diagnostic tests or to use non-invasive chromosome screening (NICS) and less-invasive chromosome screening (LICS) methods (10, 11).

This study evaluated the role of SBB in the fresh and frozen-warmed embryos (day three) on assisted reproductive outcomes. So, the correlation between embryo gender and aneuploidy (13, 18, 21, X and Y chromosomes) with embryo development potential and embryo resistance following the vitrification-warming procedure was evaluated. In addition, the pregnancy and the live birth rate were studied in the FET-PGT, fresh-PGT and fresh (without PGT) cycles.

Materials and Methods

Patients and study design

This quasi-experimental study was conducted at the Mehr infertility and research center, Rasht, Iran, from February 2018 to June 2020. The study included infertile patients undergoing ICSI cycles with/without PGT-A; subsequently, one to three euploid embryos were transferred to the patient. The age range of men and women was 24 to 59 and 21 to 49-year-old, respectively.

Four hundred fourty three embryos with grade A and 6-8 cells from ICSI cycles with or without SBB were included in this study. First, these embryos were freezes on day 3. Then, a comprehensive chromosomal screening was performed using fluorescence in situ hybridization (FISH) for 13, 18, 21, X, and Y chromosomes. Therefore, the study included three groups as follows: group I) embryos from fresh-PGT cycles (n=128), group II) embryos from FET-PGT cycles (n=149), and group III) embryos without biopsy and vitrification procedures (n=166). Each group followed the results, and the embryos' developmental potential was evaluated using the Gardner method.

Ovarian stimulation

Pituitary suppression was performed using a long-acting gonadotropin-releasing hormone (GnRH) agonist protocol based on the ovarian reserve and anti-Mullerian hormone levels. In addition, ovarian stimulation with recombinant follicle-stimulating hormone (FSH, Gonal-F, Serono, Germany) was initiated. The daily dose of either human menopausal gonadotropin (Menopur, Ferring, Germany) or FSH was set due to the ovarian response. Monitoring of follicle development was done with estradiol measurement and transvaginal ultrasonography. The oocytes were retrieved 36 to 39 hours after human chorionic gonadotropin (hCG) injection and final oocyte maturation. Then oocytes by ICSI procedure were fertilized.

Embryo culture and evaluation

The embryos were cultured and evaluated till day three after ICSI. First, the embryo classification was done based on Gardner's method into three groups; A (6 to 8 blastomeres with the exact size and ≤ 10% fragmentation rate), B (6-8 blastomeres with even or uneven size, and 10% to 20% fragmentation rate), and C (low number and uneven blastomeres with more than 20% fragmentation). Then, the frozen-thawed and/or fresh embryos were cultured until day five (blastocyst stage) and scored based on the Gardner method, which explains the extent of blastocoel expansion, establishment of TE, and inner cell mass (ICM) grade of development.

The rate of expansion was determined as follows: 1=early blastocyst; cavity starting to the formation, 2=early blastocyst; cavity less than 50% of the total embryo, 3=full blastocyst; cavity thoroughly loaded with the embryo, 4=expanded blastocyst; cavity bigger than complete blastocyst, zona slimming, 5=hatching blastocyst; TE is splitting via the zona, 6=hatched blastocyst; blastocyst fully exited of the zona. ICM was graded as follows: A=many cells; firmly compacted, B=some cells; firmly compacted, C=some cells; disordered, D=few cells; disordered. The TE grading was defined as follows: A=forming a coherent epithelium in many cells, B=moderate cells making a weak epithelium, C=some cells making a weak epithelium, and D=very few cells.

Vitrification-warming technique

The embryo transfers of patients with homogeneous hyperechogenic endometrium and serum progesterone levels greater than 2 ng/ml on the day of hCG administration were canceled, and embryos with grade A were vitrified on day three to use at subsequent cycles as a FET-PGT cycle. The vitrification and warming procedures were conducted with the suggested protocol in the Vitrification Kit from the Kitazato company. In brief, the embryos were placed in vitrification solutions for 15 minutes and 40-50 seconds in two steps. Then, embryos were transferred with minimal vitrification solution (0.1 µl or less) and lay a Cryotop. Next, the embryos were put into a nitrogen tank. For warming, the frozen embryos were submerged in a warming solution at 37°C for 1 minute. Then they were rehydrated with a 3-step dilution protocol to recover at room temperature. Finally, embryos were transferred to culture media (12).

Evaluation of embryos the following warming

After embryo warming, the quality of embryos was morphologically defined by quantifying the embryo's intact cells. In addition, intact embryos without signs of degeneration and damaged cytoplasm and/or membrane were considered. In this study, embryos were incubated to evaluate blastulation potential for another two days. The embryos were transferred in an embryo culture medium covered with oil (Global total, COOPER) in a 37°C incubator (SANYO, MCO-5AC) with 5% O_2, 6% CO_2, and 89% N_2 atmosphere to day five. Blastocysts scored with a numeric scoring system from 1-6 due to the

expansion grade and hatching situation (12).

Embryo biopsy

The SBB on day three was accomplished based on morphological evaluation. At first, the fresh and warmed embryos, at the cleavage stage of day 3, were transferred into a cation (Na^+ and Mg^{++}) free medium. Then, zona pellucida was hatched locally. So that, just a single blastomere was removed.

Then, the blastomere was gently aspirated using an appropriate biopsy microneedle. Next, the blastomeres were studied by the FISH assay. Biopsy samples were maintained in the hypotonic buffer and deferred for analysis. Following blastomere biopsy sampling, embryos were re-cultured. PGT results were described as aneuploid or euploid due to FISH outcomes. After detecting the desired signals in the PGT and control groups, a maximum of three embryos was transferred on day five.

Embryo selection for transfer

Euploid blastocyst embryos with the expansion grades 2, 3, 4, and 5 were selected for transfer. In addition, the embryo grade on day five was considered for embryo selection among the biopsied embryos by evaluating expansion, TE, and ICM morphology (13). In the control group, 1-3 embryos with the best quality were transferred. Embryos were transferred with a Cook catheter under abdominal ultrasound conduction on day five.

Embryo transfer outcomes

The primary outcomes were chemical, clinical, ongoing pregnancy, and lived birth rates. The chemical pregnancy is an early pregnancy that occurs shortly after implantation and was defined as a positive test of serum βhCG level 14 days after embryo transfer. In addition, the sonographic evidence of fetal heartbeat confirmed the clinical pregnancy. Ongoing pregnancy was determined as a viable intrauterine pregnancy observed after eight weeks of pregnancy. Live birth was defined as a live birth after 28 weeks of pregnancy. Secondary outcomes were spontaneous abortion or early pregnancy loss (EPL) and clinical pregnancy loss (CPL) rates. EPL was determined as a pregnancy loss occurring before an intrauterine gestational sac was discovered using ultrasound. Following the fetal heartbeat detection using ultrasound, a lost pregnancy was described in CPL (13).

Statistical analysis

For the pregnancy outcomes, the mixed logistic regression model was used for parameters of TE grade, ICM grade, and embryo expansion as final prophesiers to assess the effect of grades on embryo development and pregnancy outcomes. All data were adjusted for covariates, containing necessary information of semen and oocyte and the day of embryo biopsy during FET or fresh ICSI (with or without PGT-cycles) cycles. An OR table was designed to evaluate the composite development grade to define each pregnancy outcome's likelihood. Statistical analysis was done using a statistical package of the social sciences version 26 (SPSS Inc. Chicago, IL, USA). The Chi-square test for classified variables was used. A statistically significant P value was considered less than 0.05.

Ethics consideration

The Ethics Committee approved this original research at the Islamic Azad University, Rasht Branch (IR.IAU.RASHT.REC.1398.053). In addition, all participants were informed about this study.

Results

Study population and cycle characteristics

Totally 443 embryos with grade A were obtained from 115 patients (1265 mature oocytes) who underwent ICSI with or without PGT cycles. Then, 277 embryos were evaluated following blastomere biopsy in FET and fresh transfer cycles (Fig.1). The cycle characteristics and demography of patients are presented in Table 1. Less than 0.05 was considered statistically significant.

No significant difference was seen in cycle characteristics, including retrieved or fertilized oocytes, good-quality embryos, and euploid blastocysts. In addition, the blastocyst rate is not influenced by parental age, sperm parameters, and oocyte number. However, there is a significant difference between pregnancy outcomes, including chemical, clinical, and ongoing pregnancy, and live birth rate among the three groups ($P<0.001$). Also, there was a significant difference in the blastocyst rate in the three groups ($P<0.002$, Table 2).

Embryo morphology and ICSI outcomes

In the present study, 42.1% of embryos screened with X, Y, 13, 18, and 21 probes were aneuploidy, but 57.9% were euploid. However, there was no relation between 13, 18, and 21 chromosomes aneuploidy and development rate to the blastocyst stage ($P<0.12$).

Among the embryos evaluated for aneuploidy, normal chromosomes were detected in 65.40% of embryos in the FET cycle and 79.62% in the fresh process. This difference can confirm the possible adverse effect of vitrification and warming processes in the FET cycle on the embryo's 13, 18, 21, X, and Y chromosomes (Fig.2). On day five of the embryo development, the blastocyst expansion rate was observed at 26.56% of fresh PGT embryos (8.6% blastocyst expansion 3, 8.59% blastocyst expansion 4, and 9.37% blastocyst expansion 5), 30.20% of FET-PGD embryos (12.58% blastocyst expansion 3, 2.78% blastocyst expansion 4 and 14.84% blastocyst expansion 5) compared with 44.57% in the control group (10.84% blastocyst expansion 3 and 33.73% blastocyst expansion 4, $P<0.001$). Although the expansion rate increased in the control group (OR: 75% vs. 0%), the highest expansion

quality (expansion 5) was observed in the PGT groups (fresh- and FET-PGT).

In the embryos with detected signals in the FET-PGT cycle, 39.39% and 60.61% of blastocysts were aneuploid and euploid, respectively. Also, in the fresh PGT cycle, 3.57% of blastocysts were aneuploid, and 96.43% were euploid (P<0.001). The control group had no blastocyst with expansion 5 on day five. On the other hand, 14.76% and 9.37% of embryos had blastocysts with expansion 5 in FET-PGT and fresh PGT groups, respectively (P<0.01).

The blastocyst expansion grade was a better prognosticator of pregnancy outcomes than the TE and ICM grades separately (Table 3). Embryos with an expansion of grade 4 compared with grade 5 did not show significantly different successful pregnancy rates (P<0.05). But there were significant differences in the gender ratio, morphology, and development rates in the PGT groups (fresh- and FET-PGT groups). A total of 55.65% (48.15% in FET-PGT and 63.16% in fresh-PGT) of euploid embryos with expansion 4 and 5 on day five were female, and 44.35% (51.85% in FET-PGT and 37.84% in fresh-PGT) were male embryos. Also, 90.48 (92.86% in FET-PGT and 85.71% in fresh-PGT) of male blastocyst embryos developed to blastocyst expansion 5 compared with 36% (38.46% in FET-PGT and 33.33% in fresh-PGT) of female embryos (P<0.04). Thus, it reveals the higher development rate of female embryos and the faster development rate in male embryos.

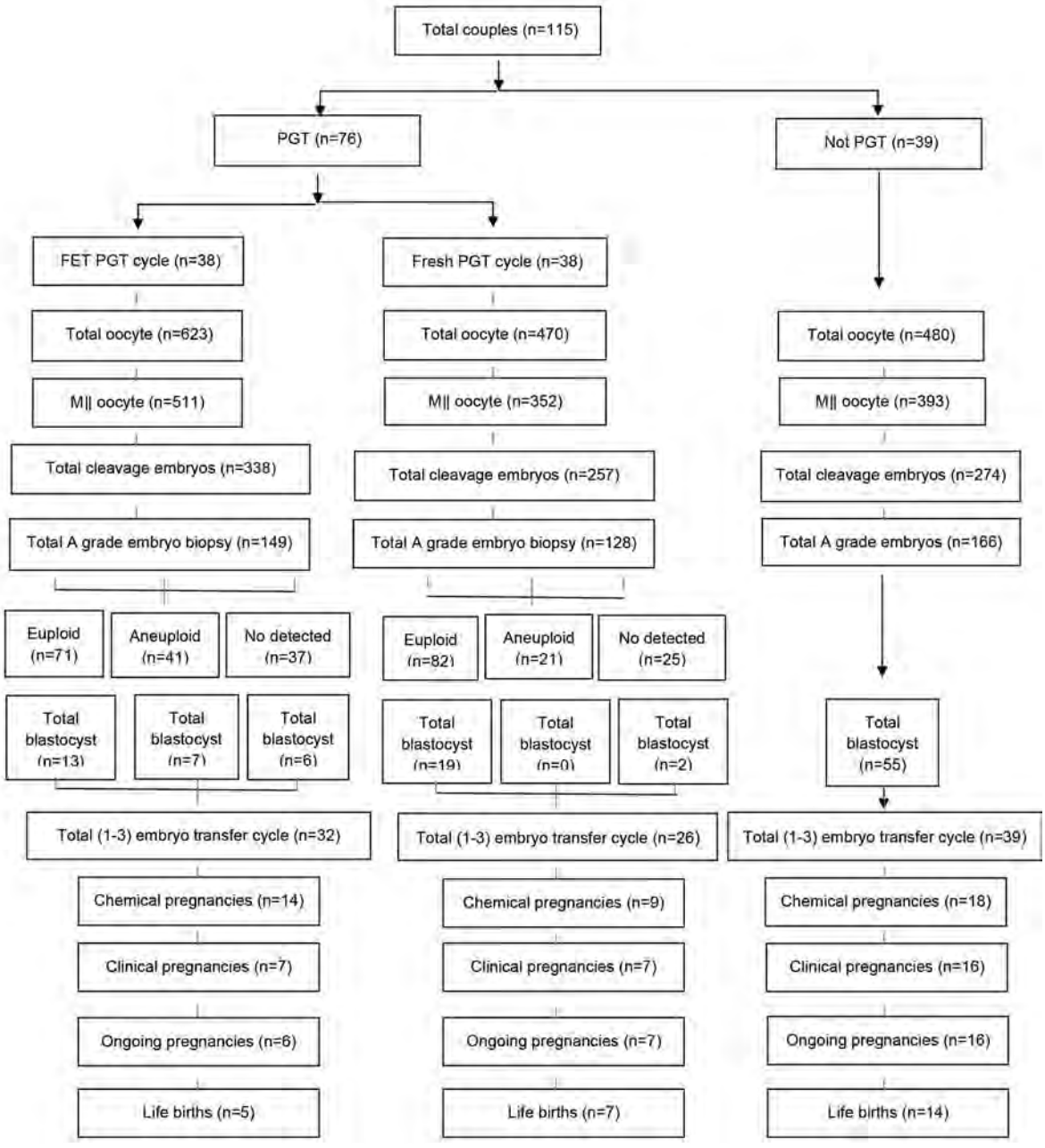

Fig.1: Schematic representation of study design and workflow (total blastocyst; blastocyst expansions 4 and 5). PGT; Preimplantation genetic testing and FET; Frozen embryo transfer.

Table 1: Demography and cycle characteristics of 115 patients

Cycle characteristics	Fresh PGT (n=38)	Freeze PGT (n=38)	Fresh without PGT (n=40)	P value
Maternal age (Y)	35.88 ± 5.18	35.66 ± 6.50	35.26 ± 7.51	0.174
Paternal age (Y)	39.85 ± 5.98	42.06 ± 6.44	38.72 ± 7.62	0.324
No. of oocytes retrieved	10.58 ± 4.06	15.41 ± 8.16	12.31 ± 9.37	0.427
No matured oocytes	9.46 ± 4.03	12.87 ± 6.75	10.8± 7.00	0.184
No cleavage embryos	7.15 ± 2.69	8.88 ± 4.77	7.03 ± 4.74	0.058
Count of sperm (million/ml)	34.71 ± 22.85	27.81 ± 16.93	30.81 ± 24.12	0.772
Motility of sperm (%)	55.69± 20.19	51.25 ± 24.16	48.44 ± 26.94	0.790
Morphology of sperm (%)	11.46 ± 5.37	10.31 ± 5.30	9.58 ± 5.70	0.027
No. of biopsy embryos	5.38 ± 1.92	5.56± 2.17	-	0.107
No. of the transferred embryo(s)	1.62 ± 0.70	2.69 ± 0.69	2.56 ± .75	0.107

Data are presented as mean ± SD. There is no significant difference among groups. N.S.; Not statistically significant and PGT; Preimplantation genetic testing.

Table 2: Embryo development and assisted reproductive outcomes following PGT and/or vitrification-warming compared with the control group

Variables	FET PGT (n=149)	Fresh PGT (n=128)	Fresh without PGT (n=166)	P value
Aneuploidy rate (%)	41/112 (36.60)*	21/103 (20.38)	-	0.001
Blastocyst rate (%)	45/149 (30.20)	34/128 (26.56)	74/166 (44.57)*	0.002
Chemical pregnancy (%)	14/32 (43.87)	9/28 (36.61)*	18/39 (46.15)	0.001
Clinical pregnancy (%)	7/3221.87))	7/28 (26.9)	16/39 (41.02)*	0.001
Ongoing pregnancy (%)	6/32 (18.75)	7/28 (26.9)	16/39 (41.02)*	0.001
Live birth rate (%)	5/32 (15.6)*	7/28 (26.9)	14/39 (35.89)*	0.001
EPL	7/14 (50)*	2/9 (22.22)	2/18 (11.11)	0.04
CPL	2/7 (28.57)*	0/7 (0)*	2/16 (14.28)	0.04

Data are presented as n (%). PGT; Preimplantation genetic testing, EPL; Early pregnancy loose, CPL; Clinical pregnancy loose, FET; Frozen embryo transfer, and *; Is meaning differences (P<0.05).

Fig.2: Specific probes of X, Y, 13, 18, and 21 chromosomes in the In-situ hybridization technique. Chromosome X is blue, chromosome Y is green, chromosome 13 is orange, chromosome 18 is purple, and chromosome 21 is red. **A.** Blastomere of normal male (X, Y, 13, 13, 18, 18, 21, and 21), **B.** Blastomere of trisomy 13 female (X, Y, 13, 13, 18, 18, 21, and 21), and **C.** Blastomere of normal female (X, X, 13, 13, 18, 18, 21, 21) (magnification: 100x).

Table 3: The evaluation of chemical, clinical, ongoing pregnancy, and live birth following PGT and/or vitrification-warming

Groups			Expansion grade			TE grade			ICM grade		
			3	4	5	A	B	C	A	B	C
FET PGT	Chemical pregnancy	No./Obs.no	9/13 (67.4)	6/9 (61.0)	8/11 (75.0)	7/10 (70.0)	10/15 (66.6)	2/4 (50.0)	7/10 (70.0)	10/15 (66.6)	2/4 (50.0)
		Adjusted OR	0.69 (0.22-.12)	0.52 (0.18-1.50)	REF	REF	1.11 (0.39-3.18)	0.51 (0.07-3.81)	REF	1.11 (0.39-3.18)	0.51 (0.07-3.81)
		P value	NS			NS			NS		
	Clinical pregnancy	No./Obs.no	6/13 (44.2)	5/9 (57.6)	6/11 (55.4)	5/10 (50.0)	8/15 (52.6)	1/4 (25.0)	5/10 (50.0)	8/15 (52.6)	1/4 (25.0)
		Adjusted OR	0.79 (0.29-2.15)	1.36 (0.52-3.52)	REF	REF	1.00 (0.37-2.68)	0.35 (0.03-3.51)	REF	1.00 (0.37-2.68)	0.35 (0.03-3.51)
		P value	NS			NS			NS		
	Ongoing pregnancy	No./Obs.no	5/13 (41.9)	5/9 (57.6)	4/11 (37.5)	5/10 (50.0)	8/15 (52.6)	¼ (25.0)	5/10 (50.0)	8/15 (52.6)	1/4 (25.0)
		Adjusted OR	1.20 (0.43-3.34)	1.36 (0.52-3.52)	REF	REF	1.00 (0.37-2.68)	0.35 (0.03-3.51)	REF	1.00 (0.37-2.68)	0.35 (0.03-3.51)
		P value	NS			NS			NS		
	Life birth	No./Obs.no	4/13 (37.2)	5/9 (52.5)	4/11 (37.5)	5/10 (50.0)	8/15 (52.6)	1/4 (25.0)	5/10 (50.0)	8/15 (52.6)	1/4 (25.0)
		Adjusted OR	0.98 (0.35-2.77)	1.84 (0.69-4.87)	REF	REF	1.00 (0.37-2.68)	0.35 (0.03-3.51)	REF	1.00 (0.37-2.68)	0.35 (0.03-3.51)
		P value	NS			NS			NS		
Fresh PGT	Chemical pregnancy	No./Obs.no	11/15 (67.4)	8/11 (61.0)	8/11 (75.0)	9/12 (70.0)	12/17 (66.6)	3/6 (50.0)	7/10 (70.0)	10/15 (66.6)	2/4 (50.0)
		Adjusted OR	0.69 (0.22-.12)	0.52 (0.18-1.50)	REF	REF	1.11 (0.39-3.18)	0.51 (0.07-3.81)	REF	1.11 (0.39-3.18)	0.51 (0.07-3.81)
		P value	NS			NS			NS		
	Clinical pregnancy	No./Obs.no	8/15 (44.2)	7/11 (57.6)	8/13 (55.4)	7/11 (50.0)	8/15 (52.6)	2/6 (33.3)	7/11 (50.0)	8/15 (52.6)	2/6 (33.3)
		Adjusted OR	0.79(0.29-2.15)	1.36 (0.52-3.52)	REF	REF	1.00 (0.37-2.68)	0.35 (0.03-3.51)	REF	1.00 (0.37-2.68)	0.35 (0.03-3.51)
		P value	NS			NS			NS		
	Ongoing pregnancy	No./Obs.no	7/15 (41.9)	7/11 (57.6)	6/13 (37.5)	7/11 (50.0)	8/15 (52.6)	2/6 (33.3)	7/11 (50.0)	8/15 (52.6)	2/6 (33.3)
		Adjusted OR	1.20 (0.43-3.34)	1.36 (0.52-3.52)	REF	REF	1.00 (0.37-2.68)	0.35 (0.03-3.51)	REF	1.00 (0.37-2.68)	0.35 (0.03-3.51)
		P value	NS			NS			NS		
	Life birth	No./Obs.no	7/15 (41.9)	7/11 (57.6)	6/13 (37.5)	7/11 (50.0)	8/15 (52.6)	2/6 (33.3)	7/11 (50.0)	8/15 (52.6)	2/6 (33.3)
		Adjusted OR	0.98 (0.35-2.77)	1.84 (0.69-4.87)	REF	REF	1.00 (0.37-2.68)	0.35 (0.03-3.51)	REF	1.00 (0.37-2.68)	0.35 (0.03-3.51)
		P value	NS			NS			NS		
Fresh without PGT	Chemical pregnancy	No./Obs.no	24/36 (66.6)	11/19 (61.0)	No sample	20/31 (64.5)	13/19 (68.5)	2/5 (40.0)	20/3 (64.5)	13/19 (68.5)	2/5 (40.0)
		Adjusted OR	0.69 (0.22-2.12)	REF	No sample	REF	1.11 (0.39-3.18)	0.41 (0.07-3.81)	REF	1.11 (0.39-3.18)	0.41 (0.07-3.81)
		P value	NS			NS			NS		
	Clinical pregnancy	No./Obs.no	16/36 (44.6)	11/19 (57.7)	No sample	16/31 (52.3)	10/19 (52.7)	1/5 (20.0)	16/3 (52.3)	10/19 (52.7)	1/5 (20.0)
		Adjusted OR	0.79 (0.29-2.15)	REF	No sample	REF	1.00 (0.37-2.68)	0.25 (0.03-3.51)	REF	1.00 (0.37-2.68)	0.25 (0.03-3.51)
		P value	NS			NS			NS		
	Ongoing pregnancy	No./Obs.no	15/36 (41.9)	11/19 (57.6)	No sample	16/31 (52.3)	10/19 (52.7)	1/5 (20.0)	16/3 (52.3)	10/19 (52.7)	1/5 (20.0)
		Adjusted OR	1.20 (0.43-3.34)	REF	No sample	REF	1.00 (0.37-2.68)	0.25 (0.03-3.51)	REF	1.00 (0.37-2.68)	0.25 (0.03-3.51)
		P value	NS			NS			NS		
	Life birth	No./Obs.no	14/36 (37.2)	10/19 (52.5)	No sample	16/31 (52.3)	10/19 (52.7)	1/5 (20.0)	16/31 (52.3)	10/19 (52.7)	1/5 (20.0)
		Adjusted OR	0.98 (0.35-2.77)	REF	No sample	REF	1.00 (0.37-2.68)	0.25 (0.03-3.51)	REF	1.00 (0.37-2.68)	0.25 (0.03-3.51)
		P value	NS			NS			NS		

Data are presented as n (%) and CI. NS; No statistically significant; REF; Reference, CI; Confidence interval, OR; Odds ratio, Obs.no; Observer, PGT; Preimplantation genetic testing, FET; Frozen embryo transfer, TE; Trophectoderm, ICM; Inner cell mass, and *; P<0.05.

Embryo grade and ICSI outcomes

In the present study, about 97 participants reached the embryo transfer step. In pentaplex PGT of embryos, pregnancy-related data could not be cited due to the tiny statistical population (n=38), and accurate statistical analysis could not be obtained from them. Therefore, their data were excluded from the pregnancy outcomes. We analyzed the pregnancy outcome according to the quality of the transferred embryos. The results showed that 34.61, 43.75, and 46.15% of patients from fresh-PGT, FET-PGT, and control groups had a positive chemical pregnancy test. Also, 26.92, 15.62, and 3 8.46% of patients from fresh-PGT, FET-PGT, and control groups had a live birth, respectively. EPL frequency in the fresh-PGT, FET-PGT, and control groups was 22, 50, and 11%, respectively. Therefore, there is a significant increase in the FET-PGT group.

Sixty percent of blastocyst transfer cycles in the control group showed chemically positive pregnancy. However, 94.44% of chemical pregnancies had blastocyst with expansions 3 and 4. In the fresh-PGT group, 57.14% of positive results had blastocyst embryos, and 44% of blastocyst transfer cycles were positive for a chemical pregnancy. In the fresh-PGT group, 75% of positive results had blastocyst embryos, and 42.85% of blastocyst transfer cycles had a clinically positive pregnancy (Fig.3).

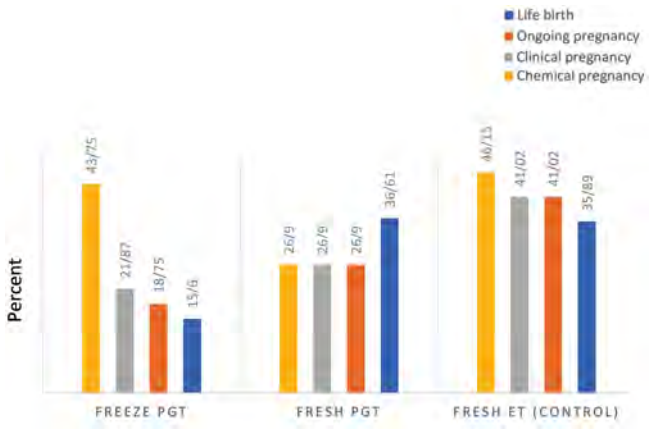

Fig.3: Pregnancy outcome in study groups. A significant difference in pregnancy results in the three groups was seen. Fresh embryo transfer has the highest rate in chemical (P=0.002), clinical (P=0.001), ongoing pregnancy (P=0.001), and live birth rate (P=0.001). PGT; Preimplantation genetic testing and ET; Embryo transfer.

Discussion

This study was designed to determine the correlated blastocysts morphology with chromosomal state and pregnancy outcome. This study is the first to assay the association between gender, SBB, and vitrification with assisted reproductive outcomes. The study shows that the probability of CPL was not associated with morphology and type of cycle. In contrast, the likelihood of EPL was affected by the cycle, especially for the FET-PGT cycle. In a recent study, Forman (14) proposed that all euploid blastocysts do not have equal implantation potential. They reported an implementation rate of 80.9% for excellent quality blastocysts (4AA, 5AA, and 6AA), which was higher than low-quality euploid blastocysts (56.3%), which is in agreement with our study.

In addition, our study evaluated the association of gender with blastocyst grade and resistance against vitrification, which can affect embryo developmental potential. According to this study, a higher percentage of male embryos reached the blastocyst stage, which shows more resistance of male embryos against freeze and warming procedures than female and aneuploid embryos. Also, male embryos reached the blastocyst stage faster than female embryos. On the other hand, Fang et al. found a relation between gender and blastocyst grade, and faster development of female embryos was reported. These differences in development could be due to the time of blastomere biopsy (1). In our study, the embryos were biopsied on day three, whereas in the mentioned study, the blastocysts were biopsied.

To the best of our knowledge, there are a limited number of studies about the association of the ICSI method with PGT outcomes. Our study refers to the embryos' ability at the cleavage stage to reach the blastocyst phase in which they undergo biopsy procedures on day three. In blastocyst development, a similar development rate was observed in the euploid and aneuploid embryos for 13, 18, 21, X, and Y chromosomes. So that, it means that abnormal chromosomal embryos have equal potential for development as normal embryos. Furthermore, using accurate techniques such as Time Laps and array CGH, it has also been reported that various chromosomal aberrations have different effects on the embryo's morpho-kinetics (15).

Our study's strength includes the number of samples in the FET and fresh-PGT cycle and the evaluation of various items and their effect on aneuploidy, blastocyst development, and pregnancy outcomes. In addition, PGT was performed on the frozen embryos and compared with fresh embryos. Therefore, this study may guide the optimal selection of euploid embryos to improve clinical pregnancy after fresh and FET-PGT cycles.

The limiting of this study was the intrinsic nature

of morphologic grading that could not evaluate the epigenetic effect of vitrification-warming and PGD on embryos. Nevertheless, Phan et al. showed the morphological parameters of the embryo, such as the fragmentation and its concentration, following an analysis of the CGH array in every 23 pairs of chromosomes in one blastomere. Although the symmetry of the blastomeres much reflects the condition of the ploidy of the embryo. However, assisted hatching does not accrue for all embryos; the expansion grades for pregnancy outcomes have predictive value (16). Future studies with embryos from more significant sample sizes and under PGT techniques like Next-Generation sequencing can teach morphology and freeze-warm effect in proposing ICSI and pregnancy outcomes.

In addition, morphology and developmental stages are affected by manipulation approaches such as embryo vitrification-warming and blastomere biopsy for PGT. Zona hatching embryos for blastomere biopsy can increase the blastocyst percentage with ICM 3, 4, 5. On the other hand, some euploid embryos have poor morphology, and a significant proportion of aneuploid embryos can get the highest morphologic scores. The implantation rate is far from the gynecologist's final goal despite transferring high-quality and euploid embryos. The impact of expansion grade after the comprehensive chromosomal screening in an optimal embryo transfer is corroborated. However, analysis of embryo valuation and embryo election for the planning of PGT could help increase healthy pregnancy rates with satisfactory outcomes. These findings offer the morphological and genomic criteria to provide supplementary data to increase the fresh-PGT and FET-PGT outcomes.

Conclusion

A significant correlation was found in the present study between SBB and/or vitrification-warming on day three, decreased embryo development potential, and assisted reproductive outcomes. The embryos' pregnancy outcome was also associated with their development stage to assess their development and live birth ability. Our findings may provide pregestational consulting for couples who decided to use PGT and FET procedures in their assisted reproductive technology (ART) process to have healthy children.

Acknowledgments

The Islamic Azad University Department of Biology approved this research Rasht in 2018 as a dissertation. The authors are thankful to Mehr's Research and Infertility clinicians and staff. This work was financial and technical supported by Mehr's Research and Infertility, Rasht, Iran. There is no conflict of interest in this study.

Authors' Contributions

Sh.A., F.Gh., M.M., A.H.; Participated in study design, statistical analysis, data collection and evaluation, and drafting. Sh.A., M.M.; Performed follicle collection and prepared oocytes for ICSI about this study component. Sh.A., A.S., F.Gh., M.M., A.H.; Contributed extensively to interpreting the data and the conclusion. Sh.A., F.Gh., M.M.; Conducted molecular experiments and PCR and FISH analysis. All authors edited and approved this paper's final version for submission, participated in finalizing the manuscript, and approved the final draft.

References

1. Fang R, Yang W, Zhao X, Xiong F, Guo C, Xiao J, et al. Chromosome screening using culture medium of embryos fertilised in vitro: a pilot clinical study. J Transl Med. 2019; 17(1): 73.
2. Ilyin I, Nikitin O, Gontar J, Buderatska N, Verlinsky OY. Application of the pronuclear scoring system for predicting the morphology and ploidy of early human embryos. Cytol Genet. 2019; 53(3): 227-232.
3. Liu XL, Xu CM, Huang HF. Application and challenge of preimplantation genetic testing in reproductive medicine. Reprod Dev Med. 2019; 3(3): 129.
4. Scarica C, Cimadomo D, Dovere L, Giancana A, Stoppa M, Capalbo A, et al. An integrated investigation of oocyte developmental competence: expression of key genes in human cumulus cells, morphokinetics of early divisions, blastulation, and euploidy. J Assist Reprod Genet. 2019; 36(5): 875-887.
5. Youm HS, Choi JR, Oh D, Rho YH. Closed versus open vitrification for human blastocyst cryopreservation: a meta-analysis. Cryobiology. 2017; 77: 64-70.
6. Wang A, Santistevan A, Cohn KH, Copperman A, Nulsen J, Miller BT, et al. Freeze-only versus fresh embryo transfer in a multicenter matched cohort study: contribution of progesterone and maternal age to success rates. Fertil Steril. 2017; 108(2): 254-261.
7. Coutifaris C. Freeze-only in vitro fertilization cycles for all? Fertil Steril. 2017; 108(2): 233-234.
8. Dviri M, Madjunkova S, Koziarz A, Antes R, Abramov R, Mashiach J, et al. Is there a correlation between paternal age and aneuploidy rate? An analysis of 3,118 embryos derived from young egg donors. Fertil Steril. 2020; 114(2): 293-300.
9. Fesahat F, Montazeri F, Sheikhha MH, Saeedi H, Firouzabadi RD, Kalantar SM. Frequency of chromosomal aneuploidy in high-quality embryos from young couples using preimplantation genetic screening. Int J Reprod Biomed. 2017; 15(5): 297-304.
10. Leaver M, Wells D. Non-invasive preimplantation genetic testing (niPGT): the next revolution in reproductive genetics? Hum Reprod Update. 2020; 26(1): 16-42.
11. Zhang J, Xia H, Chen H, Yao C, Feng L, Song X, et al. Less-invasive chromosome screening of embryos and embryo assessment by genetic studies of DNA in embryo culture medium. J Assist Reprod Genet. 2019; 36(12): 2505-2513.
12. Yu L, Jia C, Lan Y, Song R, Zhou L, Li Y, et al. Analysis of embryo intactness and developmental potential following slow freezing and vitrification. Syst Biol Reprod Med. 2017; 63(5): 285-293.

13. Nazem TG, Sekhon L, Lee JA, Overbey J, Pan S, Duke M, et al. The correlation between morphology and implantation of euploid human blastocysts. Reprod Biomed Online. 2019; 38(2): 169-176.
14. Forman EJ. Morphology matters: are all euploid blastocysts created equal? Fertil Steril. 2017; 107(3): 573-574.
15. Del Carmen Nogales M, Bronet F, Basile N, Martínez EM, Liñán A, Rodrigo L, et al. type of chromosome abnormality affects embryo morphology dynamics. Fertil Steril. 2017; 107(1): 229-235.
16. Phan V, Littman E, Harris D, La A. Correlation between embryo morphology and development and chromosomal complement. Asian Pac J Reprod. 2014; 3(2): 85-89.